Novel Mass Spectrometric Techniques for Stable Isotope Measurements in Atmospheric Halocarbons and Nitrous Oxide

By

ANNA R. RIDLEY

School of Environmental Sciences

UNIVERSITY OF EAST ANGLIA

February 2017

A thesis submitted to the School of Environmental Sciences of the University of East Anglia in partial fulfilment of the requirements for the degree of Doctor of Philosophy

Abstract

Understanding source and sink process of atmospheric species can help to constrain budgets of gases which contribute towards ozone destruction and warming of the Earth's atmosphere. The use of isotope ratio analysis is a key tool in budget quantification.

GC-MS techniques allowed quantification of $\delta(^{37}Cl)$ of CFC-11, CFC-12 and CFC-113 deeper in the stratosphere than previously recorded. Isotope enrichment increased with decreasing mixing ratios for all CFCs. A maximum ^{37}Cl enrichment in CFC-12 significantly exceeded that published to date. Apparent isotope fractionation (ε_{App}) varied with respect to latitude for ^{37}Cl analysis. The first measurements of $\delta(^{13}C)$ of CFC-11, CFC-12 and CFC-113 at stratospheric altitudes displayed increasing enrichment with altitude. Minimal correlation was observed between latitude and apparent isotope fractionation. Values of ε_{App} are significantly lower than that given by fractionation observed in laboratory photolysis experiments.

Reanalysis of samples which had undergone photolysis allowed measurements to be linked to an internationally recognised ^{13}C scale (VPDB) allowing direct comparison between photolysis rates of CFC-12 analysed using different analytical systems.

Based on the mass difference, the isotope fractionation of ^{17}O should be approximately half as much as that of ^{18}O, with respect to ^{16}O. The proportion of ^{17}O in tropospheric air is in fact higher. Identifying the source of the ^{17}O excess would identify possible non-mass dependent fractionation in sources or sinks. The development of an IR-MS measurement system allowed for the first measurements of $\Delta^{17}O$ in stratospheric N_2O above 12 km altitude. The data suggest that photolysis and reaction with $O(^1D)$ are not the source of the ^{17}O anomaly. The newly developed system allowed participation in an interlaboratory compatibility study.

Development of a measurement system capable of analysis of ^{37}Cl in CH_3Cl allowed analysis of test gas preparations of CH_3Cl in preparation for air concentrate analysis. The first steps towards the synthesis of a calibration gas of characterised isotopic composition were carried out.

Publications

Work contributing to this thesis has been published in:

MOHN, J., WOLF, B., TOYODA, S., LIN, C. T., LIANG, M. C., BRÜGGEMANN, N., WISSEL, H., STEIKER, A.E., DYCKMANS, J., SZWEC, L., OSTROM, N. E., CASCIOTTI, K. L., FORBES, M., GIESEMANN, A., WELL, R., DOUCETT, R. R., YARNES, C. T., RIDLEY, A. R., KAISER, J. & YOSHIDA, N. 2014. Interlaboratory assessment of nitrous oxide isotopomer analysis by isotope ratio mass spectrometry and laser spectroscopy: Current status and perspectives. *Rapid Communications in Mass Spectrometry,* 28**,** 1995-2007.

Table of Contents

List of Figures

List of Tables

Chapter 1: Introduction

The impact of changing atmospheric composition on the climate is of increasing interest. The effect of human-induced climate change is displayed via the warming of the Earth's atmosphere and associated effects. Additionally, depletion of the ozone layer and increased levels of pollution are of interest due to the direct and indirect effects on humans.

This research focuses on measurement of trace gases, related to both the increase in mean temperature of the Earth and gases responsible for depletion of ozone in the stratosphere. Techniques were developed for the measurement, as well as improvement of measurement of isotope ratios in CFCs and species related to global temperature increase. Details of method developments and presentation of atmospheric data are presented in Chapters two to six.

This chapter will give an overview of the structure of the atmosphere, and then the species relevant to this work will be placed in context with respect to global warming and ozone depletion. Finally, the use of isotope ratio measurements for constraining budgets of these species will be discussed.

1.1 Atmospheric structure and composition

The atmospheric composition is largely diatomic nitrogen (78 %), oxygen (21 %), argon (0.9 %) and carbon dioxide (0.04%). The remaining gases are termed 'trace gases' since their relative abundances are low. Firstly, these percentages assume the abundance of water vapour, which is very variable and can reach abundances in the percent range. Secondly, it is assumed that any given sample of air has the same composition, yet in actual fact this only is true for gases whose residence times are longer than the time required to fully mix. However, the extent to which a species is described as fully mixed is dependent on measurement precision, for example, even O_2 is not fully mixed, yet is used as a tracer. Likewise N_2/Ar ratios can be useful tracers of gravitational and thermal separation. This however, holds true for the species listed since residence times are greater than a few days to a few months, the time required for atmospheric mixing. In the context of this thesis, all species of interest are deemed trace gases, and have atmospheric abundances below that of carbon dioxide, currently 400.72 ppm (Dlugokencky and Tans, 2016).

The atmosphere can be divided into four sections: the troposphere, stratosphere, mesosphere and thermosphere, as shown in Figure 1.1.

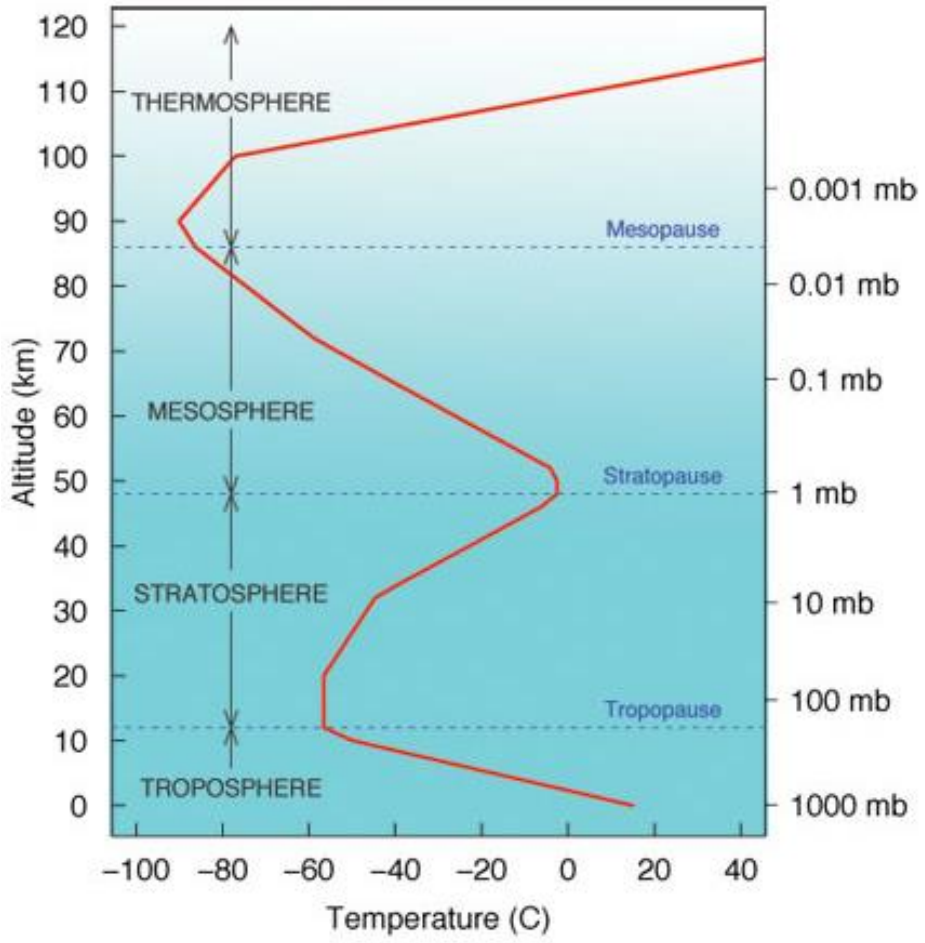

Figure 1.1 Diagram of atmospheric structure. Taken from Steven C. Wolfsy, Abbott Lawrence Ritch Professor of Atmospheric and Environmental Science, lecture notes (2006).

The lowest level of the atmosphere, the troposphere, displays a decreasing temperature gradient with height up to an altitude of approximately 10 km. The tropospheric temperature is determined mainly by radiation from the Earth's surface, decreasing at an average rate of 6.5 K km^{-1}. The temperature gradient depends on the balance between adiabatic expansion and heating. Due to instability in the air masses, there are therefore high levels of vertical transport. At the top of the troposphere lies a temperature inversion, named the tropopause. Above this lies the stratosphere, from 10 km in altitude up to approximately 50 km. Conversely, this section of the atmosphere increases in temperature with altitude due to the effects of ozone, which is a strongly influential trace gas in this region. The radiative heating due to absorption of short

wave solar radiation and long wave terrestrial radiation warms the stratosphere. The positive temperature gradient limits convection and thus the stratosphere displays limited vertical transport.

The temperature differential between the warm tropical regions and cold polar regions is the driver for atmospheric circulation. Simply described, warm air rises at the equator and is transported towards the poles in order to equilibrate temperature. However, the Earth's rotation, and the conservation of atmospheric angular momentum, causes the poleward moving air to form two cells of circulating air masses, termed Hadley cells. This transport causes warm air of subtropical origin to be transported towards the equator, where it is uplifted towards the stratosphere. This region, termed the Intertropical Convergence Zone (ITCZ), is a narrow band in which most trace gases are drawn into the stratosphere. In the context of this work, the ITCZ is a region where gases of interest are transported upwards to the tropical tropopause layer (TTL). Once in the stratosphere, large-scale Brewer-Dobson circulation pushes air masses high and polewards, thus, if collected at similar distances relative to the tropopause, samples collected in the stratosphere near the equator are atmospherically 'younger' than samples collected in the mid and polar-latitudes. At mid-latitudes there is a greater volume of mixing between the troposphere and stratosphere. However, the Brewer-Dobson circulation prevents large quantities of gases reaching the upper stratosphere, where transport towards the poles is the most significant. This means that substances entering the stratosphere at tropical latitudes are likely to have a larger impact on ozone depletion than those entering from mid-latitudes since ozone depletion is mostly significant at the poles.

1.2 Radiative forcing

The term radiative forcing is used to describe the effects of different factors on the Earth's energy budget. The energy budget is dominated by solar input, but importantly, is also affected by changes in atmospheric composition. So called 'greenhouse gases' can retain energy in the Earth's atmosphere and therefore alter the amount of energy leaving the atmosphere (Figure 1.2).

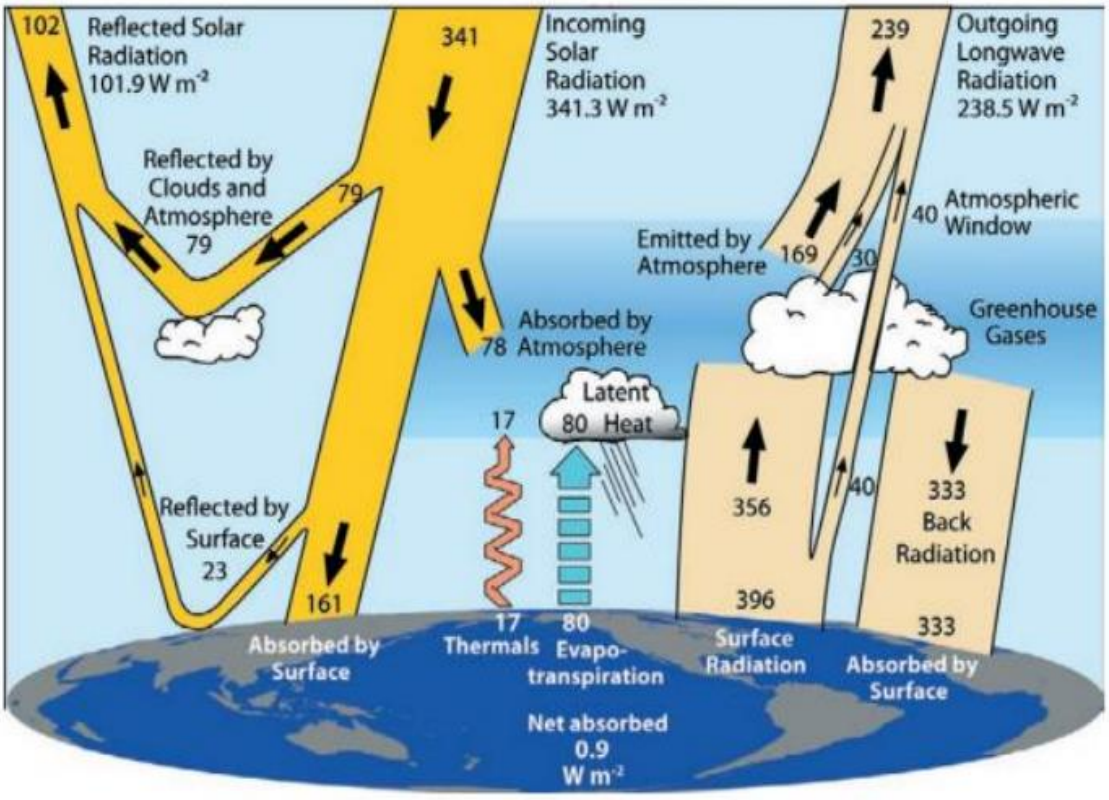

Figure 1.2 Schematic showing the Earth's annual radiation budget between March 2000 and May 2004. Taken from Trenberth et al. (2009).

Trace gases, although making make up a small proportion of the composition of the atmosphere, in fact have a significant influence on the proportion of heat energy which is retained, and in turn gives rise to the heating of the Earth.

1.2.1 Greenhouse gases

A large number of gases, both of natural and anthropogenic origin are responsible for radiative forcing. These gases, including carbon dioxide, methane and nitrous oxide all have increased significantly since preindustrial times (IPCC, 2014), and due to their absorption of terrestrial infrared radiation, are important influences on the global temperature. In terms of emissions fluxes, water vapour (H_2O) is the most significant. Of those which emissions are impacted by humans, carbon dioxide (CO_2) is the most significant greenhouse gas, along with methane (CH_4), and nitrous oxide (N_2O) (Montzka and Reimann, 2011). However, minor species with small mole fractions also contribute significantly to global temperature increase. Hydrochlorofluorocarbons (HCFCs), chlorofluorocarbons (CFCs), perfluorocarbons (PFCs) and hydrofluorocarbons (HFCs) all contribute to the warming effect.

Table 1.1. Lifetimes, global mean mole fraction 100 year time horizon global warming potentials (GWP_{100}) and ozone depletion potentials of common species related to this work. All lifetime values are taken from Montzka et al. (2011), mixing ratios from Prinn et al. (2014), GWPs from Myhre et al. (2013) and ODPs from Carpenter et al. (2014) unless otherwise stated.

Species	Formula	Lifetime	Mixing Ratio (pmol mol^{-1})	GWP_{100}	ODP
Carbon dioxide	CO_2	5-200[1]	390.5 (ppm)[1]	1	-
Methane	CH_4	12.4[1]	1803 (ppb)[1]	28	-
Nitrous Oxide	N_2O	121[1]	324.3 (ppb)[1]	265	-
CFC-11	CCl_3F	52	235.5	4660	1.0
CFC-12	CCl_2F_2	102	527.5	10200	0.82
CFC-113	$C_2Cl_3F_3$	85	73.6	5820	0.85
CFC-115	C_2ClF_5	1020	8.40	7670	0.57
HCFC-141b	CH_3CCl_2F	9.4	22.5	782	0.12
HCFC-142b	CH_3ClF_2	18	22.0	1980	0.06
HCFC-22	$CHClF_2$	11.9	219.8	1760	0.04
HFC-134a	$C_2H_2F_4$	14	67.7[3]	1300	0
HFC-152a	CH_3CHF_2	1.6	6.8[3]	174	0
HFC-227ea	CF_3CHCF_3	36	0.74[3]	3350	0
Carbon tetrachloride	CCl_4	26[3]	84.2	1730	0.82
Methyl chloride	CH_3Cl	0.9	537.1	12	0.02
Methyl bromide	CH_3Br	0.8[3]	7.07	2	0.66
Carbonyl sulphide	COS	2-8[3]	491[3]	27[2]	-
Chloroform	$CHCl_3$	149 days[3]	7.5[3]	16	-
Dichloromethane	CH_2Cl_2	144 days[3]	26.0[3]	9	-

[1]Myhre et al. (2013). [2]Brühl et al. (2012). [3]Montzka et al. (2011)

In order to quantify the magnitude of the effect of each species on the global temperature increase, a standardised measure of Global Warming Potential (GWP) is used (Equation 1.1).

$$GWP\ (x) = \frac{\int_0^{TH} a_x.[x(t)]dt}{\int_0^{TH} a_r.[r(t)]dt} \qquad \text{Equation 1.1}$$

The GWP of a species describes the total effect of a species on radiative forcing relative to a reference gas, expressed on a per kilogram basis. Since the effect of a short-lived gas may have a strong influence on radiative forcing over a short time scale, yet a minimal effect over a longer period, the GWP is dependent on the time horizon over which it is calculated. It is common to reference GWP to CO_2, given a value of 1, and expressed over a 100 year time horizon. The GWP of common greenhouse gases are shown in Table 1.1.

In the context of this thesis, the species of interest are nitrous oxide (N_2O), methyl chloride (CH_3Cl), CFC-11, CFC-12 and CFC-113. It can be seen that with respect to global warming potentials, all species are significant over the 100 year timeframe, with values of 265, 12, 4660, 10200 and 582 respectively. Although the values of GWP for N_2O and CH_3Cl are small compared to the three CFCs, the have large abundances, as shown in Table 1.1, and therefore are significant.

1.3 Ozone depletion

Ozone is a naturally occurring species in the atmosphere, and can be found in both the troposphere and stratosphere. Although found near the Earth's surface, a larger quantity of ozone is found in the stratosphere (Figure 3). The significance of ozone in the stratosphere is twofold: Firstly, the production and loss processes cause the temperature inversion signifying the lower and upper limits of the stratosphere. Secondly, ozone absorbs much of the incident Ultra-Violet B (UVB) radiation (280-315 nm). The presence of ozone has both positive and negative effects. In the troposphere, ozone is highly reactive and causes harm to biological organisms, including humans. It is responsible for reductions in crop yields. Conversely, when found in the stratosphere, the ability of ozone to absorb certain wavelengths of solar radiation results in protection for living organisms from harmful ultraviolet rays. Almost complete absorption by ozone of the shortest ultraviolet wavelengths, UVC (100-280 nm), as well as the majority of UVB (280-315 nm) radiation gives huge benefits to such organisms [Brasseur et al., 1999]. In contrast, almost all UVA radiation (315-400 nm) is transmitted to the Earth's surface.

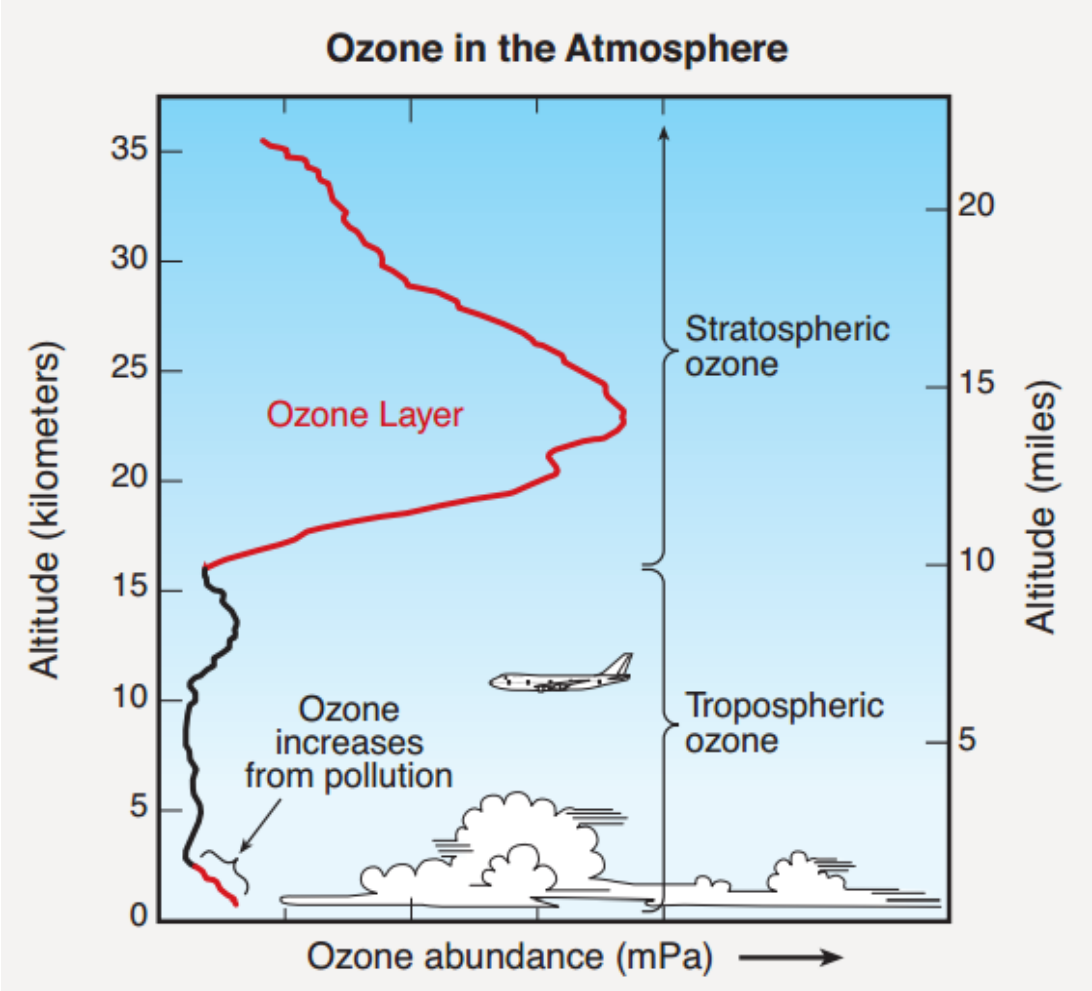

Figure 1.3 Distribution of ozone through the troposphere and stratosphere. Taken from Fahey and Hegglin (2010).

1.3.1 Ozone production

The production of ozone is via the stratospheric breakdown of diatomic oxygen by ultraviolet radiation, the recombination of the resultant oxygen atom with O_2 (Equations 1.2 and 1.3). M denotes a third body, in this case likely O_2 or N_2, required to remove excess energy formed during the reaction.

$$O_2 + h\nu \rightarrow O + O \ (\lambda < 242\ nm) \qquad \text{Equation 1.2}$$

$$O + O_2 + M \rightarrow O_3 + M \qquad \text{Equation 1.3}$$

Since the production of stratospheric ozone is reliant on the incoming solar radiation, regions with high solar radiation, such as the tropics, have a higher proportion of the total global ozone production. It is important to note however, that ozone is actually more abundant in the extra-tropics due to its longer lifetime and transport effects.

In the troposphere, ozone is transferred via downwelling from the stratosphere, but also is produced in situ via production of an oxygen atom, an example shown in Equation 1.4. Precursors such as hydrocarbons and nitrogen oxides are sourced from both natural and anthropogenic processes such as fossil fuel combustion.

$$NO_2 + h\nu \rightarrow O + NO \ (\lambda < 400\ nm) \qquad \text{Equation 1.4}$$

This free oxygen atom reacts as Equation 1.3 to give ozone.

1.3.2 Ozone loss

Ozone can be depleted naturally via photolysis in the stratosphere. As shown by Equation 1.5, ozone is broken down to give atomic and diatomic oxygen. However, this mechanism does not account for the entire loss of ozone in the stratosphere.

$$O_3 + h\nu \rightarrow O_2 + O \qquad \text{Equation 1.5}$$

Additional reactions have been identified to cause loss of ozone in the stratosphere, and mainly involve chlorine, of relevance to this thesis, as well as bromine and nitrogen oxides and HO_x.

1.3.3 Ozone depleting substances

The depletion of ozone occurs via the introduction of ozone depleting substances to the stratosphere. Ozone depleting substances are halogen-containing species that allow for the occurrence of catalytic cycles described in Section 1.3.5. Many of these substances are have been widely used as refrigerants, fire extinguishers and air conditioners, as well as solvents for cleaning and agricultural fumigants.

Ozone depleting substances can be categorised into 3 areas: chlorocarbons, as of relevance to this work, bromocarbons and iodocarbons. Bromocarbons, including halons, methyl bromide, and short lived bromocarbons, as well as iodocarbons such as methyl iodide are outside the scope of this thesis and are not discussed further.

Chlorinated ozone depleting substances of anthropogenic origin contribute approximately 83 % of chlorine from gases entering the stratosphere. Of this total chlorine, 61 % originates from CFC-11, CFC-12 and CFC-113 (as of 2012), the three most important CFCs (Carpenter et al., 2014). The effect of CFCs on ozone depletion was suggested by Molina and Rowland (1974), recognised by the Nobel Prize in 1995. CFC-11, CFC-12 and CFC-113 contribute significantly to ozone destruction due to their high global mean mixing ratios (235.5, 527.5 and 73.6 ppt in 2014 respectively) and long lifetimes (52, 102 and 85 years) (Carpenter et al., 2014). In an effort to

prevent further destruction of ozone by anthropogenic CFCs, the Montreal Protocol (1987) was introduced. This protocol outlined the phasing out and eventual cessation of the production and consumption of CFCs. Although regulated by the Montreal protocol, the long lifetimes of these species have limited their decline in the atmosphere and hence are still extremely important with respect to ozone depletion. Both CFC-11 and CFC-113 have shown a decline in mole fractions for over a decade, yet CFC-12 has only begun to decrease in recent years. Since the Montreal Protocol prevents further production and consumption of these species, their decline is expected to continue. Current sources of these CFCs are CFC 'banks' such as air conditioning units and refrigerators, illegal trade, as well as exemptions to the Montreal Protocol.

Methyl chloride, CH_3Cl, contributes approximately 16 % to the total chlorine derived from long lived gases reaching the stratosphere (Carpenter et al., 2014). As the most abundant organic chlorocarbon in the atmosphere, CH_3Cl is becoming increasingly important, in relative terms, since it is not regulated by the Montreal Protocol. Consequently there is increased interest in fully understanding source and sink processes. It is important to note, that in contrast to CFCs, the production pathways for CH_3Cl are diverse and in fact mostly not anthropogenic. The main sources of CH_3Cl include tropical vegetation (Saito et al., 2008), halophite plants found in salt marshes (Carpenter et al., 2014), and oceans (Hu et al., 2013). Minor sources include biomass burning and fossil fuel burning (Carpenter et al., 2014).

1.3.4 Ozone depletion potentials

It is necessary to use a standardised method to compare the effect of halogenated gases on stratospheric ozone depletion. The ozone depletion potential (ODP) of a given species is the quantified potential of a gas released at the Earth's surface to destroy stratospheric ozone. All species are assessed relative to a similar mass of CFC-11, which is hence assigned an ODP of 1.0, as shown in Equation 1.6.

$$ODP_i = \frac{\delta[\mathrm{O_3}]_i}{\delta[\mathrm{O_3}]_{CFC-11}}$$

Where I is the species of interest, $\delta[O_3]_i$ is the global ozone depletion produced by one unit of species I, and $\delta[O_3]_{CFC-11}$ is the global ozone depletion produced by one unit of CFC-11. ODPs of a range of ozone depleting species are given in Table 1.1.

1.3.5 Mechanisms of ozone loss

The destruction of ozone by chlorine involves a catalytic cycle producing oxygen gas, as well as further ozone destroying molecules.

This process can overall be described as:

$$X + O_3 \rightarrow XO + O_2 \quad \text{Equation 1.6}$$

$$XO + O \rightarrow X + O_2 \quad \text{Equation 1.7}$$

$$\text{Net} = O + O_3 \rightarrow 2O_2 \quad \text{Equation 1.8}$$

(Where X represents Cl, Br or I [not F])

This overall cycle begins with the breakdown of ozone by a single chlorine radical, to give ClO which continues the process as follows:

$$Cl + O_3 \rightarrow ClO + O_2 \quad \text{Equation 1.9}$$

$$ClO + HO_2 \rightarrow HOCl + O_2 \quad \text{Equation 1.10}$$

$$HOCl + h\nu \rightarrow OH + Cl \quad \text{Equation 1.11}$$

$$OH + O_3 \rightarrow HO_2 + O_2 \quad \text{Equation 1.12}$$

$$\text{Net} = 2O_3 \rightarrow 3O_2 \quad \text{Equation 1.13}$$

Steps (1.9) and (1.12) rapidly deplete ozone, giving the net production of $3O_2$ from $2O_3$. The formation of active chlorine compounds, Cl and ClO, continue to deplete ozone whereas inactive species, HCl, and later $ClONO_2$, act as long term reservoirs. A key factor in ozone depletion rates is the relative time spent in the active and inactive form. Reservoir species, HCl, and $ClONO_2$, formed by Equations 1.14 to 1.18 are deemed the longest lived and most abundant reservoir species.

$$Cl + CH_4 \rightarrow CH_3 + HCl \quad \text{Equation 1.14}$$

$$Cl + HO_2 \rightarrow HCl + O_2 \quad \text{Equation 1.15}$$

$$Cl + H_2 \rightarrow HCl + H \quad \text{Equation 1.16}$$

$$Cl + H_2O_2 \rightarrow HCl + HO_2 \quad \text{Equation 1.17}$$

$$ClO + NO_2 + M \rightarrow ClONO_2 + M \text{ (where M is a third body)} \quad \text{Equation 1.18}$$

Some reactions give a null cycle, so no overall change in the composition occurs. These reactions both deplete and form ozone:

$$ClO + NO \rightarrow Cl + NO_2$$ Equation 1.19

$$NO2 + h\nu \rightarrow NO + O$$ Equation 1.20

$$O + O_2 + M \rightarrow O_3 + M$$ Equation 1.21

$$ClO + h\nu \rightarrow Cl + O$$ Equation 1.22

$$Cl + O_3 \rightarrow ClO + O_2$$ Equation 1.23

The low atmospheric mass contained within the stratosphere, approximately 20 % of the total atmosphere, ensures mixing of air masses must occur many times to allow for the ozone depleting substances to be destroyed. Importantly, the coupling of bromine and chlorine chemistry collectively depletes ozone at a more rapid rate (Wofsy et al., 1975). Bromine chemistry is outside the scope of this thesis and hence is not discussed further.

1.4 Trace gas stable isotope measurements

To understand fully the atmospheric budgets of halocarbons, in particular methyl chloride, concentration measurements alone are not sufficient. Knowledge of the isotopic composition of a species is paramount in gleaning information about sources and sink processes [Brenninkmeijer et al., 2003]. Isotope fractionation in atmospheric gases can give detailed information about subtle yet quantifiable differences between molecules and therefore enhance knowledge of atmospheric budgets.

Gases, including halocarbons, often display particular isotopic characteristics, allowing identification and association with a specific source [Goldstein and Shaw, 2003, Miller et al., 2001]. Isotope effects during sink reactions also allow for variations in the isotope composition of gases including CH_3Cl. Sources and sinks are generally measured with respect to enrichment in the heavier isotope. Typically the lighter isotope reacts preferentially to the heavier isotope meaning the heavier isotope occurs more frequently in the phase in which it is more strongly bound or it remains unreacted. The products therefore are usually observed to be isotopically lighter compared to the original reactants. This opposes the view in which chemical behaviour of two isotope-containing compounds remains identical since their electron configuration is unchanged.

1.4.1 Abundances of stable isotopes in trace gases

Techniques for identifying sources of trace gases and calculation of source size has traditionally been via the use of concentration gradients [Cincinelli et al., 2012]. Although these calculations have provided reasonable indications towards areas of high concentration and therefore source

apportion, they are susceptible to confusion when sources are multiple, or when complex biological or physical pathways alter the original composition. The use of stable isotope analysis allows the dominant source to be identified, immediately distinguishing between anthropogenic and natural sources. Importantly, it is also possible to identify transformation reactions, whether physical or chemical processes [Schmidt et al., 2004].

Different isotopes of an element can exist due to a greater or lesser number of neutrons within the nucleus of a given atom. For example, the nucleus in a carbon atom in its most common form contains 6 protons, and 6 neutrons. This carbon atom is named carbon-12, or ^{12}C, after the atomic mass number. A less common form of carbon is carbon-13 (^{13}C), accounting for approximately 1 % of all carbon atoms, which contains 6 protons and 7 neutrons, increasing the mass number to 13. In both cases the number of electrons remains at 6. The natural abundances of stable isotopes of species of interest in this thesis are given in Table 1.2.

Table 1.2: Abundances of stable isotopes of species of interest in this chapter.

Isotope	Relative Abundance (%)
^{12}C	98.93
^{13}C	1.07
^{35}Cl	75.78
^{37}Cl	24.22
^{14}N	99.63
^{15}N	0.37
^{16}O	99.76
^{17}O	0.04
^{18}O	0.21

1.4.2 Isotope effects – kinetic and thermodynamic

A chemical reaction can be associated with an isotope effect. This causes a change in isotopic abundance of the species involved in the reaction and isotopic fractionation between reactants and products results. Isotopic fractionation can be caused by two different isotope effects: kinetic and thermodynamic isotope effects. Kinetic isotope effects occur through unidirectional

processes, whereas thermodynamic isotope effects are associated with reactions which are thermodynamically reversible.

1.4.3 Kinetic isotope effects

The first and most significant type of isotope effect is the kinetic (or primary) isotope effect. This effect occurs at the rate determining step of the reaction where a bond to an isotope in question is broken or formed. Pairs of molecules in which each contains a different isotope of a given atom, referred to as isotopologues, are found to have different rate constants for the rate determining step. Kinetic fractionations occur due to these differences in reaction rates of isotopologues in irreversible physical, chemical, or biological processes.

The vibrational energy of a bond E_{vib} is governed by the inertia (I), and the angular velocity (ω) and can be expressed as such:

$$\mathrm{E}_{vib} = \frac{1}{2}\mathrm{I}\omega^2 \qquad \text{Equation 1.24}$$

The dependence of bond energy on inertia is paramount to the relationship between bond energy and atomic mass, shown by the equation:

$$\mathrm{I} = mr^2 \qquad \text{Equation 1.25}$$

Where m is a point mass rotating around an axis, (r). When related to a molecular system, two masses will therefore move around a bond 'axis'. When referring to either two different atoms, or two isotopes in a bond, it is necessary to substitute the mass term, m, with the reduced mass μ to give:

$$\mu = \frac{m_1 m_2}{m_1 + m_2} \qquad \text{Equation 1.26}$$

In a system containing a heavier isotope, the value of reduced mass (μm) is increased and so subsequently increases inertia. Furthermore, an increase in inertia increases the vibrational energy of the bond involved. The resultant bond energy for a bond containing a heavy isotope is therefore larger than that of a bond containing a light isotope, resulting in isotope fractionation between the two isotopologues.

1.4.4 Zero point energy

Zero point energy (ZPE) is the lowest amount of energy that a quantum mechanical system may possess at 0 K, also described as the energy of the ground state. Assuming 0 K, this vibrational

energy (ϵ) is quantified as half of a quantum for each vibrational modes in each bond present [Atkins and de Paula., 2010], derived from the equation:

$$\epsilon_{\mathrm{ZPE}} = \frac{\mathrm{h}\nu}{2} + \frac{\mathrm{h}\nu}{e^{\frac{\mathrm{h}\nu}{\mathrm{kT}}} - 1}$$ Equation 1.27

Where h is Planck's constant, ν is the vibrational frequency, k is the Boltzmann constant and T is the temperature in Kelvin.

The significance of ZPE with respect to isotope effects can be drawn from this mathematical derivation of ZPE. ZPE theory states that all bonds have a characteristic vibrational frequency. This frequency is directly proportional to the mass of the atoms of that bond. A change in isotopic composition of a molecule will therefore affect the vibrational energy levels. A difference in zero point energy of a chemical bond results in a difference in bond strength. The activation energy E_a of reactions involving the heavier isotopologues is increased relative to the isotopically lighter compound. Subsequently, the ZPE of a chemical bond containing a heavy isotope compared to a bond containing a light isotope is reflected in bond cleavage rates. This means that bonds containing a heavy isotope are stronger, and therefore cleavage rates are slow compared to those containing a lighter isotope of the same atom. This theory can be used to explain the occurrence of isotopically lighter products formed during reactions where bond cleavage arises, relative to the initial reactants. Using the ZPE it is possible to predict the fractionation of isotopologues, as demonstrated by Miller and Yung (2000).

1.4.5 Thermodynamic isotope effects

The second isotope effect, the thermodynamic (or equilibrium) isotope effect, gives differences in isotopic composition during processes such as boiling and melting. Just as kinetic isotope effects, these processes are reliant on strength of bonds and reduced mass, and therefore vibrational energy levels. However, no chemical bonds are broken or formed. Thermodynamic isotope effects are more complicated as thermodynamic equilibrium is never achieved in atmospheric chemistry. Reactions at particle interfaces can be governed by equilibrium isotope effects, as can reactions in liquid particle solutions. Molecules are undergoing constant mixing and transport in addition to chemical reactions and photolysis.

1.4.6 Notation

Isotopic enrichment describes the increase in abundance of a specific isotope compared to a mixture of isotopes of a chosen element. Absolute isotope ratios are difficult and time consuming to determine, and involve calibration of mass spectrometers using pure isotopes

(Aregbe et al., 1998). For simplicity, the difference in isotopic abundance relative to a standard is used, which allows comparison between results from different laboratories. To express minute variations in atmospheric abundance of the ratio of two isotopes compared to a common standard, δ notation is used, and given in units of per mil (‰), equal to one part per thousand.

$$\delta_s = \left(\frac{R_S - R_{STD}}{R_{STD}}\right) \quad \text{Equation 1.28}$$

Where R_S is the isotope ratio of the sample, and R_{STD} the isotope ratio of the standard. For chlorine isotopes in CFCs, R_{STD} is taken from samples of tropospheric air (Laube et al., 2010) or Standard Mean Ocean Chloride (SMOC). Stable isotope ratios of chlorine therefore are expressed as:

$$\delta^{37}{}_{Sample} = \left(\frac{R_{Sample} - R_{SMOC}}{R_{SMOC}}\right) \quad \text{Equation 1.29}$$

Additionally, an enrichment factor, ε used to show enrichment of a heavy isotope with respect to the light isotope:

$$\varepsilon = \alpha - 1 \quad \text{Equation 1.30}$$

Where α represents the fractionation factor of the rate constants for the heavy, k_H, and light, k_L isotopologues:

$$\alpha = \frac{k_H}{k_L} \quad \text{Equation 1.31}$$

1.4.7 Rayleigh fractionation

Rayleigh fractionation is an exponential relationship which describes the fractionation pattern of species between two reservoirs as one reservoir decreases in size.

Rayleigh fractionation in an open system

In an open system containing two or more isotopic species where a material is constantly removed, it is important to understand how fractionation occurs over the course of a reaction, for example the $\delta(^{16}O)/\delta(^{18}O)$ system related to this thesis. It is a condition of the Rayleigh equation that the fractionation factor, α, of the removal process remains constant over time. Throughout the reaction pathway, the isotopic composition can be described by:

$$\frac{R}{R_0} = \frac{x_{(16O)}}{x_{(18O)}}^{\varepsilon} \quad \text{Equation 1.32}$$

Where R is the δ(^{16}O)/δ(^{18}O) isotope ratio in the reactant, R_0 is the initial ratio, $x_{(16\mathrm{O})}$ is the concentration of the lighter species ^{16}O, and $x_{(18\mathrm{O})}$ is the initial concentration.

Since the concentration of the most abundant isotope will always be considerably larger than the least abundant isotope, for example, [^{16}O] ≫ [^{18}O], it can be assumed that the concentration of the most abundant isotope, in this instance [^{16}O], is equal to the amount of original material in the phase. Since the fraction of material remaining, f is equal to $\frac{x_l}{x_{l^0}}$, (where x_l and x_{l^0} are the mixing ratios of the light species remaining, and the mixing ratio of the light species at time zero respectively) it follows that the fraction of material remaining in the initial phase is proportional to the initial ratio of isotopes and the amount of material remaining in the phase:

$$\mathrm{R} = \mathrm{R}_0 f^{\varepsilon} \qquad \text{Equation 1.33}$$

Conversion to δ notation shows:

$$\delta = (1 + \delta_0) f^{\varepsilon} - 1 \qquad \text{Equation 1.34}$$

This demonstrates the relationship between the fraction of material remaining in the initial phase (δ_0) with relation to the proportion of material which has been fractionated.

Rayleigh fractionation in a closed system

Rayleigh fractionation is generally used to describe the change in isotopic composition of a reservoir as material is constantly removed. However, it is possible to maintain equilibrium in a system which sees species moving not out of the system entirely, but from one reservoir to another. This type of system may be better described as two phase equilibrium. To illustrate, equilibrium is maintained between vapour and droplets in a cloud where isotopes continuously move between the liquid and gas phase reservoirs, yet there is no overall loss of isotopes from the system. Since the system is closed, and no mass is lost, the overall isotope ratio with the system remains constant, yet fractionation may occur between phases.

It is necessary to distinguish between Rayleigh fractionation within an open or closed system since there is large variability seen between both examples. In an open system, a product formed and removed immediately gives rise to a product with a definite and unchanging isotope ratio. For example, a reaction mixture may form an isotopically light gaseous product. Over time, the remaining mixture will display an isotopic signature which becomes increasingly rich in the heavy isotope. In the case of a closed system, for example, the equilibrium between liquid and gaseous form may result in the favourable production of isotopically light species in the gaseous form.

Moreover, Rayleigh fractionation processes create much larger isotope ratio variation in open systems.

1.4.8 Apparent isotope fractionation

It is known that, through Rayleigh fractionation, the isotopic composition of a species changes over time. In the case of CFCs, since the introduction of the Montreal Protocol means essentially no new sources exist, over time an enrichment of heavy isotopes is seen in gases destroyed in the stratosphere (Laube et al., 2010, Rahn and Wahlen, 1997, Röckmann et al., 2001b, Brenninkmeijer et al., 2003, Bernard et al., 2006, Blake et al., 2003, Morgan et al., 2004). These fractionation patterns can give information regarding the transport and reaction pathways related to these gases. It has been seen that the isotopic composition of a species changes with altitude, as demonstrated, for example, by Laube et al. (2010). It was suggested that stratospheric $\delta(^{37}Cl)$ increases with altitude due to faster decomposition of $CF_2{}^{35}Cl_2$ relative to $CF_2{}^{37}Cl^{35}Cl$ and $CF_2{}^{37}Cl_2$ by photolysis and by reaction with $O(^1D)$. The suggestion that photolysis is responsible for this enrichment with altitude was investigated further by Zuiderweg et al. (2012). The authors carried out photolysis experiments on a mixture of CFC-11 and CFC-12, and subsequently analysed the carbon isotope composition at various time intervals at photolytically relevant wavelengths. The apparent isotope fractionation in this study, the increase in enrichment with altitude, was much larger than expected. In comparison to that observed in chlorine isotopes by Laube et al. (2010) and $^{18}O/^{16}O$ and $^{15}N/^{14}N$ fractionation observed in N_2O (Bernard et al., 2006) it was again larger. It was suggested however that the increased fractionation could be attributed to moisture condensation on the reactor or variations in lamp intensity, as well as the fact that the lamp spectrum did not match the solar actinic flux at altitudes where CFC photolysis occurs.

1.5 Applications of isotope analysis on budgets of trace gases

The use of isotope ratio measurements has seen developments in budget determinations, including the distinction of natural and anthropogenic sources. Isotope ratio measurements are of use in the quantification of sources and sink processes, where the magnitude of fractionation detected corresponds to a distinct process.

Isotope measurements are most commonly concerned with compounds containing carbon, nitrogen, oxygen and sulfur. The use of Isotope Ratio Mass Spectrometry (IRMS) allows for analysis of isotope ratios of these elements when in the form of gases such as H_2, CO_2, CO, N_2, N_2O, O_2 and SO_2 [Kaiser and Röckmann, 2008].

An example of the use of isotope ratio analysis is the study of atmospheric methane, a strongly radiatively forcing gas produced naturally and anthropogenically. In addition to identifying methane sources, transport processes are so far poorly quantified. Constraining the atmospheric methane budget has seen the use of isotopic composition, giving rise to the distinction between methane emitted from natural and anthropogenic sources (Stevens and Engelkemeir, 1988). Stable isotope analysis is useful in resolving the variety of processes involved in the production of methane, importantly from rice paddy sources.

In the context of this work, 5 main species are relevant in terms of the influence of changing atmospheric composition by greenhouse gases and by the effect of ozone depleting substances in the stratosphere. Chapter 2 details new findings for the three most abundant CFCs: $CFCl_3$ (CFC-11), CF_2Cl_2 (CFC-12), $Cl_2FC\text{-}CClF_2$ (CFC-113). Chapter 3 describes new research on the photolysis rates of these species. In terms of global warming potential, much is already understood regarding the sources, sinks and chemical pathways of the two most anthropogenically enhanced gases, CO_2 and CH_4. The third most important greenhouse gas, nitrous oxide (N_2O), therefore is the focus of Chapters 4 and 5. Methyl chloride (CH_3Cl), a significant contributor to stratospheric ozone depletion is described in Chapter 6.

1.6 Mass spectrometric techniques

Section 1.6 provides general mass spectrometric techniques employed during this work, and describes firstly the use of gas chromatography used to separate target compounds from interfering compounds in a gas matrix. This technique can be coupled to either an Isotope Ratio Mass Spectrometer (IRMS) or a Mass Spectrometer (MS) for isotope analysis. Detection systems suitable for coupled use with gas chromatography are detailed. A brief overview of the principles of general mass spectrometry is given.

1.6.1 Gas chromatography

Gas Chromatography is a technique of analytical separation of volatile substances in the gas phase. The sample is either heated to cause it to be volatilised, or volatile gases or atmospheric trace gases introduced directly. The components in a sample are separated by distributing the sample between two phases: a stationary phase and a mobile phase. The stationary phase consists of either a solid adsorbent or a liquid held onto a support inside a column. The analytes are carried through the heated column by the mobile phase which is generally a chemically inert gas, to ensure no interaction with the analyte. Finally, the separated analytes exit the column and are detected by an in line detector.

A typical gas chromatograph consists of an injection port to introduce the sample, a column for separation of analytes, a carrier gas and flow controllers. This system is housed inside an oven to allow control of temperatures. The temperature control enables either (a) an isothermal environment to be maintained, or (b) an increase or decrease in column temperature over time firstly mobilise, then to improve separation of analytes from each other. The gas chromatograph is coupled to the detector system for quantification of analytes.

1.6.2 Analytical columns

The stationary phase of GC separation is comprised of one or more chromatography columns. These can be separated into two types; open tubular columns and packed columns.

Open tubular columns, or capillary columns, consist of either a thin layer of stationary phase coated on the inside of the column walls (wall coated open tubular), or a coating of adsorbent solid onto which the stationary phase is bound (support coated open tubular). Support coated open tubular (SCOT) columns can hold a much greater volume of stationary phase, however, wall coated open tubular (WCOT) columns in fact have greater column efficiencies. WCOT columns are generally made of fused silica to allow chemical etching and hence a rough surface to allow tighter bonding of the stationary phase to the column surface. The tubing is normally coated externally with polyimide to increase flexibility and strength. Stainless steel, aluminium, copper and plastic WCOT columns exist but bonding of stationary phase to the column is weaker. Typically capillary columns are 20-100 m in length and have internal diameters in the range 100-320 μm. Although capillary columns give a high resolution over a short period of time, overloading of capillary columns can cause peak distortions, and so limitations are placed on the quantity of sample which can be injected.

Packed columns are generally made up of glass or metal tubing packed with a solid support coated with a liquid stationary phase. These columns have only 50 % of the efficiency of WCOT columns due to the difficulty in packing the tubing uniformly. Issues regarding peak broadening also causes the efficiency of packed columns to be reduced. Packed columns are of larger diameter than tubular columns and have a limited range of length. Additionally, the packing can become deactivated over time due to adsorption of impurities.

To a large extent capillary columns have replaced packed columns, especially in the context of analysis of atmospheric gases with low atmospheric mole fraction. During this work, both PLOT columns and a molecular sieve packed column were used, as described in the relevant chapters 2 to 5.

1.6.3 The carrier gas

A carrier gas is used to move analytes along the column to allow interaction with the stationary phase. The type of gas used for this purpose varies dependent on application, but always must be chemically inert, as well as dry and oxygen free. Nitrogen, argon and hydrogen are used as carrier gases, but more commonly helium as it is compatible with many detectors and is safe to use.

The linear velocity of a gas through the system is an important factor when determining the most suitable carrier gas, and so it is necessary to balance this effect with the speed of separation. To this end, the flow rate of the carrier gas is meticulously controlled. The control of flow rate also ensures reproducibility of analyte elution times from the column. The carrier gas system generally contains methods for removing water and other contaminants, either by use of molecular sieves or by using traps.

Throughout this work helium is used as a carrier gas, for measurement of nitrous oxide, methyl chloride and CFCs.

1.6.4 Thermal control of the column

The use of an oven surrounding the chromatography column allows for regulation of temperature in an otherwise fluctuating laboratory temperature, as well as enhanced separation of co-eluting compounds. In some instances it is possible to separate all compounds of interest by holding the column temperature constant over the course of the analysis. This isothermal programme is successful if the range in boiling points of species in the sample is small. If a low isothermal column temperature is used with compounds which have a wide range in boiling points the analytes are well resolved but the chromatographic separation is slow and may cause extensive peak broadening. Conversely, if a higher isothermal temperature programme is applied then the higher boiling compounds will elute as sharp peaks but at the expense of the low boiling compounds which will be eluted so quickly that co-elution occurs.

In resolution of this issue the use of a ramped temperature programme allows cooler temperatures to separate low boiling compounds, as well as the elution of sharp peaks given by the higher boiling compounds. The column temperature can be increased at a constant rate, or in steps as the separation progresses, starting with low temperature analysis and increasing the temperature to resolve the less volatile high boiling compounds. This method is well suited for separation of mixtures of analytes with a broad range in boiling points.

1.6.5 Detection systems

In order to provide quantitative measurement of analytes in a mixture after gas chromatographic separation a detector is required. The detector exploits differences in properties of the analyte and carrier gas, as well as differences between analytes. These properties may be specific to each compound or maybe possessed by both analyte and carrier gas but to different degrees.

Any detector has two parts, which are used together to give a digital signal related to the eluted analyte. The first part of the detector is a sensor accommodated at the exit of the column, giving an analogue signal related to the analyte of interest. The second part is required to digitalise the analogue signal. The detector must have adequate sensitivity to provide a high resolution signal. The main types are detector are: Mass Spectrometer (MS), Flame Ionisation, Thermal Conductivity, Electron-Capture, Atomic Emission, Chemiluminescence and Photoionisation. Electron capture detectors and mass spectrometers are the most sensitive detectors especially with respect to electronegative species such as chlorinated hydrocarbons. Flame ionisation detectors are generally used for hydrocarbon analysis, but are limited by the fact that positive identification of the structure of a compound cannot be achieved. Identification is reliant on retention times, and hence is subject to interferences. Mass spectrometry, once coupled with gas chromatography, allows the combination of both positive identification of species, along with separation of interferences.

In this work, mass spectrometry was used, and is discussed further below. In comparison to the other detector types listed, mass spectrometry offers great flexibility for analysis of a wide range of compounds.

1.6.6 Mass spectrometry detectors

In a GC-MS system the sample exits the chromatography column and passes into the inlet of the mass spectrometer via an open split. The sample enters the ion source where it is ionised and fragmented. This commonly occurs by use of an electron-impact ion source, where energetic electrons bombard the sample causing molecules to lose electrons to become ionised. Further bombardment with energetic electrons causes fragmentation of these ions, although the role of the secondary fragmentation is small. Once ionised, the fragments pass onto a mass analyser, which sorts the fragments according to their mass to charge (m/z) ratio.

The detector output gives a mass spectrum representing the retention times of analytes in the original gas mixture. This allows quantitative determination of the unknown species.

Specifics regarding GC-MS techniques used for ultra-low detection limit measurement of carbon and chlorine isotopes in atmospheric CFC-11, CFC-12 and CFC-113 are described in Chapters Two and Three.

GC-IRMS techniques used to measure the oxygen isotope excess in stratospheric N_2O above the lowermost stratosphere are described in chapter 4. Currently such measurements exist only up to 12 km altitude (Cliff et al., 1999b). A technique developed for chlorine and carbon isotope measurements of methyl chloride in synthetic air mixes, to allow for future atmospheric analysis are described in chapters 4 and 5.

1.7 Research objectives

The use of isotope ratio measurements is essential to further understanding of source and sink processes in atmospheric species. The following section details the overarching research objectives of this thesis. The specific scientific outcomes expected are given in the relevant chapters 2 to 6.

To date, only a small number of measurements of $\delta(^{37}Cl)$ in CFCs in the tropospheric, stratospheric and from firn air currently exist. The aims of this thesis were firstly to use GC-MS techniques to increase the number of chlorine isotope ratio measurements in CFC-11, CFC-12 and CFC-113 at stratospheric altitudes. The altitude range of samples chosen was significantly larger than previously reported. With respect to carbon isotope ratio measurements in CFCs, no atmospheric measurements are currently published, only a small number of firn air analyses (Zuiderweg et al., 2013). The analysis of samples containing CFC-12 which had undergone photolysis within the laboratory by Zuiderweg et al. (2012) gave a useful indication of the expected apparent isotope fractionation. The current study aimed to present the first carbon isotope ratio measurements from these CFCs in stratospheric samples. Additionally, it was hoped that further measurement of the samples which had undergone photolysis may enhance understanding of rates of photolysis and apparent isotope fractionation in CFC-12.

Secondly, in order to improve understanding of the atmospheric budget of N_2O, the quantification of $\delta(^{17}O)$ and $\delta(^{18}O)$ are necessary. This study aimed to provide additional stratospheric measurements of $\delta(^{18}O)$ in N_2O as well as one of the first stratospheric $\delta(^{17}O)$ measurements. An analytical method was required to be developed to allow such analysis. The current study aimed to develop an analytic system capable of measuring $\delta(^{17}O)$ and $\delta(^{18}O)$ with adequate precision to form meaningful conclusions related to stratospheric sinks as well as in situ sources of N_2O.

Finally, for improved understanding of the methyl chloride budget, measurement of chlorine isotopes in this species is yet to be achieved. To date, no analytic method exists to measure this in atmospheric samples, and to this end, this work aimed to develop an analytic system capable of measuring samples of atmospheric origin. The analytical system was hoped to have the capability to measure chlorine isotopes in samples with both mole fractions and sample matrices which were atmospherically relevant.

Chapter 2: High sensitivity isotope ratio measurements of CFC-11, CFC-12 and CFC-113 in the stratosphere

CFC-11 ($CFCl_3$), CFC-12 (CF_2Cl_2) and CFC-113 ($Cl_2FC\text{-}CClF_2$) are the most abundant halocarbons of anthropogenic origin in the atmosphere (Montzka et al., 2011). Multiple industrial sources of CFC-11, CFC-12 and CFC-113 occur at the Earth's surface (Carpenter et al., 2014), yet sink processes are limited to reaction with $O(^1D)$ (3 to 7 % for CFC-12) and photolysis in the stratosphere (93 to 97 % for CFC-12). It is only at stratospheric altitudes that there is the abundant UV-C radiation to break the C-Cl bond. The photolysis reaction of CFCs produces the chlorine radical, to initiate the catalytic decomposition of ozone. Background information regarding the effect of CFCs on ozone depletion can be found in Section 1.3. Additionally, CFC-11, CFC-12 and CFC-113 have a significant global warming potential, also described further in Section 1.3.

Atmospheric mixing ratios of CFCs are well documented, and the processes which contribute to production and destruction are well understood. However, these sources, to the atmosphere, which originate from the chemical industry, although are well understood, are not well quantified, in particular those sources which are illegal or unregulated. The use of isotope ratios to aid budget calculations is explained in Section 1.4. To date there are limited studies related to isotope measurements of the three most abundant CFCs in the atmosphere: CFC-11, CFC-12 and CFC-113. The studies have mostly described isotope fractionation in tropospheric air masses, and firn air measurements, but the amount and breadth of data is limited. Stratospheric measurements are extremely limited as discussed below. Additional isotopic characterisation of these species in the stratosphere may allow for better characterisation and quantification of sink reactions, since the isotopic composition of a species displays a 'fingerprint' related to source and sink processes (Brenninkmeijer et al., 2003). The isotopic composition relates directly to the source and sink processes, and so isotopic characterisation gives information about the magnitude of such processes. Since the species are all ozone depleting, a better understanding

of sink processes, and creation of halogen radicals, may lead to better understanding of their lifetimes and therefore ozone recovery predictions.

Many processes affect the abundance and fractionation patterns of species in the atmosphere. These processes are those related to atmospheric circulation patterns. For those species by which photolysis and reaction with $O(^1D)$ are the main sink processes, as is the case with the species of interest in this thesis, it can be assumed that after production, all fractionation occurs in the stratosphere. However, it is not simply the case that air moves upwards at the tropics and towards the poles, and hence isotope fractionation is not simply proportional to altitude or latitude. As tropospheric air masses enter the stratosphere,they do indeed ascend, but are subject to mixing, at the lowermost stratosphere troposphere-stratosphere exchange will increase the amount of non-depleted species in air directly from the troposphere, as well as mixing from regions of enhanced depletion. The mean age of air, in fact is an average of the distribution of transit times of these air parcels. As the air moves polewards, the average age of air increases, and additionally the distribution of these transit times widens. The age of this average distribution therefore in turn affects the fractionation patterns seen in species of interest.

It is expected that species with photolysis as the major sink will decompose fastest in the tropical stratosphere where the actinic flux is the greatest (Laube et al., 2013). In these samples it would follow that the as this air continues to be depleted, and moves polewards, the degree of enrichment will simply become more pronounced. However, the movement of air to different latitudes exposes it to transport barriers, again affecting the abundance and measured fractionation. The tropics are isolated from mid latitudes, as well as the polar vortex, which as well as being isolated, sucks air down from the mesosphere. The age spectra of an air parcel is therefore affected. The presence of air with a concentration of zero of a species, which then mixes with the depleted air, in fact then changes the fractionation pattern. This effect was seen by Kaiser et al. (2006) via analysis of samples of N_2O in stratospheric air. In general the apparent isotope fractionation increased consistently with altitude and decreased from equator to North Pole. However, any deviations from Rayleigh fractionation patterns were explained by mixing with air from the polar vortex, containing almost nil N_2O. This could be further explained by weak mixing between intravortex and extravortex air (Plumb et al., 2000). The overall effect of mixing with air with extremely low quantities of a species of interest is a dampening effect on the observed isotope fractionation at higher latitudes.

This chapter aims to further characterise CFC-11, CFC-12 and CFC-113 with respect to ^{37}Cl isotope ratios in stratospheric samples at both mid and high-latitudes. Secondly, the first ^{13}C measurements of all three species in stratospheric air are presented.

Chapter 3 details measurement of ^{13}C and ^{37}Cl in these halocarbons in samples which had undergone photolysis, as a model of stratospheric processes. This allowed calculation of photolysis rates and quantification of the respective isotope effects from photolysis, and enabled measurements from stratospheric samples to be linked to an international ^{13}C scale.

2.1 Chlorine isotope composition in halocarbons CFC-11, CFC-12 and CFC-113 in stratospheric air

To date, the chlorine isotopic composition of only a few stratospheric gases has been investigated. For gases which are destroyed in the stratosphere, enrichment of heavier isotopologues is seen, generally displaying a profile of increasing enrichment with altitude. The degree of such isotope effects are often characteristic of specific reactions which contribute to the destruction of these compounds. This can aid improvement of our understanding of reaction pathways and transport of gases in the stratosphere.

CFC-12

The inherent fractionation in the photolysis of CFC-12 was demonstrated via the stable chlorine isotope (^{37}Cl) gradient with altitude of stratospheric balloon samples (Laube et al., 2010). Air samples were collected in 2005 and 2008 on board balloons flying in the tropical stratosphere. The data demonstrate the well-established decrease in mixing ratio with altitude. Analysis of samples from 14-34 km showed a progressing increase in $\delta(^{37}Cl)$ by up to 27 ‰ relative to tropospheric air. This is almost double the previously reported range of $\delta(^{37}Cl)$ in naturally occurring samples (Laube et al., 2010). This increase in $\delta(^{37}Cl)$ values with stratospheric altitude is likely due to the faster decomposition of $CF_2{}^{35}Cl_2$ relative to $CF_2{}^{37}Cl{}^{35}Cl$ and $CF_2{}^{37}Cl_2$ by photolysis and by reaction with $O(^1D)$. Stratospheric sink processes are limited to photolysis and reaction with $O(^1D)$, both of which are irreversible, and have constant magnitude of isotope fractionation. If these sink processes were the sole contributors to isotope fractionation in CFC-12, then the $\delta(^{37}Cl)$ values should follow a Rayleigh-type fractionation. This can therefore be expressed by the linear relationship given by Equation 2.1, where y_{sample}/y_{entry} is the ratio of stratospheric to tropospheric mixing ratios and ε_{App} is the apparent isotopic fractionation in the stratosphere:

$$\ln[1 + \delta(^{37}Cl)] \approx \varepsilon_{App} \ln(y_{sample}/y_{entry}) \quad \text{Equation 2.1}$$

Laube et al. found a correlation with ε_{App} = –12.1‰ ± 1.7‰. Due to the slow stratospheric transport and mixing, the apparent isotope fractionation observed in the stratosphere is expected to be lower than that caused by the decomposition reactions (Bernard et al., 2006). As described above, this lower than expected apparent isotope fractionation can be explained by the dampening effect due to mixing with air containing almost nil CFC-12.

Allin et al. (2015) provided additional $\delta(^{37}Cl)$ measurements in both tropospheric and stratospheric air using air archives to obtain a long-term record of chlorine isotope ratios in CFCs. The apparent isotope fractionation (ε_{app}) for mid- and high-latitude stratospheric samples are respectively −12.2±1.6 and −6.8±0.8 ‰ for CFC-12. This is in good agreement with the value of ε_{App} calculated by Laube et al. (2010). Allin et al. assumed a constant isotope composition of emissions and calculated the expected trends in the tropospheric isotope signature of these gases based on their stratospheric ^{37}Cl enrichment and stratosphere–troposphere exchange. These were compared to the long-term $\delta(^{37}Cl)$ trends using background tropospheric samples from the Cape Grim air archive (Tasmania, 1978–2010) and tropospheric firn air samples from Antarctica (Figure 2.1). When polar ice deposits are formed through the gradual build up and then compression of snow, air is incorporated into the ice, giving a record of atmospheric composition hundreds of thousands of years into the past. The uppermost layer, up to a maximum of 100 m is termed ‘firn’, and gives samples of air from the last 50-100 years (Martinerie et al., 2009, Buizert et al., 2012).

It can be seen that CFC-12 displays the strongest modelled enrichment over time compared to CFC-11 and CFC-113. The value of CFC-12 $\delta(^{37}Cl)$ is predicted to have increased 3 ‰, with maximum rates of increase since 1990 corresponding to the sharp reduction of emissions after the introduction of the Montreal Protocol. Since CFC-12 has the longest lifetime (102 years) of these species, 102 years, it follows that the rate of breakdown by photolysis is the slowest. A slow rate of destruction allows a longer time for fractionation to take place and so the remaining CFC-12 displays enrichment. It is assumed that the sources are negligible and so no addition of source material to the stratosphere reduces the amount of fractionation seen.

From 1970 to the present day, projected trends were in good agreement with tropospheric measurements, suggesting a constant emission isotope delta (δ), yet uncertainties within the analysis were high in comparison to expected changes.

CFC-11

Comprehensive analysis of ^{37}Cl in CFC-11 in tropospheric air (both air collected at Cape Grim, Tasmania, and firn air samples), as well as aircraft stratospheric samples from mid- and high-latitude sites was carried out by Allin et al. (2015). The stratospheric samples ranged from 9 to 20 km, but again, no samples represented air masses deep into the stratosphere.

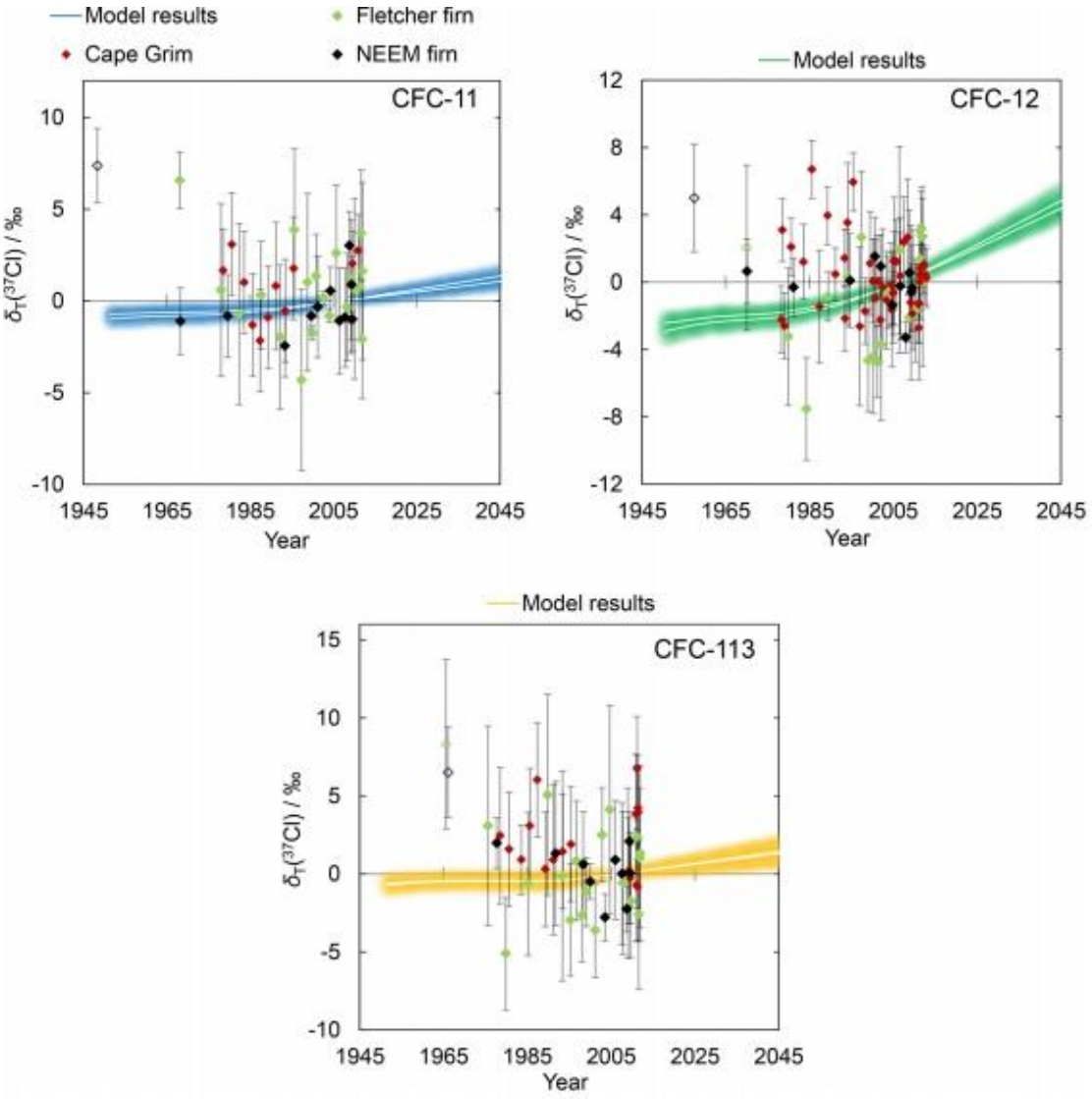

Figure 2.1: Tropospheric δ(^{37}Cl) measurements for CFC-11, CFC-12 and CFC-113, compared to model predictions. Taken from Allin (2015).

The apparent isotope fractionation (ε_{App}) for mid- and high-latitude stratospheric samples are respectively −2.4±0.5 ‰ and −2.3±0.4 ‰. Again, the expected trends in the tropospheric isotope signature of these gases based on their stratospheric ^{37}Cl enrichment and stratosphere–troposphere exchange were compared to the long-term δ(^{37}Cl) trends to background tropospheric samples (Figure 2.1). It can be see that the predicted enrichment of CFC-11 is less

significant than that of CFC-12, and displays a similar profile of CFC-113, both with a predicted $\delta(^{37}Cl)$ enrichment of 1 ‰. This is expected due to the shorter lifetimes of CFC-11 and CFC-113 respectively (52 and 85 years), compared to the lifetime of CFC-12 at 102 years. These shorter lifetimes means less time for fractionation to occur and the enrichment displayed is less. A constant average emission delta (δ) is suggested.

CFC-113

Finally, measurement of ^{37}Cl in CFC-113 has been carried out by Allin et al. (2015) in the troposphere and stratosphere. The apparent isotope fractionation (ε_{App}) for mid- and high-latitude stratospheric samples are respectively −3.5±1.5 and −3.3±1.2 ‰ for CFC-113. With respect to tropospheric air, there was good agreement between tropospheric free air (Cape Grim, Tasmania), and firn air measurements (Figure 2.1), and in line with what is expected for these well mixed gases. Observations made by Allin (2015) are consistent with an isotopically stable source signature. However, the high measurement uncertainty does not rule out the possibility that it has changed over time.

2.1.1 Research objectives

A small number of measurements of ^{37}Cl in CFCs in the tropospheric, stratospheric and from firn air currently exist. A profile of increasing enrichment in $\delta(^{37}Cl)$ with altitude has been seen, however it is not known as to whether this is representative of one sampling campaign or more widespread. Additionally, the current measurements do not reach deep into the stratosphere. The use of samples from both low and mid-latitudes gives a wider range of latitudes to provide further evidence for the observed lower apparent isotope fractionation at different latitudes. The degree of isotope effects is characteristic of destruction processes, and so this study will increase our understanding of reaction pathways and atmospheric transport. Increasing the number and altitude range of chlorine isotope ratio measurements in CFC-11, CFC-12 and CFC-113 at stratospheric altitudes will allow better understanding of the following questions:

1. Do these CFCs follow the expected profile of increasing enrichment at even higher altitudes than previously measured?
2. Do the data display Rayleigh type fractionation as expected? Any deviation from this will be apparent, and give more evidence for the dampening effect of observed isotope fractionation.

3. In comparison of ε_{App} of these measurements to existing tropospheric and firn air data by Laube et al., (2010) and Allin et al., (2015), do the data give further evidence for, or dispute, the proposed stable source signature.

2.1.2 Experimental methods

The use of GC-MS for isotope ratio analysis allows for high sensitivity measurements and therefore analysis of gases at low abundances. In this work, measurements of CFC-11, CFC-12 and CFC-113 were performed using an in-line cryogenic pre-concentration system, and an Agilent 6890 GC coupled with a VG Waters EBE Tri-Sector Mass Spectrometer 'Autospec'. This system is capable of high precision measurements at extremely low abundances, for example measurement of HCFC-133a in archived air samples at abundances of 0.02 pmol mol^{-1} by Carpenter et al. (2014). Previous analyses using the Autospec are described in Allin (2015) and Laube et al. (2010).

2.1.2.1 Sample collection

Samples were collected from two campaigns, one in December 2011 from Kiruna, Sweden, by the Institute of Marine and Atmospheric Science (IMAU), University of Utrecht and one in spring 1999 above Gap, France as summarised in Table 2.1.

Samples from Kiruna, Sweden

Stratospheric samples were collected using whole air samplers based on board the M55 Geophysica high altitude aircraft. Details of the sampling systems can be found in Bernard et al. (2006). A total of two flights departed from Kiruna, Sweden, on the 11th and 16th of December 2011 (9–19 km, 62–72◦ N, 2◦ W–24◦ E, ESSENCE campaign). A total of 39 samples were available for analysis in this study.

Samples from Gap, France

Upper tropospheric and stratospheric balloon air samples from 8.3 km to 34.4 km were collected at a mid-latitude site (Gap, France, 44.4°N) on the 22nd June 1995, using a cryogenic whole air sampler. Further details can be found in (Bernard et al., 2006). Of the 14 whole air samples collected at this site, 10 had sufficient CFC mixing ratios in the sample to give reasonable measurement precision for isotopic measurements during analysis.

Table 2.1 Summary of stratospheric sample campaigns used in this study.

Sample Site	Sampling Date	Altitude	No. of Samples
Kiruna,Sweden, 67.9-72°N	Dec 2011	9-19 km	39
Gap, France, 44.4°N	Mar-Apr 1999	13-34 km	10

2.1.2.2 Inlet system for use with the VG Waters EBE Tri-Sector mass spectrometer

Figure 2.2 shows a systematic schematic diagram of the inlet system. Before samples were introduced the inlet system was evacuated via a pump. Whole air samples were contained within Silco treated stainless steel canisters which were connected in turn using Swagelok ® stainless steel fittings to the inlet system. Approximately 32 -80 Torr (215 – 537.5 mL) of sample was passed through the system: the use of a reference volume with an attached Baratron pressure sensor (MKS, Range 0-100 Torr) giving the precise volume introduced. Gas samples passed through a glass tube containing magnesium perchlorate ($Mg(ClO_4)_2$) to remove water, before the condensable trace gases were trapped cryogenically (dry ice/ethanol mixture, -78 °C) in a stainless steel preconcentration loop (1/16th inch outside diameter), packed with HayeSep D (80/100 mesh). Once sufficient sample was trapped, the dry/ice ethanol mixture was removed and immediately replaced with hot water (approximately 95 °C) and a flow of helium (research grade, 2 mL min^{-1}) transferred the trapped gases towards the GC oven. Two different columns were used during the analysis period, a GS-GasPro porous layer open tubular column (length 30 m, i.d. 0.32 mm) and an AlPlot column (KCl-passivated, 50 m, i.d. 0.32 mm). The GC oven was cooled to -10 °C and held for 2 minutes after sample injection from the loop. After this time period, a temperature ramp was applied at 10 °C per minute up to a maximum point of 200 °C.

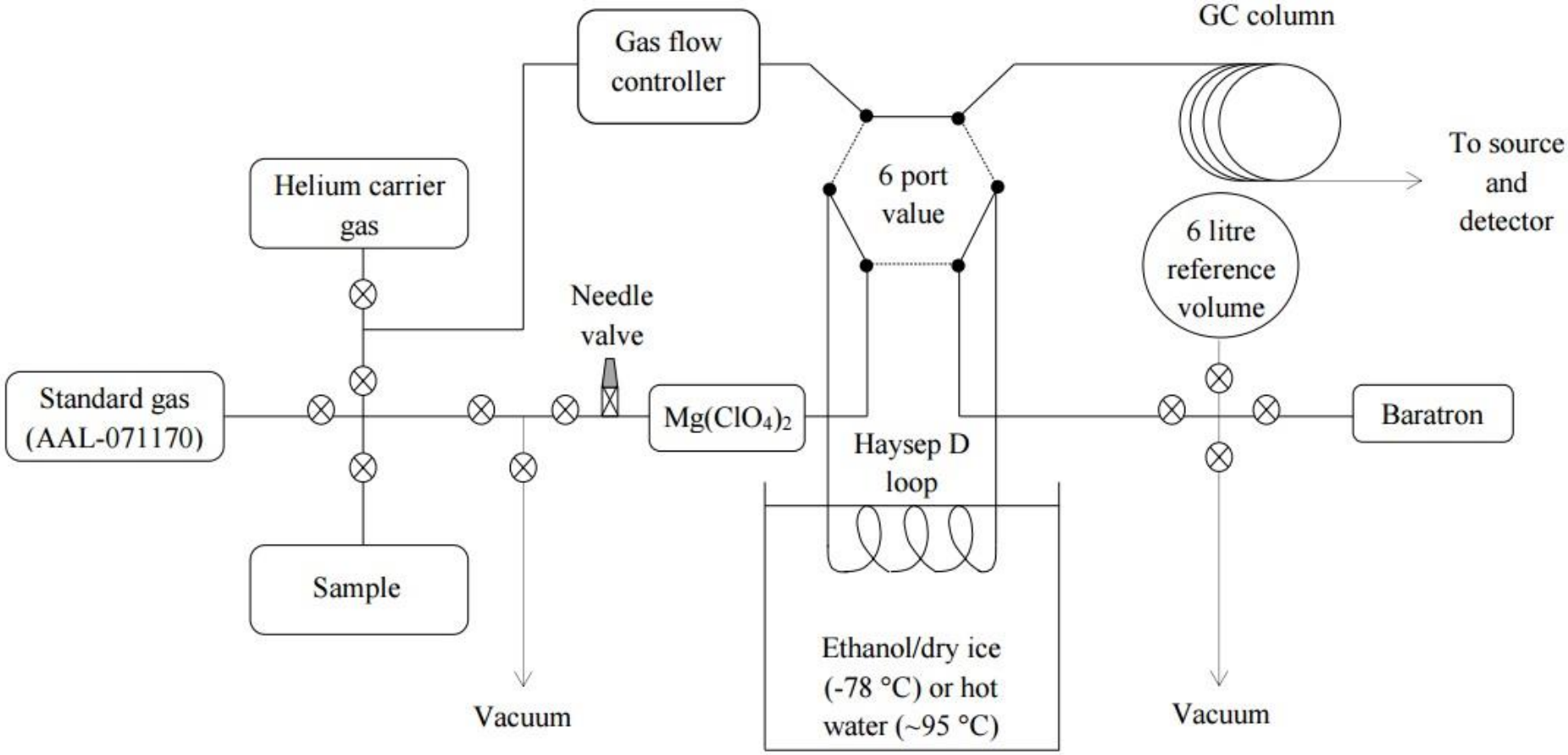

Figure 2.2 Schematic Diagram of the manual inlet set up for the GC-MS system. A cross contained within a circle represents a valve. Diagram taken from Allin (2015)

2.1.2.3 VG Waters EBE Tri-Sector mass spectrometer

Compounds eluted from the chromatography column pass to the ionisation source and are subsequently ionised and fragmented after bombardment with electrons from a heated filament as described in the above section. The Autospec instrument is of tri-sector spectrometer type, and so ions pass through an electric sector, to a magnetic sector then into a second electric sector. The magnetic sector deflects the ions towards the detector according to their mass to charge ratios. The use of a secondary electric sector improves instrument sensitivity through de-magnifying optics. Vacuum is achieved inside the flight path by scroll and diffusion pumps, preventing interaction of the sample ions with contaminants from outside air. To reduce background noise, and so improving sensitivity, metastable ions are removed in the electric sector, as well as the use of an off-axis detector. The off-axis detector prevents neutral ions reaching the detector. Once positive sample ions reach the detector, a dual conversion dynode configuration releases electrons, which then cause a phosphor screen to emit photons. In order to achieve an electronically detectable signal, a photomultiplier tube is used.

2.1.2.4 VG Waters EBE Tri-Sector mass spectrometer set up parameters

The Autospec was operated in Electron Impact-Selected Ion Recording (EI-SIR) mode. In order to control the instrument set up and analysis of samples, Waters ® provided the software package 'MassLynx'. This software works as an interface between the user and the instrument, all mass spectrometric parameters and data output are controlled via MassLynx.

To run an air sample which contains a large number of species, and therefore a number of fragment ions with differing mass-to-charge ratios, it is necessary to have a sequence of functions, moving from one analyte to the next. The MassLynx software allows for the setup of a number of 'functions' in which the mass-to-charge ratios for detection are programmed. Measurement of multiple isotopologues is possible as several fragments originating from a single parent molecule can be measured within each function. These fragment ions have unique mass-to-charge ratios which correspond to the isotope composition of the parent molecule. These functions are based on the elution times of the analytes from the chromatography column, the retention time given from the time at which the sample was injected onto the column. The mass-to-charge ratios included on each function correspond to the known ionisation products of each species of interest. Each species is generally fragmented into a wide range of ionisation products and so several fragments originating from the same species can be measured in a single function. This allows for analysis of multiple isotopologues of a species. Given the wide range of ionisation products which were able to be measured the peaks which

had the largest peak area and the least interferences from co-eluting species were generally included in the functions. It was necessary to ensure that the peak area was large enough for detection, but not so large that the detector became saturated.

Within each function, a mass related to an ionisation product of the reference gas hexadecane was measured to maintain the relatively high mass resolution of ~1000 at 5 % peak height. The hexadecane was contained within a glass vessel and attached to a stainless steel tube, the position of which allows more or less gas to be continuously introduced into the ion source. To tune the instrument, the ion repeller and a series of focussing lenses were adjusted whilst observing the hexadecane peak, to give a largest possible symmetrical peak whilst maintaining a mass resolution of ~1000 at 5 % peak height.

To optimise the instrument performance, MassLynx was used daily to tune and mass calibrate. Tuning and mass calibration was carried out using the standard reference gas, hexadecane. Given that this gas has a large number of ion fragments when ionised, there were therefore sufficient 'lock masses' for use with a large range of species including CFCs. The justification for use of a lock mass is to allow the *m/z* ratio of the targeted fragments to be detected accurately. This is possible as the resulting hexadecane ion fragments are chosen to be close in mass-to-charge ratio to those of a sample. Each time the accelerating voltage jumps between masses of fragment ions of one species, the instrument will in each cycle already include the lock mass. This ensures that ion fragment masses which have masses close to that of the hexadecane fragments are reliably detected.

2.1.2.5 Calculation of isotope ratios $(\boldsymbol{R})$

As described in Chapter 1, the isotope delta (δ) is used to denote the $^{37}Cl/^{35}Cl$ ratio difference in CFCs in an air sample relative to a standard:

$$\delta(37Cl) = \frac{R_{Sample}}{R_{Standard}} - 1 \qquad \text{Equation 2.2}$$

where R represents the $^{37}Cl/^{35}Cl$ ratio of abundance in a sample or a standard. Delta values are expressed in per mill (‰).

Currently an internationally recognised chlorine isotope standard exists, Standard Mean Ocean Chloride (SMOC), but no gaseous standard of known isotopic composition. However, to date, no link has been made between this and isotope ratios in atmospheric CFCs. Therefore, with respect to CFCs there is currently no internationally recognised isotope standard which can be used in these measurements. There are difficulties in synthesising a CFC of known isotopic composition,

importantly due to the prevention of production of CFCs via the Montreal Protocol. In this study therefore, all delta values are described relative to an in-house laboratory standard for comparison (AAL-071170). The standard comprises tropospheric background air collected in 2006 at Niwot Ridge, Colorado, by the National Oceanic and Atmospheric Administration (NOAA). It is a real air sample which is stored in a pressurised Acculife-treated aluminium cylinder. This standard has been analysed by the NOAA Climate Monitoring and Diagnostics Laboratory (CMDL) analysed the sample for a range of trace gases. The analysis of CFC-11, CFC-12 and CFC-113 means that mole fractions reported in this study are consistent with NOAA calibration scales.

Isotopologue ratios are calculated using the linear regression slope of one isotopologue against another. The ion current of any fragment ion over the course of the peak is plotted against the ion current corresponding to the most abundant ion fragment. An example plot of chromatographic peaks of all isotopologues of CFC-12 and the plot displaying the linear regression slope of one isotopologue against another is shown in Figure 2.3. With respect to CFC-11, the CCl_2F^+ fragment is the most abundant. This ion fragment is used rather than directly measuring Cl^+ ions as this fragment results larger peaks than fragmented Cl^+ ions, giving better measurement precision. In the case of CFC-12, the most abundant fragment is CF_2Cl (m/z 85), but using the CCl_2F^+ fragment eliminates potential interferences from the $CClF_2$ fragment of the nearby $CHFCl_2$. Similarly, using the CCl_2F^+ for CFC-113 analysis mimimises the influence of the isomer CFC-113a, which elutes just before CFC-113 but is much less abundant in the atmosphere. The additional fragment ions corresponding to CFC-11, CFC-12 and CFC-113 are shown in Table 2.3.

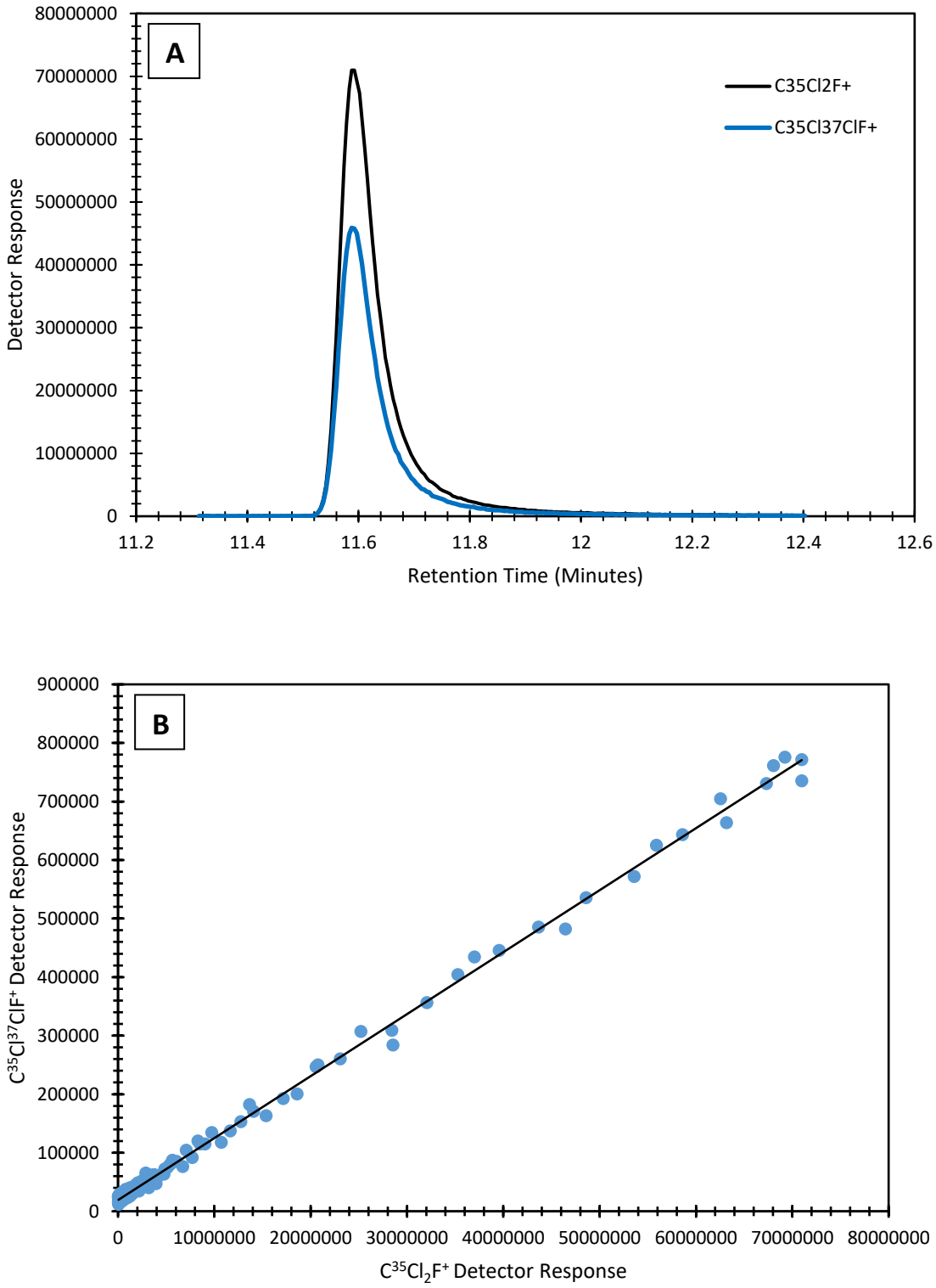

Figure 2.3 Example plot of (A) chromatographic peaks of two isotopologues of CFC-12 and (B) the linear regression slope of one isotopologue against another for $\delta(^{35}Cl)/\delta(^{37}Cl)$

Table 2.2 Fragment ions corresponding to chlorine isotopologues of CFC-11, CFC-12 and CFC-113, with *m/z* values detected by the Autospec instrument.

Species for analysis	Ion Fragment	*m/z*
CCl_2F_2 (CFC-12)	$C^{35}Cl_2F^+$	101
	$C^{35}Cl^{37}ClF^+$	103
	$C^{37}Cl_2F^+$	105
CCl_3F (CFC-11)	$C^{35}Cl_2F^+$	101
	$C^{35}Cl^{37}ClF^+$	103
	$C^{37}Cl_2F^+$	105
$C_2Cl_3F_3$ (CFC-113)	$C^{35}Cl_2F^+$	101
	$C^{35}Cl^{37}ClF^+$	103
	$C^{37}Cl_2F^+$	105

No chromatographic interferences were present close to the retention times related to CFC-11. However, in the case of CFC-12 (CCl_2F_2), HFC-125 (C_2HF_5) elutes directly in front of the peak corresponding to *m/z* 101. With respect to CFC-113 ($C_2Cl_3F_3$, 1,1,2-trichloro-1,2,2-trifluoroethane) the isomer CFC-113a ($C_2Cl_3F_3$, 1,1,1-trichloro-2,2,2-trifluoroethane) elutes very close to the CFC-113 retention time, and is detected above that of the surrounding noise. In calculating the linear regression of two isotopologues of both CFC-12 and CFC-113, the start of the analyte peak was determined only at a retention time after the end of the HFC-125 and CFC-113a peak respectively. This ensured that no correction of the data was required.

Calculation of mole fractions

In order to calculate mixing ratios of the samples, MassLynx was used to facilitate peak integrations. The peak area of the sample peak and that of the standard AAL-071170 were normalised according to the amount of air trapped. The ratio of standard to sample peak area ratio was multiplied by the known mole fraction in the standard to give the mole fraction in the sample.

2.1.2.6 Determination of background blanks and system stability

At the beginning of each measurement day, the blank value for the system is quantified, to allow subtraction of this zero point from all sample measurements. In order to determine the blank values, an aliquot of helium gas is passed through the inlet system just as a sample would be,

and injected in the GC-MS for isotope analysis. Any peak detected during this process is deemed the zero point for all subsequent measurements, however this was negligible for all measurements.

The stability of the system at the start of the measurement say is achieved by beginning with a minimum of two standard runs. Once the instrument gives a stable peak, sample analysis may begin.

Typically three samples were analysed in succession with standards bracketing at the beginning and end. In some instances, where only small amounts of sample could be trapped, sample and standard analyses were alternated to give better precision. In both cases analysis of the standard allows drift correction to be carried out throughout the course of the day, as described below. The standard used was the in house standard AAL-071170.

2.1.2.7 Drift corrections and error calculations

Drift Corrections

The Autospec instrument is not entirely consistent between runs and is seen to display a small amount of drift in the detector response over the course of a day. The calculation of $\delta(^{37}Cl)$ uses the ratio of the detector response of a sample compared to a standard. A reference peak which does not immediately precede or follow the sample peak can therefore introduce bias when calculating $\delta(^{37}Cl)$ unless the temporal distance between standard and sample peaks is always identical. Between one and three samples however were analysed between each set of bracketing standard. In order to mitigate the effect of instrumental drift the sample was compared to a weighted average of the surrounding standards. The weighting of each standard was calculated according to its temporal proximity to the samples. For example, for a sample immediately following a standard, but followed by two more sample analyses before a second standard, the average of these two standards was weighted more heavily towards the first standard since it is closer to the sample.

Calculation of Errors

The total analytical uncertainty of sample measurement is calculated by the square root of the combination of both sample and standard uncertainty. This 1σ analytical uncertainty is given by the equation:

$$Total\ Uncertainty = \sqrt{SD^2Sample + SD^2Standard} \qquad \text{Equation 2.3}$$

In the instance that the sample was measured more than two times, the standard deviation of only the samples was used, with no inclusion of the uncertainty of the standard. In the case of a repeat sample analysis not being carried out there is no value for the standard deviation for this sample. In this instance the standard deviation of a sample measured under similar instrument conditions is substituted. This relies on there being a similar mole fraction in the original sample measured and the substituting sample measurement. The reason behind this stipulation is that that the measurement precision generally increases with decreasing mole fraction. Finally, in the case that there is no suitable sample for substitution, the total measurement uncertainty for a sample is estimated using the square root of the sum of the squares of the standard deviation of the standard for that measurement day.

Outliers and poor quality measurements

In some instances it was necessary to discount a poor quality measurement from the data set. A poor quality measurement is defined as a repeated measurement with a standard deviation more than twice the standard deviation of the standard used during the measurement day.

2.1.2 Results and discussion

Data corresponding to the determination of non-linearities in the detector response is presented, then data from measurement of $\delta(^{37}Cl)$ in CFC-11, CFC-12 and CFC-113 in samples collected at stratospheric altitudes.

2.1.3.1 Determination of non-linearities

Effect of sample size on non-linearities

Since samples from both campaigns had a wide range of mole fractions for all three species of interest, it was necessary to verify as to whether isotope ratio measurements were free from bias by the response behaviour of the analytical system. An air sample collected at Niwot Ridge in 2009 (SX-0706077) was diluted with nitrogen into three litre Silco-treated stainless steel containers. Dilutions were monitored using pressure sensors, to give a series of dilutions with a wide range of mole fractions. Dilutions were based on the mole fractions of CFC-12. It was determined as whether the change in mole fraction, which gives a change in chromatographic peak area, gives rise to an effect on isotope ratio of a sample. The range of mole fractions to which the standard was diluted is representative of the range of mole fractions in the stratospheric samples. The dilution series was analysed using the identical measurement procedures to the stratospheric samples, as well as the in house standard (AAL-071170). During the stratospheric sample measurement period, the chromatographic column was changed from

a GasPro to an Alumina Plot column. This meant that the dilution series was analysed twice, once using each chromatography column to ensure that both columns give comparable results and so eliminating effects of the analytical column on the data.

The bias of the analytical system when measuring CFC-12 was previously tested by Laube et al. (2010), and also by Allin (PhD Thesis, 2015) for CFC-12, CFC-11 and CFC-113. However, the samples analysed in this thesis cover a wider range of mole fractions, as well as using two different analytical columns, and so more extensive testing of analytical bias was required. Data from Allin (2015) have been combined with data from this study to give a comprehensive analysis of analytical bias. Measurements of $\delta(^{37}Cl)$ (‰) are given relative to the same standard used for the stratospheric samples (AAL-071170). Data as shown in Figures 2.4 to 2.12 show the effect of sample size on $\delta(^{37}Cl)$ for CFC-12, CFC-11 and CFC-113 for both this study and Allin (2015).

CFC-12

Analysis of the dilution series for CFC-12 using the GasPro and Alplot column, Figure 2.4, revealed that, with respect to $\delta(^{35}Cl^{37}Cl)$, delta values derived from the smallest peak areas are

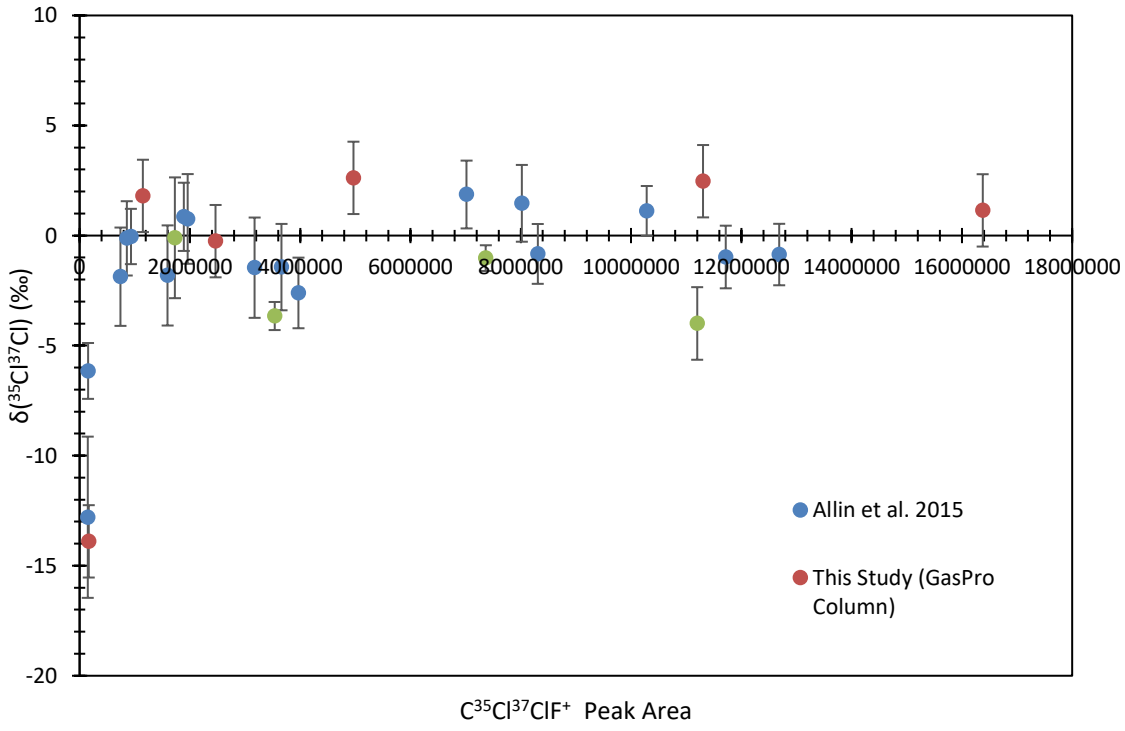

Figure 2.4: Measured $\delta(^{35}Cl^{37}Cl)$ plotted against peak area of the $C^{35}Cl^{37}ClF^{+}$ fragment ion (*m/z* 103) for CFC-12 using the Alplot column (this study), GasPro column (this study) and GasPro Column (Allin, 2015). 1σ standard deviation error bars are shown. The discarded sample is not shown. Delta values relative to standard AAL-071170.

erroneously low. Data from Allin (2015) confirms this bias of delta values with respect to the smallest peak areas. A poor quality measurement is again described as having a standard deviation of repeat analysis corresponding to greater than twice the standard deviation of the $R_{standard}$ value. Due to this large uncertainty of the smallest peak area, one dilution series sample was discarded.

With respect to $\delta(^{37}Cl_2)$, delta values derived from the smallest peak areas are again erroneously low. Data from Allin (2015) as well as this study displayed a strong deviation from a linear detector response with respect to the smallest peak areas. One dilution series measurement was discarded since the standard deviation of this repeat analysis was greater than twice that of the standard.

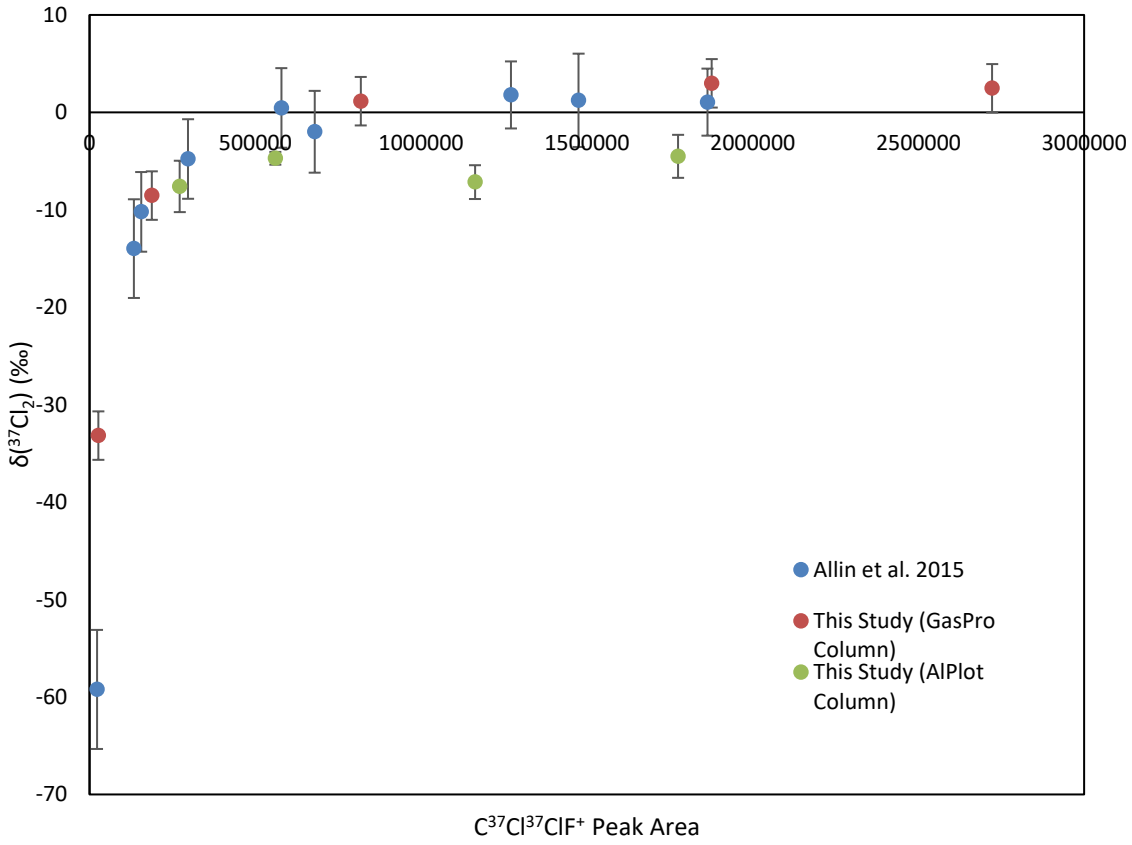

Figure 2.5: Measured $\delta(^{37}Cl_2)$ plotted against peak area of the $C^{37}Cl^{37}ClF^+$ fragment ion (*m/z* 105) for CFC-12 using the Alplot column (this study), GasPro column (this study) and GasPro column (Allin, 2015). 1σ standard deviation error bars are shown. Discarded samples not shown. Delta values relative to standard AAL-071170.

Once samples with mole fractions corresponding to peaks areas in the region of higher than average uncertainty had been discarded, the total chlorine delta was calculated for the remaining dilution series samples via Equation 2.4.

Total $\delta^{37}Cl = (^{35,37}R + 2*^{37,37}R)/(2+ ^{35,37}R)$ Equation 2.4

Since the total chlorine delta requires both $\delta(^{37}Cl_2)$ and $\delta(^{35}Cl^{37}Cl)$ data points, when either of these measurements were discarded due to uncertainties, the total chlorine delta could not be calculated for this dilution. This meant that the plot of total $\delta(^{37}Cl)$ (Figure 2.6) has a fewer number of data points compared to the corresponding $\delta(^{37}Cl_2)$ and $\delta(^{35}Cl^{37}Cl)$ plots. The total chlorine delta values of the remaining samples displayed no systematic bias with respect to peak area, as shown in Figure 2.5. This meant no correction was applied to samples with mole fractions within this linear region of peak areas. Four stratospheric samples were discarded since they had peak areas lower than that of the smallest dilution series measurements with adequate precision.

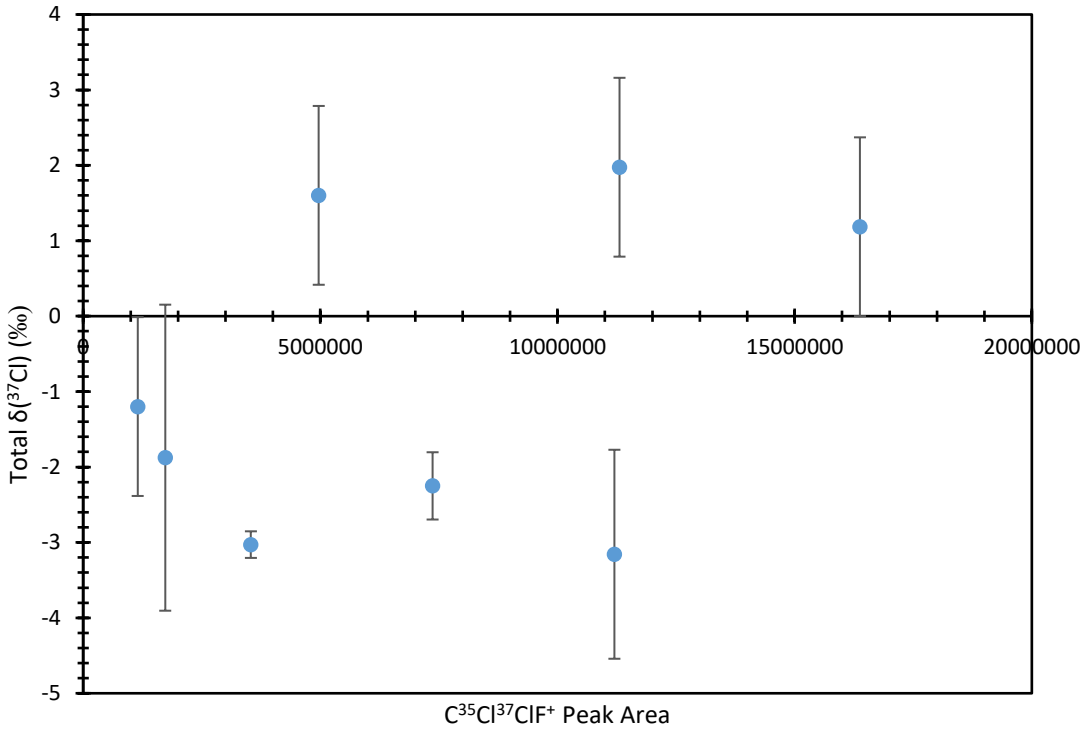

Figure 2.6: Measured Total $\delta(^{37}Cl)$ plotted against peak area of the $C^{35}Cl^{37}ClF^+$ fragment ion (*m/z* 103) for CFC-12. Data from this study and that of Allin (2015) have been combined. 1σ standard deviation error bars are shown. Delta values relative to standard AAL-071170.

CFC-11

Analysis of the dilution series for CFC-11 using the GasPro and Alplot column, Figure 2.7 showed that the isotope delta bias with respect to $\delta(^{35}Cl^{37}Cl)$ is limited to the lowest abundance samples.

Data from this study agree well with those from Allin (2015). One dilution series sample was discarded based on the large uncertainty as quantified above.

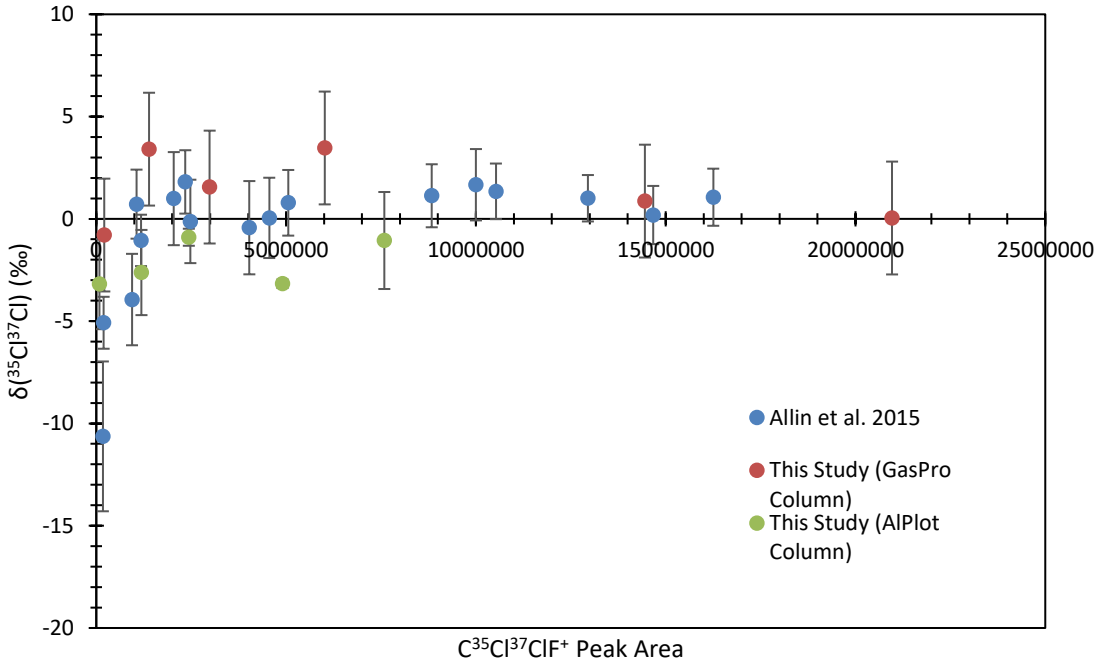

Figure 2.7: Measured $\delta(^{35}Cl^{37}Cl)$ plotted against peak area of the $C^{35}Cl^{37}ClF^{+}$ fragment ion (*m/z* 103) for CFC-11 using Alplot column and GasPro column. 1σ standard deviation error bars are shown. Discarded sample not shown. Delta values relative to standard AAL-071170.

With respect to $\delta(^{37}Cl_2)$, the data again show that the isotope delta bias is limited to the lowest abundance samples (Figure 2.8), and the lowest mixing ratio dilution series measurement was discarded due to larger than average uncertainty.

The total chlorine was calculated via Equation 2.4, the linearity of delta values with respect to peak area is shown in Figure 2.8. Again, since the total chlorine delta requires both $\delta(^{37}Cl_2)$ and $\delta(^{35}Cl^{37}Cl)$ data points, when either of these measurements were discarded the total chlorine delta could not be calculated for this dilution and so Figure 2.9 has a fewer number of data points compared to the corresponding $\delta(^{37}Cl_2)$ and $\delta(^{35}Cl^{37}Cl)$ plots. The total chlorine delta values of the remaining samples displayed a systematic biased with respect to peak area at the lowest peak areas, and hence a correction based on the slope of the non-linearity (Figure 2.9 (B)) was applied to 11 stratospheric measurements which fell in this region. 78% of the stratospheric samples analysed had peak areas in the range where there was no instrument bias and therefore no correction was required. 5 stratospheric samples were discarded due to large measurement uncertainties.

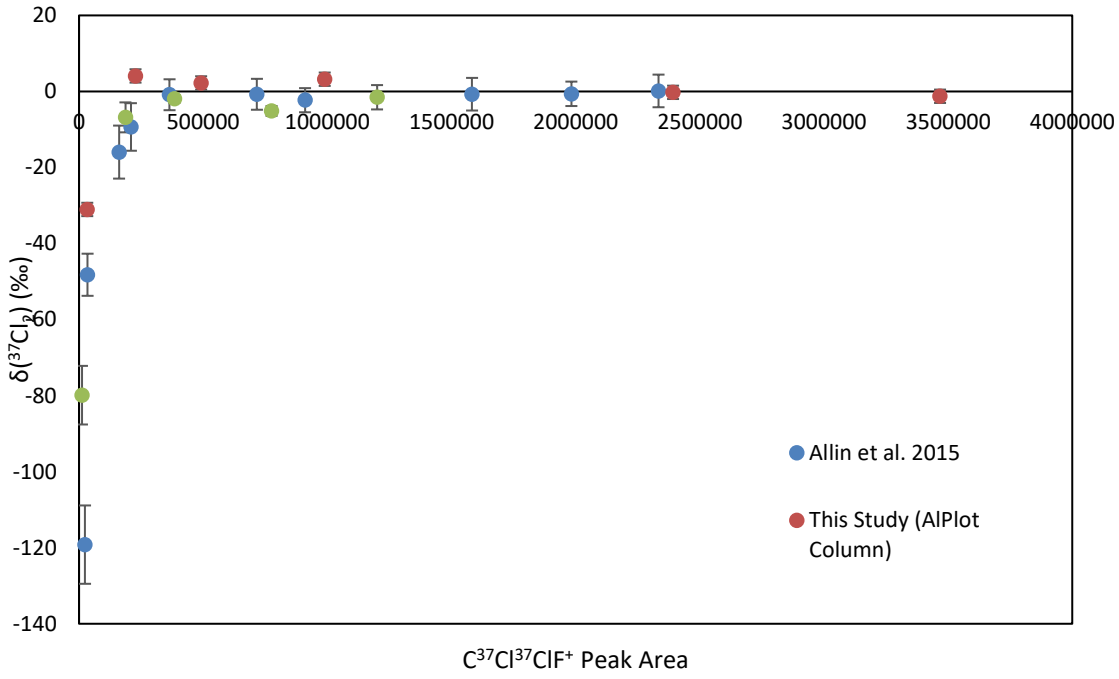

Figure 2.8: Measured $\delta(^{37}Cl_2)$ plotted against peak area of the $C^{37}Cl^{37}ClF^+$ fragment ion (*m/z* 105) for CFC-11 using Alplot column and GasPro column. 1σ standard deviation error bars are shown. Discarded sample not displayed. Delta values relative to standard AAL-071170.

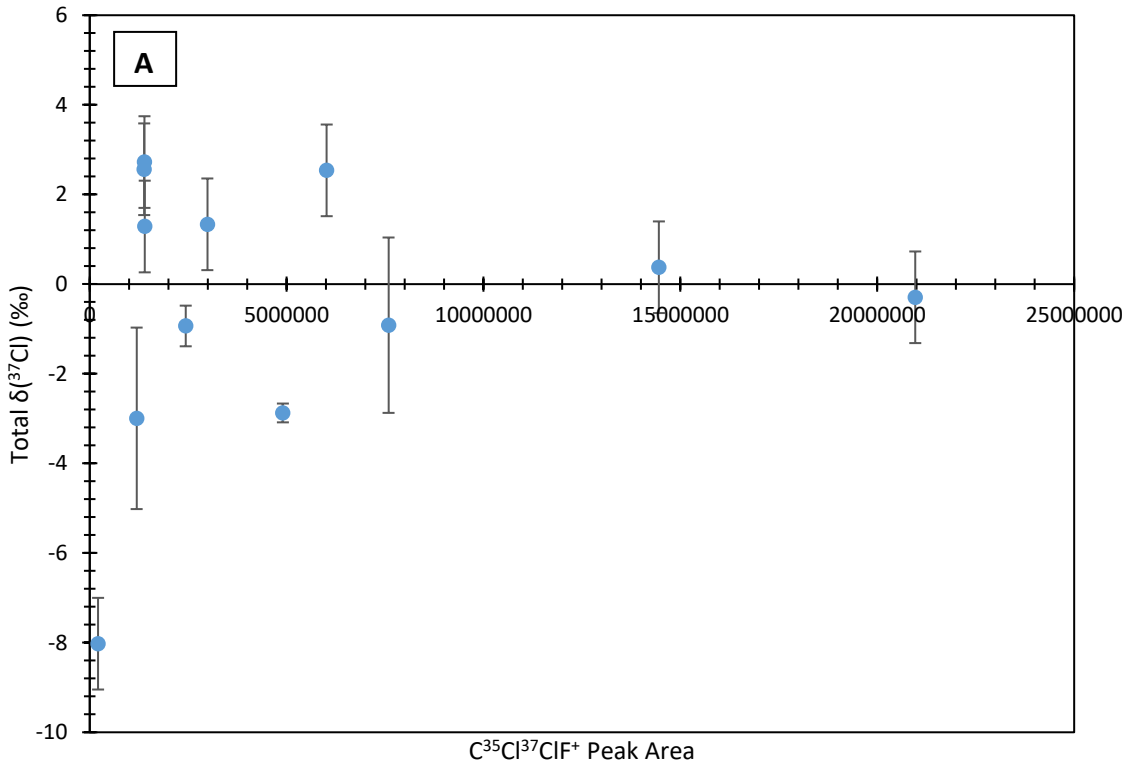

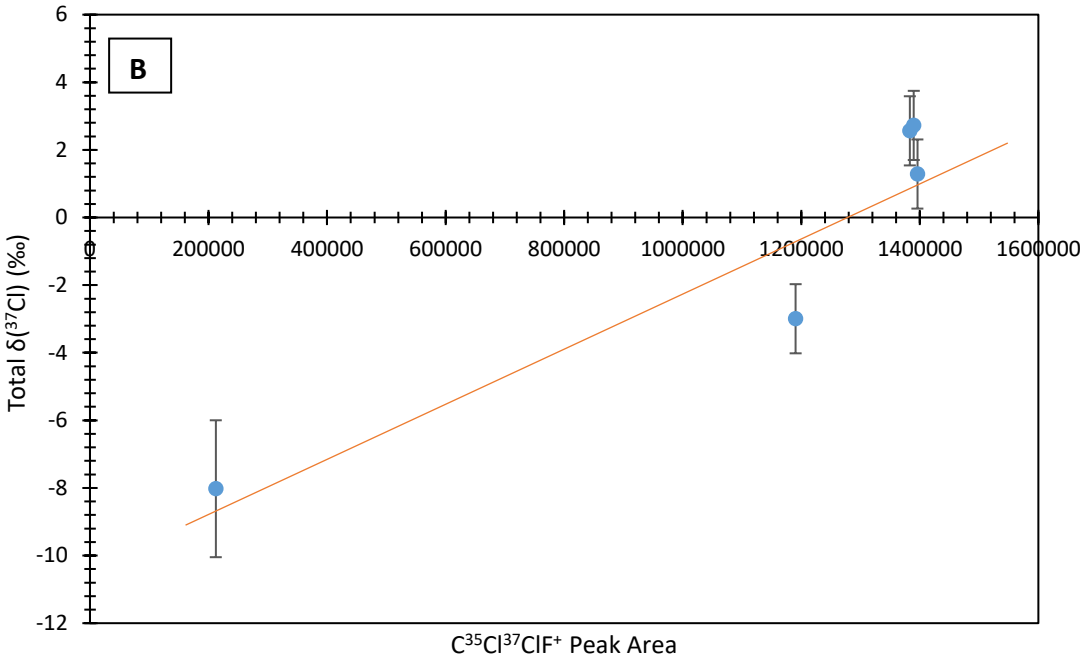

Figure 2.9: (A) Measured Total δ(^{37}Cl) plotted against peak area of the $C^{35}Cl^{37}ClF^+$ fragment ion (*m/z* 103) for CFC-11. Data from this study and that of Allin (2015) have been combined. **(B)** Region of depleted total δ(^{37}Cl) values with corresponding linear regression line used for data correction. 1σ standard deviation error bars are shown. Delta values relative to standard AAL-071170.

CFC-113

Figure 2.10 shows that, with respect to δ(^{35}Cl^{37}Cl), delta values derived from the smallest peak areas display larger than average uncertainties and are erroneously low for CFC-113. The smallest peak area derived from samples analysed using the AlPlot column displayed a much larger than average uncertainty and so was discarded. The smallest peak derived from analysis using the GasPro column showed good precision, however, the peak displays a strong positive bias and so was discarded.

With respect to δ($^{37}Cl_2$), the data again show that the isotope delta bias is limited to the lowest abundance samples (Figure 2.11). Poor precision of the smallest peak area meant one dilution series measurement was discarded.

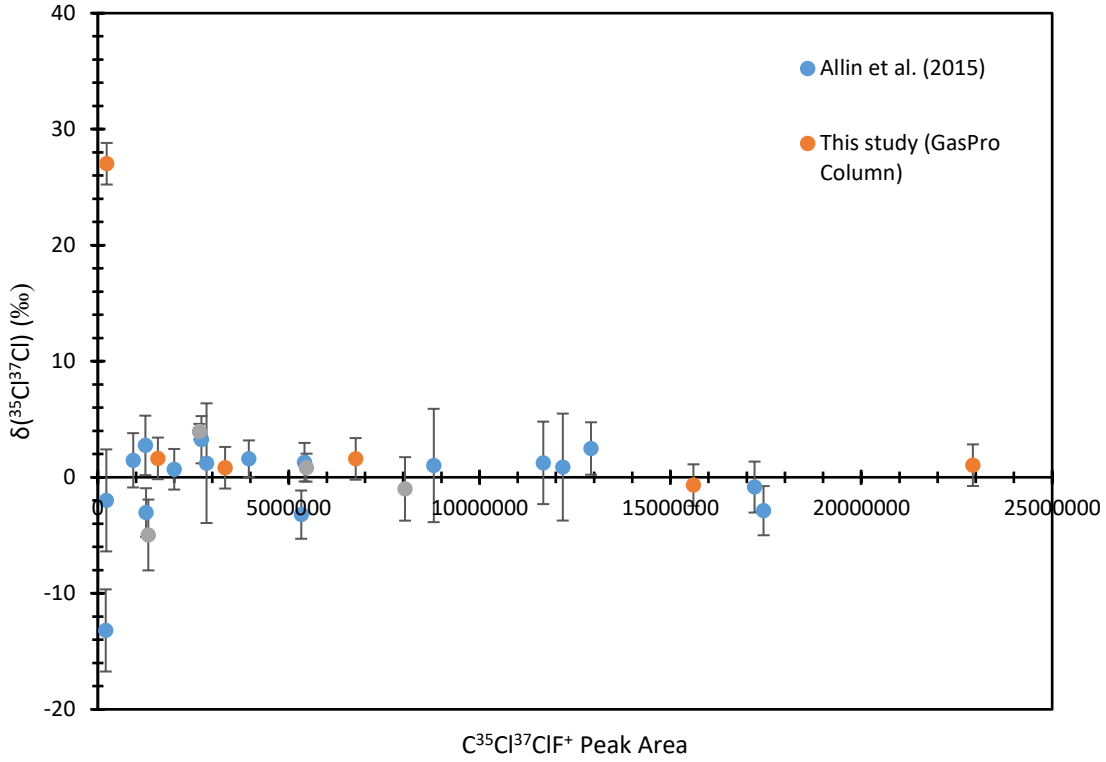

Figure 2.10: Measured $\delta(^{35}Cl^{37}Cl)$ plotted against peak area of the $C^{35}Cl^{37}ClF^+$ fragment ion (*m/z* 103) for CFC-113 using Alplot column and GasPro column. 1σ standard deviation error bars are shown. Most depleted AlPlot value removed for clarity. GasPro sample with strong positive bias displayed for information. Delta values relative to standard AAL-071170.

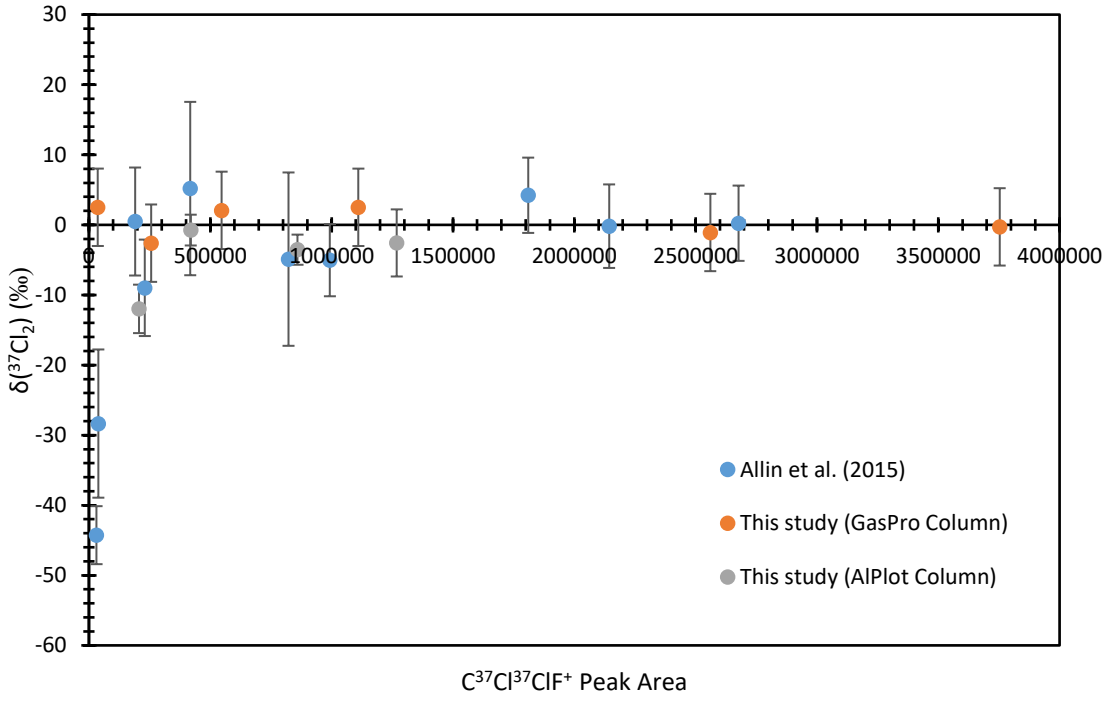

Figure 2.11: Measured $\delta(^{37}Cl_2)$ plotted against peak area of the $C^{37}Cl^{37}ClF^+$ fragment ion (*m/z* 105) for CFC-113 using Alplot column and GasPro column. 1σ standard deviation error bars are shown. Delta values relative to standard AAL-071170.

The total chlorine was calculated via Equation 2.4. The total chlorine delta values of the remaining dilution series samples displayed no systematic biased with respect to peak area (Figure 2.12). This meant no correction was applied to samples with mole fractions within this linear region of peak areas. Five stratospheric samples were discarded since they had peak areas lower than that of the smallest dilution series measurements with adequate precision

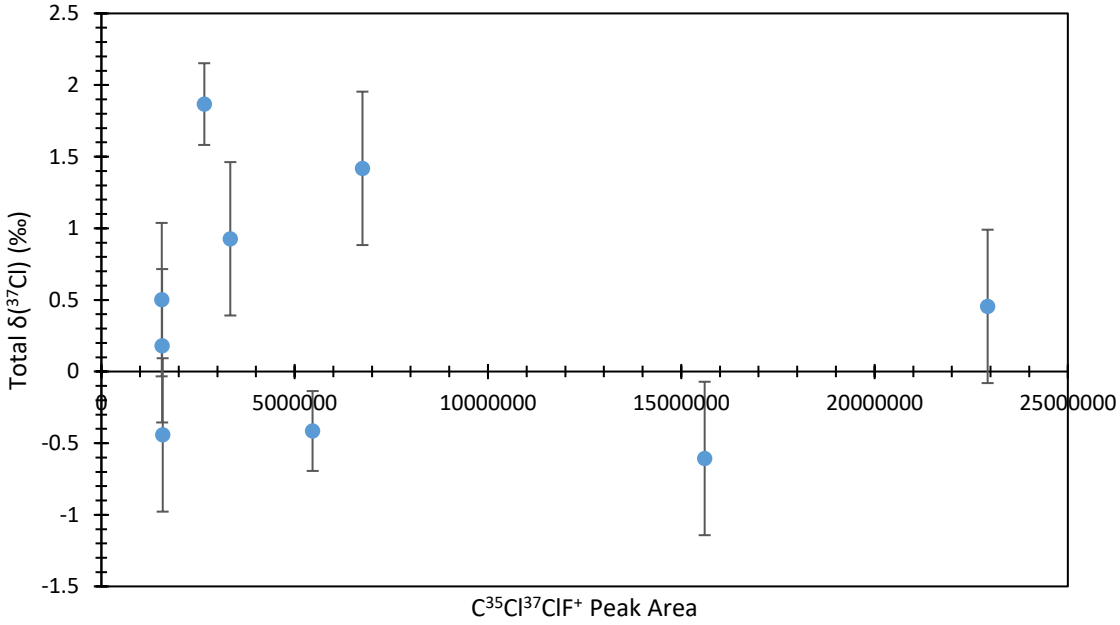

Figure 2.12: Measured Total $\delta(^{37}Cl)$ plotted against peak area of the $C^{35}Cl^{37}ClF^{+}$ fragment ion (*m/z* 103) for CFC-113 using Alplot column and GasPro column. 1σ standard deviation error bars are shown. Delta values relative to standard AAL-071170.

2.1.3.2 Stratospheric measurements

Stratospheric air samples have been analysed from both the Kiruna campaign and from balloon flights above Gap, France for the total $\delta(^{37}Cl)$ in CFC-12, CFC-11 and CFC-113. Measurements from Kiruna and Gap agree well, and show an expected increase in isotope enrichment with decreasing mixing ratios.

Apparent isotope fractionations (ε_{App})

To quantify the isotope dependence of the sink reactions, photolysis and reaction with $O(^1D)$, of these CFCs, Rayleigh fractionation plots are given in Figures 2.13 to 2.15. A Rayleigh plot displays the isotope fractionation of a species (y-axis) with respect to the proportion of species which remains relative to a start point (x-axis). In this instance, the start mixing ratio is that of the troposphere, i.e. the mixing ratio which existed before the CFC of interest was broken down in the stratosphere. Ordinarily, the mean age of air is calculated for each sample using a tracer, for

example SF_6. There is an assumed frequency distribution in each mean age of air calculated. In the case of CFCs, this matter is complicated as CFCs have a changing trend in amount of gas released over time. It is necessary therefore to carry out a correction. However, in this study, the samples were collected in December 2011, and by this point in time, due to the regulation by the Montreal Protocol, atmospheric emissions had mostly ceased and the amount of CFC in the troposphere was gradually decreasing for the three species investigated here. The error associated with the assumed frequency distribution of mean age of air on the x-axis derives from the changes in tropospheric CFC abundances up to several years before the stratospheric sampling. However, it is known from inert atmospheric tracers such as SF_6 that the mean age of air contained in these samples in fact is below 5 years (Laube et al., 2013). This means that a negligible bias is introduced to the x-axis parameters and so no correction was applied. In order to derive the total chlorine isotope fractionation, the combination of $\delta(^{37}Cl_2)$ and $\delta(^{35}Cl^{37}Cl)$ was carried out. After discarding samples based on the non-linearity of the analytical system, 46 samples remained for CFC-12 analysis, 44 for CFC-11 and 44 for CFC-113.

Calculation of ε_{App} was established by calculating the slope of the data plotted. In all three cases, negative ε_{App} values were derived, suggesting that molecules containing lighter isotopes, in this case ^{35}Cl, are broken down more quickly giving an enrichment in the heavier isotope (^{37}Cl) with increasing CFC decomposition.

It can be seen with respect to CFC-12 that the mid latitude samples display a stronger apparent isotope fractionation than high-latitude samples, -12.91±1.24 ‰ (mid-latitude) compared to -7.48±0.69 ‰ (high-latitude) for CFC-12. This agrees well with the expected trend as discussed above, demonstrating the likely effect of 'dampening' of the apparent isotope fractionation due to mixing with air containing essentially zero CFC-12. Importantly, the record of 27 ‰ set by Laube et al. (2010) has been exceeded with a maximum value of 38±0.9 ‰ in this study. It is important to note that this maximum value is an extremum and so the mid-latitude apparent isotope fractionation calculated using this value is heavily weighted on this data point. In the future it would be paramount to carry out analysis of further samples deep into the stratosphere at mid latitudes.

CFC-11 shows the same correlation, -3.19±0.46 ‰ and -2.99±0.32 ‰ for mid- and high-latitude stratospheric samples respectively. However, the values are statistically indistinguishable.

In the case of CFC-113 the correlation is reversed, the mid-latitude samples display apparent isotope fractionations of -1.87±0.98 ‰ whereas the high latitude samples display an apparent isotope fractionation of -3.56±0.65 ‰. It is expected that CFC-113 would follow the same

pattern as CFC-11 and CFC-12, with a decreased apparent isotope fractionation at higher laitudes, yet displays the opposite, which is currently unexplained. Since data presented by Allin demonstrates no statistical significance between latitudes, it would be interesting to increase the range of samples measured to identify as to whether data presented in this thesis are anomalous or present previously unrecognised correlations.

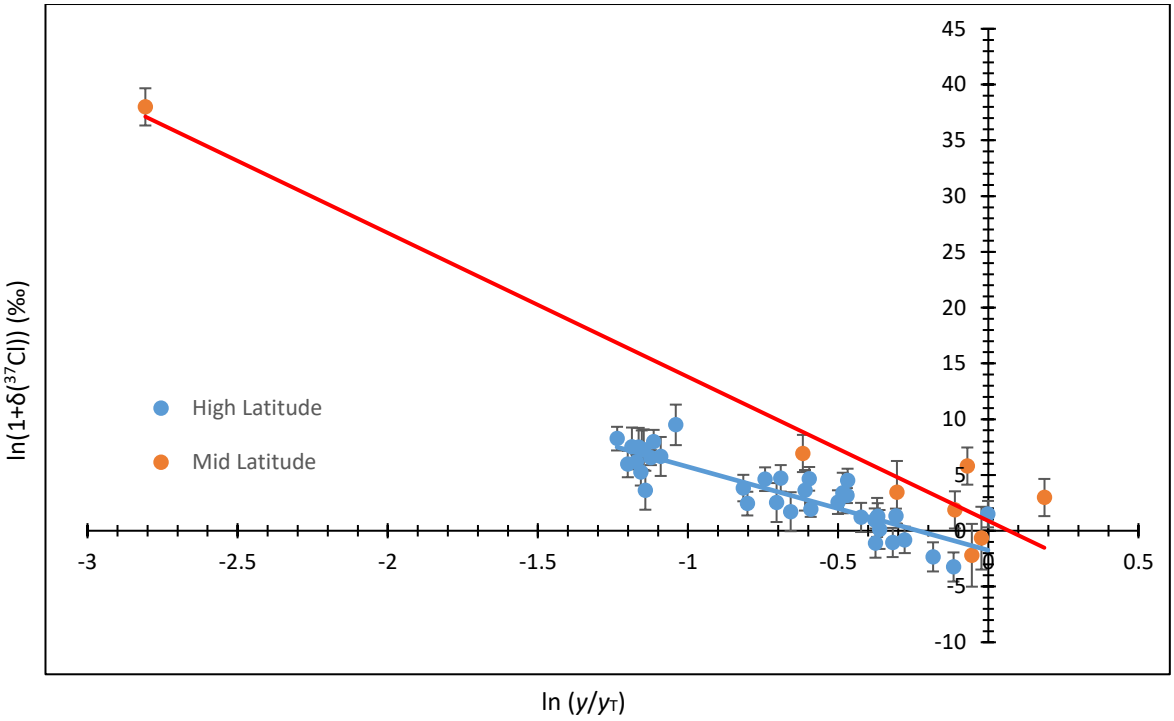

Figure 2.13. Rayleigh fractionation plot of CFC-12 chlorine isotope signature from stratospheric samples at mid (GAP, France) and high (Kiruna, Sweden) latitudes. Trend lines correspond to apparent fractionations (ε_{App}) of -12.91±1.24 ‰, -7.48±0.69 ‰ for mid and high-latitude stratospheric samples. The standard error of the gradient is quoted for ε_{App} values. 1σ standard deviation error bars are shown.

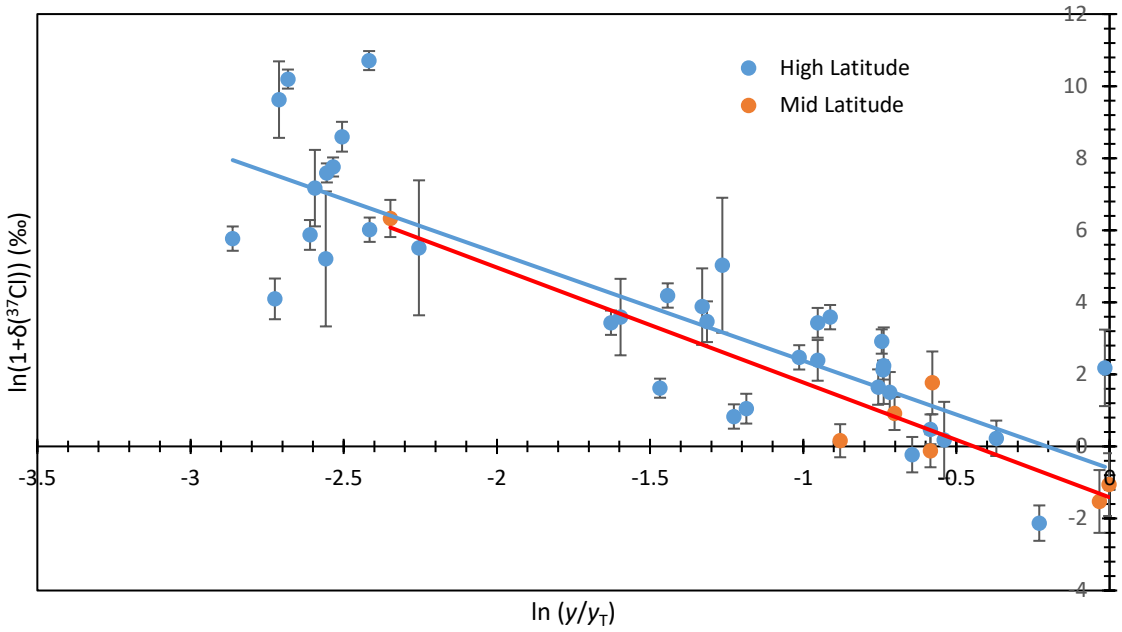

Figure 2.14 Rayleigh fractionation plot of CFC-11 chlorine isotope signature from stratospheric samples at mid (GAP, France) and high (Kiruna, Sweden) latitudes. Trend lines correspond to apparent fractionations (ε_{App}) of -3.19±0.46‰, -2.99±0.32 ‰ for mid and high-latitude stratospheric samples. The standard error of the gradient is quoted for ε_{App} values. 1σ standard deviation error bars are shown.

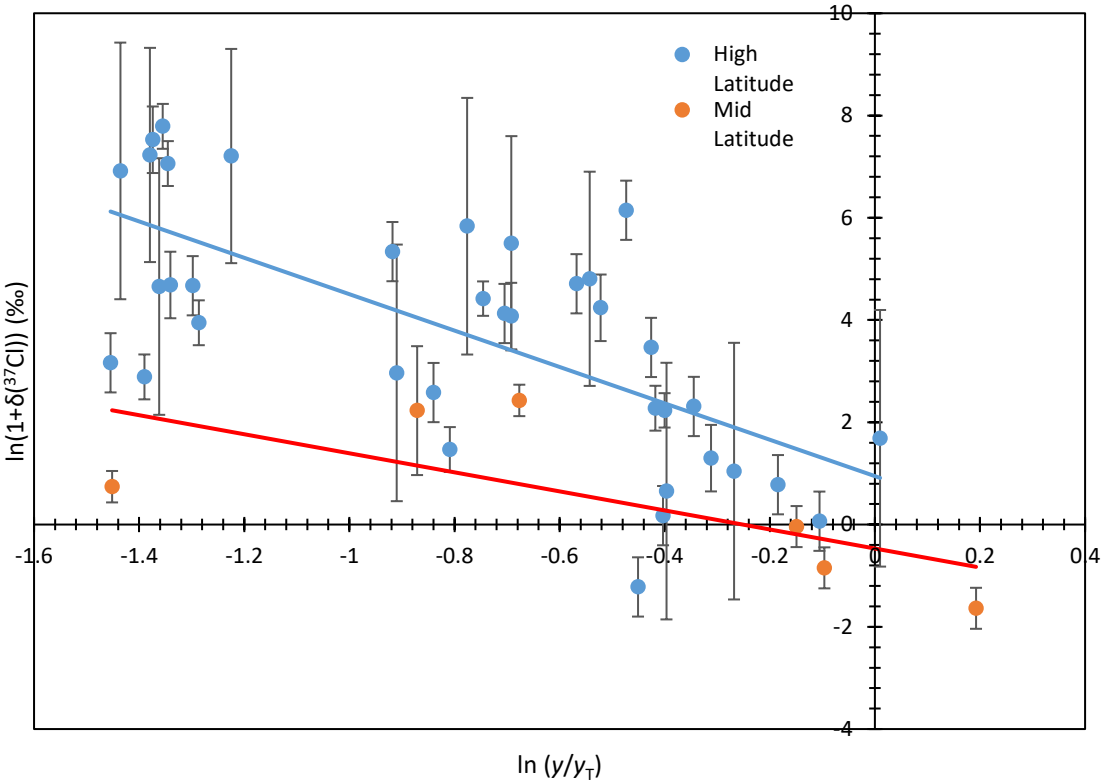

Figure 2.15. Rayleigh fractionation plot of CFC-113 chlorine isotope signature from stratospheric samples at mid (GAP, France) and high (Kiruna, Sweden) latitudes. Trend lines correspond to apparent fractionations (ε_{App}) of -1.87±1.0 ‰, -3.56±0.7 ‰ for mid and high-latitude stratospheric samples. The standard error of the gradient is quoted for ε_{App} values. 1σ standard deviation error bars are shown.

Comparison to previous studies

To date, two studies have described the apparent isotope fractionation of CFC-12. Laube et al. (2010) showed a progressive increase in $^{37}Cl/^{35}Cl$ by up to 27 ‰ relative to tropospheric air in samples from 14-34 km altitude. Laube et al. (2010) determined the ε_{App} of CFC-12 in the tropical stratosphere to be -12.1±1.7 ‰. Furthermore, Allin (2015) used air archives to enhance the number of CFC-12 measurements carried out, as well as analysis of CFC-11 and CFC-113. These two additional CFCs exhibited significant chlorine isotope fractionation in common with CFC-12. Allin (2015) gave values of ε_{App} to be −2.4±0.5 and −2.3±0.4 ‰ for CFC-11, −12.2±1.6 and −6.8±0.8 ‰ for CFC-12 and −3.5±1.5 and −3.3±1.2 ‰ for CFC-113 for mid- and high-latitude samples respectively.

Data presented in this thesis displays strong enrichment in heavy chlorine isotopes, and therefore agrees qualitatively with the data from both Laube et al. (2010) and Allin (2015), as shown in Table 2.3. It is important to note that although data from this study and that of Allin agree, the time periods over which the data covers is significantly different.

Table 2.3. Summary of total chlorine ε_{App} values from this study, (Allin, 2015) and (Laube et al., 2010). All delta values given in per mil (‰).

ε_{App} (Total Chlorine)	**This study**		**Allin et al. 2015**		**Laube et al. 2010**
Latitude	44.4°N	67.9°N	48.1-53.4°N	66.3-76.2°N	5.04°S
CFC-12	-12.91±1.24	-7.48±0.69	−12.2±1.6	−6.8±0.8	12.1±1.7
CFC-11	-3.19±0.46	-2.99±0.32	−2.4±0.5	−2.3±0.4	
CFC-113	-1.87±0.98	-3.56±0.65	−3.5±1.5	−3.3±1.2	

CFC-12 shows good correlation between all three data sets in the mid and tropical latitudes, and are indistinguishable within 1σ analytical uncertainties. The ε_{App} of the high latitude samples from this study and those of Allin (2015) agree well within the uncertainties, and are still both significantly less negative than the corresponding mid-latitude ε_{App} values.

In the case of CFC-11, ε_{App} data from this study agree within 1σ analytical uncertainties, for both high and mid-latitude samples, to that of Allin (2015). Interestingly, although both data sets agree, data from this study display more negative ε_{App} in the case of both CFC-11 and CFC-12.

CFC-113 shows the lowest apparent isotope fractionation for mid latitudes compared to CFC-11 and CFC-12. In comparison to Allin (2015) CFC-113 displays slightly higher ε_{App} for mid-latitudes yet lower ε_{App} for high-latitude samples. However, the high uncertainty range of both mid and high latitude samples, particularly with respect to the mid latitude sample presented by Allin, mean that in fact the data sets are statistically indistinguishable within 1σ (high-latitudes) and 2σ analytical uncertainties (mid-latitudes).

Importantly, data from this study displays an improvement in measurement uncertainty for all three CFCs across both mid- and high-latitudes compared to both Laube et al. (2010) and Allin et al. (2015). To date, no other studies have concerned chlorine isotope fractionation in stratospheric CFC-12, CFC-11 and CFC-113.

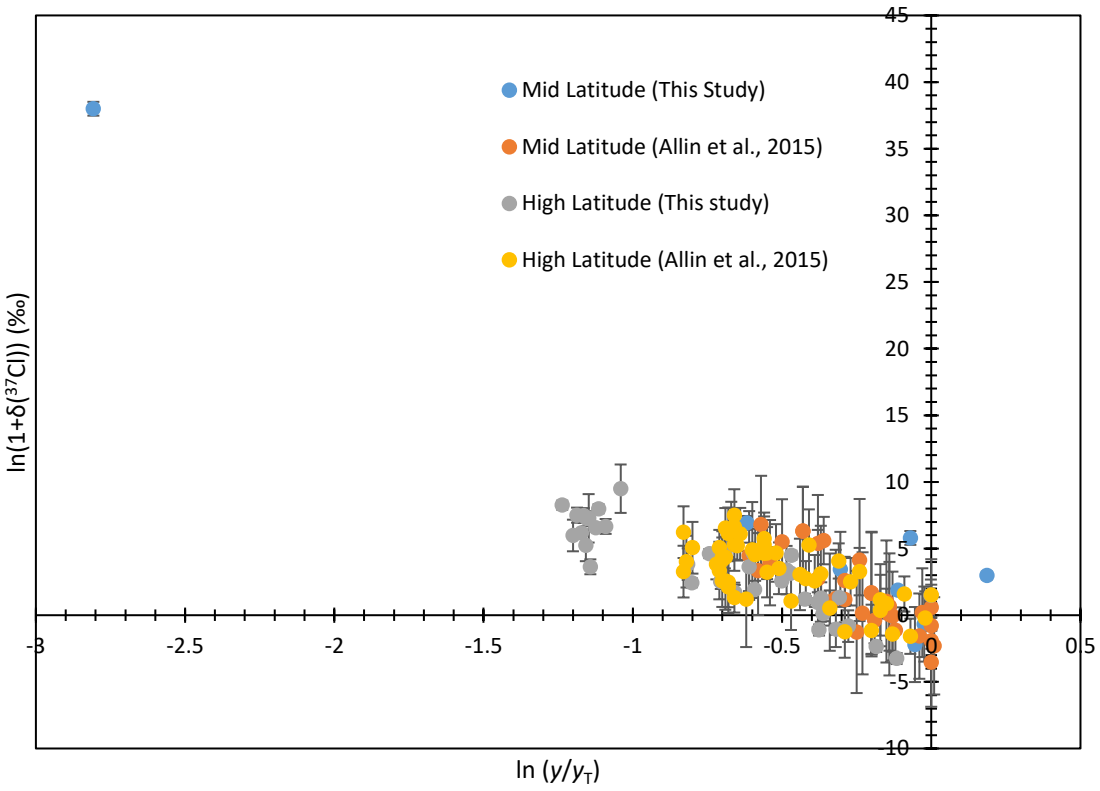

Figure 2.16: Rayleigh fractionation plot of CFC-12 chlorine isotope signature from stratospheric samples at mid and high latitudes from this study, plus mid and high latitude stratospheric samples of Allin et al., (2015). 1σ standard deviation error bars are shown.

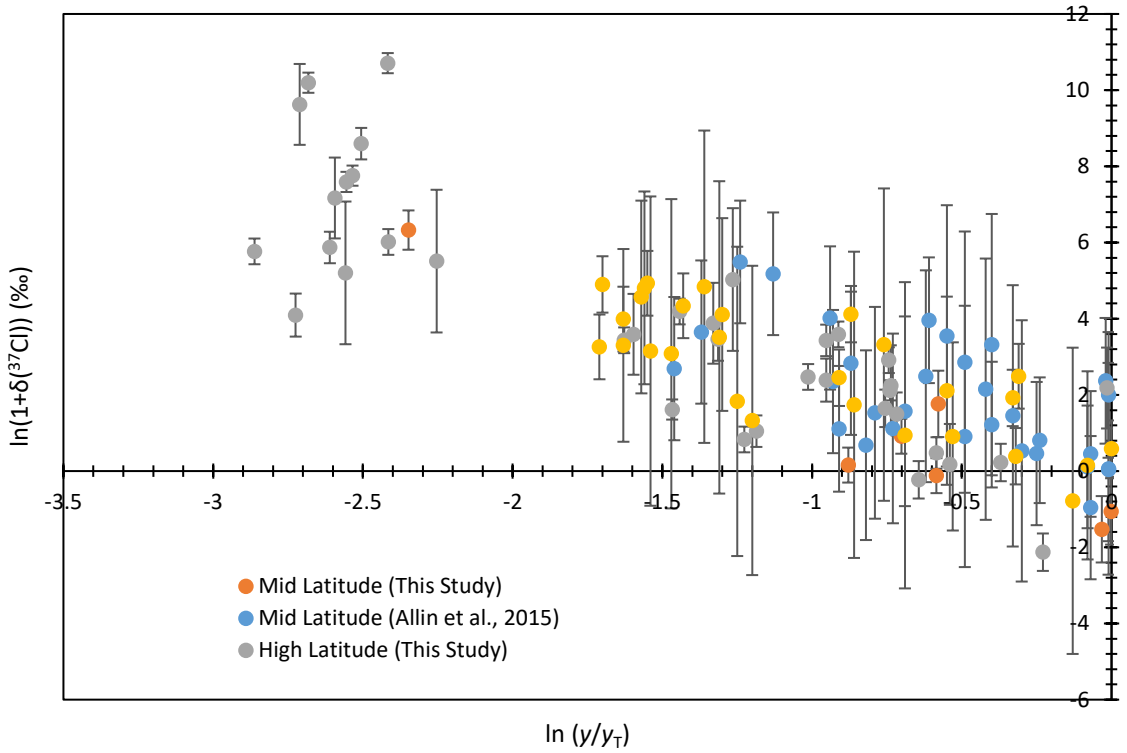

Figure 2.17: Rayleigh fractionation plot of CFC-11 chlorine isotope signature from stratospheric samples at mid and high latitudes from this study, plus mid and high latitude stratospheric samples of Allin et al., (2015). 1σ standard deviation error bars are shown.

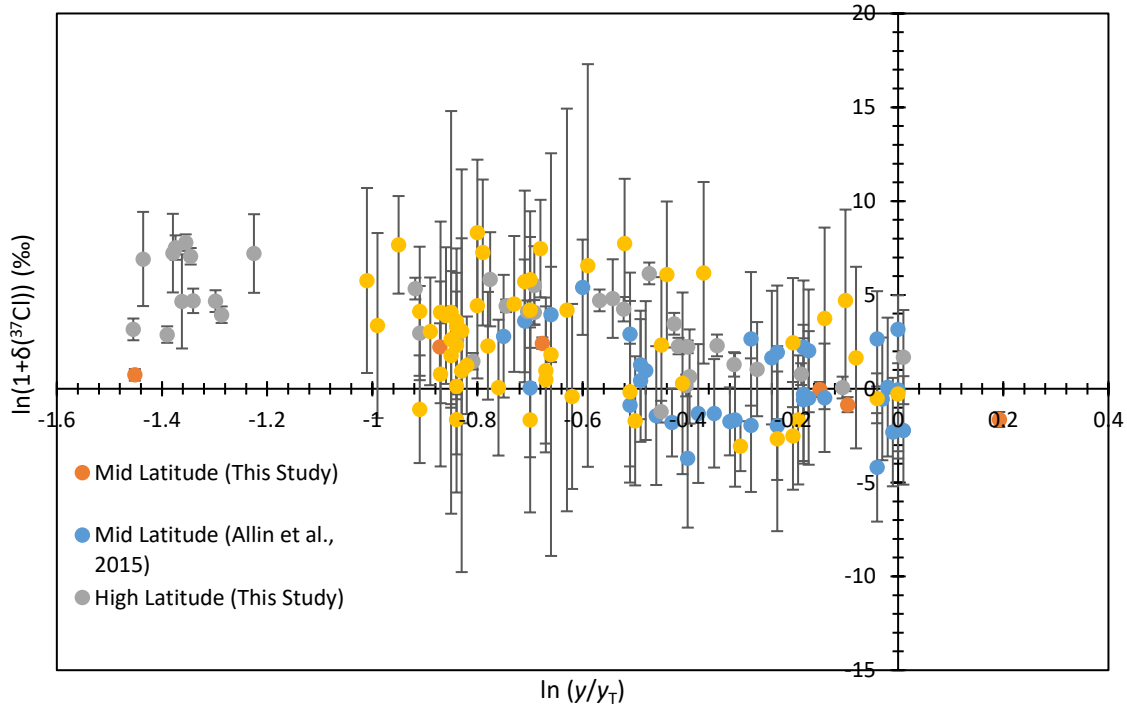

Figure 2.18: Rayleigh fractionation plot of CFC-113 chlorine isotope signature from stratospheric samples at mid and high latitudes from this study, plus mid and high latitude stratospheric samples of Allin et al., (2015). 1σ standard deviation error bars are shown.

In the case of CFC-12, it can be seen that as the stratospheric sampling point moves from mid to high latitudes, the apparent isotope fractionation decreases (Figure 2.16). This agrees well with conclusions of Allin et al (2015) and Laube (2010). Since CFC-12 is broken down via the same pathways as N_2O, this effect is mirrored (Kaiser et al 2006). Since CFC-11 and CFC-113 also are broken down via photolysis reactions and reaction with $O(^1D)$, it could be argued that this pattern in ε_{App} would also coincide. However, the mid and high-latitude CFC-11 ε_{App} values are indistinguishable within 1 standard deviation, and no latitude dependence is observed (Figure 2.17). In the case of CFC-113, the mid- and high-latitude values are indistinguishable within 2 σ analytical uncertainties (Figure 2.18). Allin et al (2015) also concluded that mid- and high-latitude data with respect to both CFC-11 and CFC-113 were indistinguishable within 1 σ. It is possible that in both cases the small isotope changes, and the possible latitude dependence as measured in CFC-12, is obscured by the size of the analytical uncertainties. It is important to note that the analytical uncertainties of the CFC-11 and CFC-113 measurements are improved by this study (0.46 ‰ and 0.32 ‰ compared to 0.5 ‰ and 0.4 ‰ for mid- and high-latitude CFC-11 respectively. 0.98 ‰ and 0.65 ‰ compared to 1.5 ‰ and 1.2 ‰ for mid- and high-latitude CFC-113 respectively).

Implications in the wider context

Stratospheric data from this study increases the range of measurements made by Allin et al (2015), yet calculated ε_{App} values are well correlated within 1σ analytical uncertainties. Figures 2.16, 2.17 and 2.18 display data from both studies, highlighting the addition range of samples and therefore the wider range of fractionation in this study, yet following the same ε_{App} trajectory, shown by the slope. Since the value of epsilon is consistent with previously published values, this demonstrates the applicability of this technique in various regions of the stratosphere. In the context of the conclusions made by Allin et al (2015), it can be seen that data from this study is in good agreement. This is further evidence that indeed the isotope composition of emissions for CFC-11, CFC-12 and CFC-113 has remained constant over time. Again, it is important to point out that although there is good agreement between data sets, the time period of which sampling took place for this study and that of Allin was not the same. It would be interesting to determine whether the average isotope enrichment has been affected in changes in CFC manufacturing processes. However, this is outside the scope of this current study.

Enrichment in $\delta(^{37}Cl)$ in all three CFCs measured is in line with that of Allin (2015) and Laube et al. (2010), as discussed above. Due to stratosphere-troposphere exchange, it is expected that

the measured enrichment in stratospheric CFC-11, CFC-12 and CFC-113 will lead to enrichment in tropospheric air in comparison to the source isotope values. Allin et al. (2015) calculated the expected trend in the tropospheric isotope signature using both the measured stratospheric enrichment and the stratosphere-troposphere exchange. A constant isotope composition of emissions of CFC-11, CFC-12 and CFC-113 was assumed. Comparison of these expected trends was made to trends of $\delta(^{37}Cl)$ measured in background tropospheric samples from the Cape Grim air archive (Tasmania, 1978–2010), tropospheric firn air samples from Greenland (North Greenland Eemian Ice Drilling (NEEM) site) and Antarctica (Fletcher Promontory site). Since the projected trends based on stratospheric measurements and stratosphere-troposphere exchange agreed with tropospheric measurements, the authors concluded that within analytical uncertainties, the isotope composition of emissions has remained constant.

In terms of emissions, CFC production increased sharply and high emissions were sustained during across the 1970s and 1980s. Since the introduction of the Montreal Protocol and subsequent amendments, a decrease in emissions was observed in the late 1980s due to the reduction of CFC production. Assuming no source variations, tropospheric $\delta(^{37}Cl)$ of CFC-11, CFC-12 and CFC-11 are predicted to have increased by 1, 3 and 1 ‰ respectively, from their first release until the present day (Allin, 2015). This is due to the reduction in anthropogenic input, meaning that sink processes cause the atmospheric pool to become increasingly enriched (Montzka et al., 2011). This long term change in the atmospheric signature was calculated by Allin et al. (2015), and can be accounted for in their tropospheric measurements. Furthermore, since the data presented in this thesis is in good agreement with the data presented by Allin et al. (2015), data presented here can be said to concur with the authors' conclusions of predicted increase in isotope signature. The high measurement uncertainty of the Allin et al. (2015) data meant that it was not possible to preclude the possibility that the average emission isotope delta has not changed over time. Data presented in this thesis, with uncertainties smaller than that of Allin et al. (2015), which although again cannot rule out the possibility, however suggests that indeed the emission delta has not changed. Improved data precision, in particular for reanalysis of long-term tropospheric air archives would help confirm whether the source isotope delta has changed over time.

2.1.4 Summary

- These measurements represent a significant addition to stratospheric measurements of $\delta(^{37}Cl)$ in all three species. 51 samples from 44.4 N and 67.9 N have been measured, representing a comparable latitude to those of Allin et al. (2015) (48.1-53.4 N and 66.3-

76.2 N). The higher altitude of samples (up to 34 km compared to 20 km) meant more samples deep into the stratosphere were analysed and therefore stronger fractionation was measured.

- Improvements have been made in uncertainty values compared to Allin et al. (2015) (1.24 and 0.69 compared to 1.6 and 0.8 ‰ for mid and high latitude CFC-12 respectively. 0.46 and 0.32 compared to 0.5 and 0.4 ‰ for mid and high latitude CFC-11 respectively. 0.98 and 0.65 compared to 1.5 and 1.2 ‰ for mid and high-latitude CFC-113 respectively).
- CFC-11, CFC-12 and CFC-113 are isotopically enriched in $\delta(^{37}Cl)$ in the stratosphere by destruction processes, namely photolysis and reaction with $O(^1D)$. This confirms the findings of Allin (2015) and Laube et al. (2010).
- A new maximum value of $\delta(^{37}Cl)$ enrichment has been measured at 38±0.9 ‰
- Stratospheric samples from high- and mid-latitudes have been used to calculate the apparent isotope fractionation (ε_{App}) of all three CFCs. CFC-12 displays ε_{App} of -12.91±1.24 ‰ (mid-latitude) compared to -7.48±0.69 ‰ (high-latitude). CFC-11 shows the same correlation, -3.19±0.46 ‰ and -2.99±0.32 ‰ for mid- and high-latitude stratospheric samples respectively. However, the values are statistically indistinguishable. In the case of CFC-113 the correlation is reversed, the mid-latitude samples display apparent isotope fractionations of -1.87±0.98 ‰ whereas the high-latitude samples display an apparent isotope fractionation of --3.56±0.65 ‰. It is also possible that some source signature biased CFC-113 was observed near the troposphere since delta values were high, and there are still considerable emissions ongoing for CFC-113.
- The calculated ε_{App} values for CFC-11, CFC-12 and CFC-113 are comparable to previous studies with respect to both mid and high-latitudes, demonstrating the applicability of this technique to various regions of the stratosphere.
- The data are consistent with a constant isotope composition of emissions, as calculated by Allin et al., (2015), for all three species.

2.2 Carbon isotope composition in halocarbons CFC-11, CFC-12 and CFC-113 in stratospheric air

Measurement of $\delta(^{13}C)$ in the three species of interest is, to date, extremely limited. A single study by Redeker (2007) detailed tropospheric measurements of $\delta(^{13}C)$ in 37 species including CFC-11, CFC-12 and CFC-113 over a year long period. No diurnal and seasonal trends were apparent within their analytical uncertainty. This study represents the first $\delta(^{13}C)$ measurements at stratospheric altitudes.

Zuiderweg et al. (2012) simulated stratospheric conditions in the laboratory and determined the carbon isotope dependence of the photolysis reaction in CFC-11 and CFC-12 using broadband UVC light (190-230 m). The calculated apparent isotope fractionations were from −23.8±0.9 to −17.7±0.4 ‰ for CFC-11 and −66.2±3.1 to −51.0±2.9 ‰ for CFC-12 between 203 and 288 K. The results inferred that these CFCs should become strongly enriched in ^{13}C in the stratosphere. However, these values are likely overestimates, since they do not account for the effect of atmospheric mixing. It is expected that the observed isotope fractionation is in fact smaller than the expected value. Unphotolysed CFCs are transferred from troposphere to stratosphere, and thus diluting the overall observed isotope fractionation (Röckmann et al., 2001b, Bernard et al., 2006, Laube et al., 2010). Zuiderweg et al. (2012) suggested that the effect of mixing causes the apparent isotope fractionation to be approximately half of that observed experimentally via photolysis experiments. The basis for this value is the impact of dynamic processes, as described by Röckmann et al. (2001a). This in turn suggests stratospheric measurements would fall in the region of -11.9 to -8.9 ‰ for CFC-11, and -33.1 to -25.5 ‰ for CFC-12.

The correlations observed via photolysis experiments (Zuiderweg et al., 2012) are in agreement with the strong chlorine isotope fractionation observed by ^{37}Cl measurements in stratospheric samples as described in Section 2.1.3.2 of this thesis. Furthermore, Zuiderweg et al., (2012) suggested that due to the variations in CFC emissions due to the introduction of the Montreal Protocol, the inferred stratospheric enrichments would lead to significant temporal increase in ^{13}C content of CFCs in the troposphere. This in turn is likely to be recorded in atmospheric air archives such as firn air. To this end, Zuiderweg et al., (2013) in fact reported a large CFC-12 carbon isotope enrichment since the 1950s via analysis of firn air. Samples collected during the North Greenland Eemian Ice Drilling (NEEM) 2009 campaign displayed extreme ^{13}C depletion in CFC-12 at 65 m depth (−80 ‰ vs. VPDB) compared to present day tropospheric measurements (−40 ‰.). Zuiderweg et al., (2013) reconstructed atmospheric measurements back to 1950 AD suggesting even larger depletions of up to -120 ‰. This suggests massive enrichment of

tropospheric air compared to the present day. The authors suggest that this may be attributed to a large change in the isotopic composition of anthropogenic CFC-12 emissions, however they acknowledge that direct evidence is lacking.

Allin (PhD Thesis, 2015) carried out measurements in firn air samples for comparison with modelled expectations. The same firn air samples from NEEM (Greenland) as measured by Zuiderweg et al., (2013) were used to infer an atmospheric history of ^{13}C in CFC-11, CFC-12 and CFC-113. Within the analytical uncertainties, there is good agreement between the modelled change in $\delta(^{13}C)$ and the firn air measurements. Again this suggests a source signature which is constant. There is therefore, a large discrepancy between the firn air measurements of Zuiderweg, and those of Allin. In fact, there are large differences in the way that the data have been treated and presented. Importantly, since Zuiderweg (2013) combusted CFC-12 to CO_2 for IRMS analysis, they are able to quote measurements to the international Vienna Pee Dee Belemnite (VPDB) scale. Allin measured fragment ions directly, for which there is no internationally recognised scale. It is possible that there is a bias between the analytical systems. To this end, chapter 3 details analysis of the photolysis samples prepared by Zuiderweg et al., (2012), using the Autospec instrument as used by Allin (2015) for the firn air measurements. This allows measurements using the Autospec instrument to be linked to the VPDB scale for direct comparison.

Allin (PhD Thesis, 2015) used the carbon dependence of the photolysis sink reaction in CFC-11 and CFC-12 calculated by Zuiderweg et al., (2012) to reconstruct expected long term changes in the tropospheric ^{13}C signatures. A constant source $\delta(^{13}C)$ value was assumed for both CFC-11 and CFC-12. The $\delta(^{13}C)$ correlations in CFC-11 and CFC-12 predicted by Allin (PhD Thesis, 2015) are small due to the long atmospheric lifetimes, and can be accounted for in tropospheric measurements. Allin predicts that from their first release until the present-day, CFC-11 and CFC-12 $\delta(^{13}C)$ values have increased by 4 and 5 ‰, respectively. The measurements carried out by Allin, therefore, do not support the changing emission scenario suggested by Zuiderweg et al., (2012).

Neither Allin nor Zuiderweg investigated the carbon isotope emissions history of CFC-113. It is expected that CFC-113 will display a similar enrichment profile to that of CFC-11 and CFC-12.

2.2.1 Research objectives

A small number of measurements of $\delta(^{13}C)$ in CFCs in the troposphere and from firn air currently exist. This study will represent the first carbon isotope ratio measurements in CFC-11, CFC-12

and CFC-113 at stratospheric altitudes. These measurements aim to give better understanding to the following questions:

1. Does $\delta(^{13}C)$ in CFC-11, CFC-12 and CFC-113 display the expected enrichment with altitude and can a latitude dependence be observed? Do they agree with modelled expectations?
2. Do real air stratospheric measurements of $\delta(^{13}C)$ agree with that suggested by Zuiderweg from photolysis experiments? Are Zuiderweg's measurements representative of atmospheric samples or do they overestimate enrichments? If data presented by Zuiderweg display larger $\delta(^{13}C)$ than stratospheric measurements from this study, does the discrepancy fit with the idea of the observed isotope fractionation being half as large in magnitude as photolysis estimates?
3. Once studies by Zuiderweg and Allin are presented relative to the VPDB scale, are the studies statistically significant?
4. Since Zuiderweg acknowledges that there is no direct evidence for massive enrichment in tropospheric air compared to today, is the modelled prediction suggested by Allin a more likely scenario?

2.2.2 Experimental methods

The analysis of $\delta(^{13}C)$ in CFC-11, CFC-12 and CFC-113 required adjustments to be made to the method outlined in Section 2.1.2. The Autospec instrument was used along with the same inlet procedure and chromatography required for $\delta(^{37}Cl)$ analysis, but parameters were adjusted to optimise measurement conditions for $\delta(^{13}C)$. Details of adjustments can be found below.

2.2.2.1 Sample collection

The same stratospheric samples were analysed for $\delta(^{13}C)$ as for $\delta(^{37}Cl)$ measurements. Eleven samples were collected from upper tropospheric and stratospheric balloon air samples from 8.3-34.4 km were collected at a mid-latitude site (Gap, France, 44.4°N) during March and April 1999. In addition, 39 samples were collected at Kiruna, Sweden in 2010. This gave a total of 50 samples for $\delta(^{13}C)$ analysis.

2.2.2.2 Chromatography

The column and chromatography remained identical to that used during the $\delta(^{37}Cl)$ analysis. However, a possible bias was identified in the form of HCFC-21, which elutes just before the CFC-11 peak, which although small, is significant for *m/z* 102. It was ensured that the baseline was flat before the start of the CFC-11 peak, and so no chromatographic interferences were present close to the retention times related to CFC-11.

2.2.2.3 MS parameters and set up

The ^{13}C isotope is naturally in lower abundance than ^{37}Cl, at 1.11% of the total carbon compared to 24.23 % of total chlorine, and hence the $^{13}C^{35}Cl_2F^+$ peak is much smaller than the $^{12}C^{35}Cl^{37}ClF^+$ peak. Alterations to the method were necessary to mitigate for the fact that the smaller peak area of $^{13}C^{35}Cl_2F^+$ would have an adverse effect on the precision values.

In order to increase the peak area corresponding to the $^{13}C^{35}Cl_2F^+$ fragment three parameters were modified. Firstly, in samples containing a low abundance of sample, the sample trapping amount was increased from 215 mL up to a maximum of 600 mL.

The slits define the width of the ion beam in the Y plane as it enters the source slit (the electrostatic analyser), and additionally when it leaves the second source slit. The sensitivity of the instrument can be increased by modifying the position of the source slits. The increase in sensitivity was quantified by monitoring the size of the hexadecane peak as the source slits were modified.

In addition, the functions which corresponded to the species of interest CFC-11, CFC-12 and CFC-113 were modified to amplify the peaks and so improve uncertainties. This was done by increasing the detector voltage from 375 V to 400 V. In the case of CFC-11 however, the higher abundance meant that the CCl_2F^+ fragment produced by CFC-11 gave a larger peak than for CFC-12 and CFC-113. In the case of CFC-11, this was sufficiently large to saturate the detector and so the detector voltage was reduced to 375 V.

It was seen that increasing the detector voltage and slit parameters increased the sensitivity of the instrument and also decreased the mass resolution to between 500 and 700 from approximately 1000. This meant that measurements were more sensitive to interferences. In the case of CFC-11 and CFC-12 no known interferences were measured, however CFC-113a partially co-elutes with CFC-113. In samples where CFC-113a was detected above that of the surrounding noise the start of the CFC-113 peak was determined only at a retention time after the end of the CFC-113a peak. This excluded the possibility of bias from this interference.

2.2.2.4 Calculation of isotope ratios $(\boldsymbol{R})$

The isotope delta (δ) is used to denote the $^{13}C/^{12}C$ ratio difference in CFCs in an air sample relative to a standard was calculated using the equation:

$$\delta(13C) = \frac{R_{Sample}}{R_{Standard}} - 1 \qquad \text{Equation 2.5}$$

Where R represents the $^{13}C/^{12}C$ ratio of abundance in a sample or a standard. Delta values are expressed in per mill (‰).

Currently, there is no link between measurements made and an internationally recognised isotope standard which can be used in measurements of $\delta(^{13}C)$. Chapter 3 addresses this issue and attempts to link data in this thesis to the Vienna Pee Dee Belemnite (VPDB) scale. All delta values in this current chapter are described relative to an in-house laboratory standard for comparison (AAL-071170), comprising tropospheric background air collected in 2006 at Niwot Ridge, Colorado, by the National Oceanic and Atmospheric Administration (NOAA).

Calculation of carbon isotope ratios was carried out using the same method as for $\delta(^{37}Cl)$. The linear regression slope of one carbon isotopologue against another is used to calculate isotopologue ratios as with $\delta(^{37}Cl)$ analysis. An example plot of chromatographic peaks of isotopologues of CFC-12 and the plot displaying the linear regression slope of one isotopologue against another is shown in Figure 2.19.

As described above, with respect to CFC-11, the CCl_2F^+ fragment is the most abundant. This ion fragment is used rather than directly measuring Cl^+ ions as this fragment results larger peaks than fragmented Cl^+ ions, giving better measurement precision. In the case of CFC-12, the most abundant fragment is CF_2Cl (m/z 85), but using the CCl_2F^+ fragment eliminates interferences. Similarly, using the CCl_2F^+ for CFC-113 analysis minimises the influence of the isomer CFC-113a.

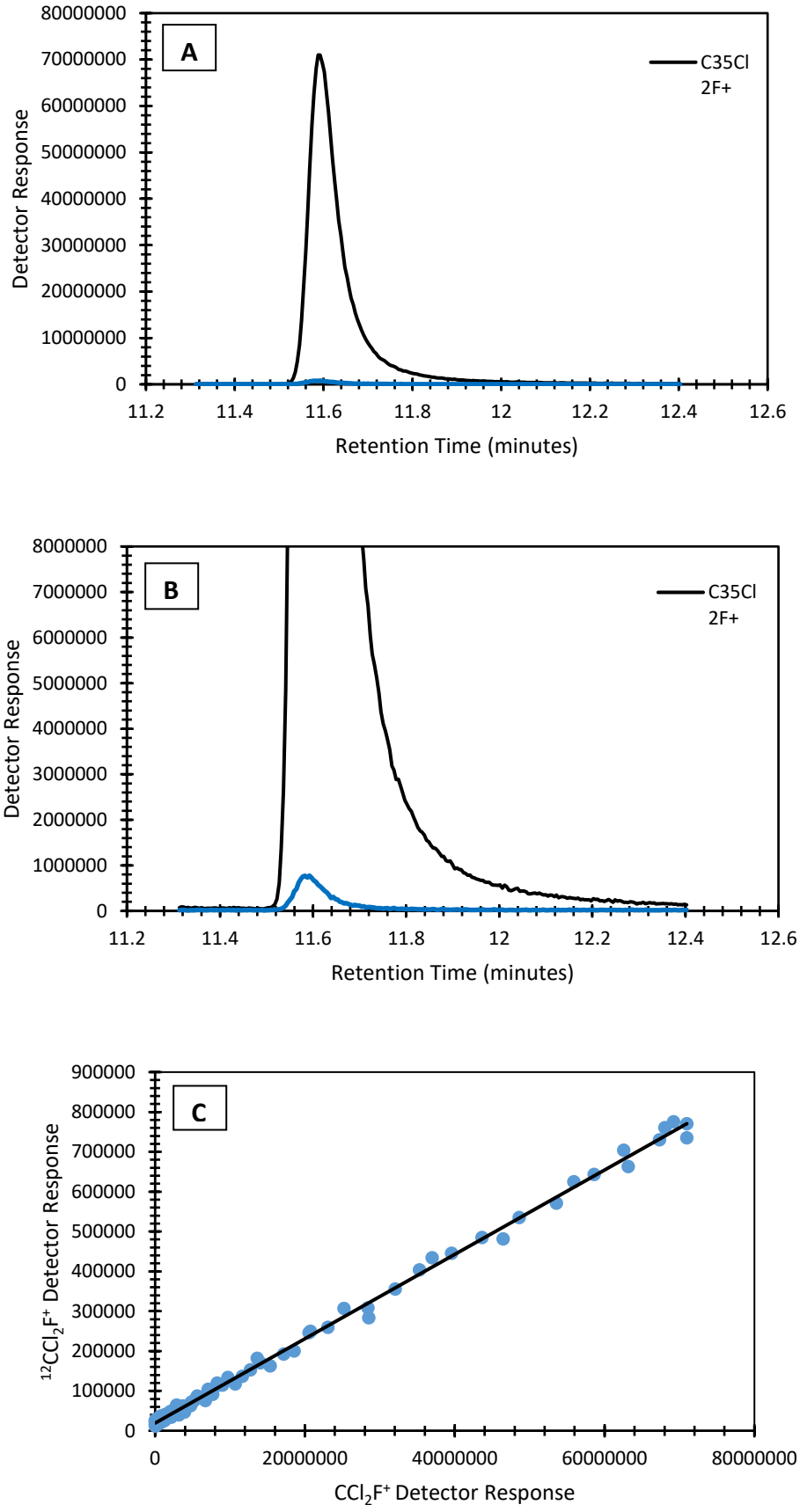

Figure 2.19. Example plots of chromatographic peaks of isotopologues of CFC-12, panel B a zoom of panel A, and the linear regression slope of one isotopologue against another.

The additional fragment ions corresponding to $\delta(^{13}C)$ analysis in CFC-11, CFC-12 and CFC-113 are shown in Table 2.4.

Table 2.4. Fragment ions corresponding to $\delta(^{13}C)$ analysis in CFC-11, CFC-12 and CFC-113, with *m/z* values detected by the Autospec.

Species for analysis	Ion Fragment	*m/z*
CCl_2F_2 (CFC-12)	CCl_2F^+	101
	$^{13}CCl_2F^+$	102
CCl_3F (CFC-11)	CCl_2F^+	101
	$^{13}CCl_2F^+$	102
$CF_2ClCFCl_2$(CFC-113)	CCl_2F^+	101
	$^{13}CCl_2F^+$	102

2.2.3 Results and discussion

2.2.3.1 Determination of non-linearities

As with analysis of $\delta(^{37}Cl)$, samples from both campaigns had a wide range of CFC mole fractions for all three species of interest. It was therefore necessary to determine whether the measured isotope ratio of a sample is dependent on its mole fraction. An air sample collected at Niwot Ridge in 2009 (SX-0706077) was diluted with nitrogen into three-litre Silco-treated stainless steel containers. Dilutions were monitored using pressure sensors, to give a series of dilutions with a wide range of mole fractions, representative of the range found in the samples analysed in this chapter. The dilution series was analysed using the identical measurement procedures to the stratospheric samples, as well as the in house standard (AAL-071170). As with analysis of $\delta(^{37}Cl)$, the dilution series was analysed twice, once using each chromatography column to eliminate effects of either analytical column on the data.

Measurements of $\delta(^{13}C)$ (‰) are given relative to the same standard used for the stratospheric samples (AAL-071170). Data as shown in Figures 2.20 to 2.22, shows the effect of sample size on $\delta(^{13}C)$ for CFC-12, CFC-11 and CFC-113.

CFC-12

Analysis of the dilution series for CFC-12 using the GasPro and Alplot column, Figure 2.20, revealed that, with respect to $\delta(^{13}C)$, delta values derived from the smallest peak areas are erroneously low (Figure 2.20 (A)). In comparison to $\delta(^{37}Cl)$ measurements, the $\delta(^{13}C)$ non-linearities are more significant. As with $\delta(^{37}Cl)$ measurements, a $\delta(^{13}C)$ measurement is rejected if the standard deviation of this repeat analysis was greater than twice that of the standard. One dilution series measurement using the GasPro column was discarded, and two from the AlPlot column based on this criteria. The remaining samples all displayed peak areas in the region of isotope delta bias and were corrected based on the linear regression plotted as shown in Figure 2.20 (B). A regression line was drawn to track the depletion across the smallest peak areas. The samples requiring correction were corrected based on their peak areas.

CFC-11

Analysis of the dilution series for CFC-11 using the GasPro and Alplot column, Figure 2.21 (A), again showed isotope delta bias for the lowest abundance samples. Two samples each from GasPro and AlPlot columns were discarded due to higher than average uncertainties. Samples of peak areas which fell in the region of non-linearity were corrected based on the linear regression as shown in Figure 2.21 (B). No correction was required for the remaining samples since peak areas displayed no instrument bias.

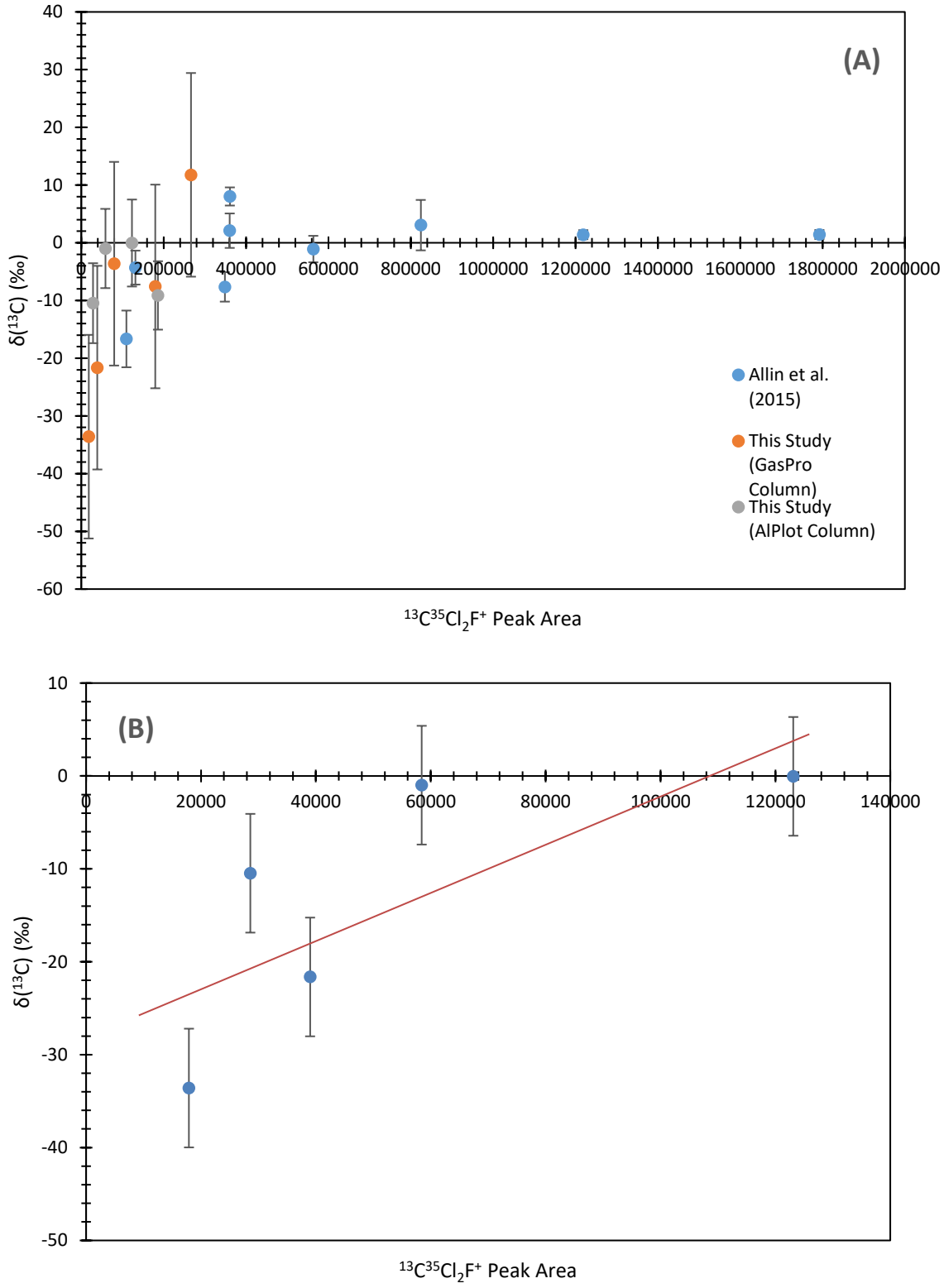

Figure 2.20. (A) Measured δ(^{13}C) plotted against peak area of the $^{13}C^{35}Cl_2F^+$ fragment ion (*m/z* 102) for CFC-12. Alplot column and GasPro column measurements have been combined. 1σ standard deviation error bars are shown. **(B)** Expanded section displays region of depleted δ(^{13}C) values with corresponding linear regression line used for data correction. Delta values relative to standard AAL-071170.

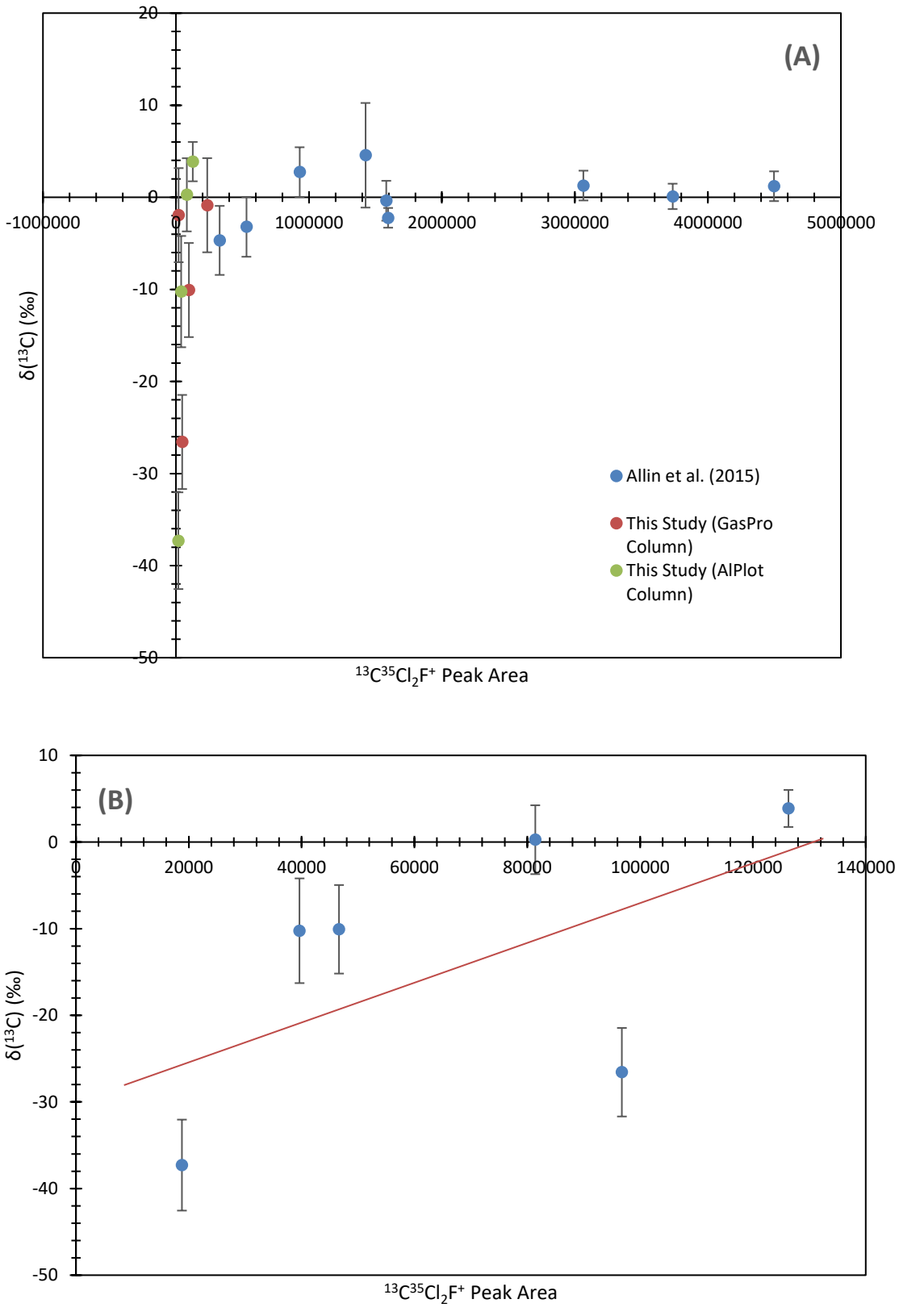

Figure 2.21. (A) Measured $\delta(^{13}C)$ plotted against peak area of the $^{13}C^{35}Cl_2F^+$ fragment ion (*m/z* 102) for CFC-11. Alplot column and GasPro column measurements have been combined. 1σ standard deviation error bars are shown. **(B)** Region of depleted $\delta(^{13}C)$ values with corresponding linear regression line used for data correction. The two most depleted value for the AlPlot column and the two most depleted GasPro column values have been removed for clarity. Delta values relative to standard AAL-071170.

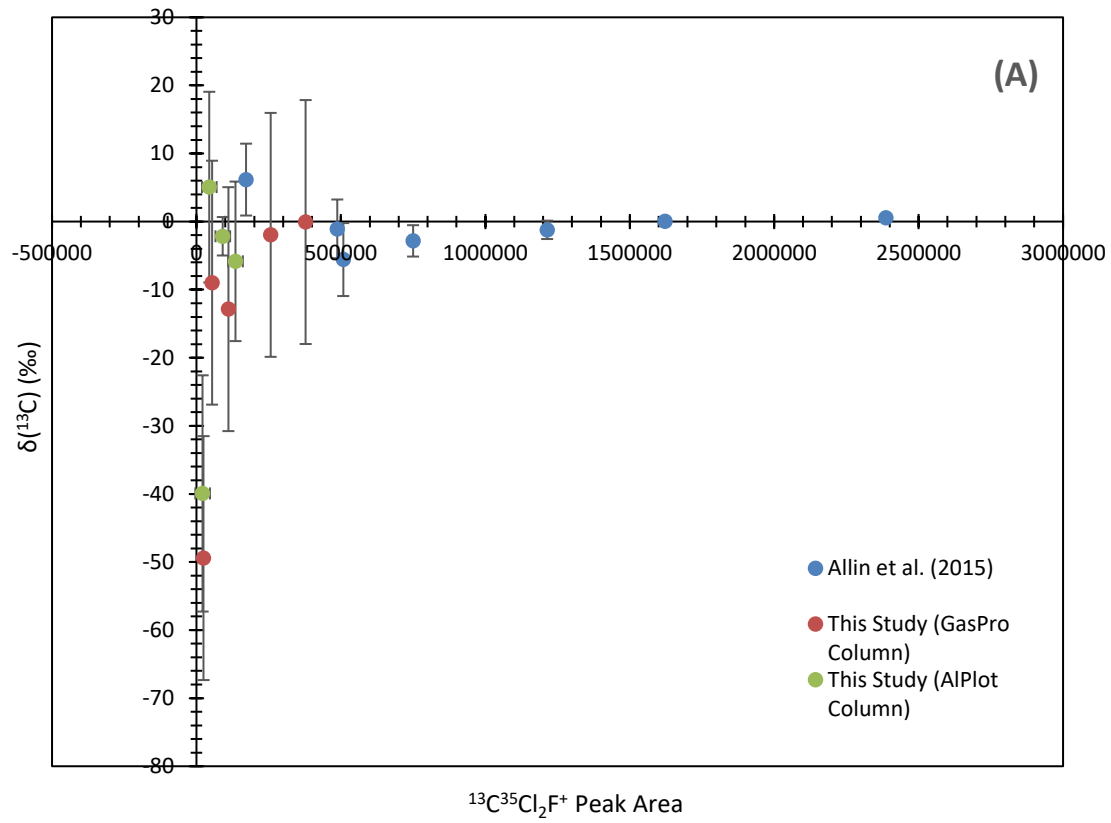

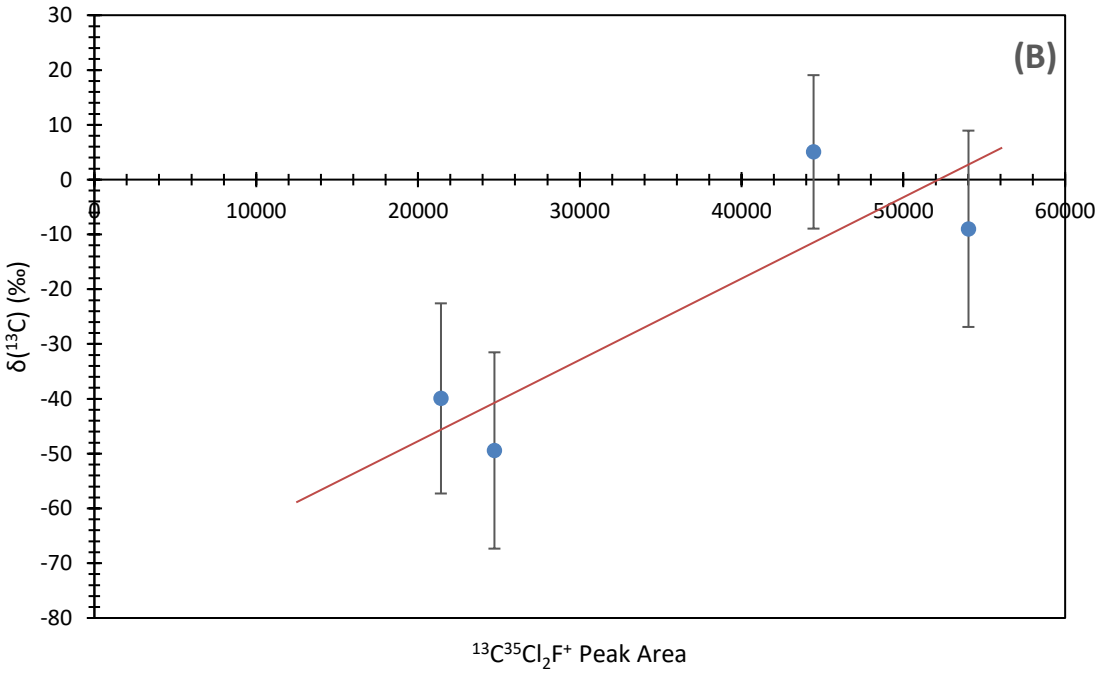

Figure 2.22. (A) Measured δ(^{13}C) plotted against peak area of the $^{13}C^{35}Cl_2F^+$ fragment ion (*m/z* 102) for CFC-113 using Alplot column and GasPro column. 1σ standard deviation error bars are shown. **(B)** Region of depleted δ(^{13}C) values with corresponding linear regression line used for data correction. Delta values relative to standard AAL-071170.

CFC-113

Figure 2.22 shows that delta values derived from the smallest peak areas exhibit larger than average uncertainties and erroneously low $\delta(^{13}C)$ values for CFC-113. One measurement using the GasPro column and two from analysis using the AlPlot column were discarded due to high uncertainty values. Samples with peak areas in the region where the dilution series showed analytical bias were corrected using the linear regression as shown in Figure 2.22.

Effect of trapping rate on non-linearity

The amount of trace gases trapped cryogenically from whole air was not constant over the measurement period. The majority of the stratospheric samples were analysed using the AlPlot column. In this case, a small amount of sample was trapped 25 Torr (167 mL) to ensure the column was not overloaded with CO_2. A small number (8 samples) was analysed using the Agilent GS-GasPro column (length 30 m, ID 0.32 mm), which allowed trapping of a larger amount of sample 80 Torr (537.5 mL). Where a larger amount of sample was trapped, the rate of trapping was increased to allow for more samples to be processed in the same period.

The effect of trapping rate on the peak area and $\delta(^{13}C)$ was investigated to ensure linearity. Analysis was carried out on a sample of 547 mL at 5 trapping rates between 0.3 mL and 1.3 mL per second.

Figure 2.23 shows the effect of trapping rate on peak area and on $\delta(^{13}C)$ of CFC-12, which is the most volatile of the three CFCs. It can be seen that the rate at which the sample is trapped has no effect on either parameter and no corrections to the data were required.

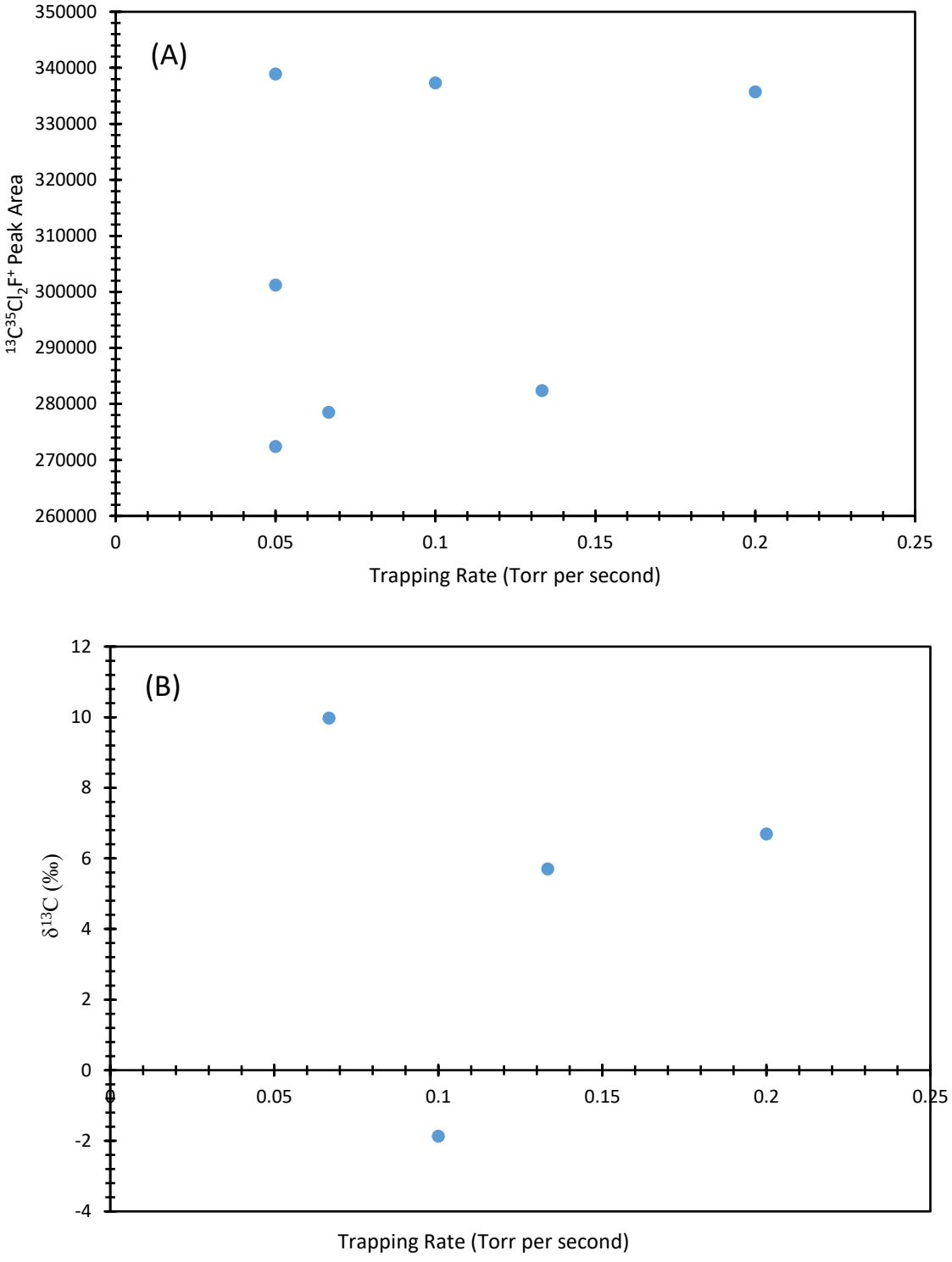

Figure 2.23. Plots of: **(A)** Trapping rate of standard (AAL_071170) (Torr per second) vs. CFC-12 $^{13}C^{35}Cl_2F^+$ Peak Area; **(B)** Trapping rate of standard (AAL_071170) (Torr per second) vs. $\delta^{13}C$ (‰). Delta values relative to standard AAL-071170.

2.2.3.2 Stratospheric samples

Stratospheric air samples have been analysed from both the Kiruna campaign and from balloon flights above Gap, France for $\delta(^{13}C)$ in CFC-12, CFC-11 and CFC-113. As with $\delta(^{37}Cl)$ measurements of $\delta(^{13}Cl)$ from Kiruna and Gap agree well, and show an expected increase in isotope enrichment with age of air.

Apparent Isotope fractionations (ε_{App})

The isotope dependence of CFC-12, CFC-11 and CFC-113 on the sink reactions, photolysis and reaction with $O(^1D)$ is shown by Rayleigh Fractionation plots given in Figures 2.24 to 2.26. After discarding samples, 46 samples remained for CFC-12 analysis, 29 for CFC-11 and 34 for CFC-113.

Calculation of ε_{App} was established by calculating the slope of the data plotted. In all three cases, negative ε_{App} values were derived, suggesting that molecules containing lighter isotopes, in this case ^{12}C, are broken down more quickly giving an enrichment in the heavier isotope (^{13}C) with age of air.

In the case of CFC-12, the calculated ε_{App} is -19.31±3.88 ‰, and -23.58±6.58 ‰ for the Kiruna and Gap samples respectively. CFC-11 shows a similar profile, but with much smaller values for ε_{App} at -4.49±2.76 ‰ for Kiruna samples and -7.38± 5.71 ‰ for the Gap samples. CFC-113 displays an ε_{App} of -5.98 ± 2.77 ‰ for Kiruna samples and -8.75± 5.53 ‰ for the Gap samples. In all instances, the negative ε_{App} value indicates that sink processes give rise to fractionation which gives enrichment in $\delta(^{13}C)$.

It can be seen that there is likely an effect of latitude on the apparent carbon isotope fraction all three CFCs. As with $\delta(^{37}Cl)$ measurements, the mid latitude samples display a higher ε_{App} than the corresponding high latitude samples for CFC-12 and CFC-11. Interestingly, although $\delta(^{13}C)$ measurements in CFC-113 display this pattern, measurements of $\delta(^{37}Cl)$ displayed the reverse. However, since these measurements represent the first $\delta(^{13}C)$ isotope measurements in stratospheric CFC-12, CFC-11 and CFC-113, the uncertainties are large, and thus in fact it cannot be concluded categorically that there is significance between latitudes within 1σ.

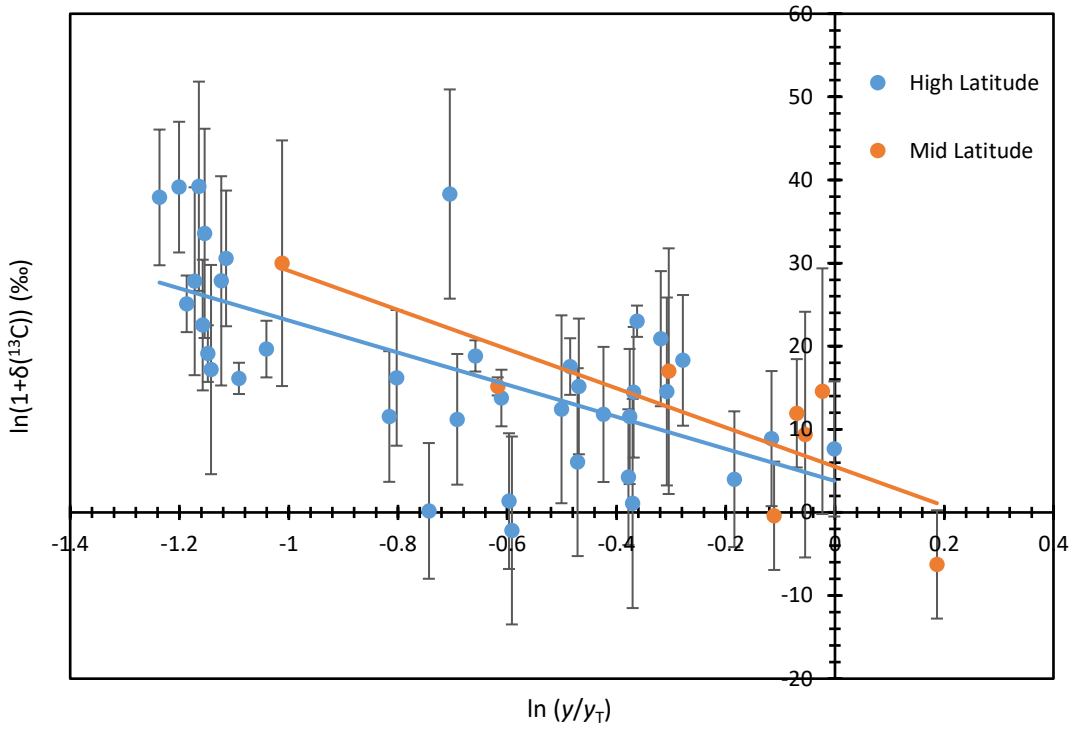

Figure 2.24. Rayleigh fractionation plot of CFC-12 carbon isotope signatures, derived from high and mid-latitude stratospheric samples Kiruna, Sweden and Gap, France respectively. Trend lines correspond to apparent isotope fractionations (ε_{App}) of is -19.31±3.88 ‰, (Kiruna), and -23.58±6.58 ‰ (Gap) The standard error of the gradient is quoted for ε_{App} values.

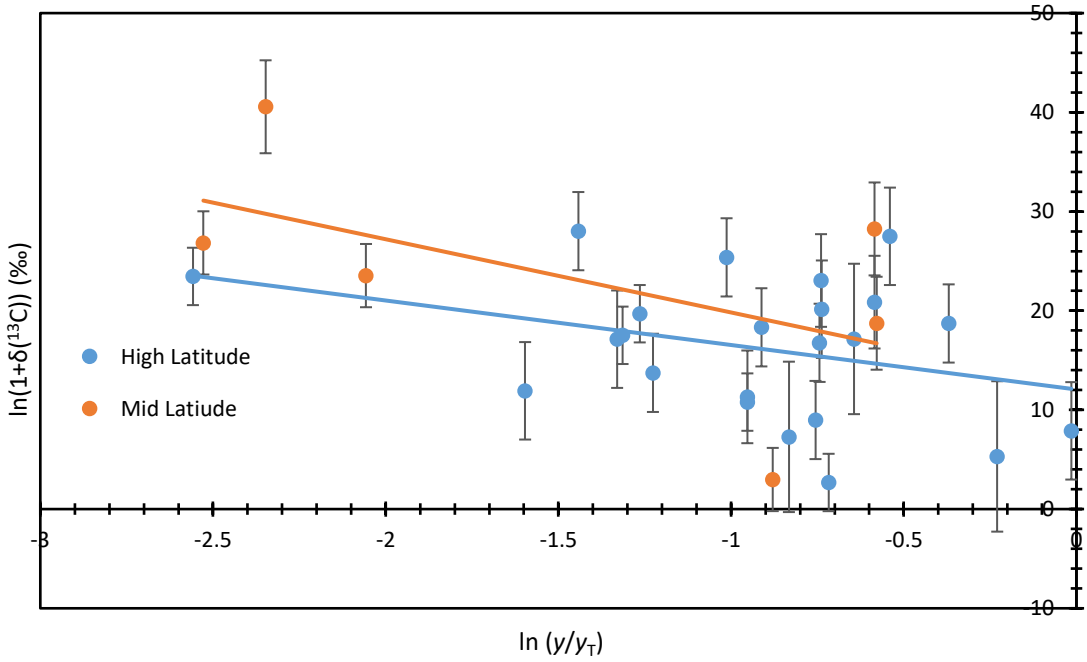

Figure 2.25. Rayleigh fractionation plots of CFC-11 carbon isotope signatures, derived from mid and high-latitude stratospheric samples, Gap and Kiruna respectively. Trend lines correspond to apparent isotope fractionations (ε_{App}) -4.49±2.76 ‰ (Kiruna), -7.38± 5.71 ‰ (Gap). The standard error of the gradient is quoted for ε_{App} values.

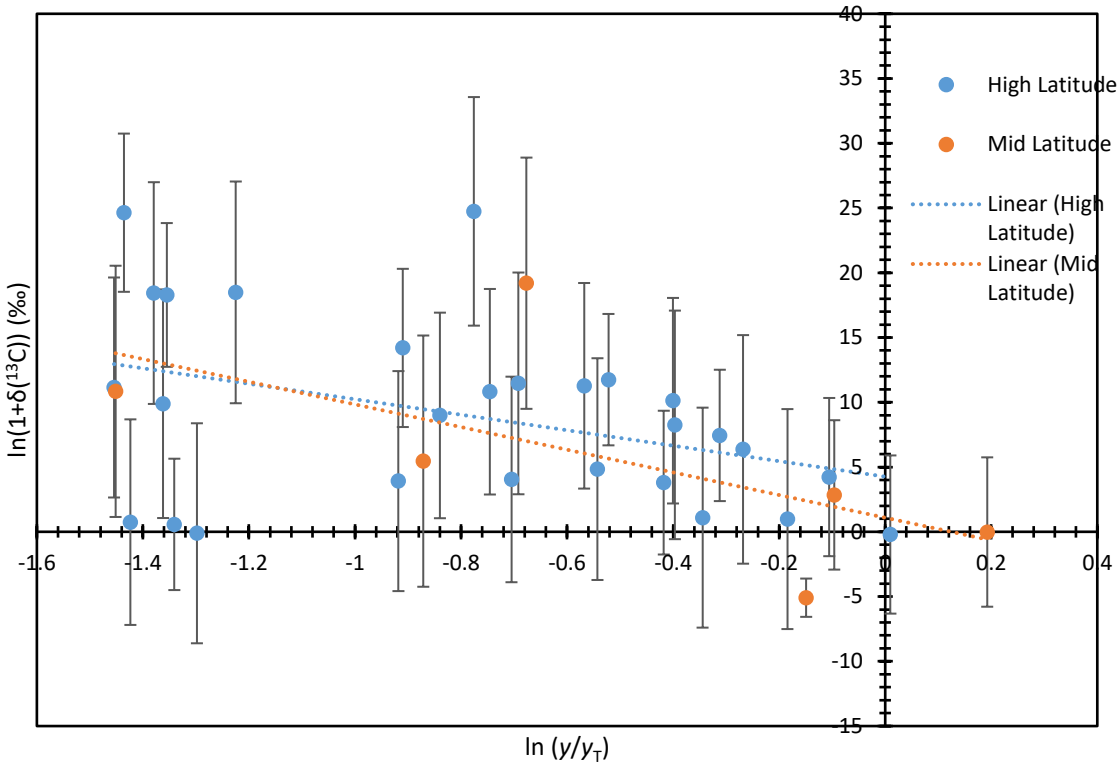

Figure 2.26. Rayleigh fractionation plots of CFC-113 carbon isotope signatures, derived from mid and high-latitude stratospheric samples, Gap and Kiruna respectively. Trend lines correspond to apparent fractionations (ε_{App}) of -5.98 ± 2.77 ‰ (Kiruna), -8.75± 5.53 ‰ (Gap). The standard error of the gradient is quoted for ε_{App} values.

Comparison to previous studies

No other studies to date detail measurements of ^{13}C in CFC-11, CFC-12 and CFC-113. Data from this study demonstrate significant ^{13}C enrichment in the stratosphere for CFC-11, CFC-12 and CFC-113, in agreement with the fractionation observed in laboratory photolysis experiments by Zuiderweg et al., (2012). However, the calculated ε_{App} value is significantly lower in magnitude than that of Zuiderweg. High- and mid-latitude samples (this study) had ε_{App} values of -4.49±2.76 ‰ and -7.38± 5.71 ‰ compared to the range −23.8±0.9 to −17.7±0.4 ‰ for CFC-11. CFC-12 gave values of 19.31±3.88 ‰, and -23.58±6.58 ‰ compared to and −66.2±3.1 to −51.0±2.9 ‰. It is important to note that the laboratory based results from Zuiderweg do not allow insights into any discrepancy between high and mid latitudes, and the ε_{App} given denotes values calculated at stratospherically relevant temperature ranges rather than latitude variations. Zuiderweg suggest that due to the effects of mixing in stratospheric air masses, the value of ε_{App} measured experimentally may be half that as suggested via photolysis experiments. This suggests stratospheric measurements would fall in the region of -11.9 to -8.9 ‰ for CFC-11, and -33.1 to -25.5 ‰ for CFC-12. For CFC-11, high latitude stratospheric measurements from this thesis still

fall outside of this predicted range, yet mid-latitude measurements are in agreement within 1σ. In the case of CFC-12, the same pattern is evident, the high latitude ε_{App} does not agree, yet mid-latitude values with a stronger enrichment profile agree within 1σ. It is important to note that although the laboratory based samples analysed by Zuiderweg contain both CFC-11 and CFC-12 which undergoes photolysis as in the stratosphere, the samples contain significantly larger quantities of both CFCs compared to samples collected in the stratosphere and analysed in this study. This means that there is possibility that molecules might recombine in the reactor resulting in bias in epsilon, which has been observed for other trace gases (Kaiser, 2008).

Implications in the wider context

The enrichment of ^{13}C in stratospheric air in turn is expected to give rise to enrichment in the troposphere. Zuiderweg et al., (2013) detailed a large ^{13}C enrichment in CFC-12 of firn origin over time, yet the conclusions of Allin (PhD Thesis, 2015) do not agree. There is a large discrepancy between data sets. Data from this study does demonstrate enrichment of ^{13}C in stratospheric air, yet does not agree with the attribution by Zuiderweg et al., (2013) to a large change in the isotopic composition of anthropogenic CFC-12 emissions. It is more likely therefore that emissions have remained close to isotopically constant over time.

Chapter 3 details the linking of both measurements made using the Autospec instrument at UEA, with that used by Zuiderweg to the international VPDB scale in order to eliminate or confirm the possibility of instrument bias.

2.2.4 Summary

- The first measurements of $\delta(^{13}C)$ of CFC-11, CFC-12 and CFC-113 at stratospheric altitudes have been carried out.
- All CFCs display isotopic enrichment in the stratosphere, likely due to fractionation by destruction processes. Enrichment in $\delta(^{13}C)$ increases with altitude.
- Apparent isotope fractionation for mid-latitude samples, ε_{App}, is calculated to be -23.58±6.58 ‰ (CFC-12), -7.38± 5.71 ‰ (CFC-11) and -8.75± 5.53 ‰ (CFC-113). For high-latitude samples, ε_{App}, is calculated to be -19.31±3.88 ‰ (CFC-12), -4.49±2.76 ‰ (CFC-11) and -5.98 ± 2.77 ‰ (CFC-113).
- Values of apparent isotope fractionation from this study are significantly lower than that given by Zuiderweg et al., (2012) (−66.2±3.1 to −51.0±2.9 ‰ CFC-12, −23.8±0.9 to −17.7±0.4 ‰ for CFC-11). However, Zuiderweg suggest that due to mixing and transport processes acting upon real sir samples, the measured stratospheric values are likely to

be half in magnitude compared to the published values. In this case, high latitude stratospheric measurements for both CFC-11 and CFC-12 from this thesis still fall outside of this predicted range, yet mid-latitude measurements are in agreement within 1 σ.

- Minimal correlation is observed between latitude and apparent isotope fractionation.
- Measurements made during this study do display enrichment of ^{13}C within the stratosphere, which in turn will cause enrichment in the troposphere. However, it is unlikely that the magnitude of enrichment is a great as that proposed by Zuiderweg et al., (2013).
- A constant isotopic source signature is suggested for emissions.

Chapter 3: Photolysis rates of CFC-12, and linkage to recognised ^{13}C calibration scale

Improved quantification of source and sink processes of CFCs leads to further understanding of atmospheric budgets. Since CFCs are responsible for both stratospheric ozone depletion as well as contributing to global temperature increase (IPCC, 2014), information related to sink processes may indicate ozone recovery rates and future warming effects.

As discussed in Chapters 1 and 2, CFCs are released at the Earth's surface and are transported through the troposphere to stratospheric altitudes. Here, in the stratosphere, they are subject to breakdown by photolysis and reaction with $O(^1D)$. Photolysis by short wave ultraviolet radiation produces free chlorine which contributes significantly to ozone depletion. Of the two loss processes, photolysis is the most significant for CFC-11, CFC-12 and CFC-113 (Laube et al., 2010). With respect to CFC-12, 93-96 % of breakdown is via photolysis, whilst reaction with $O(^1D)$ comprise the remaining 4-7 % (Patra and Lal, 1997) and is a function of the amount of incoming solar radiation, as well as the available CFC. Both of these parameters are altitude-dependent.

3.1 The photolysis process

Photolysis involves cleavage of one or more covalent bonds within a molecule, caused by absorption of a photon. Since this process is reliant on solar radiation as an energy source to overcome the bond activation energy, the rate of photolysis is directly proportional to the available light, or actinic flux, in the stratosphere. The photolysis rate coefficient, *J*, is also dependent on the wavelength of the incoming solar radiation, and the absorption cross section of the molecule as seen in Equation 3.1.

$$J = -\frac{\ln(F)}{t} \qquad \text{Equation 3.1}$$

The isotope fractionation, ε, is a combination of the total isotope fractionation effects. In relation to fractionation caused by photolysis alone, it is expressed by Equation 3.2, where *J* is again the photolysis rate coefficient, I is the actinic flux, σ the absorption cross section, and λ the wavelength.

$$\varepsilon(\lambda) = \frac{J_{Heavy}}{J_{Light}} - 1 = \frac{I(\lambda)\sigma_{Heavy}(\lambda)}{I\,(\lambda)\sigma_{Light}\,(\lambda)} - 1 = \frac{\sigma_{Heavy}(\lambda)}{\sigma_{Light}(\lambda)} - 1 \qquad \text{Equation 3.2}$$

Constraining the isotope fractionation caused by photolysis allows for better understanding and quantification of the transport and stratospheric removal processes of species depleted in the stratosphere.

It is relevant to discuss the photochemical fractionation of N_2O in the context of this chapter, since it is broken down in the stratosphere via the same processes as CFC-12 (Kaiser et al., 2004, Brenninkmeijer et al., 2003, Cliff et al., 1999b), by photolysis and reaction with $O(^1D)$. By extension, as seen in Chapter 2, both CFC-11 and CFC-113 demonstrate a similar enrichment in ^{13}C and ^{37}Cl with increasing altitude (Allin, 2015), and so are likely to undergo similar destruction processes. Assuming analogous chemistry between N_2O and CFC-12, CFC-11 and CFC-113, it could be suggested that the magnitude of photochemical fractionation could be twice as large as the apparent isotope fractionation.

3.2 Quantification of isotopic fractionation due to photolysis in CFCs

To date, a small number of studies have investigated the isotope fractionation in stratospheric sink reactions of CFC-11, CFC-12 and CFC-113.

As described in Chapter 2, with respect to CFC-12, Laube et al. (2010) and Allin (2015) detailed the increase in ^{37}Cl isotope enrichment in stratospheric samples with decreasing mixing ratio. The same correlation emerged for CFC-11 and CFC-113 in Allin's study. Furthermore, data provided in Chapter 2 of this thesis confirmed these correlations in samples at higher altitudes than demonstrated to date.

With respect to ^{13}C measurements, Redeker et al. (2007) described isotope fractionation in tropospheric measurements of 37 species including CFC-11, CFC-12 and CFC-113. Allin (2015) detailed firn air measurements of carbon isotopes (Chapter 2), giving an indication of isotopic composition over time. These firn measurements agree well with tropospheric air samples, and projected changes in isotopic composition are within the analytical uncertainties. An isotopically invariant source signature is suggested. Chapter 2 of this thesis gives the first carbon isotope ratio measurements of CFC-11, CFC-12 and CFC-113 in stratospheric samples.

Although these studies provide evidence of isotope fractionation caused by sink processes, there is no distinction between fractionation caused by photolysis or by reaction with $O(^1D)$. To improve understanding of CFC sink processes, and therefore improve the quantification of the

proportion of fractionation caused by photolysis and that caused by reaction with $O(^1D)$, further measurements are required. It has been suggested that photolysis accounts for approximately 97 % of the sink process, and reaction with $O(^1D)$ 3 % for CFC-12. To this end, a small number of recent studies attempted to determine the fractionation in CFCs caused by photolysis alone.

Firstly, Lockhart (2010) was the first to address the chlorine isotope fractionation of CFC-12 under ultraviolet photolysis. Photolysis took place on a CFC-12 mixture under laboratory conditions. It was hoped that the comparison of this experimental fractionation with the fractionation observed in stratospheric air could be used to quantify the relative contributions of both atmospheric transport and the kinetic isotope effect to the overall fractionation. The fractionation constant determined from the gradient of a Rayleigh fractionation plot was given as 20.25±6.81 ‰ at 233 K. However, although the data showed significant chlorine isotope fractionation, there were significant experimental uncertainties, and hence a large uncertainty regarding the accuracy of the fractionation constant calculated.

The temperature and wavelength dependence of chlorine isotope fractionation in CFC-12 in a photolysis reaction simulation was investigated by Martin (2011). Fractionation constants were determined to be -7.1±0.8 ‰ at 288 K compared to -12.0±0.9 ‰ at 233 K. These results agree well with the prediction based on zero point energy theory (ZPE), which suggests that a lower temperature results in higher isotope fractionation. Fractionation constants are similar to the stratospheric measurements of 12.1±1.7 ‰ carried out by Laube et al. (2010). Although measurements were in good agreement to those determined via real air samples, it was not possible to summarise the effect of temperature on isotope fractionation since only two temperatures had been investigated. Further investigations regarding this apparent correlation are required.

The use of a scavenger was included in work by Maxwell (2012), when investigating ^{37}Cl isotope fractionation during photolysis of CFC-12. Again this was performed via laboratory experiments at three stratospherically relevant temperatures, this time with the use of ethane as a scavenger to prevent recombination reactions. The fractionation constants were determined to be -8.4±0.5 ‰, -11.3±2.4 ‰ and -14.0±2.1 ‰ at 288, 233 and 203 K, respectively. Since this data agrees well with previous studies, as described above, this suggests chlorine radical recombination with CFC-12 does not occur and previous results from experiments carried out at comparable concentrations are accurate. However, it is expected that the isotope fractionation caused by photolysis in real stratospheric data to be of smaller magnitude than this photolysis study due to transport and mixing, and hence is not directly representative of atmospheric

samples. It is important to note that those carried out by Zuiderweg et al. are not at comparable CFC concentrations, as discussed further below.

Zuiderweg et al. (2012) described ^{13}C apparent isotope fractionation in laboratory based photolysis of samples containing CFC-11 and CFC-12. The UV-photolysis of such samples enabled ^{13}C kinetic isotope fractionations of CFC-11 and CFC-12 to be measured. Photolysis of samples over 0-3 hours at 0.5 hour intervals gave an indication of the strong $\delta^{13}C$ gradient with decreasing mixing ratio caused by photolytic breakdown. This correlation agrees qualitatively with the expectation from the ^{37}Cl gradient with decreasing altitude as seen in real stratospheric air samples by Laube et al. (2010). The ^{13}C fractionation constants from photolysis experiments were determined to be −23.8±0.9 ‰ to −17.7±0.4 ‰ for CFC-11 and −66.2±3.1 ‰ to −51.0±2.9 ‰ for CFC-12 between 203 and 288 K. Although this carbon isotope fractionation was determined during photolysis of samples in the laboratory, rather than real air samples, the conditions represented stratospherically relevant temperatures and wavelengths. This leads to the suggestion that real stratospheric samples should show strong enrichment with decreasing mixing ratio, in good agreement with the laboratory and stratospheric chlorine fractionation measurements. However, this study showed some non-linearity in the data possibly due to variations in reactor-lamp alignment, and lamp intensity variation.

Additionally, the lamp spectrum and the solar actinic flux at altitudes where CFC photolysis occurs did not match, meaning photolysis rates may deviate from those occurring in the stratosphere. It is important to note that these general uncertainties are relevant for the three UEA based studies (Lockhart, 2010, Martin, 2011, Maxwell, 2012). Although oxygen free nitrogen (OFN) was used to ensure no reaction with $O(^1D)$, there was the possibility that chlorine radicals formed during the photolysis process may recombine with the unreacted CFCs and distort the intrinsic photolytic fractionation. A scavenger may have provided a solution to issues related to recombination reactions. Importantly, there are two fundamental differences between the work of Zuiderweg and the UEA-related studies. Firstly Zuiderweg used a traditional IRMS system, and secondly, worked at concentrations several orders of magnitude higher.

More recently, the relationship between the Zuiderweg photolysis experiments and a modelled expectation of how ^{13}C would change over time was investigated by Allin (PhD thesis, 2015). The study used these photolysis isotope fractionation values, to approximate the effect on long term isotopic trends of increasing enrichment in ^{13}C in CFCs in stratospheric air on tropospheric values. The tropospheric predictions were higher than the corresponding ^{37}Cl values, due to the

higher isotope dependence of carbon compared to chlorine inferred by Zuiderweg et al. However, Zuiderweg's values do not take into account the transport and mixing and so stratospheric values are not directly representative. Allin demonstrated that there must be a near-constant source signature for all three CFCs, consistent with current observations and understanding of transport and sink processes. There is a large discrepancy between the data presented by Zuiderweg et al. (2012) and Allin (2015), which could in part be explained by the analytical issues faced by Zuiderweg as described above. Additionally, it is suggested that measurements carried out by Allin may not be linear with respect to the internationally recognised VPDB scale, which is discussed in the next section of this work.

3.2.1 Internationally recognised ^{13}C calibration scale

There is a significant disagreement between the conclusions of Zuiderweg et al. (2013) and Allin (2015) with respect to ^{13}C measurements, leading to the suggestion that one or both data sets contain erroneous measurements, or there is some non-linearity between the analytical systems. Although Allin (2015) described some analytical and data processing issues faced by Zuiderweg, the differences still remain unexplained. In the case of Zuiderweg et al. (2013) measurements were reported relative to an internationally recognised carbon isotope standard, Vienna Pee Dee Belemnite (VPDB), whereas Allin (2015) did not present data in this way. It is a possibility that the measurements presented by Allin (2015) are not linear with respect to the VPDB scale, and hence quantification of this is necessary to be able to compare both studies effectively. Bias between the two analytical systems cannot be ruled out until this has been carried out.

Additionally, stratospheric ^{13}C measurements presented in Chapter 2 of this thesis are reported relative to a real air sample collected in 2006 at Niwot Ridge, Colorado, by the National Oceanic and Atmospheric Administration (NOAA). It would be beneficial to relate these measurements to the VPDB scale to allow for accurate comparison to measurements from other laboratories, including those by Zuiderweg et al. (2013).

3.3 Justification and scope

To date, there have been a small number of studies concerning ^{37}Cl and ^{13}C enrichment and stratospheric fractionation of CFC-12, CFC-11 and CFC-113. Isotopic characterisation of these species may aid quantification of individual source and sink processes. One important aspect of this is the quantification of the proportion of fractionation caused by photolysis and reaction with $O(^1D)$ respectively.

Currently, studies have focused on the isotopic fractionation of chlorine during UV photolysis experiments simulating stratospheric conditions. The use of oxygen free nitrogen by Zuiderweg et al. (2012) and the use of a scavenger species by Maxwell (2011) improved conditions used by Lockhart (MSc thesis, 2010) and Martin (BSc, 2011), however a number of analytical and data processing issues were present. Allin (2015) used ^{13}C measurements from Zuiderweg et al. (2012) as a proxy for stratospheric data, as well as replicating firn air measurements carried out by Zuiderweg et al. (2013). The data sets were not in good agreement, possibly due to analytical issues, and also since Allin (2015) were not able to link their measurements to an internationally recognised calibration scale for accurate comparison.

The focus of this chapter is the isotopic fractionation of both chlorine and carbon during the UV photolysis of CFC-12. The samples are those originally used by Zuiderweg et al. (2012), in an OFN matrix and do not contain a scavenger. Results of this study will be linked to the VPDB scale. This will give a direct link for comparison between the work of Zuiderweg et al. (2012) and that of Allin (2015). Use of the same instrument as Allin (2015) in this study will help to constrain whether the two instruments are measuring the same isotopic changes in CFCs.

3.4 Research objectives

Although a number of studies have attempted to quantify the proportion of the isotope fractionation caused by photolysis, there are significant analytic issues with each study, as described above. Via the analysis of the original samples prepared and photolysed by Zuiderweg et al. (2012) for both ^{37}Cl and ^{13}C isotope fractionation in CFC-12 and calculation of photolysis rates, this works aims to address the question:

1. Are the Zuiderweg samples compromised by analytical difficulties such as high mixing ratios?

Using the same analytical system as Allin to measure the Zuiderweg samples gives a direct comparison and assessment as to whether the systems are comparable. Linkage of measurements to internationally recognised ^{13}C scale (VPDB) to allow direct comparison between the Autospec instrument (UEA) and the IRMS system used by Zuiderweg et al. (2012) is useful for direct comparison of the conclusions made by Allin and Zuiderweg. This will allow further evidence for answering the questions:

2. Are the measurements made by Allin linear with respect to VPDB?
3. Is there evidence to support the case of a constant or changing emissions scenario?

Comparison of data from this study, Allin (2015) and also Zuiderweg et al. (2012), will allow elimination of experimental issues with photolysis samples and firn samples analysed by Zuiderweg et al. (2012). Comparison of photolysis isotope fractionation in this study to work of Lockhart, Martin and Maxwell as well as stratospheric data from this study (Chapter 2), Allin (2015) and Laube et al. (2010) will allow the following questions to be addressed:

4. Are the results of these photolysis experiments indeed comparable to measured stratospheric fractionation? Do these data agree well with the predictions of Zuiderweg regarding the magnitude of apparent isotope fractionation in stratospheric samples?

3.5 Experimental methods

The methods used for analysis of photolysis samples were based on the method for analysis of CFC-12 as described in Chapter 2. Some modifications were carried out to allow for improved precision compared to the stratospheric air samples analysed in Chapter 2.

3.5.1. Sample preparation

Photolysis samples were those prepared and analysed by Zuiderweg (2012). Samples comprised of a mixture of 13 ppm CFC-11 and 530 ppb CFC-12 in oxygen free nitrogen nitrogen. Zuiderweg chose these high concentrations to provide adequate material for analysis whilst keeping sample volumes small. Samples were irradiated using the photoysis set up as shown in Figure 3.1. Photolysis at 190-230 nm occurred at 203. 233 and 288 K for times for 0 to 3 hours. After each irradiation time and aliquot was removed into a 1.75 L stainless steel canister and topped up with OFN for analysis.

Importantly, the concentrations of these prepared samples were higher than the upper limit of detection of the Autospec instrument, and would have caused saturation of the detector if not diluted. Additionally, these samples covered a range of mixing ratios of all three CFCs, and so it was necessary to eliminate any non-linearity of the analytical system. It was possible to dilute the samples to eliminate detector saturation and concentration-dependencies simultaneously. Hence, before photolysis sample analysis, a dilution was performed to give a CFC-12 mixing ratio similar to that of the standard (AAL_071170) (539.9 ppt). It was not possible to investigate both CFC-11 and CFC-12 since CFC-11 was at much higher concentrations and also decayed much faster. CFC-12 was prioritised as it is much more interesting from an isotopic point of view since higher fractionation was expected.

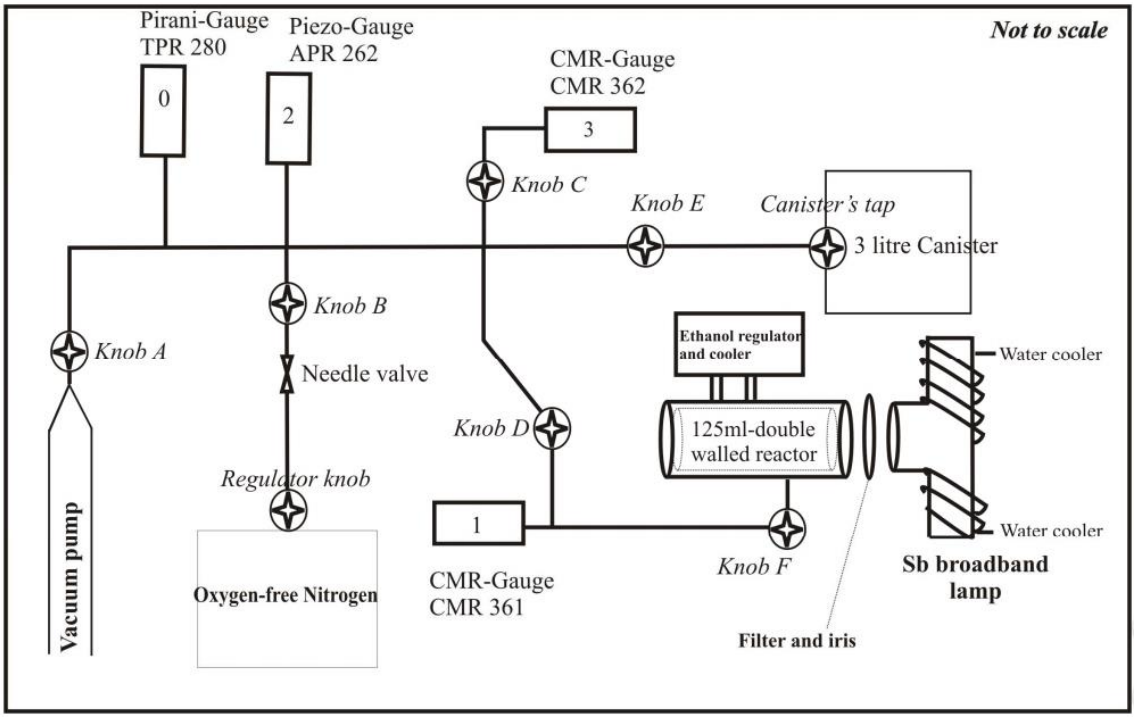

Figure 3.1. Set up of photolysis system as used by Zuiderweg for the irradiation of the CFC-11 and CFC-12 mixture which was analysed in this study. Diagram taken from (Martin, 2011).

Dilution of samples

The mixing ratios of the samples were calculated mathematically using the Time 0 mixing ratio (representing pre-photolysis), photolysis rate, and time of photolysis. It is important to note that the mixing ratios were calculated using data from the Zuiderweg study, which since it originates from an IRMS system is more precise in comparison to the Autospec instrument. An existing transfer system, housed within an oven, was modified to allow four Silco stainless steel cylinders to be filled and samples diluted simultaneously. A number of Swagelok fittings were added, and so rigorous leak checking was carried out. Cylinders were evacuated under vacuum and heated to 200 °C to remove water vapour and trace compounds. After cooling, samples were introduced into the evacuated flasks, and diluted with research grade N_2. Dilutions were between 1.9 % and 88.5 % of the original sample mixing ratio of CFC-12 in the photolysis cylinders, to give a mixing ratio close to that of the in-house standard.

Measurements were repeated in triplicate. It was not necessary to perform non-linearity corrections on the data, since photolysis samples were diluted to similar mixing ratios and hence eliminating differences in detector response.

3.5.2 Modifications to original method

The amount of whole air processed was originally 245 mL. However, although this quantity provided data for CFC-12 in the samples, the precision of the ^{13}C isotopic measurements was initially in excess of 10 ‰. In order to improve precision, the photolysis samples were later reanalysed using a larger trapping amount (550 mL). An Agilent GS-GasPro column (length 30 m, ID 0.32 mm) was used for separation of compounds.

During analysis, the drift corrected precision of the standard over the course of each measurement day was calculated.

3.6 Results and discussion

Measurement of photolysis samples allowed both photolysis rate coefficient (*J*) and isotope fractionation (ε) to be calculated.

3.6.1 Photolysis rate coefficient of CFC-12

The photolysis rate is determined by the linear regression of the plot of the photolysis time against the natural logarithm of the fraction remaining, Ln(F) (Figure 3.2).

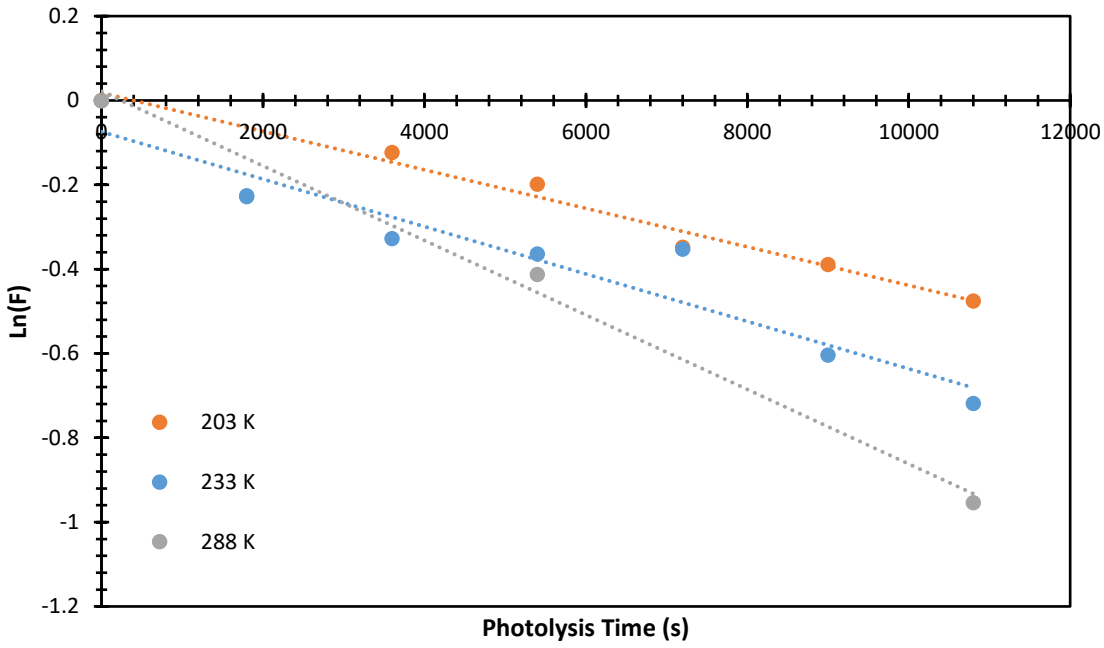

Figure 3.2: Photolysis time in seconds vs the natural logarithm of the fraction remaining, Ln(F).

As described by Zuiderweg et al. (2012), more effective breakdown of CFC-12 occurred when photolysed under high temperatures. It can be seen that the photolysis reaction which took place at highest temperatures (288 K) displays the fastest photolysis rate, *J*, at 8.8 ±0.7 x10^{-5}compared to 4.6 ± 0.3 x $10^{-5}$and 5.6 ± 0.7 x10^{-5} at 203 K and 233 K respectively. It is important to note that the photolysis rate at 288 K is based on three sample analyses only. Only three original Zuiderweg samples were available. Caution should be taken therefore with the conclusion of the 288 K data, however the data still provide an important suggestion as to photolysis rates at 288 K. The 288 K measurements in good agreement with measurements made by Zuiderweg et al. (2012) (Table 3.1), measured at 4.4 x 10^{-5} s^{-1}, 6.6 x 10^{-5} s^{-1} and 9.3 x 10-5 s^{-1} for the 203 K, 233 K and 288 K respectively. No uncertainties are given for these values from Zuiderweg et al. (2012). Taking into account the uncertainty ranges of this study only, photolysis rates at 203 K and 288 K agree well with those of Zuiderweg. At 233 K data agree within 2 σ. Assuming values at 233 K are in fact significantly different, possible reasons for this discrepancy are discussed below. Importantly, the agreement between data from this thesis and that of Zuiderweg rules out the possibility that the two different analytical systems were not comparable. Studies by Maxwell (BSc Research Project, 2012), Martin (2011) and Lockhart (2010) were carried out using the GC-MS system at UEA and so no analytical bias between these studies was present.

In comparison to measurements by Maxwell (BSc Research Project, 2012), photolysis rates are an order of magnitude lower in this study. Rates given by Maxwell are 1.6 x 10^{-4} s^{-1}, 1.1 x 10^{-4} s^{-1} and 1.4 x 10^{-4} s^{-1} at 288 K, 233 K and 203 K respectively. Importantly, much higher concentrations were used by Zuiderweg and this is likely the reason for photolysis rate differences. CFC recombination occurs more readily at higher concentrations leading to lower photolysis rates. These concentrations are first and foremost not representative of atmospheric air, and although provide interesting information about possible photolysis rates, are likely to be biased. As explained in Chapter 2, atmospheric samples would be subject to a dampening effect of the isotope fractionation caused by mixing with air parcels which contain air with almost zero concentrations of CFC, causing lower than expected isotope fractionation. Since the experimental procedure used by Zuiderweg removes each aliquot of sample after irradiation, none of these samples would ever be diluted by samples which are further irradiated, or samples in which the CFCs have been broken down completely. This again allows for more recombination reactions to take place as concentrations remain high at all stages of irradiation.

Interestingly, the use of ethane as a scavenger was used during the work of Maxwell, yet not with the samples prepared by Zuiderweg and analysed in this study. This may limit radical side

reactions and effect of the reactor wall on the photochemistry, and hence limit CFC recombination. Limiting recombination reactions within the reactor will give a faster rate of photolysis, which is seen here via the comparison of Maxwell and this study. However, caution should be taken with this interpretation, as the measurements made by Martin (2011) and Lockhart (2010) are not distinguishable from the faster rates of photolysis demonstrated by Maxwell (2012), yet do not use a scavenger to prevent recombination reactions.

In addition, Maxwell (2012) described a degree of condensation on the walls of the reactor, as well as lamp-reactor alignment variations in the photolysis set up, also described by Zuiderweg et al. (2012). Non-linearity of the data in the Maxwell study may also provide an explanation to the differences between data sets.

In relation to measurements made by Martin (2011), this study again shows photolysis rates to be smaller, again which could be attributed to Zuiderweg using a higher concentration on CFC and hence more recombination reactions. The agreement between Maxwell and Martin means that at lower concentrations there is no significant recombination. Martin suggests a number of limitations to the research, in particular the variability of pressure inside the reactor, which may in turn affect photolysis rates. Additionally, the occurrence of small leaks in the system caused minor contaminations. Drift in the detector was suggested and the data was not subsequently corrected.

In comparison to measurements made by Lockhart (2010), again, this study and that of Zuiderweg et al. (2012) display significantly lower photolysis rates. Although CFC-12 decayed under photolysis as expected, it was suggested that the rate may not only be attributed to the true photolysis rate, but additionally due to limitations with the method. Again, the effect of pressure changes within the system, in particular when aliquots were removed for analysis and the remainder continued to be irradiated, was suggested to affect the measured rate of photolysis. The precision of repeat measurements was poor, at greater than 5 ‰, and a decrease in linearity was seen with decreasing mixing ratios.

In order to confirm the reasons between the discrepancies between data sets it would be interesting to repeat the study, firstly with lower CFC concentrations. In addition, the experimental limitations, including non-linearities, build-up of condensation, variations in lamp intensities and changes in pressure would need to be addressed. This is outside of the scope of this thesis and is not discussed further.

Table 3.1: Summary of photolysis rates of CFC-12 at temperatures 203 K, 233 K and 288 K for studies between 2010 to date.

	Scavenger	*J* at 203 K (s^{-1})	*J* at 233 K (s^{-1})	*J* at 288 K (s^{-1})
This Study	None	$4.6 \pm 0.3 \times 10^{-5}$	$5.6 \pm 0.7 \times 10^{-5}$	$8.8 \pm 0.7 \times 10^{-5}$
Zuiderweg et al. 2012	None	4.4×10^{-5}	6.6×10^{-5}	9.3×10^{-5}
Maxwell (2012)	Ethane	1.4×10^{-4}	1.1×10^{-4}	1.6×10^{-4}
Martin (2011)	None	n/a	1.49×10^{-4}	1.54×10^{-4}
Lockhart (2010)	None	n/a	$1.24 \pm 0.04 \times 10^{-4}$ to $1.15 \pm 0.05 \times 10^{-4}$	$1.49 \pm 0.10 \times 10^{-4}$ to $1.98 \pm 0.01 \times 10^{-4}$

3.6.2 Chlorine isotope fractionation during photolysis of CFC-12

The chlorine isotope fractionation in CFC-12 is shown by the plot of the natural logarithm of the fraction remaining, $\ln(F/F_0)$, against $\delta(^{37}Cl)$ (Figure 3.3).

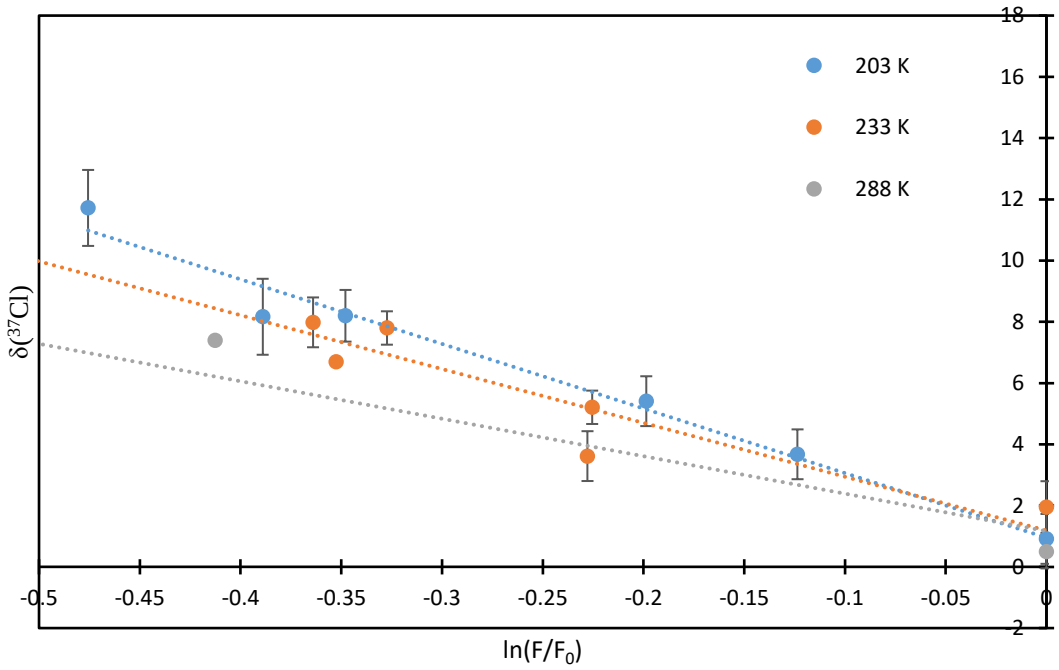

Figure 3.3: Rayleigh plot of fraction remaining ($\ln(F/F_0)$ vs $\delta^{37}(Cl)$ for CFC-12 for temperatures 203 K, 233 K and 288 K. 1 σ error bars shown. All delta values relative to an air sample collected at Niwot Ridge in 2006 (AAL-071170)

The photolysis which occurred at the lowest temperature (203 K) displayed the strongest fractionation, at -19.1±2.6 ‰, compared to -17.3±1.9 ‰ and -13.6±1.6 ‰ at 203 K, 233 K and 288 K respectively.

With respect to laboratory photolysis studies, data are not in agreement within 1 σ with data from Maxwell (2012), Martin (2011) and Lockhart (2010) as shown in Table 3.2. Since photolysis rates suggest a significant degree of recombination as described previously, this is also likely to influence isotopic fractionation. The effect of temperature on photolysis rates also is likely to affect the extent of fractionation, with lower temperatures giving a slower photolysis rate and therefore stronger fractionation. Although the data sets display a discrepancy, the data however follow this correlation. Importantly though, the photolysis data may be biased, and so may not be comparable to stratospheric data. However, it is still useful to link stratospheric measurements from Chapter 2 of this thesis, plus previous photolysis measurements to the international VPDB ^{13}C scale.

Stratospheric measurements described in Chapter 2 of this thesis show an apparent isotope fractionation of -12.91±1.24 and -7.48±0.69 at mid- and high-latitudes respectively. The mid latitude value agrees with in the 1σ uncertainty values of the photolysed samples. Stratospheric samples from the tropical stratosphere analysed by Laube et al. (2010) showed a chlorine apparent isotope fractionation of −12.1±1.7 ‰, which is in good agreement with data from this study at the highest temperature. However, this temperature (288 K) is not representative of stratospheric temperatures at altitudes samples, and so is not a reasonable comparison. The data is likely biased as suggested above. Analysis of mid- and high-latitude stratospheric air carried out by Allin (2015) displayed a similar enrichment profile, with an apparent isotope fractionation of −12.2±1.6 ‰ and −6.8±0.8 ‰ respectively.

3.6.3 Carbon isotope fractionation in CFC-12

The carbon isotope fractionation in CFC-12 is shown by the plot of the natural logarithm of the fraction remaining, ln(F), against δ(^{13}C) (Figure 3.4).

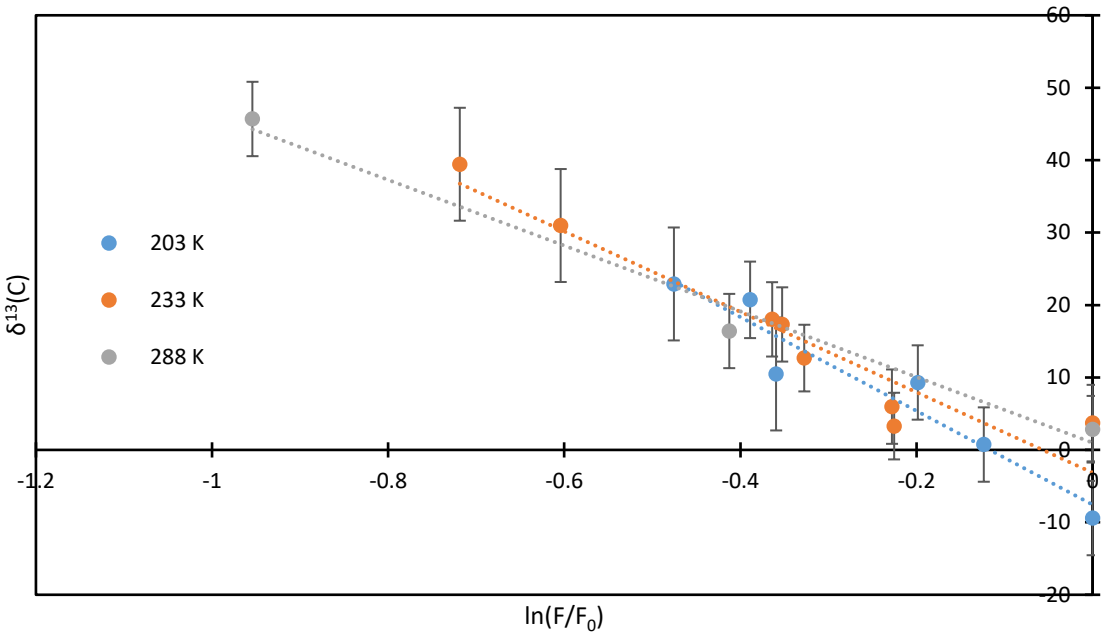

Figure 3.4: Rayleigh plot of fraction remaining ($\ln(F/F_0)$ vs d13C for CFC-12 for temperatures 203 K, 233 K and 288 K. 1 σ error bars shown. All delta values relative to an air sample collected at Niwot Ridge in 2006 (AAL-071170).

The photolysis which occurred at the lowest temperature (203 K) displayed the strongest fractionation, at -65.6±8.7 ‰, compared to -55.5±7.2 ‰ and -45.4±6.0 ‰ at 233 K and 288 K respectively. This agrees well with data from (Zuiderweg et al., 2012) at −66.2±3.1 ‰, −55.3±3.0 ‰ and −51.0±2.9 ‰ for 203 K, 233 K and 288 K (Table 3.2). No other studies have investigated the carbon isotope fractionation in the photolytic breakdown of CFC-12.

Stratospheric measurements described in Chapter 2 of this thesis show an apparent carbon isotope fractionation of -23.58±6.58 and -19.31±3.88 at mid- and high-latitudes respectively. Both mid and high-latitude samples display data with significantly lower apparent isotope fractionation than the measured photolysis samples, -65.6±8.7, -55.5±7.2 and -45.4±6.0 at 203 K, 233 K and 288 K respectively. Again the discrepancy between laboratory simulated photolysis and atmospheric samples firstly can be explained by the photolysis samples having significantly higher mixing ratios than the atmosphere causing bias. Additionally, the real air samples have been subject to atmospheric transport and mixing as described above and in Chapter 2, lessening the observed atmospheric fractionation.

Table 3.2: Summary of isotope fractionation due to photolysis of CFC-12 at temperatures 203 K, 233 K and 288 K for studies between 2010 to date.

Measurement	This study stratospheric	This study Photolysis	Zuiderweg (2012)	Maxwell (2012)	Martin (2011)	Lockhart (2010)
^{37}Cl	-12.91±1.24 (mid-latitude) -7.48±0.69 (high-latitude)	-19.12±2.6 (203 K) -17.32±1.9 (233 K) -13.6±1.6 (288 K)	n/a	-14.0±2.1 (203) -11.3±2.4 (233) -8.4±0.5 (288)	-12.0±0.9 (203) -7.1±0.8 (288)	-20.25±6.81 (233)
^{13}C	-23.58±6.58 (mid-latitude) -19.31±3.88 (high-latitude)	-65.6±8.7 (203 K) -55.5±7.2 (233 K) -45.4±6.0 (288 K)	-66.2±3.1 (203 K) -55.3±3.0 (233 K) -51.0±2.9 (288 K)	n/a	n/a	n/a

3.6.4 Discrepancies between data sets

Various factors may explain why the data in this and previous studies do not agree. It is possible that there is a systematic bias between instruments. As described previously, there may be recombination reactions occurring within the reactor since there is no presence of a scavenger. Finally, there may be contamination within the processing steps, photolysis, set and dilution of samples. Most importantly it is likely that the high concentrations use by Zuiderweg have introduced bias.

In order to establish the reasons as to why both this study and (Zuiderweg et al., 2012) display differences to other studies, it is important to identify firstly if contamination has occurred at any stage during set up or analysis.

Samples were made up of CFC-11 and CFC-12 in OFN only. However analysis revealed the presence of CFC-113 peaks, corresponding to mixing ratios between 3 and 36 ppb. Possible sources of this CFC-113 are contaminants from a leak within the system during either the original sample set up, or during the dilution phase, in addition to possible recombination reactions occurring inside the reactor. Such reactions may occur from the breakdown products formed during the photolysis of CFC-11 and CFC-12, such as ion fragments containing carbon and chlorine for recombination to 1,1,2-trichloro-1,2,2-trifluoroethane (CFC-113). Since no scavenger was present during the photolysis reactions this cannot be ruled out.

In order to determine if reactions inside the photolysis set up are causing the increase in CFC-113, CFC mixing ratio against photolysis time is presented (Figure 3.5). Interestingly, an increase in CFC-113 mixing ratio occurs with increasing photolysis time (Figure 3.5), but limited to 203 K only. Although correlated, there is no apparent increase over time for photolysis at 233 K or 288 K.

It is important to note that since the time zero concentrations are negligible, it can be said that the CFC-11 introduced to the reactor did not contain a proportion of CFC-113 and so contamination in this way can be ruled out.

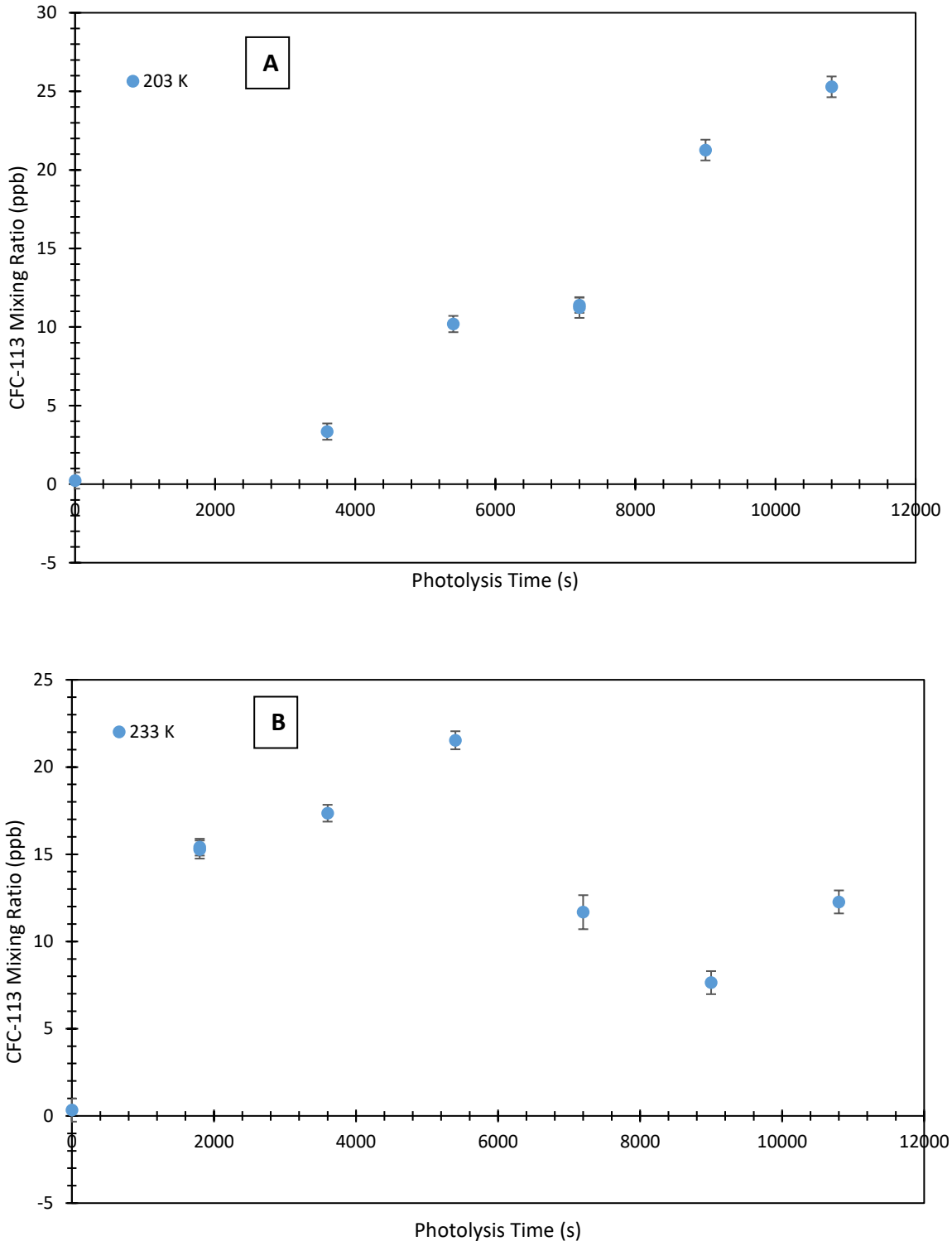

Figure 3.5: Photolysis time vs CFC-113 mixing ratio at three photolysis temperatures: (A) 203 K (B) 233 K and (C) next page.

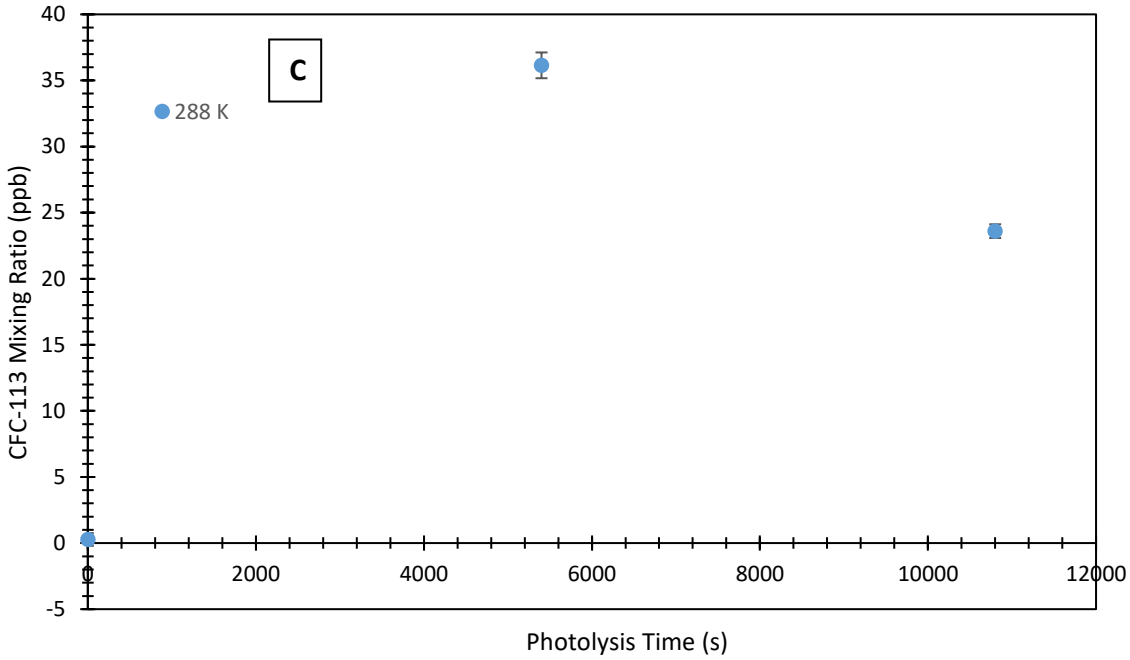

Figure 3.5: Photolysis time vs CFC-113 mixing ratio at three photolysis temperatures: (C) 288 K. 1 σ error bars shown.

These data link well to the idea of CFC-113 occurring via recombination of radicals formed during photolysis of CFC-11 and CFC-12. The reactor has a significantly higher concentration of CFC-11 (13 ppm) than CFC-12 (530 ppb) (Zuiderweg et al., 2012) and so CFC-11 only is considered here. Zuiderweg et al. (2012) demonstrate that CFC-11 is not photolysed completely at 203 K, yet at 233 K and 288 K photolysis removes CFC-11 at approximately 7000 seconds and 6000 seconds respectively. It is possible that the radicals formed during CFC-11 breakdown may recombine to form CFC-113. It is assumed that this newly formed CFC-113 is broken down via photolysis as seen in the case of CFC-12, but the proportionately large quantity of CFC-11 inside the reaction chamber means that the production of CFC-113 is larger than the breakdown even when both reactions occur simultaneously. In the case of photolysis occurring at 203 K, the rate of photolysis is slow, breakdown products of CFC-11 are being formed continuously and hence recombination reactions are significant throughout the entire photolysis time. When photolysis takes place at 233 K, the faster photolysis rate means that after approximately 7000 seconds most CFC-11 has been broken down. Once the CFC-11 cannot produce more breakdown products, and hence no more CFC-113 can be produced, the photolysis of CFC-113 formed is hence the most significant. Figure 4 demonstrates the increase of CFC-113 at the beginning of the photolysis process, where destruction of CFC-11 and therefore production of CFC-113 dominates. After 6000 seconds, it can be seen that the mixing ratio of CFC-113 decreases, due to photolysis and no source material to replenish what is depleted. At 288 K photolysis of CFC-

11 is at a faster rate still, and so is depleted by 3500 seconds. Since Figure 3.5(C) only has three data points due to one flask being empty on arrival, no firm conclusions can be drawn, but the data does suggest that CFC-113 is decreasing after 3500 seconds, since there is no additional formation.

To further confirm the explanation that the presence of CFC-113 is from recombination reactions rather than introduction via a system leak, a stable species, C_3F_8, was investigated in the same way. It would be expected that if the additional CFC-113 is caused by a leak in the system, C_3F_8 would mirror the CFC-113 data. If the increase in CFC-113 was due to a leak in the system, the increase of C_3F_8 would display the same behaviour. Figure 3.6 shows that C_3F_8 mixing ratios are low, much below atmospheric concentrations, and therefore there is no significant system leak, and also demonstrates that the change in C_3F_8 over time is not related to photolysis time. The fact that the behaviour of C_3F_8 and CFC-113 do not behave in the same way rules out the explanation for a leak causing the increasing CFC-113. It is therefore most likely to be explained by recombination reactions due to a lack of scavenger, and importantly, the high CFC concentrations within the reactor. Additionally, it is possible that there could be outgassing from interior surfaces, giving rise to the presence of CFC-113, however it is expected that this effect would be small.

3.6.5 Linking to internationally recognised ^{13}C scale

Although there is evidence that there are recombination reactions which may cause the data to be unrepresentative of atmospheric photolysis reactions, there still also maybe bias between the analytical instrument used in this study and Allin (2015), as well as that by Zuiderweg et al. (2012). In order to determine whether such analytical bias exists, analysis of the samples analysed by Zuiderweg in 2012 gives the missing link between the two data sets. Additionally, data from Zuiderweg is linked to an international calibration scale, Vienna Pee Dee Belemnite (VPDB), and so data from the Autospec intrument used during this and previous studies can be therefore linked. Linking to the VPDB scale will not change the slope displayed via Rayleigh plots, and therefore will not change the calculated apparent isotope fractionation. However, the absolute isotope changes can be reported rather than relative changes. This removes one of the main limitations of the work by Allin et al. (2015) and allows for direct comparison to the work of Zuiderweg et al. (2012).

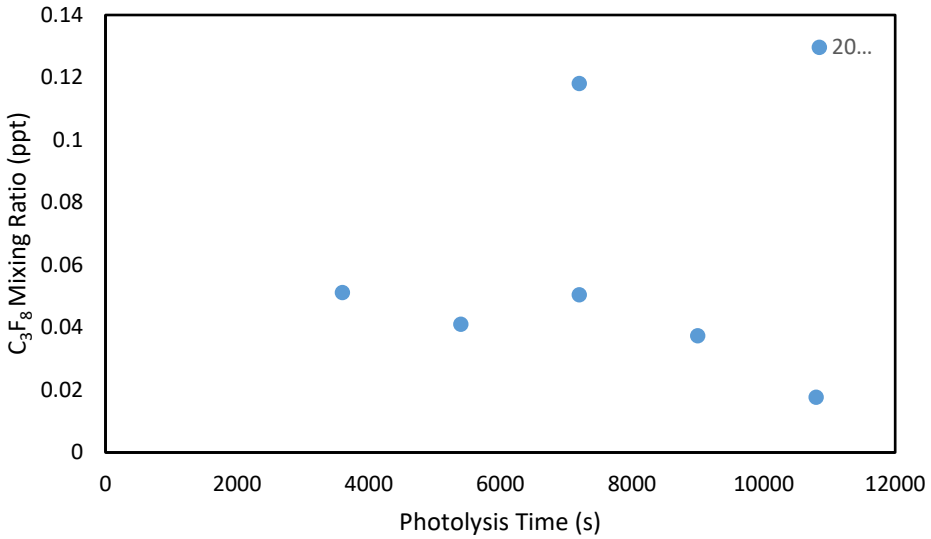

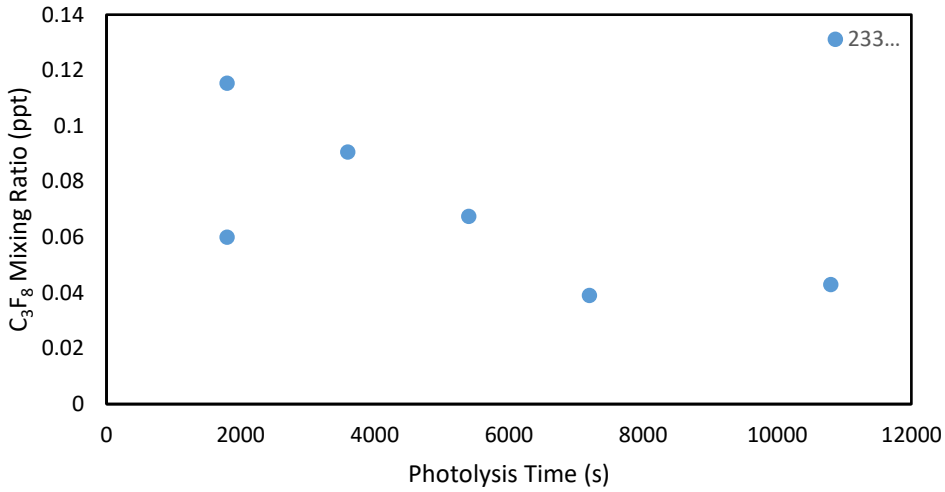

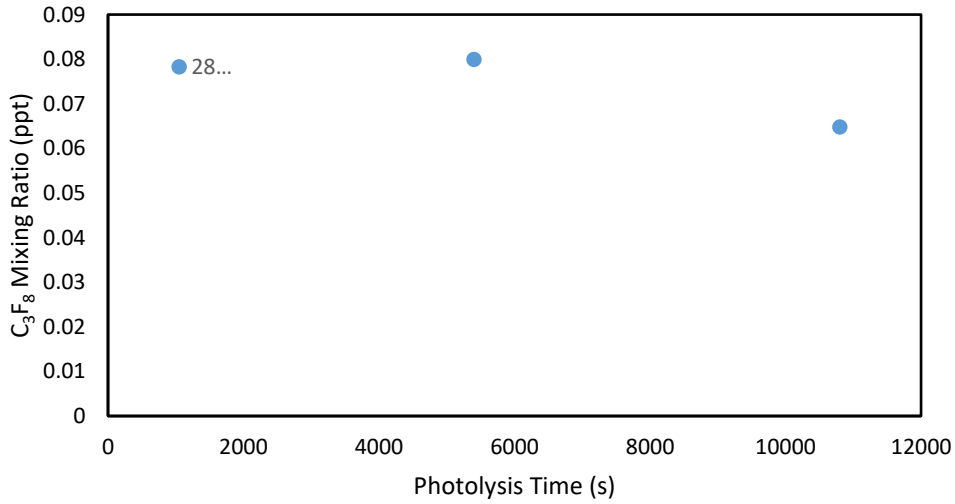

Figure 3.6: Photolysis time vs C_3F_8 mixing ratio at temperatures 203 K, 233 K and 288 K.

The samples analysed by Zuiderweg et al. (2012) are identical to the photolysis samples analysed in this thesis, and so an offset between these data sets was calculated. This offset represents the difference between relating the data to UEA in house standard (AAL_071170, a real air sample collected in 2006 at Niwot Ridge, Colorado) and the international VPDB scale. The data for each of the three photolysis temperatures (203 K, 233 K and 288 K) was plotted and the offset between each data point calculated for the three temperatures. Figure 3.6 demonstrates the comparison between CFC-12 ^{13}C data analysed in this study (vs AAL_071170) and that of Zuiderweg et al. (2012) (vs VPDB).

This offset was then applied to the data from this study, giving data from this study relative to VPDB, as shown in Figures 3.8 to 3.10.

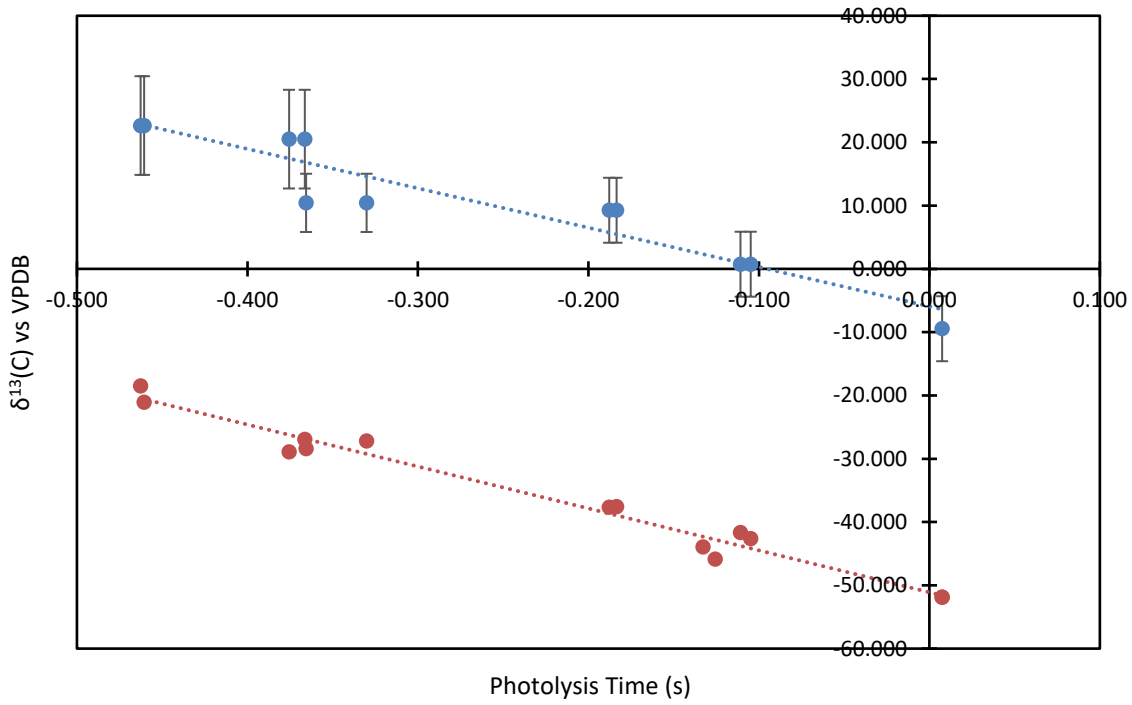

Figure 3.7: Plot of photolysis time vs $\delta^{13}(C)$ vs AAL_071170 (Blue data points) and VPDB (red data points) for CFC-12 at 203 K. 1 σ error bars are shown for data from this study, no uncertainty data was available from Zuiderweg (2012).

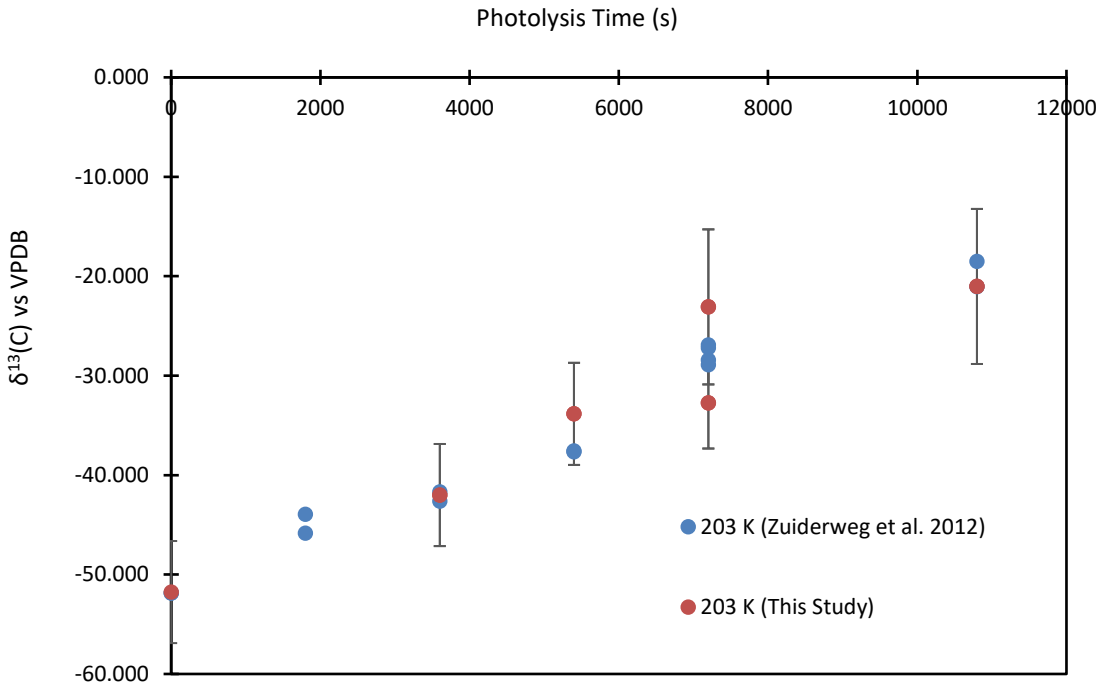

Figure 3.8: Plot of photolysis time vs δ^{13}(C) vs VPDB for CFC-12 at 203 K.

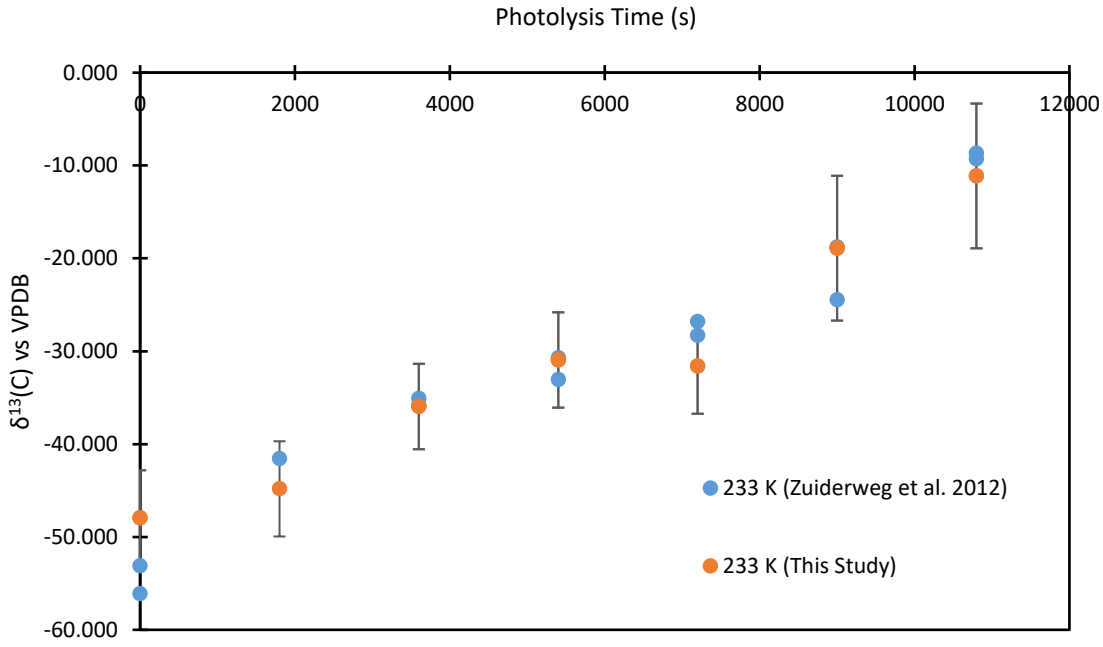

Figure 3.9: Plot of photolysis time vs δ^{13}(C) vs VPDB for CFC-12 at 233 K.

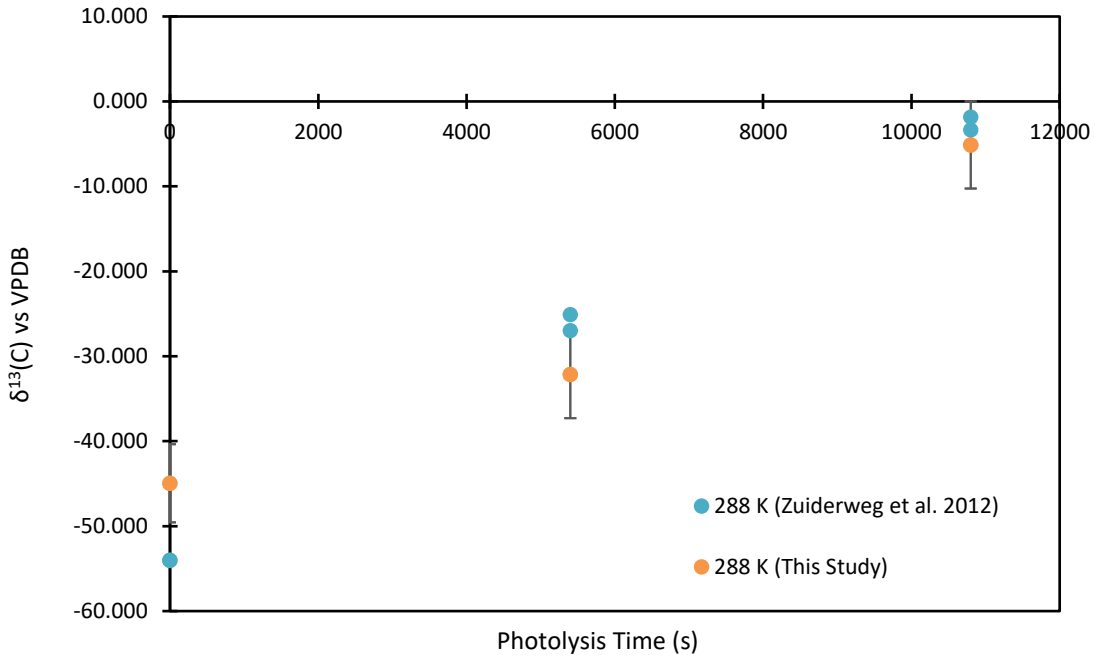

Figure 3.10: Plot of photolysis time vs δ^{13}(C) vs VPDB for CFC-12 at 288 K.

In order compare stratospheric data from this study and firn data from Allin et al. (2015) to the photolysis data a similar correction was made to give all data relative to the VPDB scale. Since tropospheric air temperatures (which result in firn air) are closest to the highest photolysis temperature, 288 K, the correction from these experiments was applied. The correction used for the stratospheric data was the average of the 203 K and 233 K values, best representing the temperature range of the stratosphere where sampling took place.

Stratospheric data from this study relative to VPDB is displayed via Figure 3.11. The slope, and hence the apparent isotope fractionation remains unchanged, but the absolute values of δ^{13}(C) are shown.

It can be seen that the firn (NEEM 2009) data of both Allin and Zuiderweg agree well to depths of 68 metres, yet there is discrepancy within the data below this value (Figure 3.12). Since samples were identical and the data of Allin has now been linked to VPDB, the data displayed should be identical, other than discrepancies caused by system non-linearities in the case of Zuiderweg, and differences in data processing between the two studies.

3.6.6 Stratospheric implications

Atmospheric transport and mixing heavily influence the apparent isotope fractionation of a species. Atmospheric measurements, from both this study and those of Laube et al. (2010) and

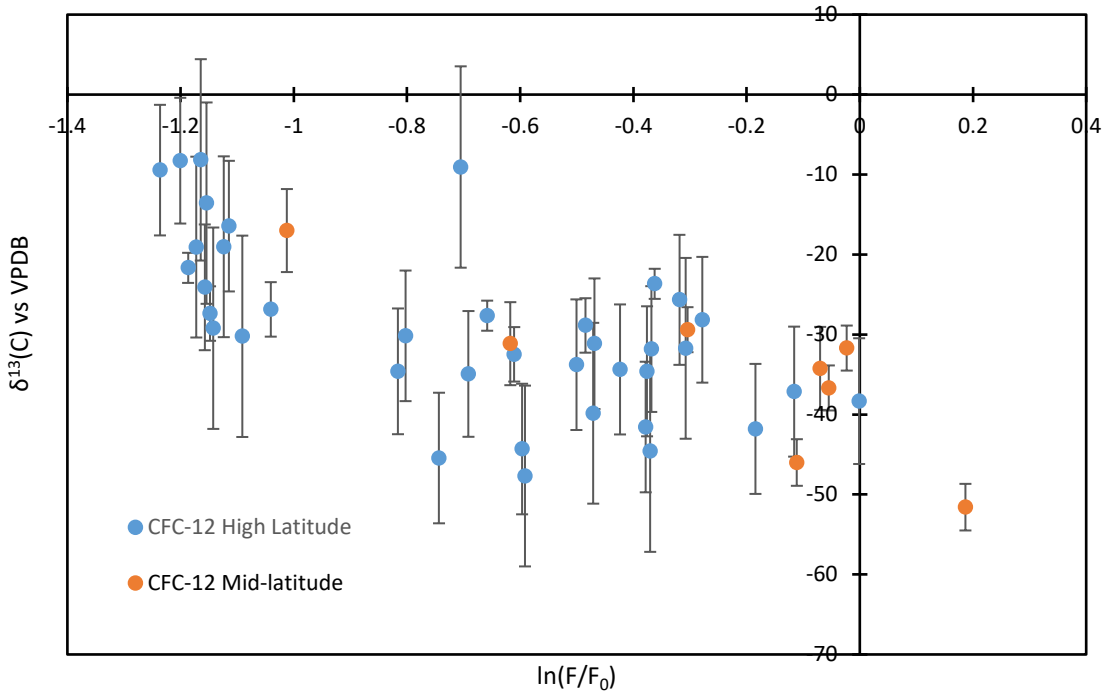

Figure 3.11: Rayleigh plot of fraction remaining ($\ln(F/F_0)$ vs $\delta^{13}(C)$ vs VPDB for CFC-12 for high- and mid-latitude stratospheric samples.

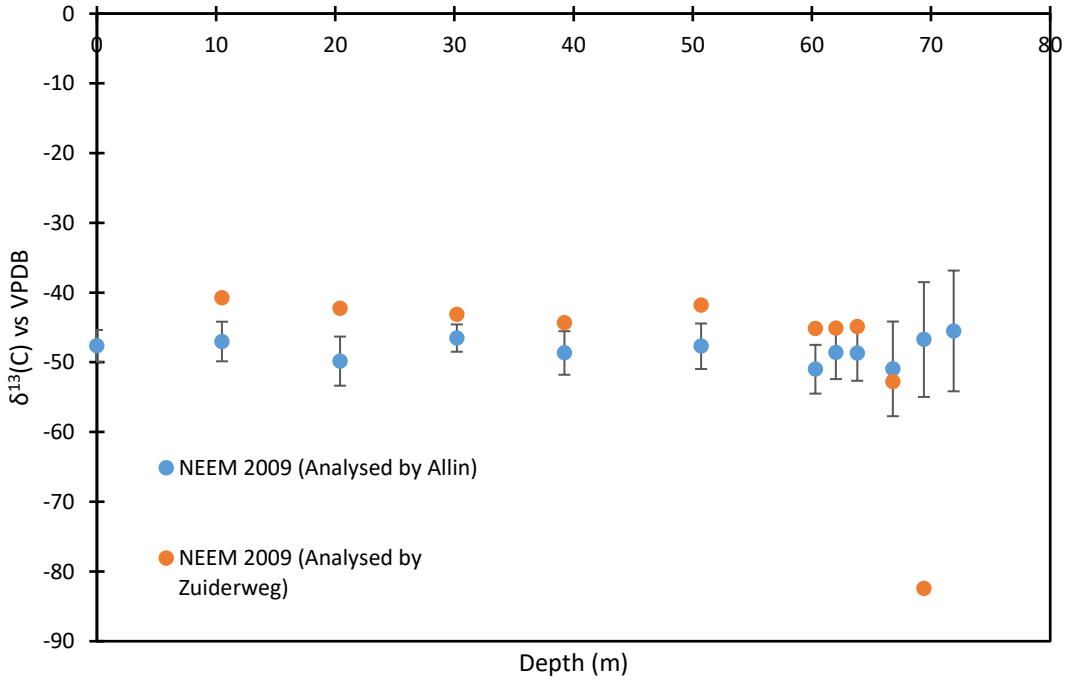

Figure 3.12: Firn air data from Allin et al. (2015) and Zuiderweg (2013) $\delta^{13}(C)$ (vs VPDB) vs profile depth for CFC-12

Allin (2015) display isotope fractionations of similar magnitude only at mid latitudes. At high-latitudes the apparent isotope fractionation is significantly lower than that of the photolysed samples, which can be explained by atmospheric transport and mixing.

With regards to photolysis rate, data show a faster photolysis rate with increased temperature as expected based in ZPE theory. Temperature increases with height in the stratosphere, and so apparent isotope fractionation should decrease with height if only temperature is considered. However, the photolysis rate of CFC-12 is also dependent on UV wavelength variations and actinic flux, and so the apparent isotope fractionation cannot be predicted on temperature alone. The highest loss rate and mixing ratio is expected in the tropics due to the actinic flux and the tropics being a significant entry point to the stratosphere. Lower enrichment near the tropopause gives rise to the significance of vertical tranport from the troposphere as a result of the Brewer Dobson circulation. Data presented in this chapter is in good agreement with stratospheric data from mid latitudes. Again, the discrepancy between the calculated photolysis rates and high-latitude stratospheric measurements can be explained by the large mixing and transport involved regarding high-latitude samples.

In comparison to Allin et al. (2015), firn air data from Zuiderweg (2013) displays a far greater magnitude of δ^{13}(C) fractionation below 68 metres depth. As described in Chapter 2, stratospheric data from this study agrees well with firn and tropospheric δ^{13}(C) of Allin, and agrees with a constant emissions scenario over time. Since after linking data from Allin to the VPDB scale a discrepancy still exists it can still be concluded that stratospheric data from this study does not agree well with the suggestions of Zuiderweg that there was a significant isotopic change in emissions over time, possibly from fluctuating manufacturing processes. A possible explanation could be that since the method adopted by Zuiderweg et al. relied on the conversion of CFC-12 to CO_2, other atmospheric trace gases may have been also converted. These may have eluted from the GC column at the same time, which is often the case when analysing air samples containing complex trace gas mixtures and especially so at ppt levels.

3.7 Conclusions

Analysis of ^{37}Cl and ^{13}C allowed calculation of photolysis rate and fractionation constants of CFC-12 in a mixture of CFC-12 and CFC-11 in OFN.

The photolysis rate, determined by the linear regression of the plot of the photolysis time against the natural logarithm of the fraction remaining, Ln(F), was 4.6±0.3 x 10^{-5} s^{-1} at 288 K compared to 5.6±0.7 x 10^{-5} s^{-1} and 8.8±0.7 x 10^{-5} s^{-1} at 233 K and 288 K respectively. This agreed well with

measurements by Zuiderweg et al. (2012), yet displayed significantly smaller photolysis rates than studies by Maxwell (2012), Martin (2011) and Lockhart (2012). Interestingly, this could be explained in part the presence of a scavenger species in the case of Maxwell, but both Martin and Lockhart did not limit recombination reactions in this way, meaning this interpretation should be taken with caution. Most importantly the high CFC concentrations are likely to give rise to significant recombination reactions inside the reactor. The data presented by Zuiderweg, therefore is most likely biased and photolysis rates not representative of those in the stratosphere. All studies had significant experimental issues such as non-linearities, condensation within the reactor, pressure and lamp intensity variabilities and detector drift. In this study detector non-linearities are not significant since dilution of samples took places deeming them of equal mixing ratio.

The ^{37}Cl isotope fractionation was determined to be -19.12±2.6 ‰, -17.32±1.9 ‰ and -13.6±1.6 ‰ at 203 K, 233 K and 288 K respectively. The chlorine isotope composition is important with respect to quantification of the atmospheric budget of CFC-12. Hence, any further understanding of the apparent isotope fractionation constant may give an insight into CFC depletion and ultimately ozone recovery rates. In comparison to stratospheric data, there is reasonable agreement between photolysis samples and stratospheric samples at mid-latitudes as described in Chapter 2, Allin (2015) and Laube et al. (2010). However, stratospheric measurements at higher latitudes had significantly lower apparent isotope fractionation

With respect to both photolysis rate and ^{37}Cl isotope fractionation, it was concluded that measurements were not representative of atmospheric values, due to recombination reactions influencing isotope fractionation. Data presented by Zuiderweg is most likely biased due to high CFC concentrations. Photolysis rates are an order of magnitude lower in this study compared to previous studies (Maxwell., 2012) demonstrating the much higher CFC concentrations used by Zuiderweg and in this study. The reason for photolysis rate differences is likely CFC recombination occurring more readily at higher concentrations leading to lower photolysis rates. Limiting recombination reactions via an ethane scavenger within the reactor will give a faster rate of photolysis, but more importantly it would be useful to repeat the photolysis experiments at stratospherically relevant concentrations.

With respect to the ^{13}C isotope fractionation, values of -65.6±8.7 ‰, compared to -55.5±7.2 ‰ and -45.4±6.0 ‰ at 203 K, 233 K and 288 K respectively. This agrees well with data from Zuiderweg (2012) at −66.2±3.1 ‰ −55.3±3.0 ‰ −51.0±2.9 ‰ for 203 K, 233 K and 288 K. Stratospheric measurements as described in Chapter 2 (-23.58±6.58 and -19.31±3.88 at mid and

high latitudes respectively) have significantly lower apparent isotope fractionation than the measured photolysis samples. This discrepancy can be attributed to the higher mixing ratio of CFC-12 in the photolysis samples compared to real air samples, likely causing a bias. Again, in addition, the real air samples have been subject to atmospheric transport and mixing, dampening the observed atmospheric fractionation.

Linking the stratospheric data from Chapter 2, as well as firn data from Allin et al. (2015) to the VPDB scale allowed direct comparison to measurements of Zuiderweg et al. (2013). Even when presented on the equivalent calibration scale, data given Zuiderweg still displays a larger magnitude in isotope fractionation with depth. It can still be concluded that stratospheric data from this thesis agrees with an emissions scenario which does not change over time

Chapter 4: Mass Spectrometric Analysis of Stratospheric Nitrous Oxide: Origin of the ^{17}O excess in tropospheric N_2O.

Nitrous oxide is a contributor to stratospheric ozone depletion and is also a significant greenhouse gas, and is not regulated by the Montreal Protocol. To date, N_2O isotopic composition in the troposphere has been measured with respect to $^{17}O/^{16}O$, $^{18}O/^{16}O$ and $^{15}N/^{14}N$ ratios. Based on the mass difference, the isotope fractionation of ^{17}O should be approximately half as much as that of ^{18}O, with respect to ^{16}O. However, tropospheric air measurements show that the proportion of ^{17}O is higher than expected. This is evidence of non-mass dependent fractionation in one or several N_2O sources or sinks. Identifying the source of the ^{17}O excess would be aided by measurement of stratospheric samples. This chapter describes the development of a measurement system capable of analysis of $\delta^{15}N$, $\delta^{17}O$, $\delta^{18}O$ and $\Delta^{17}O$ in N_2O in whole air samples. Stratospheric samples from a mid-latitude site represent the first measurements of $\Delta^{17}O$ in stratospheric N_2O above 12 km altitude.

4.1 Introduction

Nitrous oxide (N_2O) is a greenhouse gas which also contributes to stratospheric ozone depletion. The estimated global mean lifetime of N_2O is (116±9) years (Prather et al., 2015). Taking into account chemical feedback mechanisms, addressed by the 2014 IPCC report, a perturbation lifetime of 109 years (Prather et al., 2015) is determined.

A radiative forcing of (0.17±0.03) W m^{-2} (Myhre et al., 2013) relates, over a timescale of 100 years, to almost 300 times the forcing per molecule of carbon dioxide. Currently N_2O contributes approximately 6 % of all anthropogenic long-lived greenhouse gas (GHG) forcing (IPCC, 2014). Due to the decrease in the atmospheric burden of CFC-12 due to regulation by the Montreal Protocol, N_2O has replaced CFC-12 as the third most important well-mixed GHG contributing to radiative forcing (Myhre et al., 2013).

Although itself not regulated by the Montreal Protocol, N_2O has a small ozone depleting potential (ODP) of 0.017 (Ravishankara et al., 2009). However, the high mole fraction makes N_2O an extremely important contributor to stratospheric ozone depletion (Portmann et al., 2012). In terms of emissions, N_2O is expected to continue to be the largest contributor to anthropogenic ozone depleting potential (ODP) substances into the foreseeable future, and hence it is important to understand and quantify sources and sinks (Portmann et al., 2012).

The globally averaged atmospheric mole fraction of 324.2±3.2 nmol mol^{-1} in 2011 has increased by 20 % from the 1750 ice core based estimate of (270±7) nmol mol^{-1} (Prather et al., 2012). Firn air measurements indicate that this increase, at least since the early 1950s, was dominated by agricultural soil emissions due to use of nitrogen based-fertilisers (Davidson, 2009, Syakila and Kroeze, 2011).

4.1.1 Sources and sinks of N_2O

Microbial activity, both on land and in the oceans, is the most significant natural source of N_2O (IPCC, 2014). An additional natural source is the reaction of the amidogen radical and nitrogen dioxide, as shown in Equation 4.1. This source contributes approximately 0.6 Tg a^{-1} (N equivalents).

$$NH_2 + NO_2 \rightarrow N_2O + H_2O \qquad \text{Equation 4.1}$$

Anthropogenic sources including fossil fuel combustion, industrial processes, agriculture and biomass burning are significant. The sources of anthropogenic origin are not well constrained, and only marginally better quantified than natural sources. Fluxes are given in Figure 4.1. Atmospheric sources from in situ chemical processes are small in magnitude and not well understood.

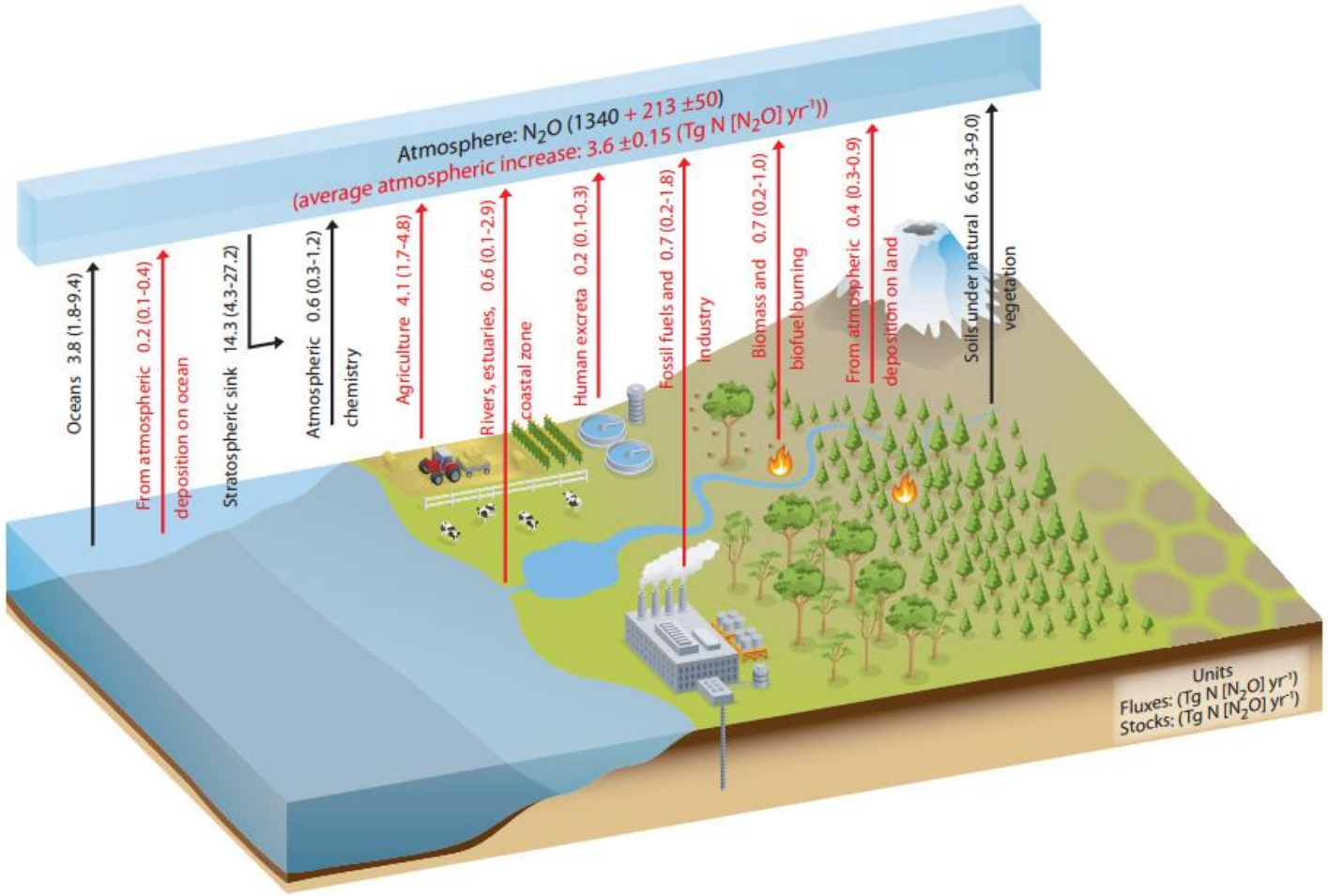

Figure 4.1. Global N_2O cycle. The stratospheric sink processes (photolysis and reaction with $O(^1D)$) equal the total source fluxes. Taken from IPCC (2014).

Photolysis and reaction with electronically excited oxygen atoms, $O(^1D)$, are the only relevant sinks of N_2O. These stratospheric processes contribute 90 % and 10 % of total N_2O loss respectively (Bernard et al., 2006). It is possible to determine the total source flux as the sum of total loss rate and atmospheric increase rate. Due to the long lifetime and the small variability of tropospheric mole fractions, relatively few measurements are sufficient to determine the atmospheric increase rate. However, the relative contributions from individual sources are difficult to quantify, in particular those processes related to land use and ecosystem changes. In order to constrain the size of individual sources or sinks, the isotopic composition of N_2O in the atmosphere can be used (Bernard et al., 2006, Cliff et al., 1999b, Brenninkmeijer et al., 2003, Yoshida and Toyoda, 2000).

4.2 Use of isotopes to constrain the N_2O budget

It is possible to constrain the N_2O budget by monitoring its isotopic composition in the atmosphere. Different source and sink processes have characteristic isotope signatures. The cause of the increase of N_2O since pre-industrial times can be determined using the simultaneous evolution of the isotopic composition (Prokopiou et al., 2016).

To date, the N_2O isotopic composition in the troposphere has been measured with respect to $^{17}O/^{16}O$, $^{18}O/^{16}O$ and $^{15}N/^{14}N$ ratios (Cliff et al., 1999b, Brenninkmeijer et al., 2003, Röckmann et al., 2001b). In the stratosphere, the discovery of N_2O enriched in ^{18}O and ^{15}N (Rahn and Wahlen, 1997, Kim and Craig, 1993, Bernard et al., 2006) suggested sink processes that give rise to kinetic isotope fractionation in N_2O, due to preferential destruction of isotopically lighter molecules in the sink reactions. Stratospheric samples with mole fractions above 200 nmol mol^{-1} show a compact relationship between $\delta^{18}O$ and $\delta^{15}N$ and the N_2O mole fraction, with little variation with latitude and season, likely due to mixing.

Land sources of N_2O are dominated by nitrification/denitrification processes. Fossil fuel combustion, biomass burning and industrial processes are only minor sources of N_2O and so the overall isotope fractionation is dominated by the inherent fractionation in the soil flux. N_2O from soils is consistently depleted in ^{15}N and ^{18}O relative to atmosphere (Kim and Craig, 1993, Toyoda et al., 2017). The use of both organic and synthetic fertilisers affect the ratio of heavy to light oxygen and nitrogen isotopes. Available nitrogen is often the limiting nutrient, but in fertilised soil, the excess nitrogen would allow microbial production to discriminate against using the heavier isotope in the case of both oxygen and nitrogen.

N_2O is generally enriched at places with high rainfall relative to dry areas. This is argued to be due to the occurrence of denitrification in wet soils. Nitrification in dry soils generally produces isotopically light N_2O (Yoshida, 1988, Wahlen and Yoshinari, 1985).

Microbial nitrification and denitrification are the main oceanic N_2O sources. Oceanic N_2O is enriched relative to that of soil origin (Rahn and Wahlen, 2000), with isotope ratios falling between tropospheric and slightly enriched values. Nitrification in deep ocean water (Kim and Craig, 1990) gives N_2O enriched in ^{15}N and ^{18}O, suggesting a heavy source to the troposphere. Near surface dissolved N_2O is depleted with respect to deep ocean N_2O, giving an enrichment profile with depth. Although enriched N_2O is brought to the surface, a strong buffering effect occurs in the surface waters, meaning the ocean source is reduced. However, despite this, the oceans still remain of a significant tropospheric source.

4.3 The ^{17}O excess in the atmosphere

Based on the mass difference, the isotope fractionation of ^{17}O should be approximately half as much as that of ^{18}O, with respect to ^{16}O. Oxygen isotopes found within atmospheric species should fall within the upper and lower limit of mass dependent-fractionation, between 0.5010 and 0.5305 (Kaiser, 2008, Young et al., 2002). The lower limit represents the gas kinetic fractionation of a heavy molecule with one oxygen atom, for example diffusion. The upper limit is the equilibrium isotope fractionation at high temperatures. The mass dependent fractionation line specific to N_2O was determined empirically. A plot of $\delta^{17}O$ against $\delta^{18}O$ (Figure 4.2) yields a slope of 0.515 (Cliff and Thiemens, 1997, Kaiser et al., 2004); a plot of $\ln(1+\delta^{17}O)$ against $\ln(1+\delta^{18}O)$ gives a slope of 0.516 (Kaiser et al., 2004). Any deviation from this mass dependent fractionation line suggests processes which cause fractionation in addition to that due to mass alone. Any deviation from the mass dependent fractionation line is termed the ^{17}O excess. Tropospheric air measurements show a deviation from this line, meaning the proportion of ^{17}O is higher than expected and therefore evidence of non-mass dependent fractionation in one or several N_2O sources or sinks.

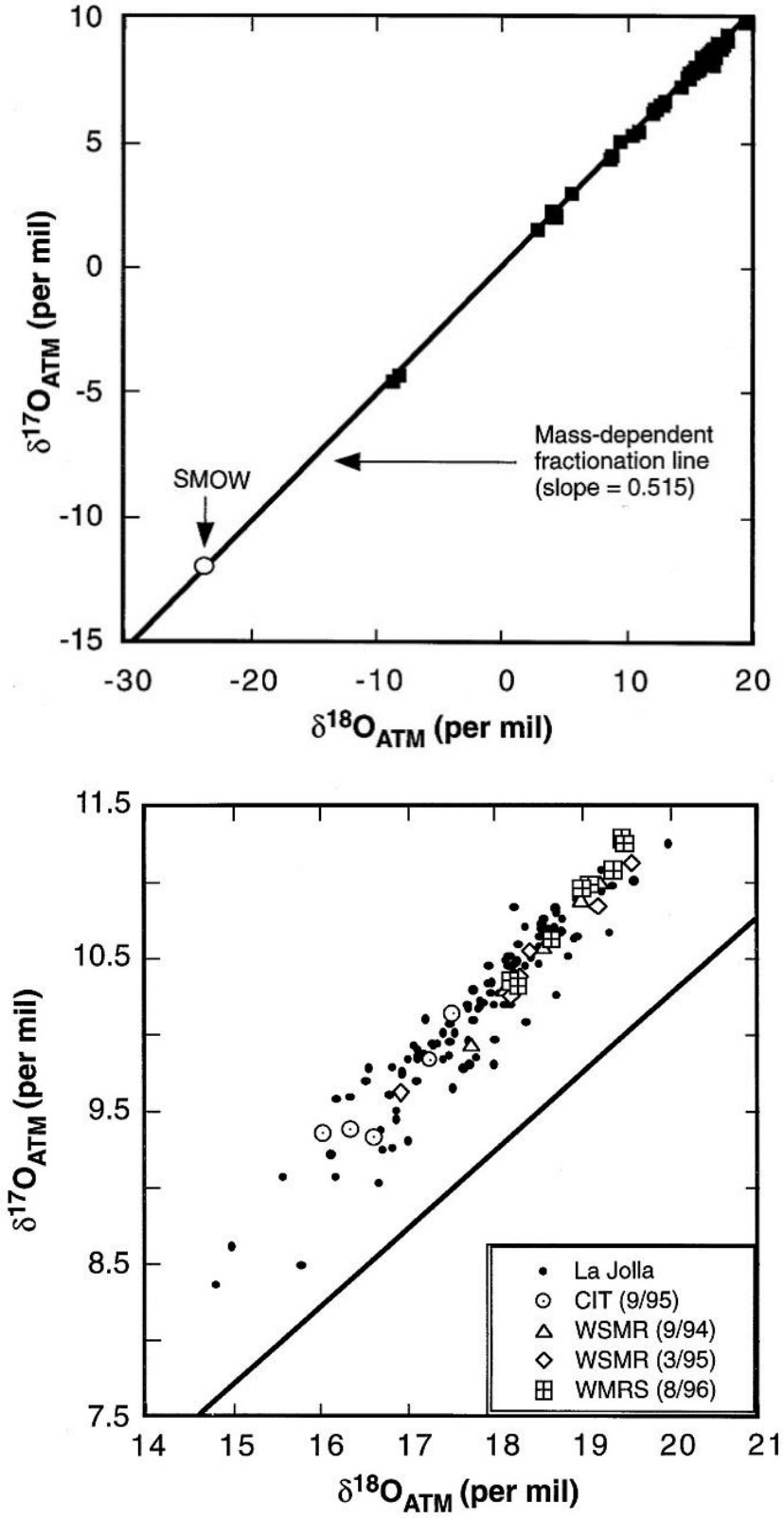

Figure 4.2. (A) The mass dependent fractionation line determined empirically with a slope of 0.515. Standard Mean Ocean Water (SMOW) is shown for comparison. (B) The mass dependent fractionation line at slope = 0.515 alongside atmospheric measurements. Data from La Jolla, California Institute of Technology (CIT), White Sands Missile Range (WSMR) and White Mountain Research Station (WMRS) The ^{17}O excess (isotope anomaly) is represented by the distance of atmospheric measurements from the slope of $\delta^{18}O$ vs $\delta^{17}O$. Taken from Cliff et al. (1999b).

The magnitude of this ^{17}O excess, i.e. the deviation from the mass dependent fractionation line, was determined to be (0.9 ± 0.1) ‰ (Cliff et al., 1999b, Röckmann et al., 2001b, Brenninkmeijer et al., 2003). The origin of this ^{17}O isotope excess, $\Delta(^{17}O)$, can be attributed to either transfer of the isotopic signature from substrates, or fractionation processes. These fractionation processes must be non-mass dependent in order to lead to non-zero $\Delta(^{17}O)$ values. The inherent fractionation in source and sink processes of N_2O will influence the proportion of ^{17}O in the atmosphere. Since the sources and sink of N_2O are not entirely quantified, ^{17}O isotope excess may be caused by either a process which is well understood but the magnitude ill defined, or due to an unrealised atmospheric process. The ^{17}O excess could originate from processes either in the troposphere or stratosphere, and so the source of $\Delta(^{17}O)$ may be related to downwelling of stratospheric N_2O across the tropopause rather than in situ chemistry in the troposphere.

A number of sources of the positive ^{17}O excess in the troposphere are discussed, and fall broadly into 3 categories: biological sources; in situ atmospheric chemistry; and stratospheric sink processes. Additionally, it has been proposed that the ^{17}O excess is due to a numerical peculiarity, as described below.

Biological sources

Biological sources, both land and ocean are likely to contribute to the isotope anomaly in N_2O.

Atmospheric nitrate is seen to have excess ^{17}O (Michalski et al., 2003), so excess ^{17}O could be transferred to N_2O via biological denitrification (Kaiser et al., 2004). In order to quantify the contribution of biological sources to the ^{17}O excess, it is necessary to determine the isotopic composition of N_2O from soils and water (Lewicka-Szczebak et al., 2016). In fact, the first measurements of ^{17}O from soil emissions showed a small positive oxygen anomaly 0.21 ‰ (Komatsu et al., 2008). This was attributed to denitrification of atmospheric NO_3^-. It is important to note that biologically produced N_2O is extremely complex with respect to ^{17}O. Nitrification is a source of N_2O, however, depending on oxygen concentrations, denitrification can be a source or a sink mechanism. A ^{17}O excess of up to 0.4 ‰ is expected from microbial nitrification and denitrification (Meijer and Li, 1998, Barkan and Luz, 2005). Biological variability may have an effect on fractionation patterns and thus should be interpreted carefully.

In contrast to these terrestrial sources which contribute to the ^{17}O excess, N_2O produced from biomass burning is likely to inherit the isotope composition of O_2. Since this O_2 is in fact relatively depleted in ^{17}O, biomass burning is in fact expected to diminish the anomaly slightly (Kaiser and

Röckmann, 2005). This also is relevant for N_2O produced by industrial processes, which likely derive the oxygen isotopic composition from atmospheric O_2.

Importantly, biological sources of the ^{17}O excess are linked to the numerical source, as described below.

In-situ atmospheric chemistry

If terrestrial sources are not considered the source of the ^{17}O excess, then atmospheric chemistry may be of importance. In situ chemistry both in the troposphere and the stratosphere may prove to be a significant source of the ^{17}O excess to the troposphere. Tropospheric and low altitude stratospheric samples showed enrichment in ^{17}O relative to ^{18}O (Cliff et al., 1999b, Röckmann et al., 2001b, Brenninkmeijer et al., 2003). It is not possible to determine as to whether there is an increase in ^{17}O with altitude since the measurements of Cliff et al. (1999b) are not adequately precise to make this conclusion, and they do not penetrate deep into the stratosphere. In theory, stratospheric chemistry could give rise to an increase of ^{17}O excess with altitude. Importantly, however, many of the originally proposed reaction pathways which could lead to enrichment of ^{17}O have now been ruled out experimentally. Additional production and destruction pathways proposed are described below (Yung and Miller, 1997, Brenninkmeijer et al., 2003).

Oxidation of NH_3 then formation of N_2O and NO_2 takes place in the troposphere (Röckmann et al., 2001b). In the tropics, a subsequent reaction with NO_2 is significant in the tropics (Dentener and Crutzen, 1994), especially due to the production of NO_2 biomass burning via Equation 4.2 and 4.3.

$$NH_3 + OH \rightarrow NH_2 + H_2O \qquad \text{Equation 4.2}$$

$$NH_2 + NO_2 \rightarrow N_2O + H_2O \qquad \text{Equation 4.3}$$

It is reasonable that the enriched isotope signature of the substrate species is transferred indirectly to N_2O via this reaction pathway, giving a possible source of the ^{17}O excess. However this reaction cannot account for the increase in anomaly with altitude since it is coupled with surface NH_3 cycling.

Cliff and Thiemens (1997) suggested unrecognised atmospheric processes may give rise to fractionation, for example, the transfer of isotope signature from O_3. A number of mechanisms involving O_3 have been proposed. Direct reaction of excited O_3 with N_2 via Equation 4.4 claimed to show significant N_2O yields (Zipf and Prasad, 1998, Prasad and Zipf, 2000).

$$O_3^* + N_2 \rightarrow N_2O + O_2$$ Equation 4.4

However the high yield means the ^{17}O signature that would be transferred to N_2O from O_3 would exceed the observed ^{17}O anomaly. This suggests that all other sources of N_2O are largely overestimated or sink reactions underestimated.

A different experimental set up investigated these inconsistencies using direct irradiation at 532 nm to avoid production of $O(^1D)$. Previous studies had irradiated at 115-300 nm for dissociation of O_2 to give O_3*. Results showed lower yields so less importance of this reaction (Estupiñán et al., 2000, Estupiñán et al., 2002). This experimental evidence essentially rules out the importance of the direct reaction of O_3 with N_2 as the source of the ^{17}O excess.

An alternate experiment gave detectable yields at 266 nm irradiation:

$$O(^1D) + N_2 + M \rightarrow N_2O + M$$ Equation 4.5

This source is small but could account for a significant part of the ^{17}O excess, since $O(^1D)$ is generated by the photolysis of enriched O_3 (Estupiñán et al., 2002). This reaction in fact takes place in the stratosphere so could account for the increase in the anomaly with altitude.

The reaction of CO_2 with $O(^1D)$ causing oxygen exchange between O_3 and CO_2 is analogous to the reaction involving N_2O. This reaction gives enrichment in heavy isotopes in CO_2. The implication of this reaction is that intermediate in this reaction could react with N_2 to give N_2O to give enrichment in heavy O isotopes. This proposed oxygen isotope exchange during the reaction of $O(^1D)$ and N_2O, suggested by Morgan et al. (2004), could cause the ^{17}O excess to be close to the 1 ‰ measured in the troposphere. This would then explain the ^{17}O excess. However Kaiser and Röckmann (2005) suggest that isotope exchange accounts for less than 1 % of the reaction rate and can therefore be neglected as the source of the ^{17}O excess.

The transfer of the oxygen isotope signature from O_3 was demonstrated by production of excited NO_2* and NO_3* which then react with N_2 to give NO + N_2O (Zellner et al., 1992). However N_2O yield was likely due to artefact production. Later studies (Estupiñán et al., 2000) showed no N_2O production in this way.

Stratospheric sink processes

Light ground and ocean sources, as well as little contribution from in situ atmospheric chemistry means that sink processes in the stratosphere atmosphere may be the source of the ^{17}O excess, via reaction with $O(^1D)$ or photolysis. However, the reaction of N_2O with $O(^1D)$ was ruled out by Kaiser and Röckmann (2005) and Schmidt et al. (2011). Additionally, the suggested source from

photolysis of N_2O was ruled out by Kaiser et al. (2004). However it is important to note that no measurements of $\Delta^{17}O$ have been made at stratospheric altitudes, which is addressed in this chapter. Johnston et al. (1995) didn't show any significant fractionation for photolysis, but the experiments in fact had inadequate wavelengths

The modelled effect of stratospheric photolysis on the isotopic composition of N_2O showed only a very small contribution towards the ^{17}O excess (Schmidt et al., 2011, Schmidt and Johnson, 2015), suggesting that the photolysis sink process is not the source of the ^{17}O anomaly. Schmidt in fact predicted photolysis to produce an isotope anomaly of (0.1–0.3) ‰. There is however, an altitude dependent photolysis rates. This is due to the wavelength dependence of isotopic dependence of N_2O photolysis, as shown in laboratory experiments (Kaiser et al., 2002). The photolysis of N_2O showed ^{17}O excess to be essentially equal to zero, meaning the photolysis is strictly mass dependent.

Numerical source

Budget calculations have suggested that a significant of the ^{17}O excess can be attributed to a 'numerical source'. There is general acceptance that N_2O from biological production follows the mass-dependent fractionation line. However, Young et al. (2002) noted that a non-zero ^{17}O isotope excess can occur even with mass-dependent fractionation. This means that the source of the ^{17}O excess may in fact be unrelated to source and sink processes, or to isotopic composition of substrates.

The ^{17}O excess is, by definition, the deviation of measured values from the slope of the three isotope exponent (Figure 4.2). Since the slope, β, is itself a function of the relative abundances of ^{18}O, ^{17}O and ^{16}O, any variation on these individual abundance values will influence the slope. If mass-dependent processes are assumed to follow a different fractionation line to the 0.516 slope, the atmospheric values may in fact be closer to this line, and the ^{17}O excess is resolved (Kaiser and Röckmann, 2005, Kaiser et al., 2004). For example, microbial nitrification and denitrification could follow a fractionation line of (0.5279±0.0001) ‰ (Barkan and Luz, 2005), and therefore reduce the apparent excess by 0.4 ‰ (Meijer and Li, 1998). This variety in calculated β (the three isotope exponent) is a possible explanation of the 'source' of the ^{17}O excess.

In summary, the ^{17}O excess in atmospheric N_2O is likely to be, at least in part, due to contributions from mass-dependent processes. These processes may either transfer the isotope

signature of O_3 which has been fractionated non-mass dependently, or follow a different fractionation line to the arbitrary line deduced for N_2O.

4.4 Scope and justification of study

The origin of the ^{17}O excess in the troposphere remains under debate. It seems unlikely that the source is of stratospheric origin, or if so, only accounts for a negligible proportion of N_2O enriched in ^{17}O. In order to determine the origin of the ^{17}O excess in the troposphere, it is necessary to confirm the suggestion that the stratospheric sink processes, photolysis and reaction with $O(^1D)$ coupled with downwelling to the troposphere do not cause excess ^{17}O. Measurements by Cliff et al. (1999b) between 8 and 12 km, displayed good agreement of ^{17}O data with tropospheric measurements. This was interpreted to mean that the ^{17}O excess source did not originate from the stratosphere. The study by (Cliff et al., 1999b) demonstrated that up to 12 km sink processes appear to give non mass-dependent fractionation of ^{17}O. However, to date no studies have provided measurements of ^{17}O in stratospheric N_2O above 12 km, In order to determine whether the ^{17}O excess is of stratospheric origin, these measurements are required. The research aims to provide evidence for answering the questions:

1. Is the origin of the ^{17}O isotope excess due to fractionation processes in the stratosphere, followed by downwelling?
2. If not, can a stratospheric source be ruled out, and what is the most likely alternative scenario?

This study presents measurements of the ^{17}O excess of stratospheric N_2O, from above the lowermost stratosphere. A set of balloon samples taken from 10.4 to 26.6 km over Gap, France (44° N) were analysed using a MAT 253 Isotope Ratio Mass Spectrometer (IRMS). These results represent additional $\delta^{18}O$ and $\delta^{15}N$ data to that of Bernard et al. (2006), as well as the first $\delta^{17}O$ measurements of N_2O above 12 km.

Before analysis, it was necessary to develop an inlet system for atmospheric samples containing low mole fractions of N_2O. Significant modifications were made to an existing inlet system to allow such samples to be measured with adequate precision to form conclusions regarding the origin of the ^{17}O excess.

4.5 Experimental methods

During this work, a Finnigan MAT 253 Spectrometer (Thermo Fisher Scientific) was used to measure isotopes in N_2O. The use of the Isodat 3.0 software allowed for analysis of isotope

ratios, and was used for further automation of the inlet system. The existing set up consisted of a continuous flow inlet system to separate analytes from interfering substances and introduce these analytes into the mass spectrometer. To control the helium load to the spectrometer ion source an open split periphery was used as a transition point between the high helium loaded sample gas and the vacuum of the mass spectrometer. It was necessary to convert the N_2O to O_2 and N_2 via an in-line gold furnace for subsequent isotope analysis.

The provided inlet system was rapidly determined to be insufficient for N_2O isotope analysis in atmospheric samples with low mole fractions, and so significant modifications were carried out. The modified system was used to carry out the first measurements of $\Delta^{17}O$ in stratospheric N_2O above 12 km.

4.5.1 Extraction of N_2O from bulk air

In order to produce highly reproducible measurements of $\Delta^{17}O$ in whole air samples, an existing inlet system required modification and improvement. An extraction system for continuous flow gas chromatography was originally intended for use with seawater samples. Via this method, as described by Grefe (*PhD Thesis, September 2013*), and based on systems of McIlvin and Casciotti (2010) and Kaiser (2008), N_2O is extracted, purified on line and analysed for $\delta^{18}O$, $\delta^{17}O$ as well as $\delta^{15}N$. For the purpose of measurement of N_2O from atmospheric samples, modifications to the inlet system were carried out.

The existing extraction system was modified to accommodate atmospheric samples in three ways:

(i) Replacement of seawater components with those more suitable for use with air samples. This enabled dead volume within the system to be reduced.

(ii) The sample inlet was modified to accommodate:
(a) Alternation of a sample and standard without the need to disconnect cylinders
(b) The use of samples of differing mole fractions of N_2O
(c) The introduction of samples entirely automatically, thus limiting manual errors.

(iii) The system was optimised to give highly reproducible $\Delta^{17}O$ measurements in whole air samples.

The replacement of seawater-compatible components consisted of removal of a number of flasks and chemical traps (Figure 4.3). A solenoid valve, V2, was added to allow additional samples to be introduced without the need to disconnect and reconnect cylinders thus ensuring that once leak tight, no interferences were introduced. Both inlets to V2 allowed sample to flow

through a mass flow controller to ensure consistency of sample flow rates. The chemical trap prior to V3 was changed from Carbosorb, a carbon dioxide absorbant (0.7-1.2 mm, *Elemental Microanalysis*) only, to half Carbosorb and half magnesium perchlorate ($Mg(ClO_4)_2$, *Merck*) for removal of water generated by the reaction of sodium hydroxide and carbon dioxide within the trap. Carbosorb and magnesium perchlorate (*Sigma Aldrich*) were separated with quartz wool. A pump was added at the vent at V3 to allow either (a) samples to be pumped through the liquid nitrogen trap (T1), or (b) use high flow helium as a carrier gas. The use of a pump allowed samples to be extracted under reduced pressure thus reducing the amount of oxygen frozen out during cryogenic extraction. These modifications additionally allowed dead volumes to be reduced.

To allow the system to be fully automated, and therefore improve reproducibility, the system needed to be suitable for use with a variety of samples with different mole fractions, and without the need to change cylinders frequently. Modifications allowed gases to be fed from three sources, two suitable for a variety of mole fractions, and one for samples of high mole fractions only. All three were able to alternate automatically as required. All tubing was 1/16 inch outer diameter stainless steel tubing.

At the right hand inlet to V2, an original 16 gauge needle was removed and an additional 6-port valve, V1, was fitted. Helium at 36 ml/min (STP: 1 bar, 20 ºC) flowed into V1 via a mass flow controller (port 5) as well as flow from an attached sample cylinder (port 3). A sample loop was connected at both ends to V1 (ports 1 and 4). A vent was fitted with a needle valve to control sample flow at port 2. Port 6 allowed sample to enter the main inlet system for cryogenic trapping. Once the sample cylinder was attached, V1 was set to the load position, and the sample introduced through the sample loop and out through the vent at the same valve using the cylinder pressure only. Sample flow was controlled to be in excess of 20 mL min^{-1} (STP) for 1 minute using the needle valve. The sample cylinder was then closed to allow the pressure inside the loop to equilibrate. Varying the length of 1/16 inch stainless steel tubing was fitted as the sample loop (lengths 200 cm and 396 cm) depending on the concentration and therefore quantity of sample required for analysis. Once equilibrated, V1 was switched to inject to allow the sample to flow towards T1 via V2. High flow helium was used as a carried gas, which was controlled to 36 mL min^{-1} (STP) by a mass flow controller. Helium passed through a Nafion dryer (Perma Pure) with nitrogen counter-flow at 160 mL min^{-1} for initial drying.

Samples with mole fractions close to that of tropospheric air were extracted directly into LN_2 without the use of a sample loop. V2 was opened, plus either sample valve 1 or valve 2, all

automated. Flow was controlled at 36 mL min^{-1} by an additional mass flow controller at V2. Pumping at V3 in addition to cylinder pressure allowed samples to travel towards T1 for cryogenic extraction. Originally, samples were extracted using a helium carrier gas at the flow of 36 mL min^{-1}. The use of helium to push the sample was replaced with use of a pump at V3 to improve precision.

After passing V2, samples were introduced via 1/16 inch stainless steel tubing (*Alltech*, 0.05 inch inner diameter (i.d.)), pumped at 24 mL min^{-1} through a multiport 6 port Valco valve (V3), to a sample loop (T1) immersed in liquid nitrogen (77 K). Passing through the on-line chemical trap, containing Carbosorb and magnesium perchlorate, removed carbon dioxide (CO_2) and water (H_2O) from the sample. Cryogenic extraction times were varied to trap equivalent N_2O sample sizes to that of tropospheric air.

After extraction into T1 was complete, trap 2 (T2) was lowered into liquid nitrogen (77 K) for 20 seconds. V3 was switched from load to inject and T1 lifted out of the liquid nitrogen to enable low flow helium (0.7 mL min^{-1}) to transfer the collected N_2O sample from T1 into the cryofocus trap, T3. Focussing took place for 500 seconds after which T3 was lifted and V2 returned to the load position to allow helium to purge any remaining sample out of the tubing. T3 consisted of a fused silica capillary, protected by a 1/16 inch stainless steel tubing loop in liquid nitrogen.

4.5.2 Gas chromatographic purification and conversion of N_2O to N_2 and O_2

After transfer from T1 to T2 was complete, the sample was released and passed over a pre-column (30 m long, 0.32 mm i.d. PoraPlot Q, *Thermo Fisher Scientific*) at 0.9 mL min^{-1}. Once the N_2O peak had eluted, a 6-port 2-position Valco valve was switched to the opposite position to remove late eluting substances from the column. For $\Delta^{17}O$ analysis, the sample was passed through a furnace containing a gold catalyst tube (50 cm long, 0.6 mm i.d., 1.6 mm o.d.) held isothermally at 900 °C, where the catalyst decomposed N_2O to N_2 and O_2. By measuring the stable isotope composition of nitrogen and oxygen separately, $\Delta^{17}O$ can be determined.

Separation of O_2, N_2 and interferences was achieved via a 5 Å molecular sieve column downstream of the furnace (30 m long, 0.32 mm i.d., *Restek*). The original 15 m-molecular

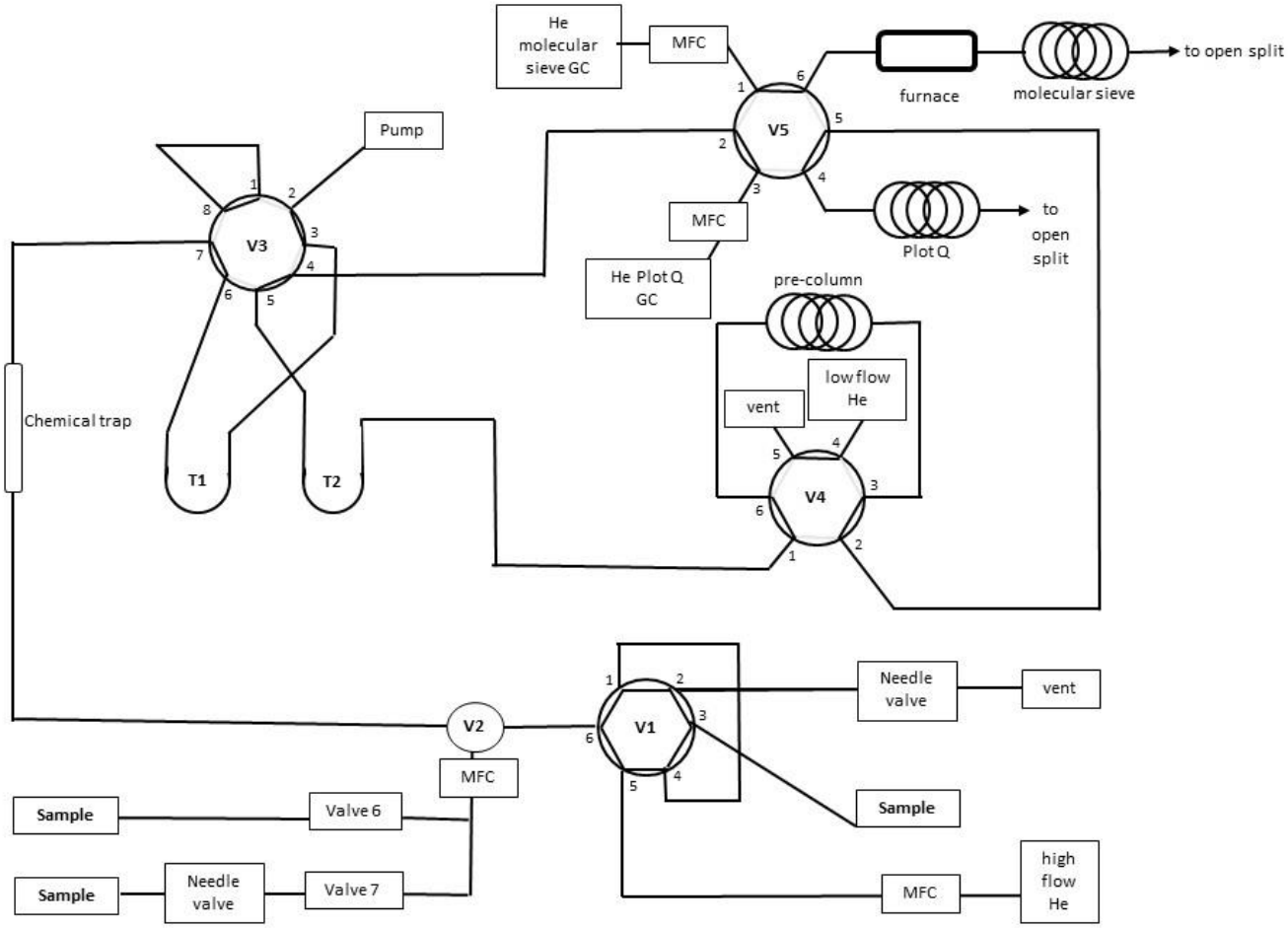

Figure 4.3. Modified inlet system used for N_2O analysis. V1, V4 and V5 denote 6 port valco valves. V3 is an 8 port valco valve and V2 a solenoid valve. MFC denotes mass flow controllers

sieve column used for the seawater setup was replaced by a 30 m-column of the same type to give improved separation of N_2O from CO_2 and O_2. Both the PlotQ and molecular sieve column were held at 37 °C.

4.5.3 Mass spectrometric analysis

Samples were introduced to the spectrometer via an open split interface, modified from the default setup of the reference open split in the GasBench II (*Thermo Fisher Scientific*). Masses *m*/z 32, 33, 34 were measured simultaneously for O_2 analysis, switching to masses *m/z* 28 and 29 when the N_2 peak eluted.

4.5.4 Optimisation of system

The peak size dependence was the main challenge in achieving precision of $\Delta^{17}O$ below 0.3 ‰. It was found that any small variation in the sample peak area gave variations in $\delta^{15}N$, $\delta^{18}O$, and in particular $\delta^{17}O$. Three parameters influenced the sample peak area: the amount of N_2O trapped cryogenically, the speed at which the sample was trapped, plus the temperature of the furnace giving conversion from N_2O to O_2 and N_2.

4.5.6 Linearity testing

Stratospheric samples were collected from between 10.4 km and 26.6 km, and hence contained non-equivalent N_2O mole fractions. If flow rate and trapping time remained constant, the amount of pure N_2O trapped was thus variable dependent on age of air (or altitude of collection). This in turn gave a variety of measurement peak areas. It was necessary to determine the linearity of the delta values with respect to the sample size. This was achieved by using a laboratory standard (BOC) and varying the trapping time at 5, 15, 30, 45 and 60 minutes using the pump method (Figure 4.4). Sample flow remained at 20 mL min^{-1}, with a helium carrier gas at 36 mL min^{-1}.

In the case of $\delta^{15}N$, it can be seen that there is no definite correlation with changing trapping time, but the measurements have large variability. It can be seen that $\delta^{17}O$ and $\delta^{18}O$ increase with increased trapping time, however, the correlation is not linear. It is necessary therefore to ensure that peak areas remain as constant as possible across all measurements to reduce the effect of this non-linearity on the data. In order to achieve this, the amount of standard trapped was matched to the amount of sample trapped to ensure peak areas remained constant.

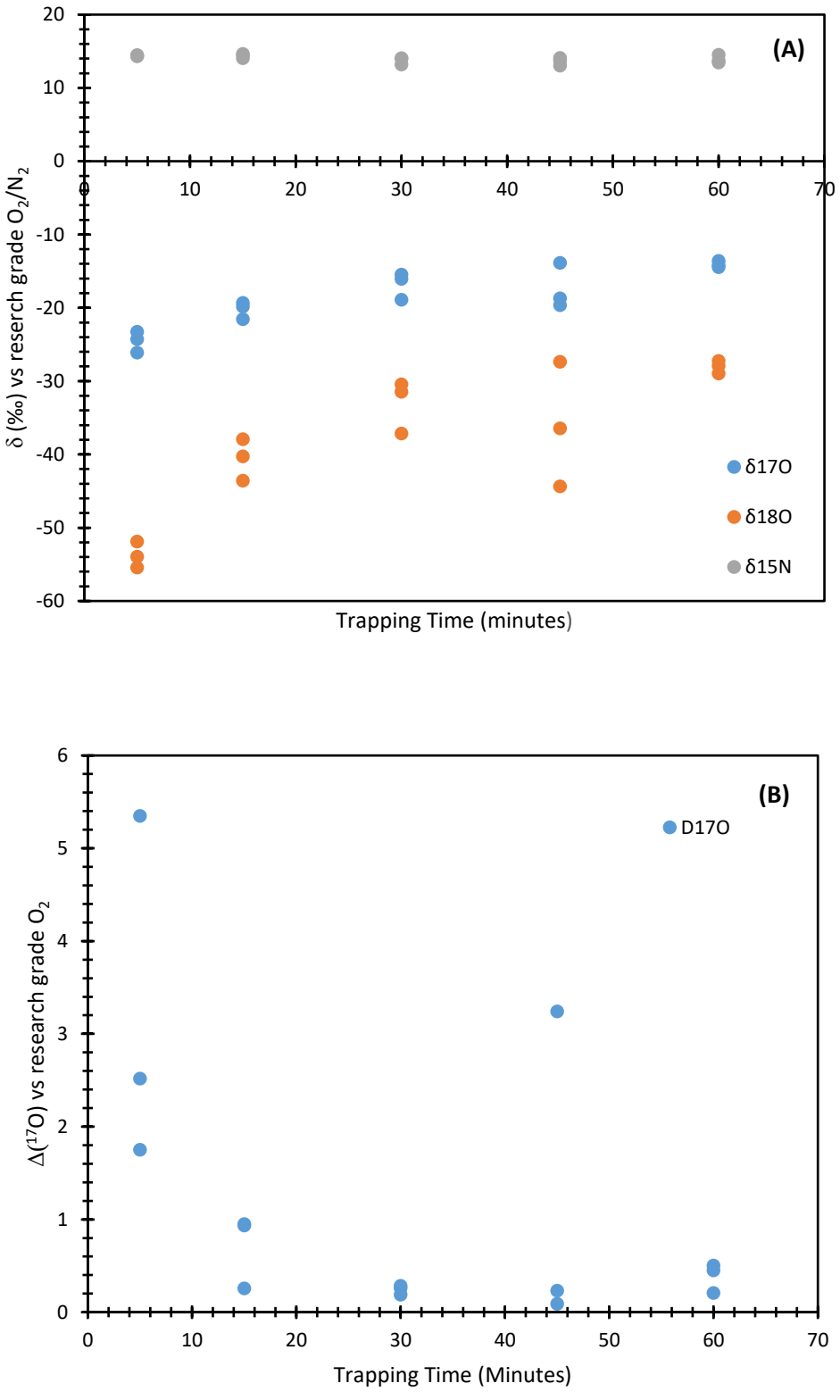

Figure 4.4. (A) Linearity tests showing effect of sample size, quantified by trapping time (minutes), on $\delta^{17}O$ (blue circles) $\delta^{18}O$ (red circles) and $\delta^{15}N$ (grey circles). All delta values are relative to research grade oxygen ($\delta^{17}O$, $\delta^{18}O$) and research grade nitrogen ($\delta^{15}N$). **(B)** Effect of sample size on $\Delta(^{17}O)$ calculated relative to 3-isotope exponent slope at 0.516 of in-house tropospheric air standard.

The stratospheric samples all contained mole fractions equal to or lower than tropospheric air, and so were trapped cryogenically using the inlet from Valve 7 to Valve 2 directly. To ensure peak areas remained as constant as possible, extraction flow rates remained constant using the MFC before V7, but the time of extraction was varied to give equivalent amounts of N_2O frozen out in liquid nitrogen. For high mole fraction samples, i.e. those with mole fractions equal to or higher than tropospheric air, sample loops were filled with sample, the cylinder isolated, and then the sample extracted cryogenically from the loop as described above. This method required the length of the stainless steel loop to be modified to contain the equivalent amount of N_2O to tropospheric air to enable the measurement peak area to remain constant.

4.5.7 Furnace temperature

The temperature of the furnace had an influence on the conversion of N_2O to O_2 and N_2, and hence the measured peak area as shown by Figure 4.5. Since $\delta^{15}N$, $\delta^{18}O$, and $\delta^{17}O$ are affected by sample peak are, it follows that furnace temperature influences these measurements (Figure 4.6). Although the peak area of both *m/z* 32 and *m/z* 28 increased with furnace temperature, the precision was determined at the intermediate value of 900 °C.

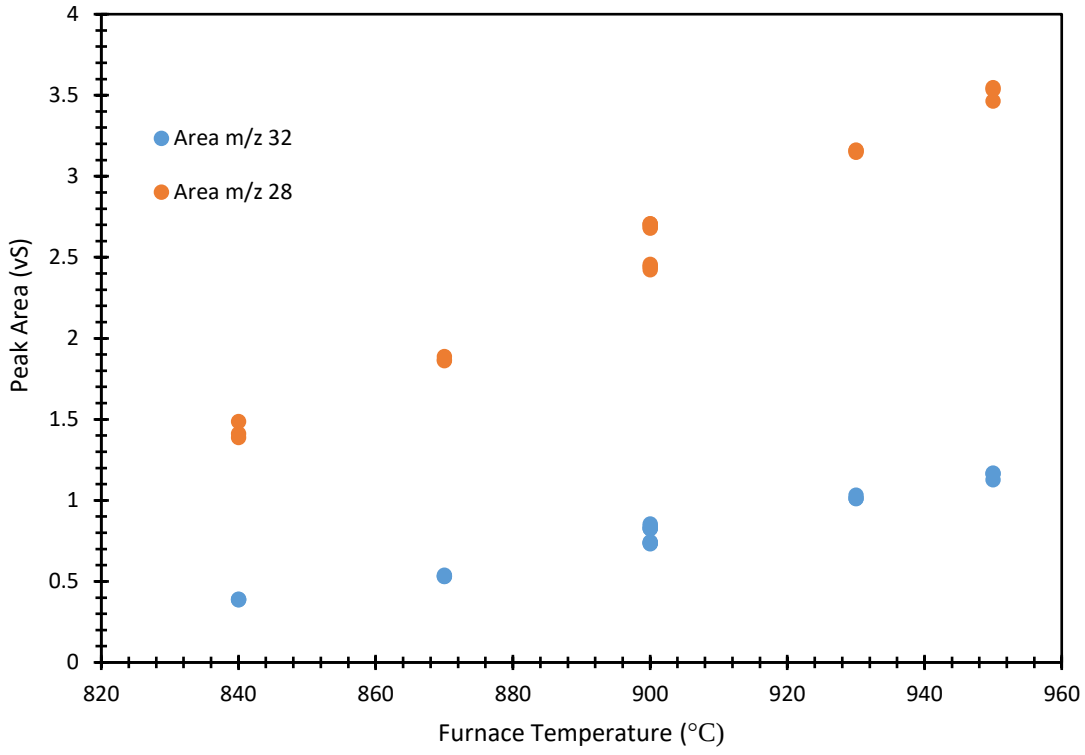

Figure 4.5. Effect of furnace temperature (°C) on peak area (Vs) for *m/z* 32 (blue circles) and *m/z* 28 (red circles).

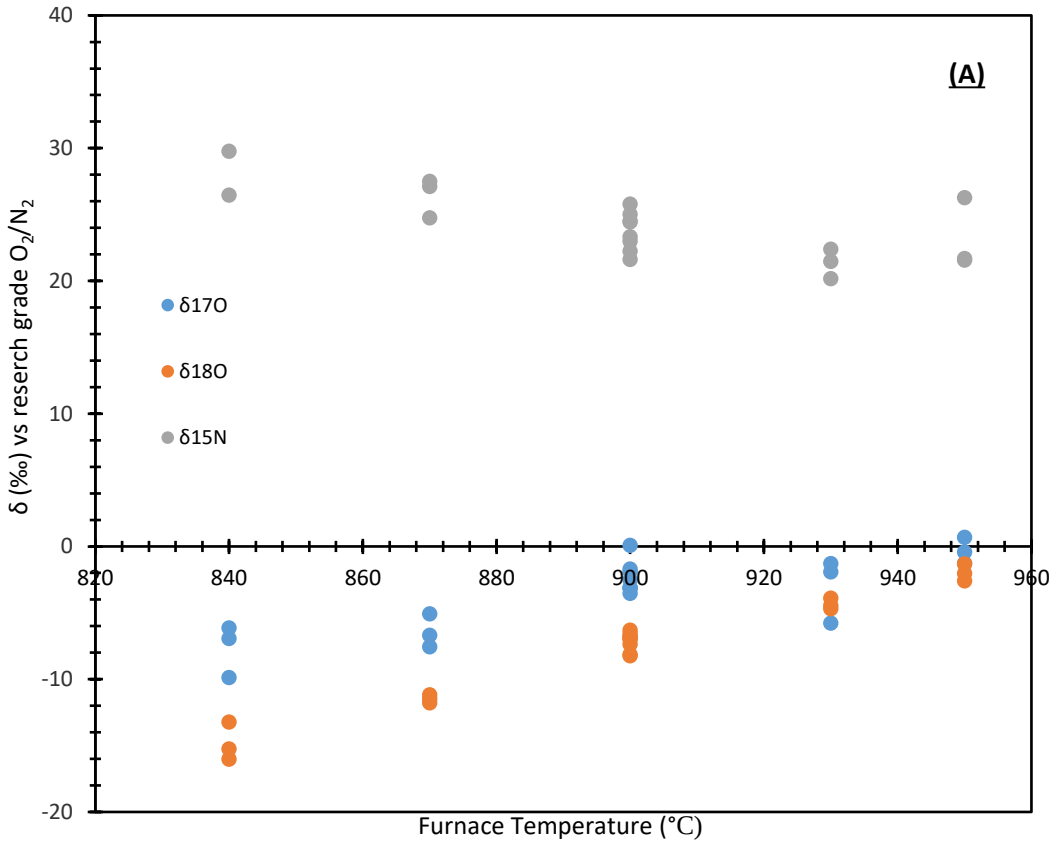

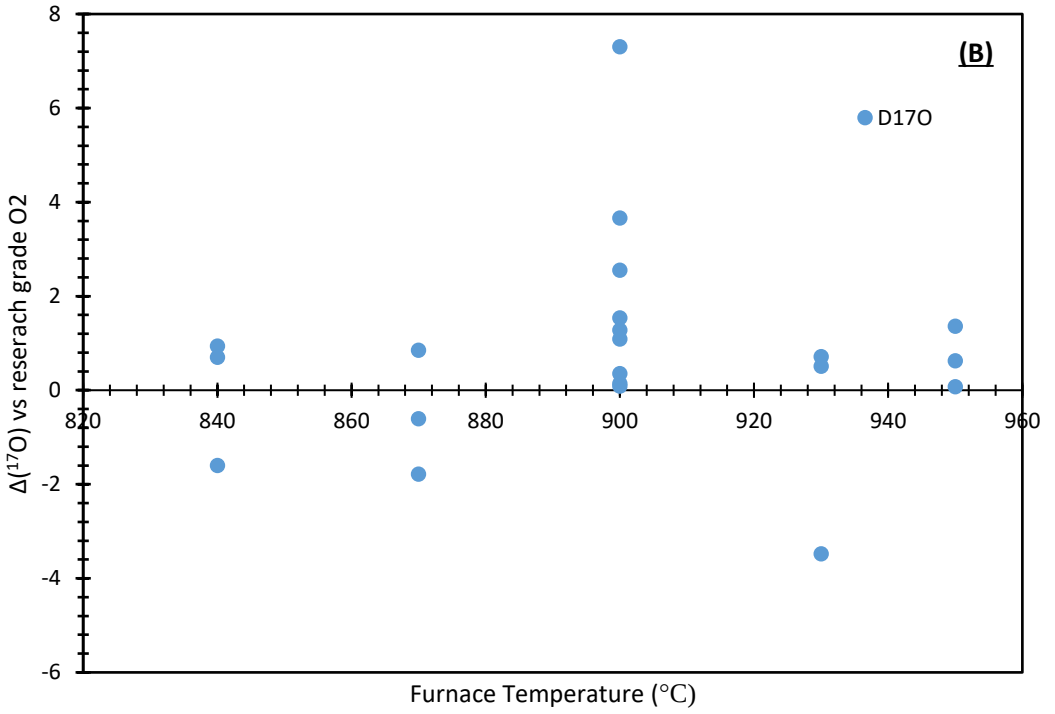

Figure 4.6. (A) Effect of furnace temperature (°C) on $\delta^{17}O$ (blue circles), $\delta^{18}O$ (red circles) and $\delta^{15}N$ (grey circles). All delta values are relative to research grade oxygen ($\delta^{17}O$, $\delta^{18}O$) and research grade nitrogen ($\delta^{15}N$). **(B)** Effect of furnace temperature on $\Delta(^{17}O)$ calculated relative to 3-isotope exponent slope at 0.516 in an in-house tropospheric air standard.

It was possible to achieve $\delta^{17}O$ precision below 0.3 ‰ at 900 °C enabling the running temperature of the furnace to be well below that of the melting point of gold (1064 °C) and thereby preventing damage to the gold catalyst.

4.5.8 Use of the backflush function

Using a backflush function ensures that late eluting compounds are removed from the system before they can reach the precolumn and main column. The time in the sample sequence at which the back flush is activated was determined to have an impact on the precision. The optimum backflush position was determined, to ensure no interferents eluted at the same retention time as the sample peak, but ensuring unwanted compounds were removed. This improved the precision.

4.5.9 Optimisation of flow rates

The retention time of sample peaks was not stable, so additional mass flow controllers were added to improve this, as well as investigating the optimum flow through each part of the extraction system, including the 3 columns. Optimum flows are shown in Table 1. The flow rate through the sample loop ensured that minimal sample was used, yet ensuring that the loop was completely purged of helium. The sample pump flow was adjusted to 24 mL min^{-1} using a mass flow controller (MFC) for the same reason. The flows at the sample loop to T1 and from T1 to T2 were optimised to ensure that all of the sample was transferred from one component to the next, leaving no trace and ensuring no fractionation occurred. The flow rate through both the precolumn and main column were set at 0.9 mL min^{-1} to enable maximum separation of nitrogen and oxygen peaks, yet ensuring no interference from CO_2. The altered flow meant that the position of capillaries in the open split were modified to give maximum peak areas.

4.5.10 Column temperature

The optimum temperatures to run both the Plot Q and Mol Sieve columns were investigated (Table 1). The original set up used a GC temperature of 37 °C; however, separation was greatly improved with decreased temperature. The measurement precision of tropospheric air samples was improved with added separation.

4.5.11 Stratospheric air sampling

Upper tropospheric and stratospheric balloon air samples from 8.3 km to 34.4 km were collected at a mid-latitude site (Gap, France, 44.4° N) during March and April 1999, using a cryogenic whole air sampler. Further details can be found in (Bernard et al., 2006).

Table 4.1. Optimum flows for components in inlet system after testing of flow rate for optimum precision

Component	Gas	Flow rate
Sample loop fill	Sample, Helium blank, Standard	20 mL min^{-1}
Sample pump	Sample, Helium blank, Standard	24 mL min^{-1}
High flow carrier gas	Helium	36 mL min^{-1}
Nafion drier counter flow	Nitrogen	160 mL min^{-1}
Transfer from loop to Trap 1	Helium	36 mL min^{-1}
Transfer from Trap 1 to Trap 2	Helium	0.7 mL min^{-1}
Precolumn and main column	Helium	0.9 mL min^{-1}

Of the 14 whole air samples collected at this site, 8 were analysed in this study, based on there being sufficient N_2O present in the sample to extract and purify via an on-line continuous flow preparation system.

4.6 Repeatability

The repeatability of measurements combines the repeatability of both the instrument, as determined by direct injection of reference gases, and the inlet system, measured by introducing the tropospheric air standard (BOC) repeatedly through the system.

Table 4.2. Comparison of average values of $\delta^{17}O$, $\delta^{18}O$, $\Delta^{17}O$ and precision achieved (n=6) at two column temperatures for tropospheric air (BOC). Delta values relative to research grade O_2/N_2.Temperature is displayed in °C. Averages and σ values in ‰.

GC Temperature	Average $\delta^{17}O$	σ $\delta^{17}O$	Average $\delta^{18}O$	σ $\delta^{18}O$	Average $\Delta^{17}O$	σ $\Delta^{17}O$
37 °C	0.97	0.42	-2.84	0.54	2.44	0.29
19 °C	1.36	0.63	-3.09	0.74	2.95	0.75

4.6.1 Repeatability of the O_2 reference gas.

Repetition of injection of the O_2 reference gas into the open split interface was carried out. The O_2 reference peaks showed significant variation in peak area over the first 3-5 peaks of the day, as shown in Figure 10. Precision over the first 5 peak was 2.84 Vs. The effect of reference peak area δ values is shown in Figure 12. Delta values are calculated with respect to the central reference peak 10. By definition, reference peak 10 therefore had a δ value of 0, as plotted (Figure 4.7). It was necessary to keep the peak area of reference peak constant for better measurement precision. The amount of reference peaks was increased, and only when the reference peak area had been stable for 5 peaks, was a peak used to reference a sample peak. This improved precision to 0.14 Vs over the last 5 peaks. Improvements in precision of $\delta^{17}O$ was from 0.43 to 0.05 ‰ and from 0.24 to 0.19 ‰ for $\delta^{18}O$. Since the precision was greatly improved by increasing the amount of reference peaks, each sample analysis was with respect to the final peak in a set of 20 reference peaks. The position of the peak jump between detection of O_2 and N_2 was optimised to give minimum disruption to eluting sample peaks.

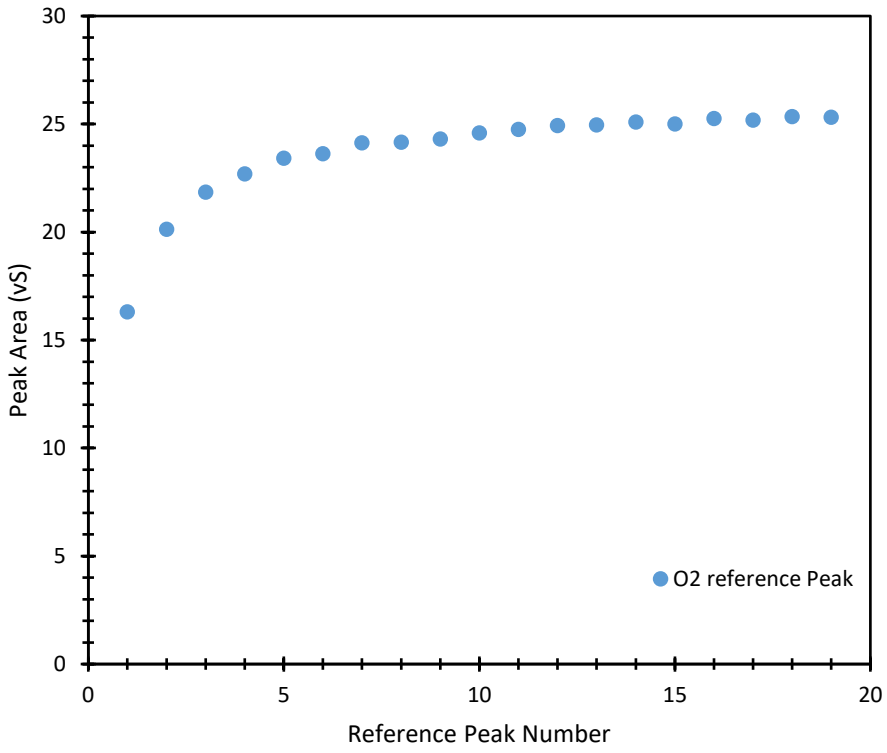

Figure 4.7. Repetition of O_2 reference peaks to identify repeatability of peak area (vS). 1σ precision of peak area over first 5 peaks is 2.84 Vs, and over last 5 peaks 0.14 Vs.

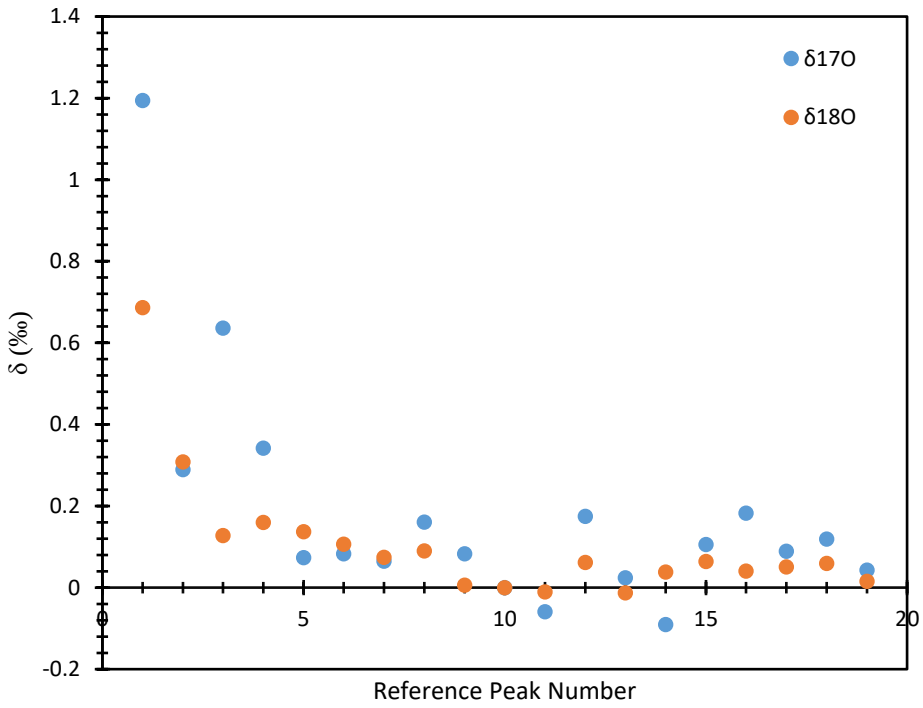

Figure 4.8. Repetition of O_2 reference peaks to identify repeatability of $\delta^{17}O$ (blue circles) and $\delta^{18}O$ (red circles). Each data point is a single measurement. 1σ precision of $\delta^{17}O$ was 0.43 ‰ over first 5 peaks is, and 0.05 ‰ over last 5 peaks. 1σ precision of $\delta^{18}O$ was from 0.24 ‰ over first 5 peaks is, and 0.19 ‰ over last 5 peaks. All delta values are relative to research grade O_2.

4.6.2 Repeatability of tropospheric air standard

After modifications to the inlet system and optimisation were carried out, the final measurement precision was identified. Repetition of introduction of the tropospheric air standard (6 nmol) into the inlet system was carried out. This was repeated 6 times to mimic that of a standard sample run of the stratospheric samples (Figure 4.9). After 6 runs, the 1σ precision of $\delta^{17}O$ is 0.50 ‰ (n=6). However it was seen that eliminating the first data point improved precision to 0.34 ‰ (n=5). For $\delta^{18}O$ the 1σ precision was 0.37 (n=6) and 0.30 (n=5). The 1σ precision of $\Delta(^{17}O)$ was found to be 0.34 (n=6) and 0.23 (n=5). In conclusion, it was determined that the new inlet system had sufficient precision to allow analysis of stratospheric air samples, in particular when repeats were carried out 6 times and the fist data point in each set discarded.

4.7 Results and discussion

4.7.1 Data correction

The lack of an internationally agreed atmospheric standard for N_2O means that reported measurements are generally described relative to standard mean ocean water (SMOW) for oxygen isotopes, and Air-N_2 for nitrogen isotopes. In order to compare data from this study to that published elsewhere, it was necessary to relate the new data to a recognised calibration gas such as these. It was therefore useful to relate this new data to previously published data, which had been related to a recognised calibration scale.

Isotope ratios in samples in this study were corrected relative to previously published measurements, allowing for a relationship between the new measurements in this study and a recognised standard. Measurements of $\delta^{18}O$ and $\delta^{15}N$ of samples used here have already been reported by Bernard et al. (2006). Comparison was made between measurements of ^{18}O and

^{15}N from Kaiser et al. and $\delta^{15}N$, $\delta^{17}O$ and $\delta^{17}O$ data from this study, and the latter corrected accordingly in order to relate measurements from this study to SMOW. Measurements of $\delta^{18}O$ and $\delta^{15}N$ from 2006 gave a reproducibility for a 2 nmol N_2O sample of 0.15 ‰. Bernard et al. (2006) reported nitrogen and oxygen isotopes relative to SMOW, Air-N_2 and an in house

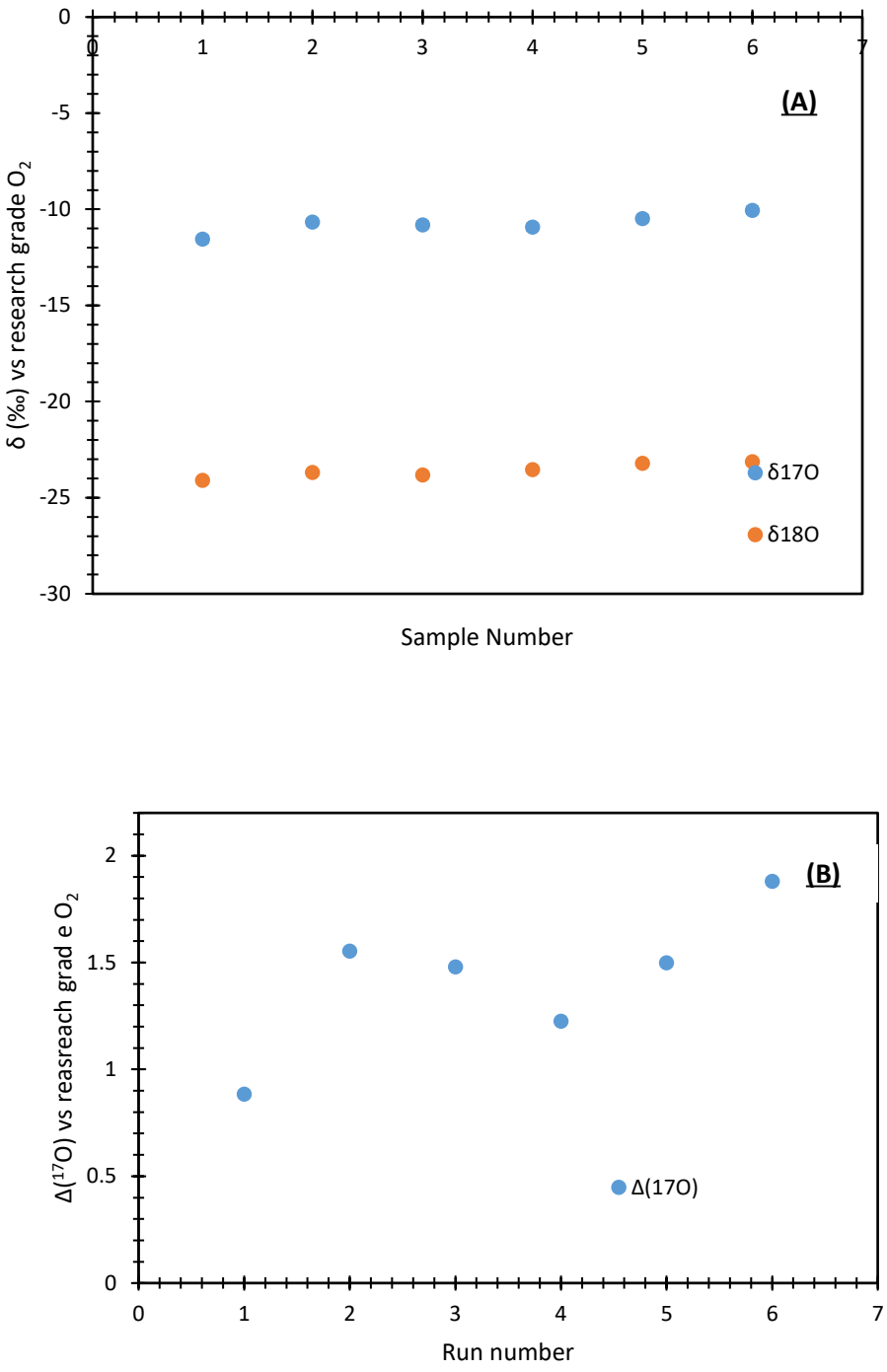

Figure 4.9. (A) Repetition of 6 x 6 nmol tropospheric air standard (BOC) passed through the inlet system to identify reproducibility of $\delta^{17}O$ and $\delta^{18}O$. 1σ precision $\delta^{17}O$ is 0.50 ‰ (n=6), and 0.34 (n=5), $\delta^{18}O$ is 0.37 (n=6) and 0.30 (n=5) **(B)** Repetition of 6 x 6 nmol tropospheric air standard passed through the inlet system to identify reproducibility of $\Delta(^{17}O)$. 1σ precision is 0.34 (n=6) and 0.23 (n=5). All delta values are relative to research grade O_2.

tropospheric air standard. This study calculates delta values relative to an in house tropospheric air standard, and so data was corrected relative to the Kaiser 2006 tropospheric air standard using a simple linear regression.

Figures 4.10 and 4.11 show the relationship between the data from this study and those from 2006. Even though both data sets are relative to tropospheric air, the data do not display identical $\delta^{15}N$ or $\delta^{18}O$ values. This can be attributed to the fact that although both of tropospheric origin, the reference gas was sourced from different locations at different points in time, and analysed using different analytical methods. However, there is good correlation in both cases ($r^2 = 0.98$) for $\delta^{18}O$, and for $\delta^{15}N$ ($r^2 = 0.99$). The linear regression slope was applied as a correction factor to the data in this study giving data. This means that all data points from both studies are relative to tropospheric air used in 2006. Since the 2006 tropospheric standard is related to Air-N_2 and SMOW, this study is now related to the same internationally recognised standards.

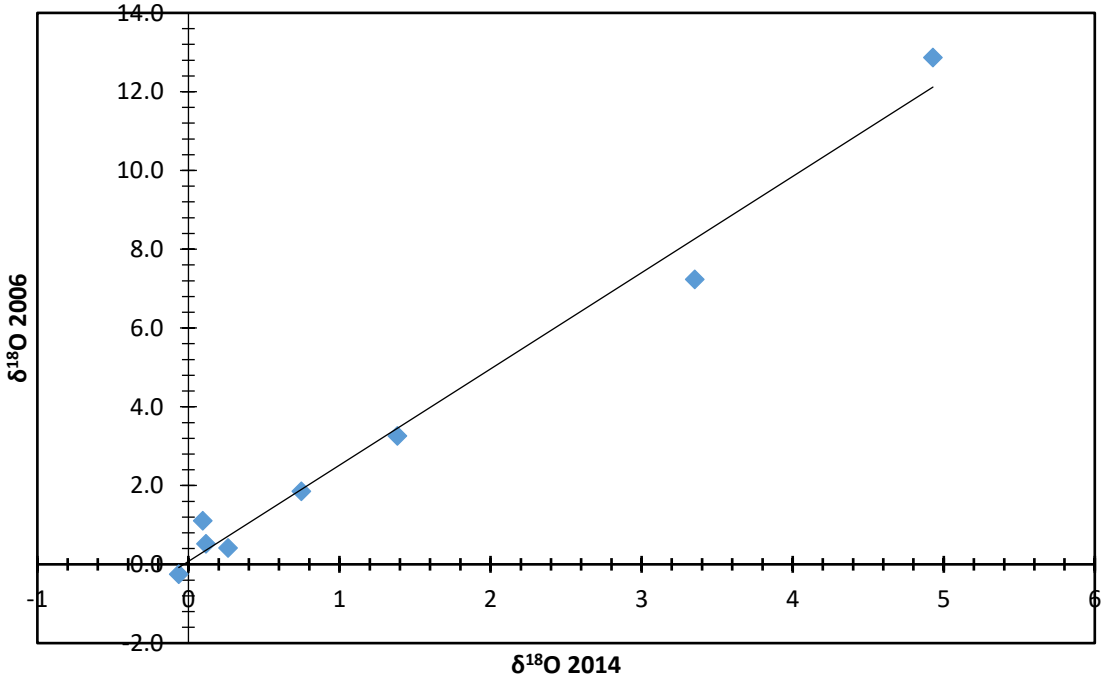

Figure 4.10. Correlation between $\delta^{18}O$ measurements from 2014 data (this study) and $\delta^{18}O$ measurements from Bernard et al. (2006). All delta values are relative to tropospheric air. $r^2 = 0.98$. Slope used for correction of 2014 data = 2.44.

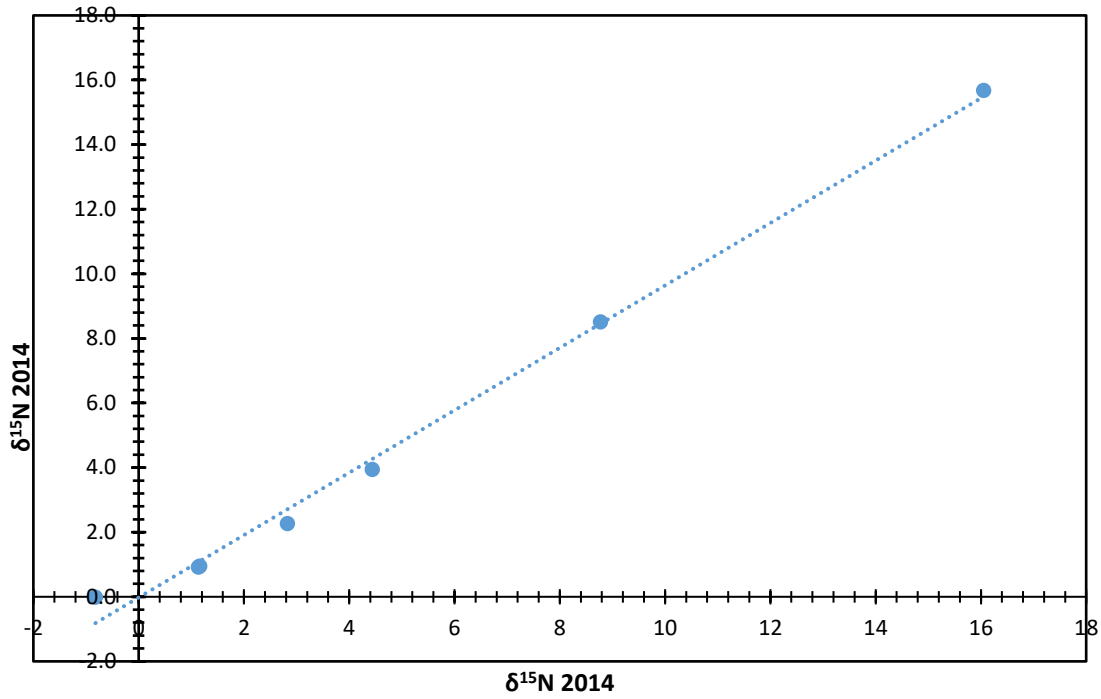

Figure 4.11. Correlation between $\delta^{15}N$ measurements from 2014 data (this study) and $\delta^{18}O$ measurements from Bernard et al. (2006). All delta values are relative to tropospheric air. $r^2 = 0.99$. Slope used for correction of 2014 data = 0.97.

It was assumed that the $\delta^{17}O$ measurements follow the same correlation as the $\delta^{18}O$ Kaiser data. Therefore, for comparison, $\Delta^{17}O$ data was corrected with respect to the 2006 data by using the slope (0.244) of the $\delta^{18}O$ correlation plot. All delta values are relative to tropospheric air.

4.7.2 Measurement of stratospheric samples

Results from stratospheric samples are presented using the standard delta notation with respect to tropospheric N_2O.

The data for the 8 stratospheric samples (n=6) is plotted as a function of mole fraction (Figure 4.12) for bulk oxygen and nitrogen isotope signatures. In general the magnitude of isotope fractionation for ^{17}O, ^{18}O and ^{15}N increased with altitude. This enrichment agrees with the suggestion that kinetic isotope fractionation occurs in sink processes in the stratosphere, either ultraviolet photolysis or reaction with $O(^1D)$. The value at 143 nmol mol^{-1} is significantly lower than expected based on the correlation as shown by the remaining data. Insufficient sample at this altitude, and therefore low mol fraction, meant that no repeat measurement could be carried out. Although interesting, and is not discarded as a poor quality measurement at this stage, it was deemed appropriate to not use this measurement in further calculations as the

work was progressed. This data point therefore has not been included in the remainder of this chapter.

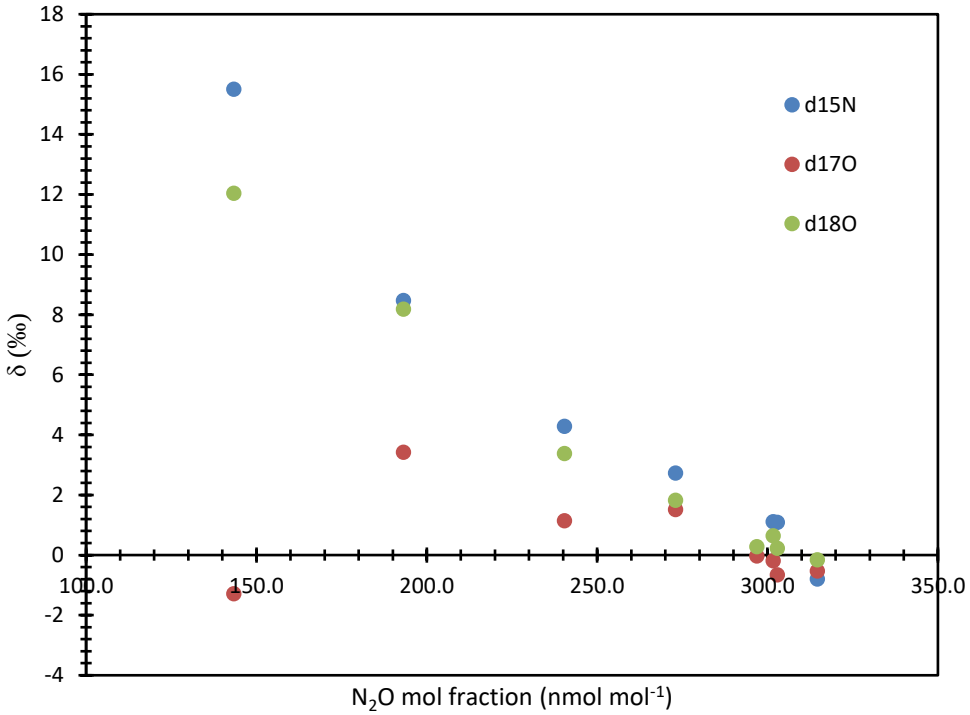

Figure 4.12. Relationship between $\delta^{15}N$ (blue circles), $\delta^{17}O$ (red circles), $\delta^{18}O$ (green circles) and mole fraction of stratospheric samples. All delta values are relative to tropospheric N_2O.

The relationship of ^{17}O isotope excess with decreasing N_2O mole fraction is shown in Figure 4.13. It can be seen that in general there is an increasing correlation in $\Delta(^{17}O)$ with decreasing mole fraction. However, the high value at $\Delta(^{17}O)$ = 0.6 ‰ has a large effect on this correlation. If this data point is treated as an outlier the increase in $\Delta(^{17}O)$ with decreasing mole fraction is essentially zero.

4.7.3 Source of the ^{17}O excess in the troposphere

In order to determine if the stratospheric $\Delta^{17}O$ measurements are significantly different to tropospheric measurements, Figure 4.14 is presented. All measurements are again presented with respect to research grade O_2. Later, measurements are presented in relation to VSMOW for comparison to previously published data. Tropospheric air measurements (BOC, filled 12.06.13, Ipswich, UK) are displayed as blue circles. Data from stratospheric samples collected from over GAP, France are shown as red circles, repeat measurements are visible. It can be seen that the stratospheric data are well correlated with the tropospheric data. The published $\Delta^{17}O$ is (0.9±0.1) ‰ for tropospheric air. Since the published data and this study are not referenced

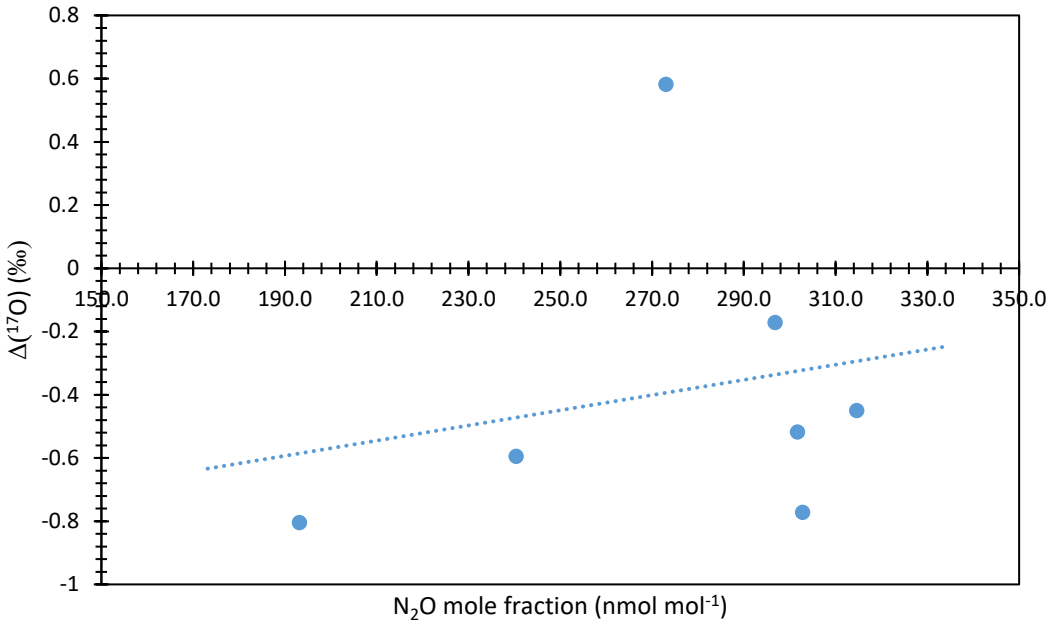

Figure 4.13. Relationship between $\Delta(^{17}O)$ and mole fraction of stratospheric samples. Delta values are relative to tropospheric air.

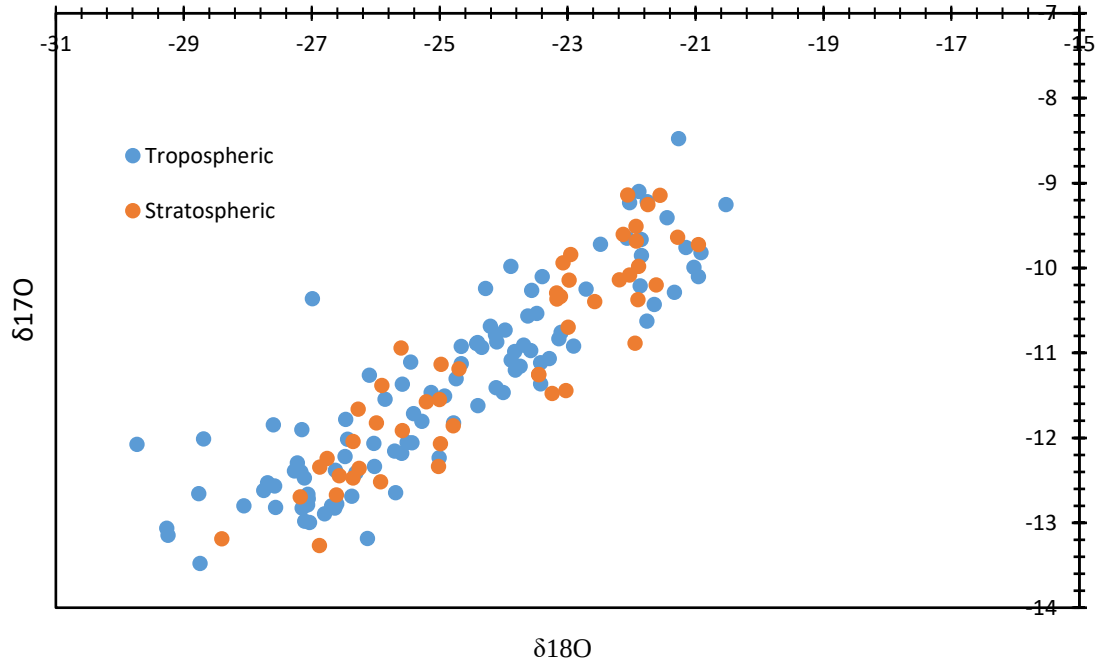

Figure 4.14. Relationship between $\delta^{18}O$ and $\delta^{17}O$. Tropospheric measurements are shown as blue circles and stratospheric measurements as orange circles Each GAP data set contains 6 measurements, the first point has been discarded in each case. GAP 6 and Gap 8 consist of 3 repeated measurements. GAP 14 contains a single data point due to insufficient sample. All delta values are relative to research grade oxygen ($\delta^{17}O$, $\delta^{18}O$).

using the same material, the deviation of stratospheric $\Delta^{17}O$ from tropospheric (BOC) is calculated at (-0.14 ± 0.84) ‰. Within the measurement error, the measured $\Delta^{17}O$ is therefore comparable to the previously published data. This means that even in the stratosphere, above 12 km, the ^{17}O isotope excess is the same as the tropospheric value. Each stratospheric sample was repeated 6 times, not including the sample from the highest altitude which had insufficient N_2O for repeat measurements. This sample is displayed as a single data point. It was necessary to identify if the stratospheric data are significantly different to the tropospheric data within the 1σ error margin. Figure 4.15 is presented displaying the relationship between $\delta^{18}O$ and $\delta^{17}O$ for both stratospheric and tropospheric data, yet with the stratospheric data averaged over the repeat measurements. 1σ error bars are displayed, showing that the stratospheric data are still not significantly different to the tropospheric data.

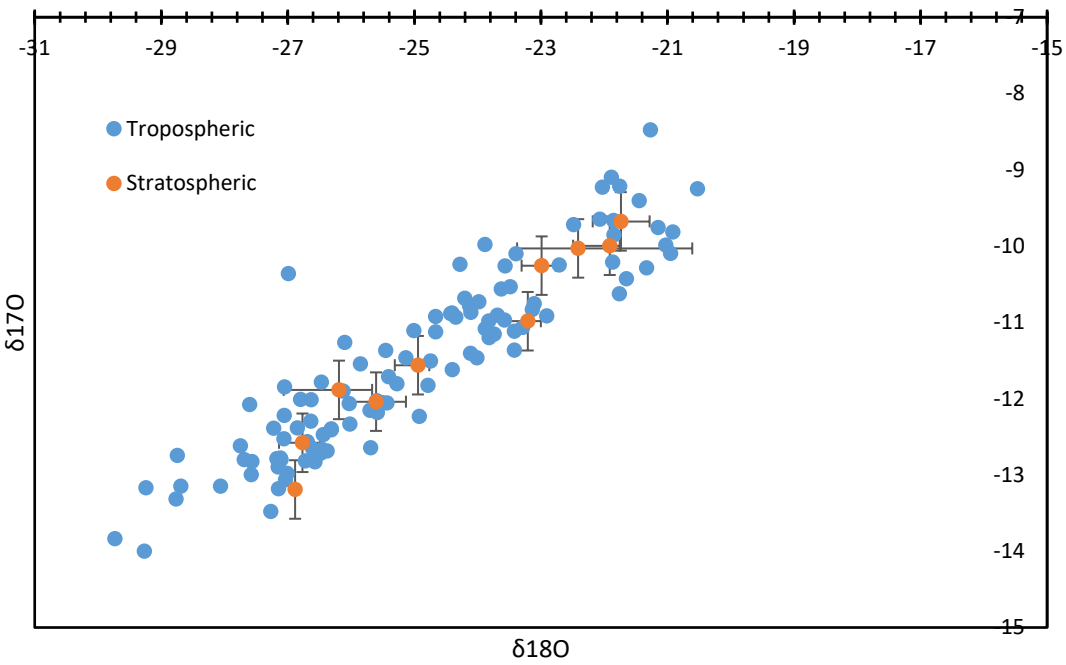

Figure 4.15. Relationship between $\delta^{18}O$ and $\delta^{17}O$. Tropospheric measurements are shown as blue circles. Stratospheric measurements are shown as red circles. Gap data are shown as averaged values. GAP 14 contains a single data point due to insufficient sample. 1 sigma error bars are shown. All delta values are relative to research grade oxygen ($\delta^{17}O$, $\delta^{18}O$).

Stratospheric measurements fall well within the range of the tropospheric measurements. This means that the measured stratospheric $\Delta^{17}O$ is comparable to the $\Delta^{17}O$ in the troposphere.

The agreement of tropospheric and stratospheric measurements means that $\Delta^{17}O$ in the stratosphere appears is in good agreement with that between 8 and 12 km (Cliff et al., 1999b).

Figure 4.16 displays the three isotope plot along with the mass dependent fractionation line. Both tropospheric and stratospheric measurements from Cliff and from this study sit above this line, indicating a positive ^{17}O excess. It can be seen that the stratospheric data form this study display considerably more fractionation, due to the sampling points being deeper into the stratosphere than the sample analysed by Cliff. Importantly, data from this study continue to agree that stratospheric data display an equal ^{17}O excess to tropospheric and low altitude stratospheric data, shown by the positioning of data above the mass dependent fractionation line. Reasons for this are discussed below.

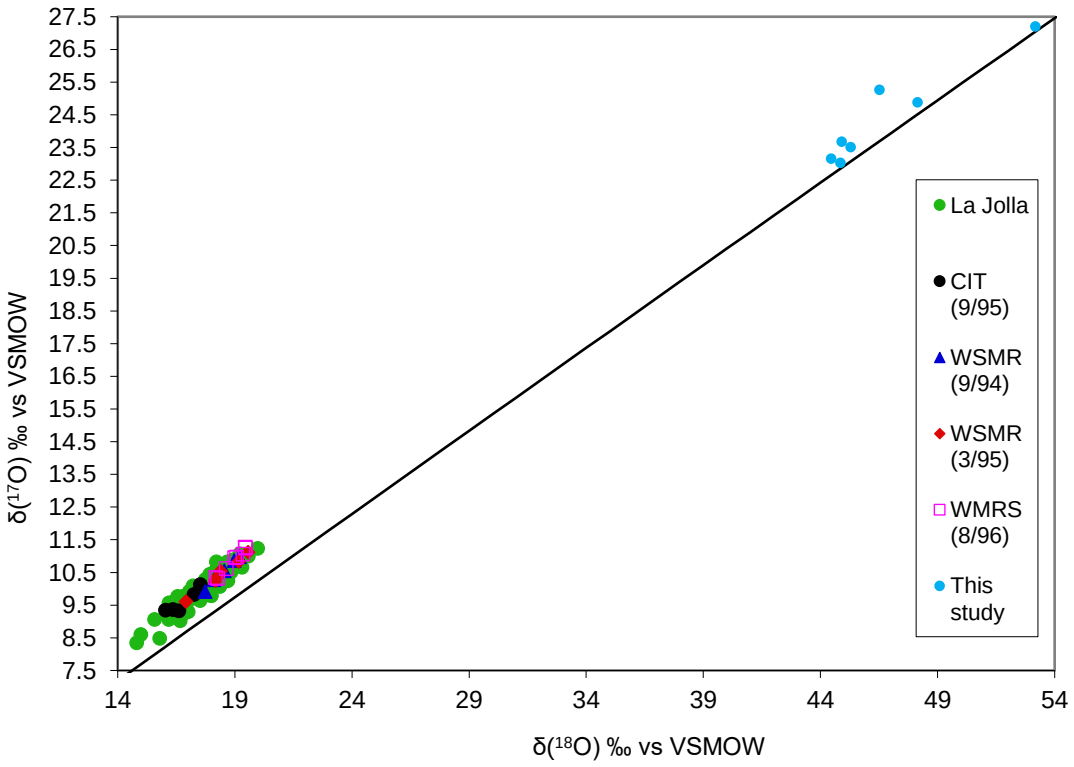

Figure 4.16. Three isotope plot of $\delta^{18}O$ vs. $\delta^{17}O$ for tropospheric (La Jolla, California Institute of Technology (CIT), White Sands Missile Range (WSMR), White Mountain Research Station (WMRS)) and Stratospheric measurements 8-12 kM) (Strat.) from Cliff et al. (1999b). Data from this study overlaid (This study). The mass-dependent fractionation line is shown in black.

4.7.4 Photolysis as the source of the ^{17}O excess

If the source of the ^{17}O excess was due to photolysis, the proportion of ^{17}O in the stratosphere would be larger at altitudes where photolysis occurs. In particular the ^{17}O excess would be much larger in the stratosphere in relation to the troposphere where no photolysis is taking place. The ^{17}O excess would therefore be altitude dependent. As displayed in Figure 4.13 the relationship

between $\Delta(^{17}O)$ and mole fraction of stratospheric samples appears to be independent of altitude, assuming mole fraction is proportional to altitude.

The suggestion that photolysis is responsible for producing excess ^{17}O seems therefore unlikely, since the proportion of ^{17}O in the stratosphere is equal to the troposphere. If the source of ^{17}O was of stratospheric origin, followed by downwelling in the stratosphere, the ^{17}O excess in the stratosphere would be larger than in the troposphere. There would also be increased $\Delta^{17}O$ at altitudes which are influenced by wavelengths of light suitable for photolysis. The prediction of the effect of photolysis on N_2O (Schmidt et al., 2011) depicted an isotope anomaly of (0.1–0.3)‰, thus suggesting that the effect of photolysis on increasing the amount of ^{17}O in the stratosphere to be small. This study agrees with the suggestion that photolysis essentially follows mass-dependent fractionation. Taking the wavelength dependence of fractionation during N_2O photolysis, it would be interesting to complete analysis on samples higher in the stratosphere, about 26.6 km. There is the possibility that fractionation in the upper stratosphere is stronger with respect to ^{17}O, due to differences in wavelengths of incident radiation, and thus causing the proportion of ^{17}O at high altitudes to be higher. If this were the case, downwelling would cause this excess ^{17}O to travel through the mid and lower stratosphere. However there is insufficient N_2O in the upper stratosphere to influence the proportion of ^{17}O in lower to mid altitudes. This in turn means that the tropospheric ^{17}O excess would be unaffected. Measurements from this study show that even though there may be a wavelength dependence of N_2O fractionation, photolysis overall must still be essentially mass dependent.

4.7.5 Reaction with $O(^1D)$ as the source of the ^{17}O excess

If the reaction of N_2O with $O(^1D)$ is the source of the ^{17}O anomaly, the ^{17}O excess in the stratosphere would be larger than the troposphere, and downwelling would cause a proportion of this excess ^{17}O to reach the troposphere. Since the stratospheric data falls within the range of the tropospheric data this cannot be the case. The data therefore do not agree with the suggestion proposed by Morgan et al. (2004) that the reaction with $O(^1D)$ would explain the $\Delta^{17}O$ excess. However, this does not mean that the reaction with $O(^1D)$ does not cause enrichment in ^{17}O, but the magnitude of the reaction is small. It is likely that this isotope exchange accounts for less than 1 % of this reaction and can therefore be neglected as the source of the ^{17}O excess (Kaiser and Röckmann, 2005).

4.7.6 Chemical processes as the source of the ^{17}O excess

Since photolysis and reaction with $O(^1D)$ were discarded mathematically as the source of the ^{17}O (Kaiser et al., 2004), and this study provides empirical evidence, atmospheric chemistry may in fact be an important source. However, regardless of pathway leading to enrichment, these processes must occur equally both in the stratosphere and in the troposphere. If this was not the case then there would be a higher proportion of ^{17}O in the region in which the source process is taking place. The fact that the stratospheric data are in good agreement with the tropospheric data means that this cannot be the case. The three possible chemical pathways for ^{17}O enrichment are (a) the reaction $NH_2 + NO_2$ (Röckmann et al., 2001b); (b) $N_2 + O(^1D) + M$ (Estupiñán et al., 2002), and (c) $N + NO_2$ (McLinden et al., 2003).

It is important to note that for each of these possibilities; photolysis; reaction with $O(^1D)$ and in situ chemistry, there needs to be careful interpretation of future experimental data. Unmodified tropospheric air by mid-latitude cross-tropopause transport could alter the stratospheric N_2O isotopic signature by diluting the fractionation imparted by loss processes.

4.7.7 Numerical sources of the ^{17}O excess

The suggestion that the origin of the ^{17}O excess is due to terrestrial biological production is still valid. If the slope of the 3 isotope exponent, β, is in fact 0.528 rather than 0.516, the excess ^{17}O is accounted for. Figure 4.17 shows these two mass dependent fractionation lines with the stratospheric data (blue circles) overlaid. It can be seen that the 0.516 slope is used to describe the mass dependent fractionation line, the data generally fall on or above this line, indicating a positive ^{17}O excess. However, the upper mass-dependent fractionation line with a slope of 0.528 shows that in fact the majority of data falls below this line. Within experimental error, it can be seen that stratospheric data fall between the two mass-dependent fractionation lines. This indicates that the ^{17}O excess is simply a product of the arbitrary mass-dependent fractionation line for N_2O being low. The data fall within the range of lines (Figure 4.17) range so not because of a non-mass dependent process but because of a numerical 'source'.

The stratospheric ^{17}O excess measured in this study therefore can be explained in the same way as the tropospheric ^{17}O excess. This suggests the mathematical origin as significant, with stratospheric loss processes unlikely causing additional ^{17}O. The data fits well with this conclusion, which shows no distinction between stratospheric and tropospheric air. The suggested source of the 0.528 value for β is from water as a substrate for the biological production of N_2O. The groundwater itself may either be generally enriched in ^{17}O, or N_2O

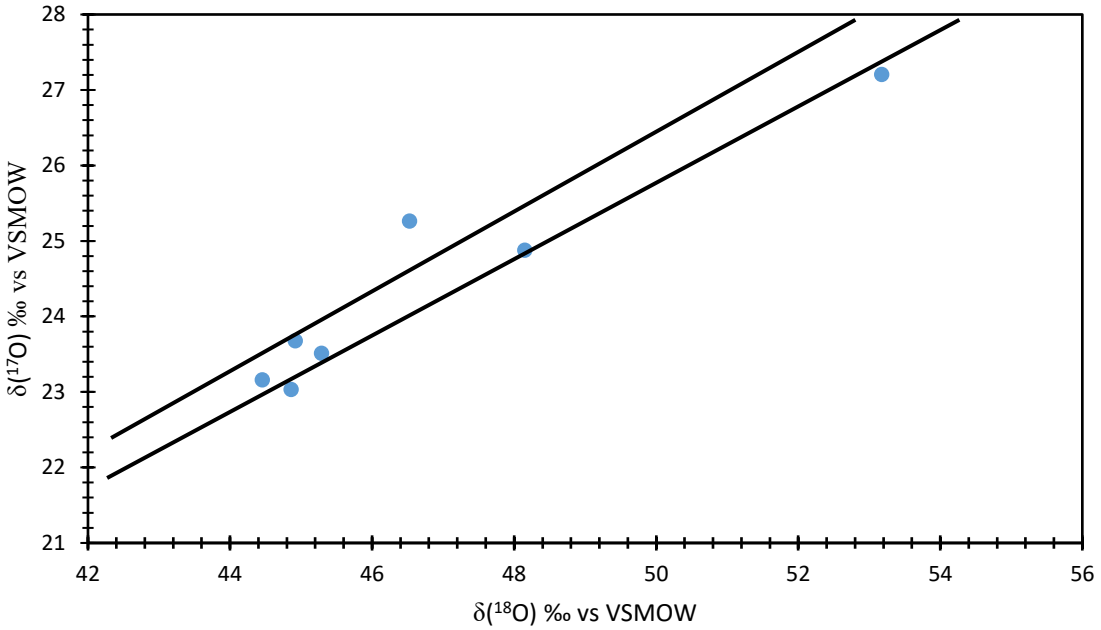

Figure 4.17. Three isotope plot of $\delta^{18}O$ vs. $\delta^{17}O$ for mass dependent fractionation lines 0.528 (upper slope) and (0.516 (lower slope). Stratospheric $\Delta^{17}O$ for this study shown to generally fall between these two lines. All delta values are relative to VSMOW.

formation is dominated by regions in which the water is enriched compared to other regions. Importantly, there is significant isotope fractionation during the formation of N_2O during

denitrification, explaining the large difference between the $\delta^{18}O$ of water and N_2O (Lewicka-Szczebak et al., 2016). Although large quantities of N_2O is formed in temperate regions due to frequent precipitation, N_2O formed in these locations is in fact depleted. This is due to the precipitation at mid latitudes being lighter than that from tropical regions. If the value of β is in fact 0.528 then N_2O production must occur more readily in areas with enriched precipitation such as tropical areas. N_2O is generally enriched at places with high rainfall due to the occurrence of denitrification in wet soils. In the future it would be useful to further analyse the proportion of ^{17}O in N_2O from terrestrial biological sources, which follow the 0.528 fractionation line.

4.8 Conclusions

Modifications were carried out to an existing inlet system for use with whole air samples, for analysis of $\delta^{15}N$, $\delta^{17}O$, $\delta^{18}O$ and $\Delta^{17}O$. Precision of measurements made using this system are comparable to previous systems for measurement of $\delta^{15}N$, $\delta^{17}O$, $\delta^{18}O$. The inlet system was

successfully used to analyse a standard as part of a laboratory intercomparison study. Eight stratospheric samples, collected from 10.4 km to 26.6 km over Gap, France were analysed for $\delta^{17}O$, $\delta^{18}O$ and $\Delta^{17}O$. These are the first measurements of $\Delta^{17}O$ in stratospheric N_2O above 12 km. Stratospheric samples are increasingly enriched with altitude, and display a similar ^{17}O anomaly to that in the troposphere. The data suggest that processes which only occur in the stratosphere, photolysis and reaction with $O(^1D)$ are not the source of the ^{17}O anomaly. Assuming this conclusion, the ^{17}O excess may therefore be attributed to either (a) chemical processes which occur in both the stratosphere and troposphere, or (b), the three isotope exponent of N_2O sources having the value of 0.528 rather than the accepted 0.516. This conclusion agrees well with both Cliff et al. (1999b) and Bernard et al. (2006) and would be enhanced by an additional number of stratospheric samples at different locations and altitudes. Additionally, it would be useful to further analyse N_2O from terrestrial sources to identify the proportion, which follow the 0.528 fractionation line.

Chapter 5: Use of the developed N_2O inlet system in an interlaboratory comparison study

This chapter is based on a published paper, for which I am a co-author:

MOHN, J., WOLF, B., TOYODA, S., LIN, C. T., LIANG, M. C., BRÜGGEMANN, N., WISSEL, H., STEIKER, A.E., DYCKMANS, J., SZWEC, L., OSTROM, N. E., CASCIOTTI, K. L., FORBES, M., GIESEMANN, A., WELL, R., DOUCETT, R. R., YARNES, C. T., RIDLEY, A. R., KAISER, J. & YOSHIDA, N. 2014. Interlaboratory assessment of nitrous oxide isotopomer analysis by isotope ratio mass spectrometry and laser spectroscopy: Current status and perspectives. *Rapid Communications in Mass Spectrometry,* 28**,** 1995-2007.

My contributions are stated clearly below, and involved using the developed inlet system, as described in Chapter 4, to analyse a series of samples provided by J. Mohn, Laboratory for Air Pollution and Environmental Technology, EMPA, Switzerland, as part of a interlaboratory comparison study. This was important in the context of this thesis as it gave information regarding the performance of the developed inlet system compared to that of various systems which had been developed for similar purposes. In order to demonstrate that the modified inlet system was suitable for use with atmospheric samples, the involvement in an interlaboratory study was a useful indication of precision compared to similar systems.

5.1 Context and rationale

The analysis of the distribution of intramolecular ^{15}N within linear assymetric N_2O is of interest since its quantification increases understanding of the contribution of N_2O to the anthropogenic greenhouse effect (Toyoda et al., 2013). Studies of N_2O sources have used analysis of isotopologues to disentangle microbial N_2O production and consumption pathways . Examples of such pathways are hydroxylamine oxidation (Heil et al., 2014), or nitrite reduction during

autotrophic nitrification and heterotropic denitrification (Frame and Casciotti, 2010, Jinuntuya-Nortman et al., 2008). The development of novel techniques which can determine the average $\delta^{15}N$ in addition to the $\delta^{18}O$ in N_2O have aided the understanding of N_2O transfomation processes. An important and relavant technique which has been developed is the quantification of so called 'site preference', the difference between the $\delta^{15}N$ values of the central and terminal nitrogen within N_2O. Analysis of $\delta^{15}N$ site preference within N_2O was first carried out by Friedman and Bigeleisen (1950), and rediscoverd by Toyoda and Yoshida (1999), and Cliff et al. (1999a). Results are always reported in δ notation, where δ denotes the difference in isotope ratios of a sample and a standard. Most laboratories refer their measurements to a tank of high purity N_2O, used as a working standard. The isotopic composition of this working standard is often determined relative to the international calibration material VSMOW or Air N_2. Most laboratories rely on the position dependent calibration of Yoshida and Toyoda (2000). The lack of an internationally agreed gaseous N_2O reference material means there is uncertainty between different laboratories and analytical techniques. Data on the consistency of measurements made across different laboratories, or different analytical techniques is, to date, limited to one study only (Köster et al., 2013). The campaign involved N_2O emitted from soils, and compared two different techniques only. The study on which this chapter is based, organised by EMPA and Tokyo Tech (Earth-Life Science Institute, Tokyo Institute of Technology, Tokyo, Japan), examined the compatibility of eleven laboratories on analysis of N_2O site preference, using both mass spectrometry and laser-spectroscopy based analysis. Data from the study was then used in the context of this thesis to determine if the developed inlet system described in Chapter 4 has adequate precision compared to similar systems.

5.2 Experimental methods

Eleven laboratories were each provided with N_2O at tropospheric mole fractions (target gas T) and two reference gases (REF1 and REF2). The isotopocule data for T, REF1 and REF2 was assessed to give compatibility between laboratories: each laboratory analysed the three the gas samples for $\delta^{15}N$, ^{15}N site preference and $\delta^{18}O$. Standardisation of T in relation to REF1 and REF2 was carried out in order to evaluate the potential of N_2O reference materials for improving compatibility between laboratories.

The isotopic composition of each of the gases remained unknown to each laboratory until they had completed analysis using their individual analytical techniques and calibration procedures. Eight laboratories carried out IRMS, and four used laser spectroscopy (one laboratory carried out both analytical techniques), giving a total of 12 sets of isotopic data.

The experimental procedure, and a small number of modifications made to the inlet system used in the analysis carried out as part of this thesis is described below. All experimental work was carried out by myself, other than the mathematical calculation of ^{15}N site preference which was carried out by Professor Jan Kaiser, UEA. Details of the experimental procedures of laboratories other than used for this thesis are given by Heil et al. (2014).

5.2.1 Inlet system modifications

The modified and improved inlet system as described in Chapter 4 was optimised to allow site specific ^{15}N analysis, rather than $\delta^{17}O$ analysis of the three target gases. The same Finnigan MAT 253 Spectrometer (Thermo Fisher Scientific) was used as described previously, but the inlet system modified slightly. In this study, samples were introduced into the system using the stainless steel sample loops with helium carrier gas, rather than the use of a pump for the ^{17}O measurements. N_2O was not converted to O_2 and N_2, but analysed as N_2O directly by bypassing the gold furnace. All other aspects of the analysis process remained identical to those described in Chapter 4.

5.2.1 Memory effects

It was of concern that when repeat measurements of a sample were carried out, the previous sample was affecting the result of the next sample processed (so called memory effects), perhaps by residue being left over in traps. Repetition of 9 measurements of $\delta^{15}N^{14}N^{16}O$ and $\delta^{14}N^{14}N^{18}O$ in tropospheric air (BOC) indicated that $\delta^{15}N^{14}N^{16}O$ was variable over the first 3 samples, then appeared to increase with each successive measurement (Figure 5.1). In an attempt to reduce the effect of one sample on the next, a blank sample of helium carrier gas was run between each real sample, to flush out the system; however this seemed not to improve the precision (Figure 5.2).

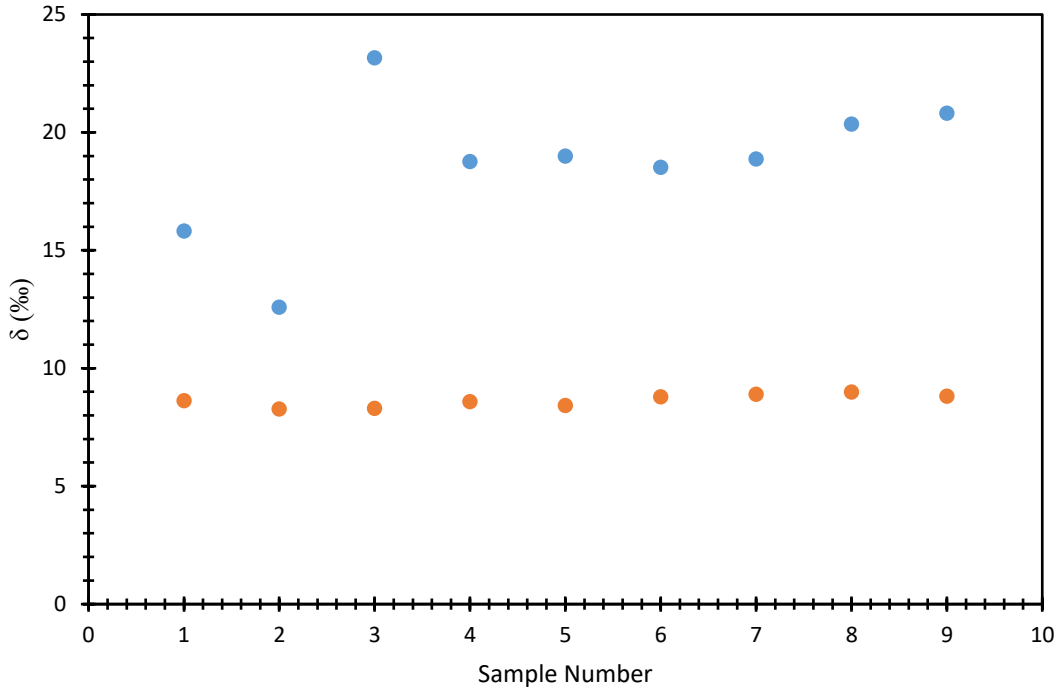

Figure 5.1. Evidence of effect of a sample on the following sample over the course of 9 repeated measurements of $\delta^{15}N^{14}N^{16}O$ (blue circles) and $\delta^{14}N^{14}N^{18}O$ (red circles) in tropospheric air (BOC). All delta values are relative to research grade N_2O.

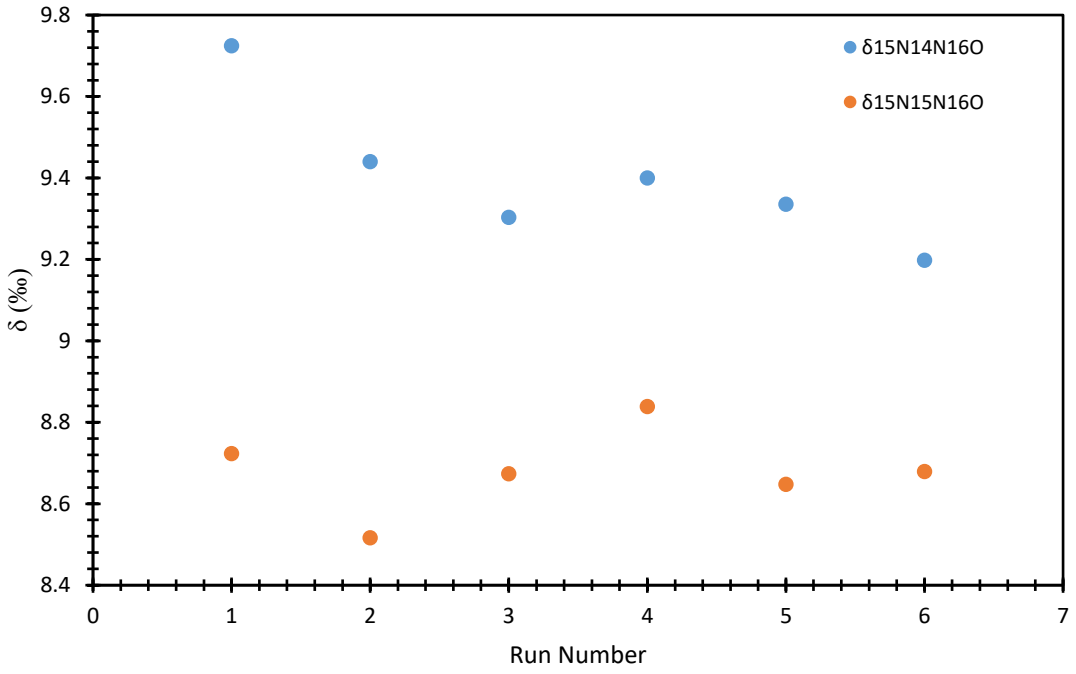

Figure 5.2. Effect of the addition of blanks between samples over the course of 6 measurements of $\delta^{15}N^{14}N^{16}O$ (blue circles) and $\delta^{14}N^{14}N^{18}O$ (red circles) in tropospheric air (BOC). All delta values are relative to research grade N_2O.

A second approach was to increase the time the sample was flushed from the cold trap, T1, to the cryofocus trap, T2. Precision improved via this method (Figure 5.3). A fixed quantity of tropospheric air was analysed for $\delta^{15}N^{14}N^{16}O$ and $\delta^{14}N^{14}N^{18}O$ 8 times in succession with a flushing time of 500 to 1000 seconds.

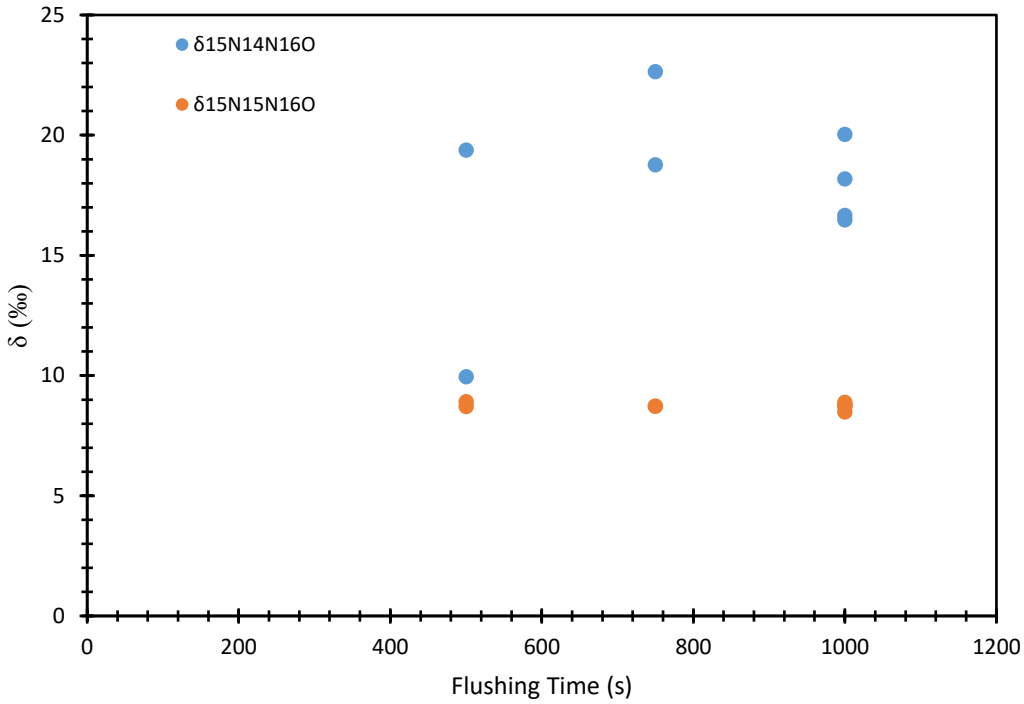

Figure 5.3. Effect of longer flushing from cryogenic trap 1 (T1) and cryofocus trap (T2) between samples over the course of 8 measurements of $\delta^{15}N^{14}N^{16}O$ (blue circles) and $\delta^{14}N^{14}N^{18}O$ (red circles) in tropospheric air (BOC). All delta values are relative to research grade N_2O.

Given a flushing time of 500 seconds, $\delta^{15}N^{14}N^{16}O$ displayed large variability, single data points ranging from 9.95 ‰ to 19.38 ‰. Increasing the flushing time to 1000 seconds reduced the variability, from the lowest value of 16.48 ‰ to 20.03 ‰. In all cases, $\delta^{14}N^{14}N^{18}O$ displayed no effect from the previous sample, and was unaffected by additional blanks or longer flushing between cryogenic traps.

5.3 Results and discussion

The $\delta^{15}N$, $\delta^{18}O$ and ^{15}N site preference data of the target gas T are given in Table 5.1. Samples analysed as part of this thesis represent Laboratory 7. The complete dataset N_2O isotopic composition of T, REF1 and REF2 provided by all laboratories is provided in the supplementary information of the described publication. Table 5.1 displays results based on the normal

calibration procedures of the 11 different laboratories and therefore illustrates the current compatibility of N_2O isotopocules.

Table 5.1 $\delta^{15}N$, $\delta^{18}O$ and ^{15}N site preference data taken from Heil et al. (2014)

Laboratory	$\delta^{15}N$	$\delta^{18}O$	^{15}N site preference
Tokyo Tech	2.54±0.08	42.43±0.05	19.12±0.64
0	2.26±0.05	42.71±0.12	22.97±0.35
1	2.03±0.17	42.03±0.34	17.45±1.08
2	2.60±0.11	42.76±0.17	None calculated
3	1.16±0.22	40.61±0.62	13.85±0.61
4	2.86±0.35	43.26±0.58	25.46±2.05
5	2.64±0.32	44.08±0.22	15.14±0.56
6	1.96±0.15	42.95±0.24	None calculated
7	0.97±0.27	43.22±0.12	22.10±0.54
8	2.04±0.13	41.91±0.04	19.39±0.24
9	-2.09±0.29	No data reported	18.43±0.37
10	1.25±0.51	No data reported	25.47±1.10

For $\delta^{15}N$ data, the laboratories which use mass spectrometry (laboratories 0-7) display good agreement with that of Tokyo Tech, within a root mean square deviation (RMSD) of 0.8 ‰. Laboratories which used laser spectrometry (laboratories 8-10) were less successful with a RMSD of 2.8 %. In the case of ^{15}N site preference, laboratories which used laser spectrometry showed better agreement with Tokyo Tech data than laboratories using mass spectrometry, with a RMSD of 3.7 % compared to 4.3 % respectively.

In the context of this thesis, confirmation of the ability of the system to measure samples satisfactorily was determined by analysis of N_2O samples with good precision. Precision of the

modified inlet system for $\delta^{18}O$ measurements was (0.13 to 0.49) ‰, which was well within the range of the uncertainties for the remaining 10 laboratories (0.05 to 2.01).

5.4 Conclusions and further work

The development of novel techniques which can determine the of $\delta^{15}N$ site preference within N_2O, as well as the average $\delta^{15}N$ and $\delta^{18}O$ in N_2O have aided the understanding of N_2O transfomation processes and therefore increases understanding of the contribution of N_2O to the anthropogenic greenhouse effect. In carriying out such measurements, most laboratories refer their measurements to a tank of high purity N_2O, used as a working standard, of which the isotopic composition is relative to the international calibration material VSMOW or Air N_2. The lack of an internationally agreed gaseous N_2O reference material means there is uncertainty between different laboratories and analytical techniques.

The compatibility of eleven laboratories on analysis of N_2O site preference, $\delta^{15}N$ and $\delta^{18}O$ using both mass spectrometry and laser-spectroscopy was carried out. Data showed that for $\delta^{15}N$ measurements, the use of mass spectrometry gave good agreement, and displayed a root mean square deviation (RMSD) of 0.8 ‰. Laser spectrometry was less successful with a RMSD of 2.8 %. The opposite conclusion was drawn with respect to ^{15}N site preference measurements, with laser spectrometry showing better agreement than mass spectrometry techniques, RMSD of 3.7 % and 4.3 % respectively. It was concluded that for future research on N_2O isotopocules, standardisation against N_2O reference material is essential to improve interlaboratory compatibility.

Data from the study was then used in the context of this thesis to determine if the developed inlet system described in Chapter 4 has adequate precision compared to similar systems. The ability of the system to measure samples satisfactorily was determined by comparison of uncertainties of N_2O analysis carried out using the novel inlet system developed in this thesis, and other laboratories in the study by Heil et al. (2014). The uncertainties of the modified inlet system for $\delta^{18}O$ measurements was (0.13 to 0.49) ‰, compared to that of the remaining 10 laboratories (0.05 to 2.01). The novel inlet system is suitable for $\delta^{18}O$ in N_2O, with uncertainties comparable and in some cases better than those of the 10 other laboratories.

Chapter 6: Development of novel mass spectrometric techniques towards the measurement of isotopes in atmospheric methyl chloride

Methyl chloride (CH_3Cl) accounts for a significant proportion of all natural chlorine reaching the stratosphere and therefore has a significant influence on ozone destruction. Sources are dominated by natural processes, with higher mole fractions occurring at tropical latitudes. Reaction with OH in the troposphere is the most significant loss process.

Use of isotope ratios in methyl chloride to aid budget calculations are, to date, not widespread. Measurements of isotopes in methyl chloride samples of non-atmospheric origin have been carried out extensively, but do not provide data useful for constraining the atmospheric budget. Carbon isotope ratios have been determined in atmospheric samples, but as yet, no successful measurements of hydrogen or chlorine isotopes in atmospheric methyl chloride have been published.

It is necessary to link isotope ratio measurements to an internationally recognised calibration standard. Currently, measurements of isotope ratios in methyl chloride are generally compared via relation to standard mean ocean water chloride ($\delta^{37}Cl_{SMOC}$) and Vienna Pee Dee Belemnite ($\delta^{13}C_{VPDB}$). There is no known methyl chloride calibration gas of characterised isotopic composition.

This chapter aims to develop a measurement system capable of analysis of chlorine isotopes in methyl chloride in air concentrates. Additionally, the first steps towards the synthesis of a calibration gas of known isotopic composition are described, to allow comparison between different laboratories and analytical techniques.

6.1 Abundance of CH_3Cl

As the most abundant natural chlorine containing compound in the atmosphere, CH_3Cl contributes to 16 % of total tropospheric chlorine flux (Carpenter et al., 2014). Atmospheric mole fractions of CH_3Cl are in the region of 540 pmol mol^{-1} (Carpenter et al., 2014) and subject to variation related to latitude and season (Butler et al., 1999). CH_3Cl has an intermediate lifetime of approximately 1 year allowing long-range transport and hence mixing in the troposphere. The effect of global transport and mixing allow for only relatively small global variations in CH_3Cl mole fractions. Mole fractions in the stratosphere are considerably lower than the troposphere and CH_3Cl is subject to rapid horizontal mixing before entry into the lower stratosphere. The most significant point of entry of gases from the troposphere to the lower stratosphere is in the tropics (Holton et al., 1995).

6.1.1 Sources of CH_3Cl

Sources of methyl chloride are dominated by natural processes over anthropogenic (Table 5.1). In most cases, CH_3Cl is released in the gaseous form directly to the atmosphere. There is wide variation, but it is thought that over 90% of methyl chloride emissions are from non-anthropogenic sources. There are considerably higher mole fractions of CH_3Cl at tropical and sub-tropical latitudes compared to polar regions, with highest values occurring between 30° S and 30° N. No emissions are recorded at the poles. The majority of gases enter the stratosphere via the tropics. The necessary transport to tropical regions and subsequent mixing therefore affects the distribution of CH_3Cl at higher altitudes.

Natural sources of CH_3Cl

Early measurements showed natural global sources of CH_3Cl to be dominated by ocean emissions (Singh et al., 1983), caused by sunlight on ocean biomass and chlorine contained in sea foam. Conversely, more recent calculations fall between 0.6 and 0.7 Tg a^{-1} (Keppler et al., 2005, Hu et al., 2013), which although significant, does not account for the majority of the flux the atmosphere, but 10-20 % of CH_3Cl emissions (Moore et al., 1996, Keppler et al., 2005). This implies land-based emissions are of greater importance globally. Both (a) terrestrial vegetation biogenesis and (b) biomass burning, whether human-initiated vegetation burning for land clearing purposes or natural fires, constitute the major and most significant sources of CH_3Cl (Yokouchi et al., 2002, Keene et al., 1999, Gebhardt et al., 2008). Estimates suggest up to 55% of CH_3Cl emissions come from tropical terrestrial sources (Montzka et al., 2011), with the combined biomass burning and tropical plant emissions standing at two thirds

Table 6.1: Source and sink strength of tropospheric CH_3Cl. Possible ranges are indicated in parentheses. Adapted from Carpenter et al. (2014)

	Source strength (Gg a^{-1})	Sink Strength (Gg a^{-1})
Biomass Burning	113 (56-169)	
Tropical plants	2040 (1430-2650)	
Mangroves	12 (11-12)	
Fungi	145 (128-162)	
Salt marshes	85 (1.1-170)	
Wetlands	27 (5.5-48)	
Coal Combustion	162 (29-295)	
Shrublands	15 (9-21)	
Rice	3.7 (2.7-4.9)	
Oceans	700 (510-910)	370 (296-445)
Reaction with OH in troposphere		2832 (2470-3420)
Loss to stratosphere		146
Degradation in soils		1058 (664-1482)
Total	3658	-4406

of all CH_3Cl emissions (Table 6.1). Methyl chloride produced by wood rotting fungi is little understood, but is thought to contribute approximately 0.6 Tg a^{-1} to the atmosphere (Harper, 1985). Small emissions from fumaroles, solid rocket fuels and aggressive volcanic eruptions may inject methyl chloride directly into the stratosphere (Cronin, 1971).

Anthropogenic sources of CH_3Cl

Small anthropogenic sources are dominated by the use of methyl chloride as a chemical intermediate, for example in drug synthesis and silicon polymer production as well as use as a general methylating agent. The once widespread use of CH_3Cl as a refrigerant has been discontinued due to concerns over toxicity. Other uses include those as a solvent, propellant and extractant in various chemical industries. All the CH_3Cl used industrially is produced by synthetic means via the reaction of methanol and hydrogen chloride. However, the low CH_3Cl outputs from these processes deem them to be relatively unimportant factors in global concentrations.

6.1.2 Sinks of CH_3Cl

Losses of CH_3Cl can be categorised into: terrestrial sinks; those occurring in the troposphere; and those in the stratosphere.

Minor terrestrial losses occur by uptake by soils, suggested to be in the region of 0.18 to 1.6 Tg a^{-1} (Keppler et al., 2005), as well as loss to high latitude ocean waters. It is worth noting that although waters in polar regions constitute a small sink, ocean waters overall give a net source due to output processes in tropical regions as shown in Table 6.1.

Reaction with hydroxyl radicals in the troposphere significantly reduces the mixing ratio of CH_3Cl which can migrate through the tropopause. Loss via reaction with OH is estimated at approximately 3 Tg a^{-1} (Derendorp et al., 2012). The rate constant of reaction of CH_3Cl with OH, Equation (1.2), measured to be in the region of 3.1 x 10^{-14} to 4.4 x 10^{-14} cm^3 mol^{-1} s^{-1} (Hsu and DeMore, 1994) denotes a lifetime in the troposphere of approximately 1.5 years. Small quantities of CH_3Cl, equivalent to chlorine in the region of 0.2 Tg a^{-1} therefore reach the stratosphere, as shown in Table 6.1. The total contribution of Cl from CH_3Cl in the lower stratosphere is estimated at 0.2 % of total Cl emissions (Schauffler et al., 1993).

Two main sinks of CH_3Cl in the stratosphere involve photodissociation, shown by Equation (6.1) and reaction with hydroxyl radicals, Equation (6.2). Importantly, stratospheric photodissociation gives the formation of free chlorine atoms, aggressive ozone depleting substances.

$$CH_3Cl + h\nu \rightarrow CH_3 + H_2O \qquad \text{Equation 6.1}$$

$$CH_3Cl + OH \rightarrow CH_2Cl + H_2O \qquad \text{Equation 6.2}$$

Although removal processes in the stratosphere include those which also take place in the troposphere, the stratospheric lifetime of CH_3Cl is longer than in troposphere. The temperature dependence of reaction with hydroxyl means rate coefficients at higher latitudes are smaller and therefore CH_3Cl is more stable (Fabian et al., 1996).

6.1.3 Global warming potential

The overall global warming potential of a gas is dependent on not only the radiative efficiency, but the atmospheric concentration and lifetime. As shown by Equation 1.1 (chapter 1).

Thus in the troposphere, CH_3Cl is not thought to contribute significantly to global warming even though, per molecule, it causes 267 times more radiative forcing than carbon dioxide (Grossman et al., 1997). However, the dependence of GWP on low concentration and short lifetime of

CH_3Cl, deem the contribution of this gas to global warming to be negligible (Grossman et al., 1997).

6.1.4 Importance of CH_3Cl with respect to ozone

As the most abundant halocarbon in the atmosphere, the photochemical breakdown of CH_3Cl is of major importance as a source of chlorine atoms in the stratosphere. CH_3Cl is considered the largest reservoir of gaseous chlorine in the atmosphere at 5 Tg (Keene et al., 1999), which in turn affects the rate of breakdown, and therefore concentration, of stratospheric ozone, O_3.

Mixing ratios of CH_3Cl are of importance with respect to the effect on the flux of chlorine to the stratosphere. Estimates of 0.5-0.6 nmol mol^{-1} of chlorine entering the lower stratosphere from CH_3Cl are significantly lower than chlorine from chlorofluorocarbons (3.0 nmol mol^{-1}). It is however somewhat more significant than contributions from HCl (0.5-0.6 nmol mol^{-1}) (Schauffler et al., 1993).

The introduction and subsequent amendments of the Montreal Protocol has meant substantial decreases in the emissions of chlorofluorocarbons (CFCs) and hydrochlorofluorocarbons (HCFCs) to the atmosphere. Although the impact of CH_3Cl to stratospheric ozone depletion is significant, its emissions are not currently regulated. Therefore, since the emissions of regulated CFCs and HCFCs released have reduced, the relative contribution of CH_3Cl to the production of chlorine radicals therefore will increase. This in turn means the relative effect of CH_3Cl on O_3 will increase. This effect is not confined to CH_3Cl, in fact other species not regulated by the Montreal Protocol, such as N_2O, are becoming relatively more important with respect to ozone destruction.

6.2 Isotopic budget of CH_3Cl

Although the sources, lifetime and abundance of CH_3Cl are well constrained, the use of isotope ratios can provide addition information into processes which affect this important species. Firstly, to provide a historical picture of the CH_3Cl isotope ratios, analysis of firn air samples would give an excellent insight. It would be possible to determine whether the source signature has changed over time. It would be expected that in recent times that the source signature is changing due to increased anthropogenic output compared to preindustrial times. It would be interesting to distinguish between biogenic and anthropogenic source signatures, and quantify the anthropogenic input, since CH_3Cl is not regulated by the Montreal Protocol. To give an integrated global picture, analysis of aircraft-based samples, such as CARIBIC would give rise to an overview of the current CH_3Cl isotope ratios and how it has changed over time. The use of

air archives would allow for identification of historical CH_3Cl isotope analysis, but it is important to note that CH_3Cl degrades when contained in canisters and so firn air analysis removes this issue. Additionally, an aircraft-based campaign could provide distinction between various biogenic sources. For instance a flight over a wetland area would firstly collect samples of high mixing ratios and therefore improved measurement precision, and additionally may provide a distinct source signature compared to sampling over a different biogenic source.

Determination of the isotopic budget of CH_3Cl can be described in terms of sample origin, both atmospheric and non-atmospheric. It is important to note that CH_3Cl comprises of only carbon, hydrogen and chlorine, all of which have stable isotopes available for analysis. Measurements of samples of non-atmospheric origin have been carried out extensively, but do not provide data useful for constraining the atmospheric budget. Measurements of atmospheric CH_3Cl carbon isotope ratios have been carried out, whereas hydrogen isotope measurements are very much in the development stages. To date, no measurements of chlorine isotope measurements in atmospheric samples of methyl chloride have been published.

6.2.1 Non-atmospheric measurements of isotope ratios in CH_3Cl

To date, determinations of chlorine isotope ratios have been carried out extensively for samples of methyl chloride. However, samples have not been of atmospheric origin, and rather are those which have been produced for analysis of chloride ions in geological and hydrological samples (Long et al., 1993, Taylor and Grimsrud, 1969, Holt et al., 1997, Hamilton et al., 2003). Generally, samples are dissolved, hydrolysed or leached, then converted to CH_3Cl via formation of AgCl and reaction with CH_3CI. Mass Spectrometry using peak hopping for *m/z* 50 and 52 is commonly used. A series of comparisons of the ratio of *m/z* 52 to 50 are compared to commercial CH_3Cl used as a standard. Since neither hydrogen nor carbon have mass differences between the two most common isotopes, the ratio of *m/z* 50 to 52 must be completely attributed to the ratio of ^{37}Cl to ^{35}Cl in the sample.

The most recent success in measurement of chlorine isotopes in methyl chloride is demonstrated by Konno et al. (2013). Development of a suitable analytical system allowed analysis of a 'Test Gas' preparation of methyl chloride in helium. The analytical accuracy of their measurements could not be determined as an analytical material of known chlorine composition other than seawater has not been distributed. The authors determined that the analytical system caused only negligible fractionation. Analytical precision (standard deviation of a single

measurement) of greater than 0.6 nmol of CH_3Cl was 0.1 ‰. With respect to analysis of atmospheric samples, the volume of air required to give 0.6 nmol of CH_3Cl would require samples of gas of unfeasibly large volume. Additionally, it is not known how the matrix effects of real atmospheric samples would differ from the test sample in a helium matrix. Hydrogen isotope ratios of CH_3Cl released thermally from the leaves of dried halophite plants, have been measured down to the lowest mixing ratios of 1 μmol mol^{-1} (Greule et al., 2012).

6.2.2 Atmospheric measurements of isotope ratios in CH_3Cl

Knowledge of the isotopic variation of not just carbon, but hydrogen and chlorine within chlorine containing molecules can be used as a 'fingerprint' of the sources and sinks, and therefore budgets in the atmosphere (Goldstein and Shaw, 2003, Brenninkmeijer et al., 2003).

Atmospheric carbon isotope measurements in CH_3Cl

Measurement of carbon isotopic composition of methyl chloride in atmospheric samples was first demonstrated by Rudolph et al. (1997) and allowed further understanding of sources, sinks and conversion reactions within the atmosphere. Using this carbon isotope signature technique allowed the first construction of an isotopic mass balance for methyl chloride (Thompson et al., 2002), however, in situ atmospheric data available was limited.

To enhance the data set for mass balance calculations, in situ measurement of carbon isotope ratios in methyl chloride emissions from living salt marsh plants (Bill et al., 2002), tropical ferns (Hamilton et al., 2003), as well as foliar emissions from dipterocarp trees (Saito et al., 2008) have been determined. Additionally, carbon isotope ratios of methyl chloride emitted from methylotrophic bacteria (Miller et al., 2001) is a useful parameter for mass balance calculations. Such analyses are useful with respect to this study, as although do not provide atmospheric data as such, yet do present values of isotope ratios expected for individual sources. For example, measurement of carbon isotope ratios of methyl chloride and methyl bromide emitted from salt marshes was determined – 65 ‰ and -12 ‰ (vs VPDB) for day and night time samples respectively (Bill et al., 2002). Since salt marshes represent an extremely important CH_3Cl source, it would be expected that atmospheric samples collected close to these areas may display a similar values.

Carbon isotopic composition has not been purely derived from in situ measurements. Measurements of plant derived emissions from freshly collected plant material which has then

been heated strongly gives rise to isotopic composition of methyl chloride from a known source. Carbon isotope signatures were depleted in ^{14}C from methyl chloride emissions derived from fresh C_3 and C_4 plant tissue (Keppler et al., 2004). Using this drying and heating technique gives an indication of isotopic composition of plant derived atmospheric composition, as well as suggesting the composition of emissions from biomass burning at similar temperatures. Further measurements of carbon isotopic composition of emissions from senescent or dead leaves have been recorded (Hamilton et al., 2003).

Atmospheric hydrogen isotope measurements in CH_3Cl

To date there are no hydrogen isotope measurements of CH_3Cl in background air. Measurements of hydrogen isotopes in methyl chloride are in the preliminary stages. Compound specific thermal conversion isotope ratio mass spectrometry has recently been used to measure the stable hydrogen isotope ratios of methyl chloride released thermally from halophyte plants (Greule et al., 2012). Analyses showed normal isotope effects for both $^{13}C/^{12}C$ and $^{2}H/^{1}H$.

6.2.3 Isotopically calibrated CH_3Cl standard gas

In order to allow comparison of the isotopic composition of methyl chloride between samples and different analytical methods, it is necessary to link to an internationally recognised calibration standard. Measurement of isotope ratios in methyl chloride are generally compared via relation to standard mean ocean water chloride ($\delta^{37}Cl_{SMOC}$) and Vienna Pee Dee Belemnite ($\delta^{13}C_{VPDB}$). This chapter describes a methodology used to synthesise a calibration gas of known isotopic composition via firstly the reaction of pectin with sodium chloride, which was further heated to produce a gaseous mixture containing methyl chloride, since a calibrated CH_3Cl isotopologue standard is was not available.

6.3 Research objectives

By developing an inlet system suitable for use in measurement of chlorine isotopes in CH_3Cl, it is possible to identify the ability if this system for measurement of real air samples:

1. Is the system suitable for samples of CH_3Cl in synthetic matrices such as N_2 and CO_2?
2. Is the precision achieved via this system suitable for real air analysis?

Synthesis of a methyl chloride standard gas for intercomparison of future CH_3Cl measurements requires consideration of the following:

1. Does the propose reaction scheme give production of CH_3Cl?
2. Does the reaction give large amounts of product for analysis?
3. Is significant clean up required to remove byproducts before use as an isotopically characterised reference material?

6.4 Experimental methods

A Thermo Finnigan 253 Spectrometer, provided by Thermo Fisher Scientific, was used in this work to measure isotopes in CH_3Cl. The use of the software Isodat 3.0 allowed for analysis of isotope ratios, and for automation of the inlet system.

6.4.1 Set up of dual inlet system

In order to allow measurement of methyl chloride using the MAT 253 Spectrometer it was necessary to set the measured masses to *m/z* 49,50,51,52 and 53 to account for all isotopes in methyl chloride, Table 6.2.

Table 6.2 Fragments detected by *m/z* 49 to 53

m/z	**47**	**48**	**49**	**50**	**51**	**52**	**53**
Fragment	$^{12}C^{35}Cl^+$	$^{12}C^1H^{35}Cl^+$	$^{12}C^1H_2{}^{35}Cl^+$	$^{12}C^1H_3{}^{35}Cl^+$	$^{13}C^1H_3{}^{35}Cl^+$	$^{12}C^1H_3{}^{37}Cl^+$	$^{13}C^1H_3{}^{37}Cl^+$
		$^{13}C^{35}Cl^+$	$^{12}C^1H_2{}^{35}Cl^+$	$^{13}C^1H_2{}^{35}Cl^+$	$^{12}C^1H_2{}^{37}Cl^+$	$^{13}C^1H_2{}^{37}Cl^+$	
			$^{13}C^1H^{35}Cl^+$	$^{12}C^1H^{37}Cl^+$	$^{13}C^1H^{37}Cl^+$		
			$^{12}C^{37}Cl^+$				

Testing of detection of these masses was carried out using the dual inlet function, to eliminate effects caused by the inlet system. Mass scale calibration was carried out on peaks at *m/z* 15, 35 and 47. The background signal detected for all masses was zero.

A zero enrichment was tested using standard UMCIS (UEA Methyl Chloride Isotopologue Standard) using the automated bellow pressure adjust. The system displayed unstable peak

areas corresponding to unequal bellow pressures caused by the inadequate pressure adjust feature. To rectify the issues caused by the automated pressure adjust, the system was bypassed and the bellow pressure adjusted manually. A pressure corresponding to a signal of 40000 mV (*m/z* 50) was used. Manual adjustment increased the stability of peak areas and therefore isotope ratios. Manual adjustment of the bellows was used for all future measurements.

6.4.2 Basic set up of continuous-flow inlet system

Once it had been determined that the spectrometer could adequately determine the masses required for CH_3Cl analysis, a suitable inlet system was required. The inlet system set up for CH_3Cl isotope analysis in atmospheric samples with low mole fractions had different requirements to N_2O analysis and so the N_2O system was determined to be unsuitable. Although many suitable aspects of the described inlet system remained, significant modifications were carried out as described below:

The set up developed for analysis of N_2O (Figure 4.3, chapter 4) consisted of a continuous flow inlet system to separate analytes from interferences and to introduce these analytes into the mass spectrometer. An open split periphery was used as a transition point between the high helium loaded sample gas and the vacuum of the mass spectrometer.

To begin set up of the inlet system, it was necessary to identify a peak corresponding to the methyl chloride after passing though the existing inlet system before modifications took place. For continuity, the same standard used for the dual inlet set up (UMCIS) was diluted to 1.86 ppm in He to mimic that of approximately tropospheric values. This was connected to the existing stainless steel tubing at the inlet as described in chapter 4.

Chromatography

Initially, peaks were multiple and too small in magnitude to be accurately quantified, and so it was necessary to address the chromatography as a priority. In order to improve separation of CH_3Cl chromatographic peaks from interferences, namely CO_2 and N_2O, as well as CFC-12 and CFC-114a, a Plot Q column (30 m long, 0.32 mm i.d. PoraPlot Q, *Thermo Fisher Scientific*) was fitted. In the first instance, for simplicity, the precolumn was bypassed, and the run time of the spectrometer lengthened to 2500 s to ensure that all peaks were detected. The retention time of the CH_3Cl was not known at this stage but it was assumed that it would elute at a similar time to both CO_2 and N_2O. Broad peaks indicated perhaps two or more compounds poorly resolved, and so it was decided to increase the GC oven temperature from 37 °C to 100 °C in the first

instance. This allowed for separation of the large broad 'peak' into one broad peak and one sharp peak eluting shortly afterwards.

Since resolution of two unknown peaks had been achieved, the next step was to begin use of the precolumn. It was hoped that the use of the precolumn as well as the main column would allow both better separation of the broad and sharp peaks, but also may give rise to separation of the large broad peak into in fact more than one peak. In fact, the peaks were indeed separated further, yet the broad peak remained broad yet as a single peak, indicating that this in fact was a single compound.

In order to optimise the peak shape of, in particular, the broad peak, the temperature of the GC oven was increased to 170 °C. This improved the peak shape and so this temperature was retained isothermally. The improved peak shape is shown in Figure 6.1.

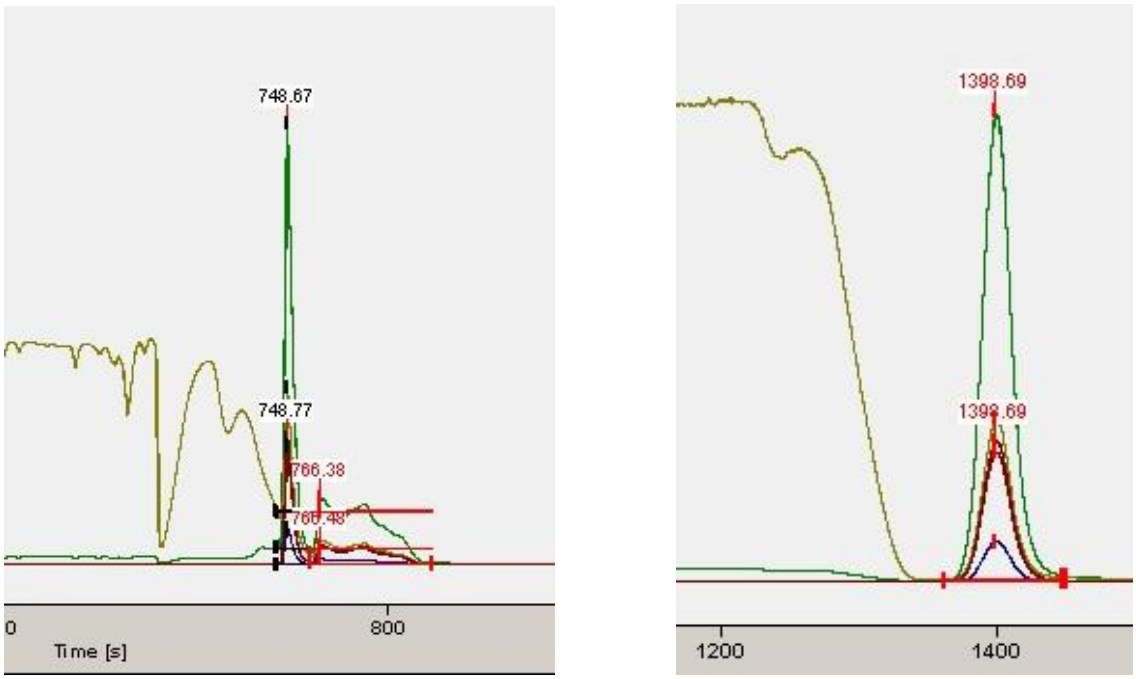

Figure 6.1 Peak shape optimisation via introduction of precolumn, and separation from interference and improved baseline by increasing oven temperature from 37 °C (left) to 170 °C (right). x-axis corresponds to Time (s), y-axis to intensity (mV).

To quantify the precision after separation and peak shape optimisation appeared to have been achieved, a 340 mL aliquot of 1.86 ppm sample of CH_3Cl in He was analysed repeatedly (n=38) and the stability of retention time and peak area identified. Sample trapping rate was 27.2 mL min^{-1}. Flows through the high flow system were maintained at 24 mL min^{-1}, and 1.42 mL min^{-1}

through the low flow side of the system. The retention time remained constant, and precision of 0.32 ‰ (*m/z* = 50/49), 0.69 ‰ (*m/z* = 51/49), 0.71 ‰ (*m/z* = 52/49), 0.76 ‰ (*m/z* = 51/50), 0.06 ‰ (*m/z* = 52/50) and 2.17 ‰ (*m/z* = 53/50) achieved. All delta values are with respect to UMCIS via the bellows of the dual inlet system.

Amount of liquid N_2 used for trapping sample

Although the precision of repeat measurements was good, it was noticed that the peak shape was variable and appeared to be related to the amount of liquid nitrogen in the dewar (Figure 6.2).

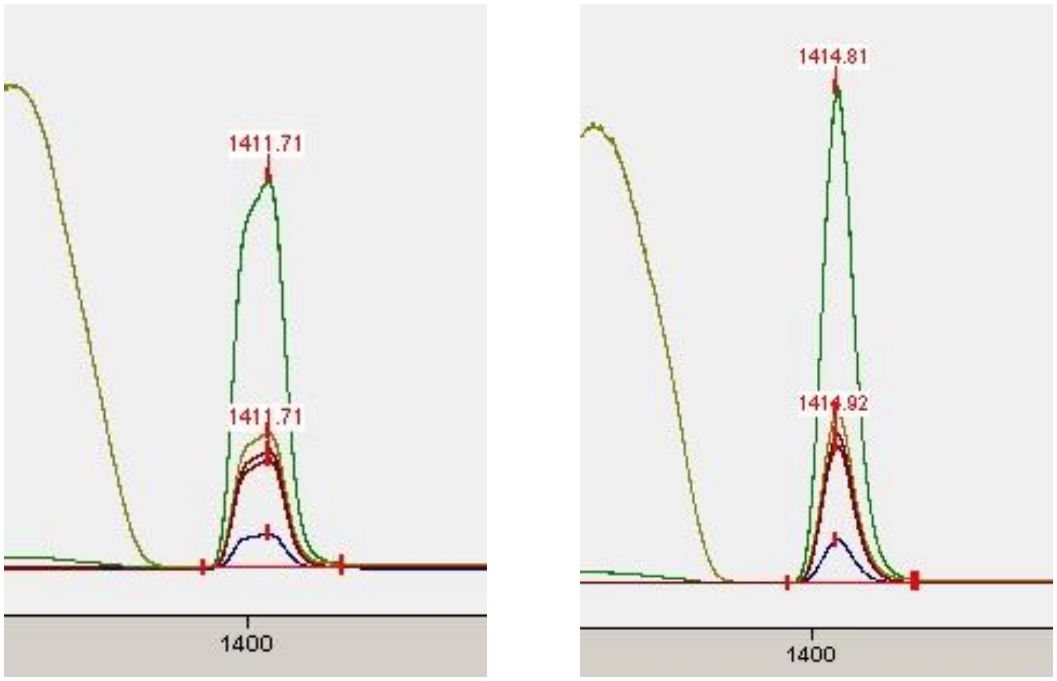

Figure 6.2 Poor peak shape (left) due to decrease in liquid nitrogen level. Improved peak shape (right) on keeping liquid nitrogen levels constantly at maximum.

It was necessary to determine if the quantity of liquid nitrogen adversely affected the quantity trapped and therefore affected the fractionation measured. The liquid nitrogen was filled to the top of the dewar, and 340 mL analysed repeatedly as described above, yet the liquid nitrogen was not topped up at any point during the analyses.

Over the course of 10 analyses, the CH_3Cl peak area significantly reduced from 30.671 mV to 9.418 Vs (Figure 6.3), yet the precision on raw areas remained below 2.5 ‰ for all masses. It was concluded that although the precision remained good when the liquid nitrogen levels became low, in order to allow for symmetric peaks, the levels should be kept topped up and peak areas to remain constant.

6.4.3. Use of inlet system for continuous flow measurements of CH_3Cl in N_2

The method determined above was sufficient to allow for analysis of large quantities (340 mL) of a synthetic laboratory standard diluted with helium. However, although a good starting point for the setup of a system for analysis of methyl chloride in real air samples, this laboratory standard was not representative of the matrix and small quantities which would be encountered on analysis of real air samples. The next stage towards a system capable of real air samples was the use of a mix of 1.3 ppm CH_3Cl in N_2. This allowed the system to measure

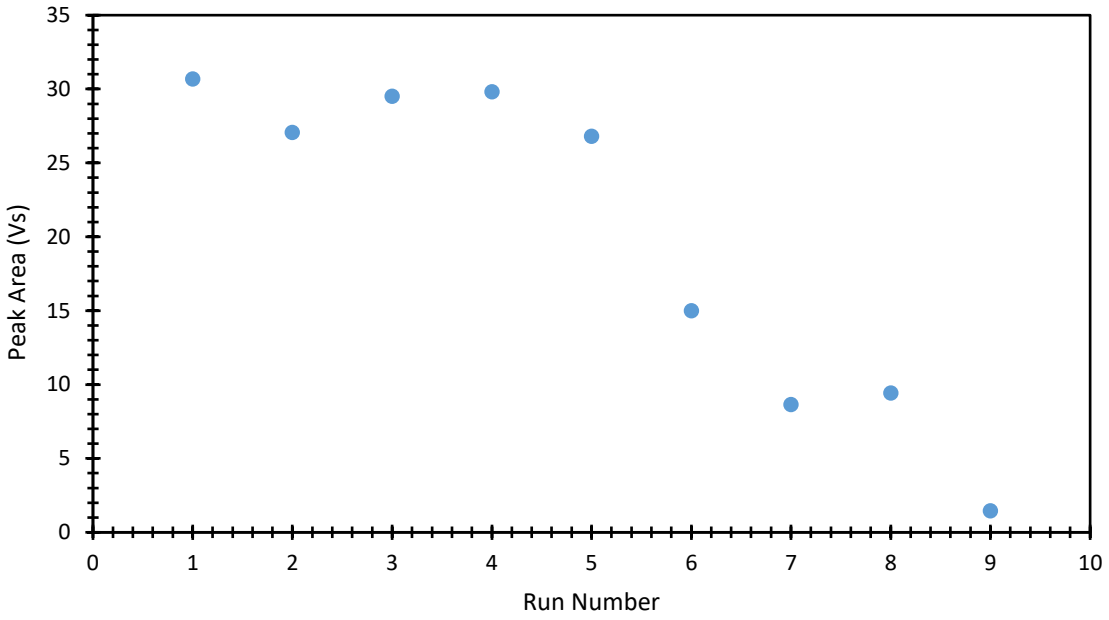

Figure 6.3 Effect of decreasing liquid nitrogen amount over time on the *m/z* 52/50 peak area, determined by repeat analysis of 10 runs over the course of a measurement day, without topping up liquid nitrogen in cryogenic trap.

methyl chloride in a nitrogen matrix, without the complications of large interferences such as CO_2.

Since real air samples would be small in volume, the minimum volume of CH_3Cl which could be analysed whilst retaining good precision was determined. It was necessary to further modify the inlet system for use with a 'sample' of methyl chloride in nitrogen. Until this point, extractions had consisted of 750 second extractions at 27.2 mL min^{-1}. The flow rate was retained, but the trapping amount reduced to 30 s, 60 s, 100 s and 150 s to be more representative of sample sizes in real air samples. Trapping for as little as 30 and 60 seconds did not allow for peaks of

suitable size for reliable integration. Trapping for 100 seconds was possible but data was not reproducible and so it was necessary to trap further sample. Trapping for 150 seconds (68 mL) allowed reproducible data with precision values between 0.4 and 6 ‰ for all masses vs UMCIS.

6.4.4 Use of inlet system for continuous flow measurements of CH_3Cl in carbon dioxide

The method developed so far was suitable for measurement of methyl chloride in whole air samples, of volumes greater than 160 L. However, once real air samples had been identified, it was apparent that the main gaseous components, nitrogen and oxygen, had been removed, giving samples which were essentially a trace gas mix in a CO_2 matrix. It was necessary therefore to modify the system further again to allow for measurement of CH_3Cl in CO_2. A cylinder of 1.3 ppm CH_3Cl in CO_2 was purchased for this development stage.

In general, this stage of the development proved to be the most challenging, arriving at multiple difficulties with the analysis of the methyl chloride 'sample' in carbon dioxide. Mainly these consisted of issues relating to the chemical trap, flow rates, gas pressure, issues with cryogenic traps, carbon dioxide not being sufficiently removed from the gas stream and loss of chromatographic peaks.

Removal of interferences

When using the inlet system for analysis of methyl chloride in nitrogen, the trace amount of CO_2 present was separated from the CH_3Cl peak. However, it was necessary to ensure that any excess CO_2 was removed so as not to overload the column or spectrometer. A chemical trap containing a CO_2 scrubbing reagent (Carbosorb Granular, 0.7-1.2 mm, Elemental Microanalysis) and a drying agent magnesium perchlorate, (self-indicating, Granular 0.7-1.2 mm, Elemental Microanalysis) deemed suitable for this purpose. Once the chemical trap was in line, the CO_2 peak had no influence on the CH_3Cl peak, and the spectrometer was not adversely affected by the small volume of CO_2 which was introduced.

However, once the matrix was switched from N_2 to CO_2, a number of issues arose. The primary aim at this stage was to ensure that the CO_2 did not interfere with the CH_3Cl peaks or overload the column. Although initial testing of CH_3Cl in CO_2 (50 s extraction, 0.8 bar cylinder pressure) gave precision comparable to analysis using the N_2 matrix, continued analysis eventually caused the instrument to trip out due to overloading the spectrometer with CO_2. The issue was rectified by replacement of the CO_2 scrubbing reagent and drying agent. However, since continually replacing the chemical trap would not allow multiple samples to be run back to back, and

alternative solution was needed. The trap was replaced with a larger version, 12 mm wide by 80 cm long, filled again with magnesium perchlorate and CO_2 scrubbing reagent separated with glass wool.

Although in the short term this large trap enabled a larger quantity of measurements to be performed with seemingly no issues, eventually it resulted in loss of peak symmetry, retention time shifts due to column overloading, and eventually reduced flow rates once magnesium perchlorate became saturated with the resultant H_2O. Simultaneously, flow rates appeared reduced at other points around the system, in particular the low flow side of the setup, containing not only the chemical trap, but the first cryogenic trap (liquid nitrogen).

Attempts to rectify these issues included replacement of the liquid nitrogen filled dewar with an ethanol/ dry ice slush (-72 °C) to remove possible blockages caused by solid CO_2 build up, attempts to try a variety of old style CO_2 scrubbing agents (Ascarite (charcoal-bound) (Elemental Microanalysis), Ascarite (asbestos-bound) (Elemental Microanalysis), Ascarite II (sodium hydroxide coated silica)), and varying the quatity of CO_2 scrubbing reagent compared to the magnesium perchlorate. Many attempts were unsuccessful due to loss of peaks, further loss of peak shape and again blockages.

This did not resolve the issue and so the stainless steel tubing was heated to remove any traces of condensed material. Flow issues were not resolved by removing debris from the cryogenic trap and so the liquid nitrogen dewar was reinstated.

Finally, it was concluded that the large 80 cm long trap would contain predominantly CO_2 scrubbing reagent Carbosorb (Granular, 0.7-1.2 mm, Elemental Microanalysis), since it was effective at removing the CO_2, but only a small amount of magnesium perchlorate immediately afterwards. It was hoped that the larger amount of CO_2 scrubbing reagent carbosorb would ensure that the CO_2 was removed, yet there would be insufficient magnesium perchlorate available to cause a blockage once wet. The liquid nitrogen dewar was reinstated. Although the instrument did not get overloaded with CO_2, peak shapes improved, and there were no effects on flow rates, there was a concern that H_2O may pass into the column and cause retention time shifts. In order to minimise the amount of H_2O retained on the column over long periods of time, the column was regularly baked at 200 °C to remove water and all 'sticky' compounds.

Flow optimisation

During the setup of the inlet system for the analysis of CH_3Cl in CO_2, there were numerous issues related to maintaining the flow rate throughout the system. Many of the flow rate issues were

directly related to the chemical trap. Leaks were suspected, and leak checking was performed extensively and multiple times over the course of the method development. Once the flow rate issues were resolved, the flows through the high flow system was optimised at 24.0 mL min^{-1}. Through the low flow section of the inlet system, including the chromatography column, flows were optimal at 1.42 mL min^{-1}.

The change in flow rate in the low flow part of the system meant that in order to optimise the detected CH_3Cl signal, the position of the capillary from the column into the open split periphery need to be altered. The small size of the CH_3Cl sample meant it was important to ensure that there was no sample dilution by helium in the open split periphery. The helium dilution capillary was positioned further upwards than before, away from the sample capillary, when not in the 'inject' position.

Sample trapping

In the case of a real air sample, the volume of gas is smaller than previously introduced via the inlet system. In the first instance, it was thought that the use of a pump may be suitable to transfer small volumes of gas through the cryogenic trap. However, this method would use up the small volume of sample very quickly, and may cause fractionation during the pumping process, and so the use of a pump was discarded. The solution was the addition of a stainless steel sample loop, 2.5 metres long (volume 35 mL), attached to a 6-port valve. On opening the small sample cylinder, there was sufficient gas pressure to completely fill the loop at least twice over to allow for flushing and removal of contaminants. Filling was controlled using at mass flow controller set to 25 mL min^{-1} for 6 minutes to ensure that the loop was filled more than twice, flushing gases out of the loop during filling and therefore removing contaminants. The 6 port valve was then switched to the inject position, and a helium carrier gas stream at 80 mL min^{-1} pushed the sample into the cryogenic trap.

Once collected into the first cryogenic trap (T1), the 6 port valve would return to the 'fill' position, and the second cryogenic trap (T2) lowered to cool in the liquid nitrogen for 20 s before T1 was lifted out of the LN_2. Traps were continually under He flow at 80 mL min^{-1} whilst not collecting sample, to ensure no contamination or memory effects from the previous sample.

Testing of time to transfer between loop and T1

It was necessary to ensure that all material was transferred between the sample loop and the first cryogenic trap T1, to ensure no fractionation was imparted during the inlet system stage. The effect of transfer time was investigated by running a series of test transfers from 5 to 35

minutes, and the resultant peak area monitored. It can be seen in Figure 6.4 that the peak area increased with increasing transfer time up to approximately 25 minutes, where it stabilised.

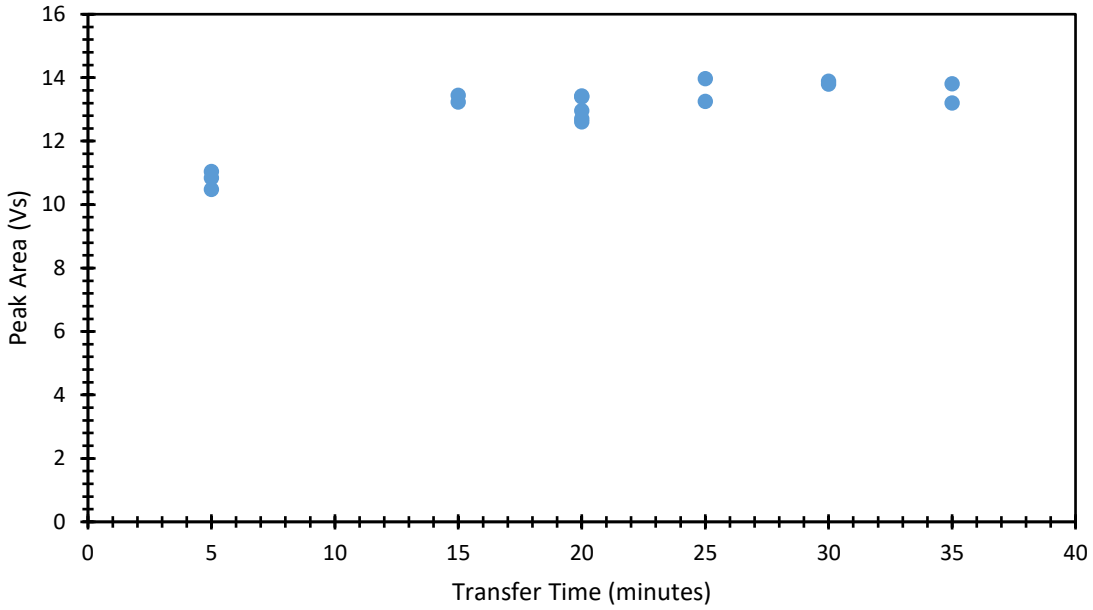

Figure 6.4 Effect of transfer time (minutes) between sample loop and cryogenc trap 1 on the peak area (Vs).

The values of δ52/50 and δ51/50 from these tests are shown in Figure 6.5. It can be seen that fractionation occurs below transfers of 25 minutes in the case of both δ52/50 and δ51/50. All delta values are with respect to UMCIS via the bellows of the dual inlet system.

It was concluded therefore that the loop would be flushed for 25 minutes to transfer the sample into trap 1.

Testing of different loop sizes

Testing of a range of different sized loops had two purposes. Firstly, it enabled determination of the smallest sample size which gave good precision, and secondly, gave information regarding the linearity of the system. A series of samples loops were prepared with sizes from 30 cm to 250 cm, which were attached one after the other to the 6-port valve. The CH_3Cl in CO_2 mixture was used to mimic closely the atmospheric air concentrates (with N_2 and O_2 removed), using a 25 minute transfer as determined previously. Figure 6.6 shows that the system is linear with regards to a linear increase in length of sample loop.

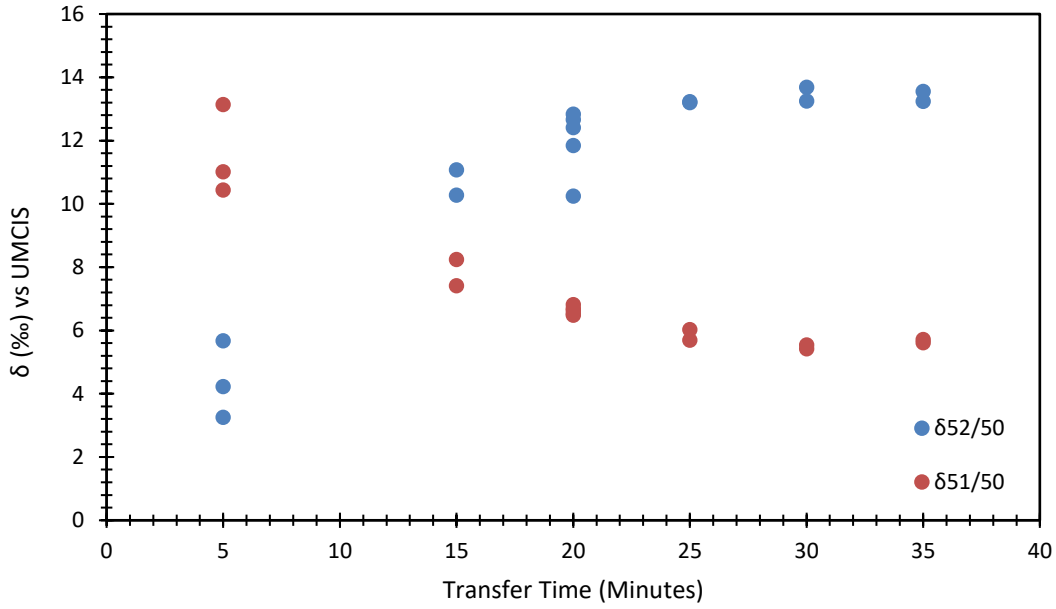

Figure 6.5 Effect of transfer time (minutes) between sample loop and cryogenc trap 1 on δ (‰). All delta values are with respect to UMCIS via the bellows of the dual inlet system.

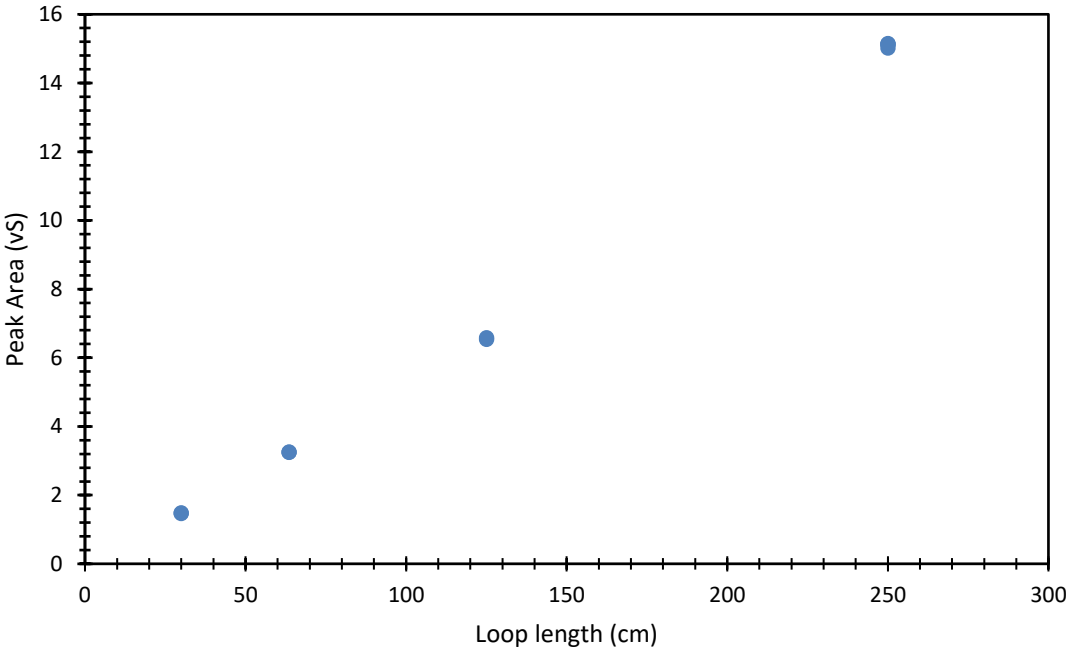

Figure 6.6 Effect of sample loop length (cm) on peak area (Vs).

The effect of loop length on δ values is shown in Figure 6.7. With respect to δ52/50 there is an increase in delta with increasing loop length, it appears linear. However the data at 250 cm loop length display considerable variability. The data at 250 cm length point which falls at higher δ than the others at the same loop length was in fact measured at a later point in the day than the first, indicating instrument drift.

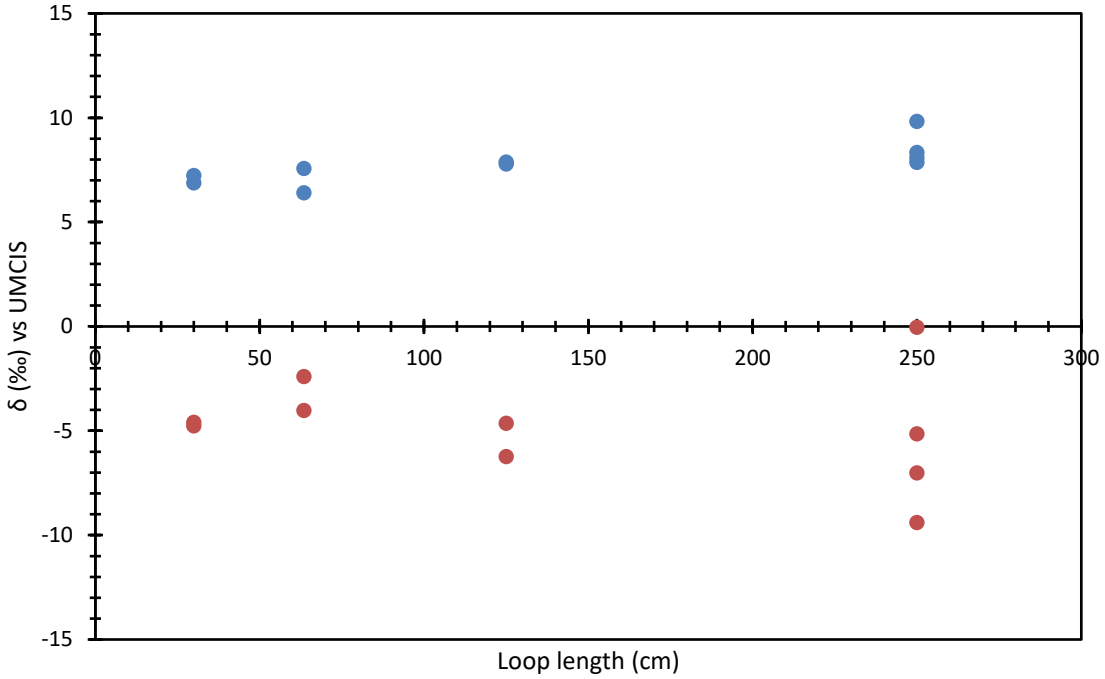

Figure 6.7 Effect of sample loop length (cm) on δ (‰).All delta values are with respect to UMCIS via the bellows of the dual inlet system.

Data displayed for δ51/50 show a changing δ with loop length and again have a spread of values at the 250 cm loop length, again indicating drift over the course of the day. The effect of loop length on delta values therefore could not be accurately attained without first removing the effect of drift on the data.

Drift observations

A sample was analysed in the identical way 6 times over the course of the day to quantify the instrument drift. The sample filled the loop for 6 minutes, transferred from the 250 cm loop to the cryogenic trap for 25 minutes. Figure 6.8 identifies a small decrease in peak area over the measurement period. Over the course of 6 identical runs, a change of only 2 % indicates that the system is in fact very stable.

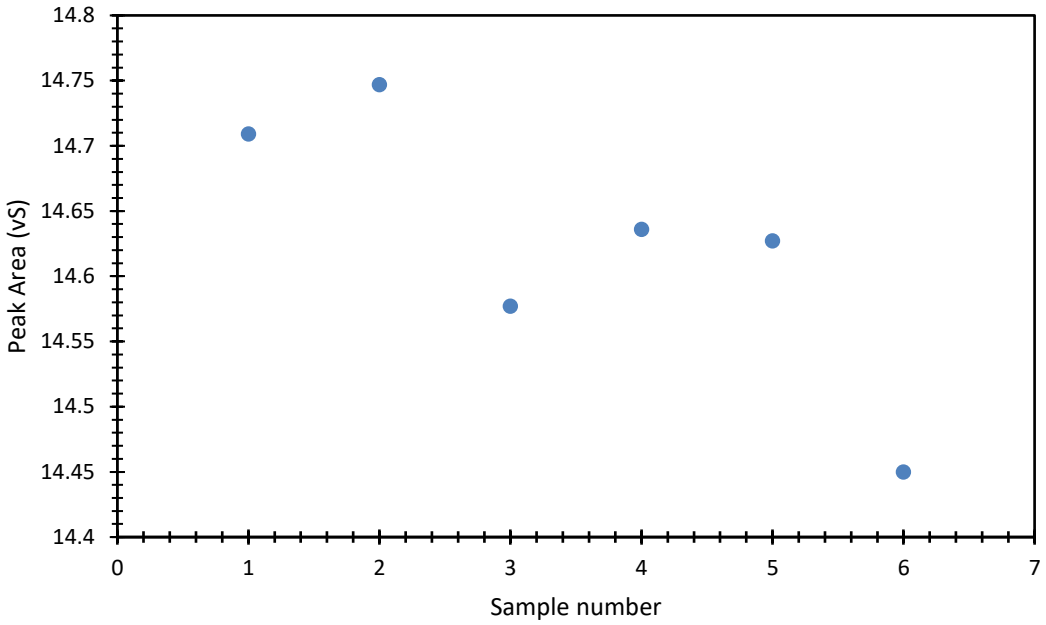

Figure 6.8 Observed peak area instrument drift over the course of 6 identical sample runs.

Interestingly, the δ52/50 data display instability, yet are not correlated to the decrease in peak area over the measurement period as shown in Figure 6.9. However, the δ52/50 measurments show a poitive bias in delta values with decreasing peak area.

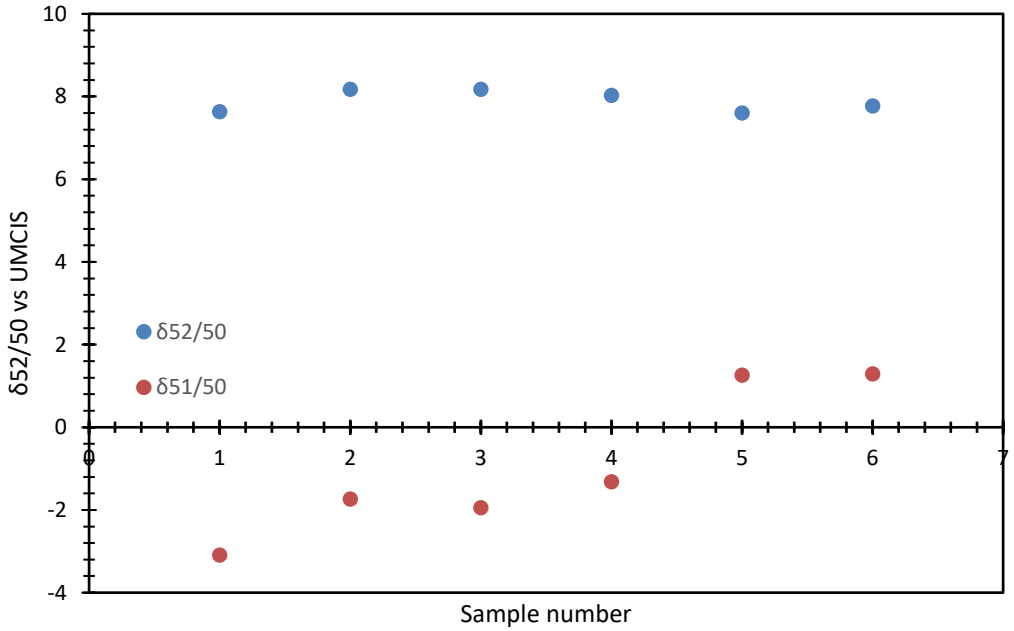

Figure 6.9 Observed δ instrument drift over the course of 6 identical sample runs. All delta values are with respect to UMCIS via the bellows of the dual inlet system.

Before attempting mathematical drift corrections it was necessary to rule out the effect of instability in the methyl chloride reference peaks on the drift in delta values.

Reference peaks via dual inlet

The position of the CH_3Cl reference peaks was investigated to ensure continuity of the reference peak shape and therefore maintaining reproducibility of isotope deltas. The reference peaks were positioned before the elution of the sample peaks from the column. Reference peaks were not consistent in shape or peak areas each time, yet the issue resolved when a number of reference peaks were run in succession.

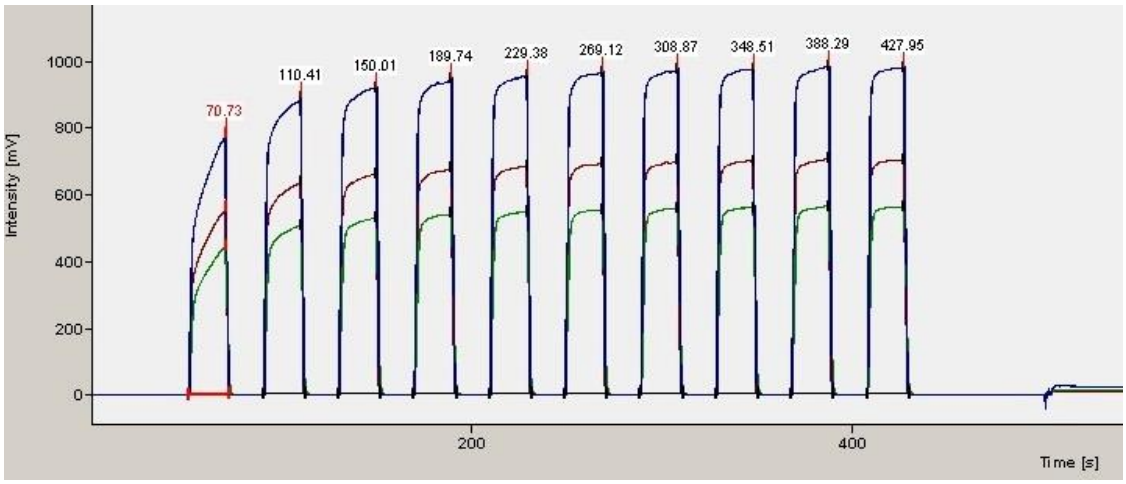

Figure 6.10 Sample chromatogram to show change in peak shape of CH_3Cl reference peaks over multiple repeats.

As shown in Figure 6.10, the reference peaks are not stable in area to begin with, but repeating in excess of 10 reference peaks gives reproducible shape and peak area. Therefore, the last reference peak in the series was used to calculate isotope deltas of the sample CH_3Cl peaks. Originally, the baseline of the chromatogram was not flat at the point of the 10th reference peak introduced to the spectrometer. It was thought that the use of the backflush function might be useful to remove interferences from the column, but was deemed not necessary as both CO_2 and N_2O are retained on the column similarly in retention time to methyl chloride. This being the case, these interferences are removed from the column during each run, and so the backflush function is redundant.

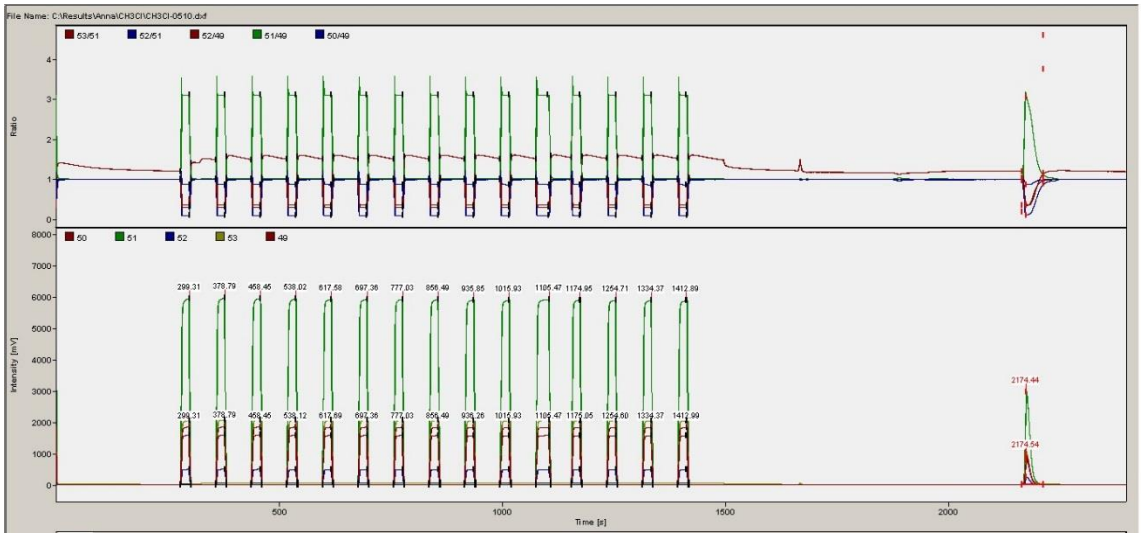

Figure 6.11 Sample chromatogram to show flat baseline after reference peaks and before CH_3Cl peak.

The issue with the baseline was resolved by increasing the amount of reference peaks to 18, and so the 18th reference peak occurred where there was a flat smooth baseline, which improved the reproducibility of the samples peaks. Figure 6.11 demonstrates the flat baseline immediately before the methyl chloride peak elutes.

6.4.5 Synthesis of CH_3Cl standard gas

To date no internationally recognised calibration gas has been distributed to allow comparison of the isotopic composition of methyl chloride between samples and different analytical methods. Measurement of isotope ratios in methyl chloride are generally compared via relation to standard mean ocean water chloride ($\delta^{37}Cl_{SMOC}$) and Vienna Pee Dee Belemnite ($\delta^{13}C_{VPDB}$). There is no recognised international standard of atmospheric origin. The use of an isotopically characterised sodium chloride and the ester group of a pectin moiety was identified as a possible mechanism to form isotopically characterised methyl chloride upon heating.

Pectin describes a family of complex polysaccharides present in the cell walls in plants (Ridley et al., 2001). Three pectin moieties exist; homogalacturonan, rhamnogalacturonan-I, and substituted galacturonans (Visser and Voragen, 1996), each comprising of a polymeric chain containing 1,4-linked α-d-galactosyluronic acid residues, as shown in Figure 6.12.

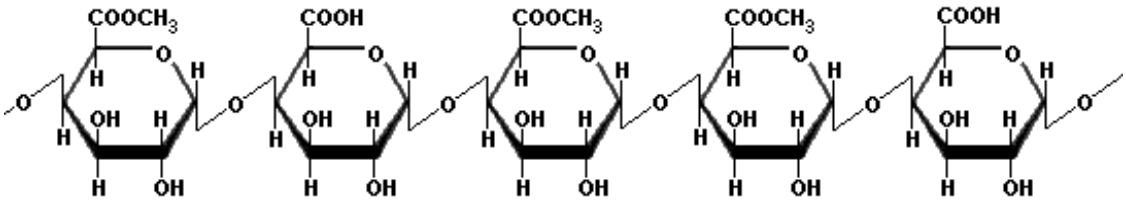

Figure 6.12 Polymeric chain containing 1,4-linked α-d-galactosyluronic acid residues of a pectin polysaccharide.

In the case of homogalacturonan a number of carboxylates of the α-d-galactosyluronic acid residues are either esterified with methanol or acetic acid to give methyl esters or O-acetyl esters. The degree of esterification gives rise to different varieties of homogalacturan pectins across a range of plant material. The backbone of the rhamnogalacturonan-I family displays alternating α-d-galactosyluronic acid and rhamnosyl residues. No side chains have been observed at the α-d-galactosyluronic acid position, whereas 20-80 % of rhamnosyl residues have been shown to be substituted with oligosaccharide side chains (O'Neill et al., 1990). Although there is no conclusive evidence that the alternating a-d-galactosyluronic acid residues are methyl esterified, they may however be O-acetylated (Komalavilas and Mort, 1989) to give available methyl groups for chlorination. Substituted galacturonans combine the α-d-galactosyluronic acid residue polymeric chain, with multiple and diverse substitutions. No rhamnosyl residues are present. Side chains are typically saccharides (O'Neill et al., 1990), β-D-xylosyl (Kikuchi et al., 1996), or β-D-apiofuranosyl (Cheng and Kindel, 1997) residues.

Methyl chloride formation from pectin as a precursor can be via one of two mechanisms. Firstly, the chlorination of the methyl group can occur at either the methyl ester or O-acetyl ester position in homogalacturonan pectin, the O-acetyl ester position in rhamnogalacturonan-I pectins. It is possible that the substituted side chains of substituted galacturonans contain esterified functional groups.

Preparation of sodium chloride/pectin gel

Pectin (0.5 g) was weighed, lyophilised and reweighed to allow determination of water content by weight. Sodium chloride solution (0.0705 M, 50 mL) was heated to 50°C and dry Pectin (5 g) added slowly with rapid stirring to give a uniform gel. The gel was transferred to a crystallising dish and allow to cool for 2 hours. The resultant gel was transferred as a thin layer to a

crystallising dish, covered with aluminium foil and frozen at -10°C. The frozen sample was lyophilised until constant weight, and ground to approximately 3 mm particle size.

Heating experiments

A 1 L quickfit vessel was modified with a valve to sample the headspace and a 24/29 ground glass fitting to allow connection of a test tube containing the sample. The sodium chloride fortified pectin sample (35 mg) was placed in the test tube, the test tube connected to the modified flask via the quickfit fitting and lowered into the oven as described. The sample was heated for 30 minutes at 240 °C, and the headspace gases collected. The procedure was repeated with distilled water rather than sodium chloride solution to account for the contamination of the commercially acquired pectin with Cl-.

6.5 Results and discussion

To date, no measurements of ^{37}Cl have been published for atmospheric samples of CH_3Cl. The most successful analysis of CH_3Cl in gaseous samples so far is that of Konno et al. (2013), demonstrating development of a suitable analytical system which allowed for analysis of a 'Test Gas' preparation of methyl chloride in helium. Analytical precision of this system (standard deviation of a single measurement) of greater than 0.6 nmol of CH_3Cl was 0.1 ‰ (vs UMCIS) (n = 48). With respect to analysis of atmospheric samples, three issues mean that the system developed by Konno et al. (2013) requires further improvements which are addressed in this chapter. Firstly, the authors describe good precision with samples greater than 0.6 nmol CH_3Cl, however, in order to analyse samples of atmospheric origin the system would require samples of gas of unfeasibly large volume. The system developed in this chapter aims to significantly reduce the amount of gas required, and so can be applicable for analysis of air concentrates. Secondly, it is not known how the matrix effects of real atmospheric samples would differ from the test sample in a helium matrix used by Konno et al. This chapter improves on this helium matrix firstly by using a test sample in nitrogen rather than helium. Additionally, since atmospheric samples may be stored as trace gases only (nitrogen and oxygen removed), the samples are effectively in a CO_2 matrix. The system developed in this chapter allows analysis of CH_3Cl in CO_2.

The ability of the overall measurement system to be used for CH_3Cl analysis with adequate precision was ascertained in three ways:

1. Use of the dual inlet system to measure isotopes in CH_3Cl.

2. Use of the new inlet system to measure 1.3 µmol mol^{-1} CH_3Cl l in Nitrogen 'synthetic' sample to adequate precision.
3. Use of the new inlet system to measure 1.3 µmol mol^{-1} CH_3Cl in CO_2 'synthetic' sample to adequate precision.

6.5.1 Use of the dual inlet system to measure isotopes in CH_3Cl

Use of the MAT 253 spectrometer for analysis of CH_3Cl was successful in the first instance using the dual inlet function. Use a zero enrichment was tested using standard UMCIS, using manual bellow pressure adjust corresponding to a signal of 40000 mV. Manual adjustment increased the stability of peak areas and therefore isotope ratios. Precision of measurements over 10 cycles are shown in Table 6.3.

Table 6.3 1 σ uncertainty of measurements using the dual inlet system.

m/z	**53/50**	**52/50**	**51/50**	**52/49**	**51/49**	**50/49**
Mean δ (‰)	-0.50	-0.14	-0.10	-0.26	-0.21	-0.11
σ	0.05	0.01	0.14	0.19	0.05	0.19

In comparison to measurements carried out by Konno et al. (2013), the standard UMCIS comprises CH_3Cl in helium. However, Konno in fact uses an inlet system to trap and process the gases before introduction to the MS. Since data displayed in Table 6.3 represents CH_3Cl in He injected directly into the MS via a dual inlet system, it is to be expected that this study has improved precision compared to Konno et al. (2013). The published 1 σ uncertainty is 0.1 ‰ when a sample greater than 0.6 nmol CH_3Cl was introduced, ten times the uncertainty (0.01 ‰) of the *m/z* 52/50 peak in the study.

6.5.2 Use of the newly developed inlet system to measure chlorine isotopes in CH_3Cl

Measurement of CH_3Cl in nitrogen matrix

The use of a mix of 1.3 ppm CH_3Cl in N_2 allowed the system to measure 'real' air quantities of methyl chloride in a nitrogen matrix, without the complications of large interferences such as CO_2. This also gave a more comparable data set to that of Konno et al. (2013).

Since real air samples would be small in volume, the minimum volume of CH_3Cl which could be analysed whilst retaining good precision was determined. Until this point, extractions had consisted of 750 second extractions at 27.2 mL min^{-1}. The flow rate was retained, but the trapping amount reduced to 30 s, 60 s, 100 s and 150 s to be more representative of sample sizes in real air samples. Trapping for as little as 30 and 60 seconds did not allow for peaks of suitable size for reliable integration. Trapping for 100 seconds (45 mL, 1.16 nmol CH_3Cl) allowed reproducible data with precision values between 0.4 and 6 ‰ (vs UMCIS) for all masses. Although this value is larger than that of the Konno et al. (2013) system (1 σ = 0.1).The Konno samples, although contained perhaps less CH_3Cl, the matrix helium, and less representative of a real atmospheric sample. There may be matrix effects involved in a mixture of CH_3Cl in nitrogen which are not present in a mixture of CH_3Cl in helium.

Measurement of CH_3Cl in CO_2 matrix

Atmospheric samples from suitable measurement campaigns such as CARIBIC (Civil Aircraft for the Regular Investigation of the atmosphere Based on an Instrument Container) are not whole air samples but have had the N_2 and O_2 removed, giving essentially CO_2 with trace gases. The above 'sample' of CH_3Cl in N_2 is representative of whole air sample analysis. It was necessary to ensure the system could process samples which could measure CH_3Cl in a CO_2 matrix. A cylinder of 1.3 ppm CH_3Cl in CO_2 was purchased for this purpose. Filling the 250 cm loop used 35 mL of sample, equivalent to 0.90 nmol CH_3Cl. This again is larger than the 0.6 nmol CH_3Cl sampled during the Konno measurements. Delta values (vs UMCIS) of 2.15 ‰ (*m/z* 51/50) and 9.71 ‰ (*m/z* 52/50) were calculated. The 1 σ uncertainty of 6 repeats of 0.90 nmol CH_3Cl in CO_2 was 0.58 ‰ for δ51/50 and 0.12 ‰ for δ 52/50. This is comparable to the value of 1 σ = 0.1 ‰ given by Konno for the δ52/50, yet the uncertainty is larger for δ51/50. This is expected due to the use of a CO_2 matrix 'test gas' rather than the CH_3Cl in He sample as used by Konno et al. (2013). In fact, considering the extent of the challenges presented by using a CO_2 matrix, these precision values are indeed a positive step towards measurement of real samples. Importantly however, in an atmospheric contest, the precision achieved is suitable for analysis of air concentrated collected by CARIBIC. As described above, $\delta^{13}C$ measurements of methyl chloride and methyl bromide emitted from salt marshes was determined to be – 65 ‰ and -12 ‰ (vs VPDB) (Bill et al., 2002). Samples by CARIBIC collected directly over such areas would be expected to display a similar values, however mixing and transport effects would cause the dampening effect of isotope ratios, leading to values approximately half of the expected values as described by Zuiderweg (2012). The precision achieved in this study is therefore well below the -32.5 ‰ and

-6 ‰ values, half of those determined by Bill et al., (2002), meaning the system is suitable for real air analysis.

6.5.3 Atmospheric CH_3Cl standard material

Since no internationally recognised calibration gas has been distributed to date, comparison of the isotopic composition of atmospheric methyl chloride between samples and different analytical methods is not possible. The use of standard mean ocean water chloride ($\delta^{37}Cl_{SMOC}$) and Vienna Pee Dee Belemnite ($\delta^{13}C_{VPDB}$) is accepted as a fair alternative in place of a recognised international standard of atmospheric origin.

The reaction of an isotopically characterised sodium chloride with a pectin chain was identified as a possible mechanism to form isotopically characterised methyl chloride. Once the reaction had taken place, the resultant headspace gases were analysed using the dual inlet method. Delta values of 9.57 ‰ and 22.02 ‰ were measured, for *m/z* 52/50 and *m/z* 51/50 respectively, relative to UMCIS. Precision over 10 cycles of the dual inlet method was 0.01 ‰ (*m/z* 52/50) and 0.26 ‰ (*m/z* 51/50) (vs UMCIS).

The isotopic composition is likely to have undergone some fractionation during the synthesis, and it would be interesting to determine the degree of fractionation, if any. It would be beneficial to undergo cleanup of the sample, to remove products which are not CH_3Cl, then to characterise the sample to ensure purity. Nuclear Magnetic Resonance spectroscopy (NMR) for both ^{2}H and ^{13}C would be useful, whereas ^{37}Cl is slightly less sensitive. Infrared spectroscopy (IR) may also aid characterisation.

Finally, in order to establish whether the reaction of sodium and chloride had in fact produced methyl chloride with the isotopic composition of the reactant sodium chloride, it would be necessary to measure the isotopic composition of the original sodium chloride using the MAT 253 spectrometer.

6.6 Conclusions

To date, no measurements of chlorine isotope measurements in atmospheric samples of methyl chloride have been successfully measured. These method developments represent the first steps towards measurement of chlorine isotopes in atmospheric methyl chloride.

The analytic system of Konno et al. (2013) allowed measurement of chlorine isotopes in a preparation of CH_3Cl in helium. The authors determined the 1 σ analytical precision of greater

than 0.6 nmol of CH_3Cl to 0.1 ‰. Samples of gas required would be of unfeasibly large volume for real atmospheric application. Additionally, it is not known how the matrix effects of real atmospheric samples would differ from the test sample in a helium matrix. The analytical accuracy of their measurements could not be determined since no internationally recognised atmospheric standard for chlorine isotopes in methyl chloride has been distributed.

Dual inlet measurements

Use of a MAT 253 spectrometer allowed dual inlet measurements of carbon and chlorine isotopes of methyl chloride in helium. The 1 σ uncertainty was 0.01 ‰ and 0.14 ‰ (vs UMCIS) for *m/z* 52/50 and *m/z* 51/50 respectively. This is an order or magnitude smaller, and therefore more analytically precise than the that of Konno et al. (2013). However, since the Konno system uses an inlet system, it would be expected that the analytical precision is improved using the dual inlet method employed in this study.

Measurement of isotopes of CH_3Cl in a N_2 matrix using the newly developed inlet system

A preparation of 1.3 ppm CH_3Cl in N_2 gave a greater indication of the ability of the inlet system to process whole air samples. Additionally it allowed better comparison to the capabilities of the inlet system to that of Konno et al. (2013). The minimum sample volume which could be analysed with reasonable precision was determined to be 45 mL (1.16 nmol CH_3Cl). 1 σ uncertainty lay between 0.4 ‰ and 6 ‰ (vs UMCIS) for all masses. This uncertainty is larger (more uncertain) than that of Konno (1σ = 0.1 ‰), yet can be explained by differences in the analytical processes. There may be matrix effects involved in a mixture of CH_3Cl in nitrogen which are not present in a mixture of CH_3Cl in helium, leading Konno to establish better measurement uncertainty. Although the use of nitrogen in this study is more representative of a whole air sample than the helium used by Konno, it is important to note that there in effect are no other gases present other than CH_3Cl. This means that the inlet system does not need the capability to remove large quantities of trace gases as would be required with whole air samples. In effect, the precision would be likely adversely affected if a whole air sample was introduced, highlighting a limitation of this system. It would be interesting to attempt to analyse a whole air sample using this inlet system.

Measurement of isotopes of CH_3Cl in a CO_2 matrix using the newly developed inlet system

For measurement of atmospheric samples from real campaigns such as CARIBIC, the system is required to measure air concentrates . Samples essentially comprise CH_3Cl in a CO_2 matrix. The smallest sample size of 1.3 ppm CH_3Cl in CO_2 used in this study was 35 mL, equivalent to 0.90 nmol CH_3Cl. This is larger than the 0.6 nmol CH_3Cl sampled during the Konno measurements. The 1 σ uncertainty (vs UMCIS, n=6) of 0.90 nmol CH_3Cl in CO_2 was 0.58 ‰ for δ51/50 and 0.12 ‰ for δ52/50. The δ52/50 is comparable to the value of 1σ = 0.1 ‰ given by Konno, yet the uncertainty is larger for δ51/50. Considerable challenges were faced in the development stages, yet this system still represents good precision, and is capable of measurement of real samples in a CO_2 matrix. It would be necessary now to attempt measurement of a sample from a campaign such as CARIBIC to identify measurement precision.

Synthesis of a CH_3Cl standard from isotopically characterised sodium chloride

No internationally recognised atmospheric CH_3Cl calibration gas has been distributed to date. The use of standard mean ocean water chloride ($\delta^{37}Cl_{SMOC}$) and Vienna Pee Dee Belemnite ($\delta^{13}C_{VPDB}$) is the current alternative.

Isotopically characterised sodium chloride was reacted with apple pectin in an attempt to form isotopically characterised methyl chloride. Headspace analysis took place using the dual inlet method, and CH_3Cl was indeed detected. Precision over 10 cycles of the dual inlet method was 0.01 ‰ (*m/z* 52/50) and 0.26 ‰ (*m/z* 51/50) (vs UMCIS).

It is likely that fractionation occurred during synthesis, and the proportion of CH_3Cl to other products is currently unknown, so cleanup would be necessary as a next step. It would also be useful to characterise the CH_3Cl content using ^{2}H, ^{13}C and ^{37}Cl NMR.

Chapter 7: Conclusions and Future Research

This chapter summarises the main findings of this thesis and outlines future enquiry for isotope measurements in CFC-11, CFC-12, CFC-113, N_2O and CH_3Cl. The measurements carried out have firstly provided valuable novel findings with respect to the individual species studied. However, it is important to discuss the interesting comparison of behaviour across all species. Sections 7.1 to 7.5 detail and summarise the main findings from the corresponding chapters 2 to 6. The following section, 7.6, compares and contrasts the isotopic behaviour of all these species, and highlights the implications of continued and improved measurements of this type.

7.1 High sensitivity isotope ratio measurements of CFC-11, CFC-12 and CFC-113 in the stratosphere

CFC-11, CFC-12 and CFC-113 are three of the most abundant halocarbons of anthropogenic origin in the atmosphere, and have multiple industrial sources at the Earth's surface. Sink processes are limited to reaction with $O(^1D)$ and photolysis in the stratosphere, which produces the chlorine radical initiating the catalytic decomposition of ozone. Chapter 2 further characterised CFC-11, CFC-12 and CFC-113 with respect to ^{37}Cl and ^{13}C isotope ratios in stratospheric samples.

^{37}Cl Isotope ratio measurements

- A significant number of $\delta(^{37}Cl)$ measurements of CFC-11, CFC-12 and CFC-113 in stratospheric air from mid- to high-latitudes have been carried out. These samples represent measurements deeper into the stratosphere than previously reported.
- Measurements display improvements in uncertainties compared to previous studies for both mid- and high-latitudes, for all three species of interest.
- Measurements from high- and mid-latitudes show an expected increase in isotope enrichment with decreasing mixing ratios for all CFCs. A maximum enrichment value of 38±0.9 ‰ significantly exceeds published ^{37}Cl enrichment in CFC-12 to date.

- Apparent isotope fractionation varies with respect to latitude:
    - ε_{App} is higher in mid latitude samples compared to high latitudes in CFC-12.
    - CFC-11 displays the same correlation however values are statistically indistinguishable.
    - The correlation in ε_{App} is reversed with respect to CFC-113.
    - The calculated ε_{App} values for CFC-11, CFC-12 and CFC-113 agree well with expected values based on previous studies with respect to both mid and high-latitudes.
- Since the value of epsilon is consistent with previously published values, this demonstrates that this technique can be applied to various regions of the stratosphere
- The data are consistent with a constant isotope composition of emissions over time for all three species.

^{13}C Isotope ratio measurements

- The first measurements of $\delta(^{13}C)$ of CFC-11, CFC-12 and CFC-113 at stratospheric altitudes have been carried out
- All CFCs display isotopic enrichment in the stratosphere, likely due to fractionation by destruction processes. Enrichment in $\delta(^{13}C)$ increases with altitude.
- Minimal correlation is observed between latitude and apparent isotope fractionation.
- No other studies to date detail measurements of ^{13}C in CFC-11, CFC-12 and CFC-113 in the stratosphere. Data from this study demonstrate significant ^{13}C enrichment in the stratosphere yet values of apparent isotope fractionation are significantly lower than that given by fractionation observed in laboratory photolysis experiments.
- The measured enrichment of ^{13}C in the stratosphere, will in turn will cause enrichment in the troposphere. However, it is unlikely that the magnitude of enrichment is a great as that proposed by Zuiderweg et al., (2013).
- A constant isotopic source signature is suggested for emissions

For analysis of $\delta(^{37}Cl)$ in CFC-12 it is possible to draw conclusions regarding the change in isotope fractionation at mid- and high-latitudes, the apparent isotope fractionation decreases as expected. However, the CFC-11 mid and high-latitude ε_{App} values are indistinguishable within 1 standard deviation, and no latitude dependence is observed. In the case of CFC-113, the mid and high-latitude values are indistinguishable within 2σ analytical uncertainties. It is possible that in both cases the small isotope changes, and the possible latitude dependence as measured in CFC-12, is obscured by the size of the analytical uncertainties. It is also possible that some

source signature biased CFC-113 was observed near the troposphere since delta values were high and there are still considerable emissions ongoing for CFC-113.

With respect to $\delta(^{13}C)$ measurements, no correlation of isotope fractionation with latitude is observed. However, since these are the first measurements of $\delta(^{13}C)$ in stratospheric air, the analytical uncertainties could again obscure any small isotope changes. A priority for ongoing work would be the development of the system further to improve analytical uncertainties for both $\delta(^{37}Cl)$ and $\delta(^{13}C)$ measurements.

The high measurement uncertainty of the Allin et al. (2015) data meant that it was not possible to preclude the possibility that the average emission isotope delta has not changed over time. Data presented in this thesis, with uncertainties smaller than that of Allin et al. (2015), which although again cannot rule out the possibility, however suggests that indeed the emission delta has not changed. Improved data precision, in particular for reanalysis of long-term tropospheric air archives would help confirm whether the source isotope delta has changed over time. It would be interesting to determine whether the average isotope enrichment has been affected in changes in CFC manufacturing processes.

7.2 Photolysis rates of CFC-12 and linkage to recognised ^{13}C calibration scale

After release at the Earth's surface, CFCs are transported to the stratosphere, where they are subject to breakdown by photolysis and reaction with $O(^1D)$. Photolysis by short wave ultraviolet radiation produces free chlorine which contributes significantly to ozone depletion. A study by Zuiderweg et al. (2012) detailed ^{37}Cl and ^{13}C isotope analysis of samples which had undergone laboratory photolysis at stratospherically relevant wavelength and temperatures, plus the corresponding photolysis rates. Chapter 3 presents a reanalysis of these samples, to link measurements to internationally recognised ^{13}C scale (VPDB) to allow direct comparison between the Autospec instrument (UEA) and the IRMS system used by Zuiderweg et al. (2012). It was then possible to compare data from this study, Allin (2015) and Zuiderweg et al. (2012), to eliminate experimental issues with photolysis samples and firn samples analysed by Zuiderweg et al. (2012). Additionally, the photolysis isotope fractionation in this study could be compared to the work of Lockhart (2010), Martin (2011) and Maxwell (2012) as well as stratospheric data from this study (chapter 2), Allin (2015) and Laube et al. (2010).

- The photolysis rate of CFC-12 agreed well with measurements by Zuiderweg et al. (2012), yet displayed significantly smaller photolysis rates than studies by Maxwell (2012), Martin (2011) and Lockhart (2012). This could be explained in part the presence

of a scavenger species in the case of Maxwell, but both Martin and Lockhart did not limit recombination reactions in this way. All studies had significant experimental issues such as non-linearities, condensation within the reactor, pressure and lamp intensity variabilities and detector drift.

- In comparison to stratospheric data, there is reasonable agreement between the ^{37}Cl isotope fractionation in photolysis samples and stratospheric samples at mid latitudes as described in chapter 2. A strong influence of mixing and transport on ^{37}Cl isotope fractionation is suggested.
- With respect to both photolysis rate and ^{37}Cl isotope fractionation, it was concluded that measurements were not representative of atmospheric values, due to recombination reactions influencing isotope fractionation.
- Measurements of ^{13}C isotope fractionation agrees well with data from Zuiderweg (2012) for all temperatures. However, stratospheric measurements as described in Chapter 2 have significantly lower apparent isotope fractionation than the measured photolysis samples. This discrepancy can be attributed to the higher mixing ratio of CFC-12 in the photolysis samples compared to real air samples, likely causing a bias. Again, in addition, the real air samples have been subject to atmospheric transport and mixing, lessening the observed atmospheric fractionation.
- Stratospheric data from Chapter 2, as well as firn data from Allin et al. (2015) was linked to the VPDB scale to allowed direct comparison between studies. Data given by Zuiderweg still displays a larger magnitude in isotope fractionation with depth.
- Stratospheric data from this thesis agrees with an emissions scenario which does not change over time.

The analysis of ^{37}Cl and ^{13}C allowed calculation of photolysis rate and fractionation constants of CFC-12 in a mixture of CFC-12 and CFC-11 in OFN. However comparisons between studies was complicated by experimental issues that the other studies described.

The samples prepared by Zuiderweg, which were analysed in this study, had mole fractions which were significantly higher than atmospheric values. This influences the measured photolysis rates. CFC recombination occurs more readily at higher concentrations leading to lower photolysis rates.

There is reasonable agreement between ^{37}Cl and ^{13}C isotope fractionation in the photolysis samples and stratospheric samples at mid latitudes as described in Chapter 2. However, stratospheric measurements at higher latitudes had significantly lower apparent isotope

fractionation, and therefore suggests a strong influence of mixing and transport. This can be attributed to the higher mixing ratio of CFC-12 in the photolysis samples compared to real air samples, as well as the fact that real air samples are subject to atmospheric transport and mixing.

It would be useful to prepare samples of CFC-11 and CFC in OFN at atmospherically relevant mixing ratios. Limiting recombination reactions via an ethane scavenger within the reactor will give a faster rate of photolysis.

7.3 Mass Spectrometric Analysis of Stratospheric Nitrous Oxide: Origin of the ^{17}O excess in tropospheric N_2O.

Nitrous oxide is a contributor to stratospheric ozone depletion and is also a significant greenhouse gas, yet is not regulated by the Montreal Protocol. Based on the mass difference, the isotope fractionation of ^{17}O should be approximately half as much as that of ^{18}O, with respect to ^{16}O, however, tropospheric air measurements show that the proportion of ^{17}O is higher than expected. Identifying the source of the ^{17}O excess would identify possible non-mass dependent fractionation in one or several N_2O sources or sinks. Chapter 4 described the development of a measurement system capable of analysis of $\delta^{15}N$, $\delta^{17}O$, $\delta^{18}O$ and $\Delta^{17}O$ in N_2O in whole air samples. Stratospheric samples from a mid-latitude site represent the first measurements of $\Delta^{17}O$ in stratospheric N_2O above 12 km altitude.

- Stratospheric samples are increasingly enriched with altitude, and display a similar ^{17}O anomaly to that in the troposphere.
- The data suggest that processes which only occur in the stratosphere, photolysis and reaction with $O(^1D)$ are not the source of the ^{17}O anomaly.
- Assuming this conclusion, the ^{17}O excess may therefore be attributed to either (a) chemical processes which occur in both the stratosphere and troposphere, or (b), the three isotope exponent of N_2O sources having the value of 0.528 rather than the accepted 0.516. Conclusion (b) agrees well with both, Cliff et al. (1999b) and Bernard et al. (2006).

Precision of measurements made using the new inlet system are comparable to previous systems for measurement of $\delta^{15}N$, $\delta^{17}O$, $\delta^{18}O$. The conclusions of this chapter, as stated above, agree well with the literature. However, it is important to note that the sample size of this study is small. Although the measurement uncertainties of the system were comparable to similar systems elsewhere, the conclusions would be enhanced by an additional number of

stratospheric samples at different locations and altitudes. Additionally, it would be useful to further analyse N_2O from terrestrial sources to identify the proportion which follow the 0.528 fractionation line.

7.4 Use of the developed N_2O inlet system in an interlaboratory comparison study

This chapter is based on a published paper, for which I am a co-author (Heil et al., 2014).

Detrermination of the of $\delta^{15}N$ site preference within N_2O, as well as the average $\delta^{15}N$ and $\delta^{18}O$ in N_2O have aided the understanding of N_2O source and sink processes. This increases understanding of the contribution of N_2O to the anthropogenic greenhouse effect. During analysis, laboratories generally refer their measurements to a tank of high purity N_2O, used as a working standard, of which the isotopic composition is relative to the international calibration material VSMOW or Air N_2. The lack of an internationally agreed gaseous N_2O reference material means there is uncertainty between different laboratories and analytical techniques. Chapter 5 detailed the use of the newly developed system for the participation in an interlaboratory compatibility study, in order to determine the current state of compatibility of different laboratories and techniques.

- The compatibility of eleven laboratories on analysis of ^{15}N site preference, $\delta^{15}N$ and $\delta^{18}O$ in N_2O using both mass spectrometry and laser-spectroscopy was carried out.
- Data showed that for $\delta^{15}N$ measurements, the use of mass spectrometry gave good agreement between laboratories. Laser spectrometry was less successful.
- The opposite conclusion was drawn with respect to ^{15}N site preference measurements, with laser spectrometry showing better agreement than mass spectrometry techniques
- It was concluded that for future research on N_2O isotopocules, standardisation against N_2O reference material is essential to improve interlaboratory compatibility.

Data from the study was then used in the context of this thesis to determine if the newly developed inlet system described in chapter 4 has adequate precision compared to similar systems. This was quantified by comparison of uncertainties of N_2O analysis carried out using the novel inlet system developed in this thesis with other laboratories in the study by Heil et al. (2014).

- The uncertainties of the modified inlet system for $\delta^{18}O$ measurements are well within the range of the remaining 10 laboratories

- The novel inlet system is suitable therefore for $\delta^{18}O$ in N_2O, with uncertainties comparable to and in some cases better than those of the 10 other laboratories.

The use of an interlaboratory comparison study was extremely useful in determining the success of the novel inlet system in the context of this thesis. In the wider context, it was concluded that for future research on N_2O isotopocules, standardisation against N_2O reference material is essential to improve interlaboratory compatibility.

7.5 Development of novel mass spectrometric techniques towards the measurement of isotopes in atmospheric methyl chloride

Methyl chloride accounts for a significant proportion of all natural chlorine reaching the stratosphere and therefore has a significant influence on ozone destruction. Measurements of methyl chloride samples of non-atmospheric origin have been carried out extensively, but do not provide data useful for constraining the atmospheric budget. Carbon isotope ratios have been determined in atmospheric samples, but as yet, no successful measurements of hydrogen or chlorine isotopes in atmospheric methyl chloride have been published.

Currently, measurements of isotope ratios in methyl chloride are generally compared via relation to standard mean ocean water chloride ($\delta^{37}Cl_{SMOC}$) and Vienna Pee Dee Belemnite ($\delta^{13}C_{VPDB}$). There is no known methyl chloride calibration gas of characterised isotopic composition.

Chapter 6 aimed to develop a measurement system capable of analysis of chlorine isotopes in methyl chloride in air concentrates. Additionally, the first steps towards the synthesis of a calibration gas of known isotopic composition were described, to allow comparison between different laboratories and analytical techniques.

Dual Inlet Measurements

- Use of a MAT 253 spectrometer allowed dual inlet measurements of carbon and chlorine isotopes of methyl chloride in helium.
- The analytic system of Konno et al. (2013) allowed measurement of chlorine isotopes in a preparation of CH_3Cl in helium. The 1 σ uncertainty of dual inlet measurements in this chapter was an order or magnitude smaller, and therefore more analytically precise than the that of Konno et al. (2013). However, since the Konno system uses an inlet system, it would be expected that the analytical precision is improved using the dual inlet method employed in this study.

Measurement of isotopes of methyl chloride in a N_2 matrix using the newly developed inlet system

- Analysis of a preparation 1.3 ppm MeCl in N_2 gave a greater indication of the ability of the inlet system to process whole air samples. Additionally it allowed better comparison to the capabilities of the inlet system to that of Konno et al. (2013).
- The minimum sample volume which could be analysed with reasonable precision was determined to be 45 mL (1.16 nmol CH_3Cl). The 1σ uncertainty is larger (more uncertain) than that of Konno yet can be explained by the possibility of matrix effects involved in a mixture of CH_3Cl in nitrogen which are not present in a mixture of CH_3Cl in helium.

Measurement of isotopes of methyl chloride in a CO_2 matrix using the newly developed inlet system

- For measurement of air concentrates, the inlet system was modified to analyse samples of CH_3Cl in a CO_2 matrix.
- The smallest sample size of 1.3 ppm CH_3 in CO_2 used in this study was 35 mL, equivalent to 0.90 nmol CH_3Cl. The 1 σ uncertainty of δ52/50 is comparable to the value determined by Konno, yet the uncertainty is larger for δ51/50. This higher uncertainty can be explained in part by possible CO_2 matrix effects.
- Considerable challenges were faced in the development stages, yet this system still represents good precision and looks capable of measurement of real samples in a CO_2 matrix

Synthesis of a methyl chloride standard from isotopically characterised sodium chloride

- No internationally recognised atmospheric CH_3Cl calibration gas has been distributed to date. The use of standard mean ocean water chloride ($\delta^{37}Cl_{SMOC}$) and Vienna Pee Dee Belemnite ($\delta^{13}C_{VPDB}$) is the current alternative.
- Isotopically characterised sodium chloride was reacted with apple pectin in an attempt to form isotopically characterised methyl chloride.
- Headspace analysis took place using the dual inlet method, and CH_3Cl was indeed detected.
- Delta values of 9.57 ‰ and 22.02 ‰ were measured, for *m/z* 52/50 and *m/z* 51/50 respectively, relative to UMCIS.
- Precision over 10 cycles of the dual inlet method was 0.01 ‰ (m/z 52/50) and 0.26 ‰ (m/z 51/50) (vs UMCIS).

It is not known how the matrix effects of real atmospheric samples would differ from the test sample in a helium matrix. Although the use of nitrogen in this study is more representative of a whole air sample than the helium used by Konno, it is important to note that there in effect are no other gases present other than CH_3Cl. This means that the inlet system does not need the capability to remove large quantities of trace gases as would be required with whole air samples. In effect, the precision would be likely adversely affected if a whole air sample was introduced, highlighting a limitation of this system. It would be interesting to attempt to analyse a whole air sample using the N_2 inlet system**.** Considerable challenges were faced in the development stages of the system for samples in CO_2, ready for analysis of air concentrates. The system however, still represents good precision, and looks capable of measurement of real samples in a CO_2 matrix. It would be necessary now to attempt measurement of a sample from a campaign such as CARIBIC to identify measurement precision.

The analytical accuracy of measurements could not be determined since no internationally recognised atmospheric standard for chlorine isotopes in methyl chloride has been distributed. The synthesis of CH_3Cl from reactants of known isotopic composition is a positive step towards an atmospheric CH_3Cl standard. However, it is likely that fractionation occurred during synthesis, and the proportion of CH_3Cl to other products currently unknown, and so cleanup would be necessary as a next step. It would also be useful to characterise the CH_3Cl content using ^{2}H, ^{13}C and ^{37}Cl NMR.

7.6 Comparison of isotopic behaviour of all species of interest

In addition to the valuable new findings as described in sections 7.1 to 7.5, a comparison of the isotopic behaviour of all the species of interest in this thesis is relevant. Better understanding the drivers of similarities and differences between species will enable more thorough understanding of relevant atmospheric processes and well as enable a direction for future enquiry to be identified more fully.

With respect to the isotopic fractionation with increasing altitude, all species display an increasing trend; measurements from high- and mid-latitudes show an expected increase in $\delta(^{13}C)$ and $\delta(^{37}Cl)$ enrichment with decreasing mixing ratios for all CFCs. The previously found similarity between CFC-12 and N_2O is confirmed by data from this study, stratospheric N_2O samples are increasingly enriched in $\delta(^{17}O)$ $\delta(^{18}O)$ and $\delta(^{15}N)$ with altitude. These data are expected based on the presumption that all species of interest here have similar destruction pathways, dominated by photolysis in the stratosphere. However this correlation between species is not seen with respect to apparent isotope fractionation. It can be seen clearly

between the three CFCs of interest that the ε_{App} varies depending on the species. This difference is likely driven by the difference in lifetimes, caused by either faster or slower chemistry involved in the destruction of the species. This is demonstrated well by the weak ε_{App} displayed by CFC-11, indicative of the fast rate at which it is broken down, and fast chemistry meaning less time for fractionation to occur. This also is the case for the comparison of $\delta(^{13}C)$ and $\delta(^{37}Cl)$, the latter displaying the smaller ε_{App} since the reaction proceeds at a faster rate. This gives a clear indication that the apparent isotope fractionation is affected by both the species, but also largely by the element involved. The faster chemistry allowing for less fractionation to occur during the destruction process. This conclusion is valuable for the application to unknown CFCs. It is important to note however that the speed of the reaction is only one factor. The most important factor is how different the absorption spectra look for the different isotopologues of each of the CFCs, and whether there is significant radiation at these wavelengths at stratospheric altitudes. For example, if the spectra look very similar for $CF(^{35}Cl)_3$ and $CF(^{35}Cl)_2(^{37}Cl)$ then they the amount of fractionation is likely to be low, unless the radiation intensity is higher at one of the wavelengths. This demonstrates that the causes of isotope fractionation are related to the quantum physics and are significantly more complex than the correlation between shorter lifetime giving less fractionation. However, it still gives a useful indication of fractionation. Mixing ratios are sufficient to calculate rates of destruction of species, however the use of isotopes as demonstrated in this thesis give an additional method of calculation. If the apparent isotope fractionation can be measured via the analytical procedure used in this thesis, an indication of the rate of reaction, and therefore rate of destruction can be inferred. By extension, this information aids budget calculations and additionally, may help to determine ozone recovery rates. Future work could look into fractionation from reaction with $O(^1D)$, to aim to deduce the proportions of CFC which are destroyed by either photolysis or $O(^1D)$. The weak fractionation demonstrated by CFC-11 gives weight to the argument suggested by Allin that the troposphere has seen little change in isotopic composition. Of relevance here is the long term trend of the N_2O isotopologues, demonstrating long term flux from the stratosphere to the troposphere. It is likely that CFC-12 also has a long term flux towards the troposphere, however, this would require improved precision to quantify. To further this application, the measurement of weak apparent isotope fractionation of CFC-11 essentially means that air returning to the troposphere from the stratosphere would not have a largely different isotopic composition compared to air leaving the troposphere. This means that the isotopic composition is not likely to change considerably over time. More broadly, and to use comparison to other species of interest, it is likely that

those with fast rates of destruction, and hence weaker apparent isotope fractionation are less likely to have significant changes in isotopic composition in tropospheric air over time. This is extremely useful in the case of methyl chloride, since sources are well understood but not well quantified, the understanding of changes in isotopic composition over time will aid constraint of source signatures.

In an ideal scenario of precision, an integrated global picture could be achieved. Use of samples such as those from the CARIBIC campaigns, and new aircraft based samples which show global picture and how it changes over time. This approach would be suitable for the three CFCs of interest as well as N_2O. However it is important to note that since CH_3Cl degrades in canisters, in order to measure this species historically, firn samples would be required. It would be interesting to use findings to identify if the Brewer-Dobson circulation has changed. By comparing historical samples with recently sourced air it would be possible to identify changes in circulation. Assuming no variation in photolysis, (or by a comparison of actinic flux), if dampening of the fractionation at altitude has changed over time, it is likely that this is due to changes in circulation data. Future work might include N_2O isotope analysis of further Geophysica samples from Gap, France, both the same region and mid latitudes for example, but at a later date than those presented in this thesis.

Since the techniques and data provided in this work could be further to answer some interesting questions regarding atmospheric circulation and transport, it follows that in the future there may be an impact on policy making. Isotopic information leading to a better understanding of stratospheric ozone depletion as well as the Brewer-Dobson circulation has implications for the policy making through the respective international agreements: The Montreal Protocol on Substances That Deplete the Ozone Layer, and the Paris Climate Deal. The latter is relevant as stratospheric circulation changes are of importance for understanding future climate change. In addition, CFC-12 exhibits similar fractionation to N_2O. The latter has been used for studies to constrain mass transport between the stratosphere and the troposphere, which is another important parameter for climate models, and so CFC-12 could be used to validate these results

Major abbreviations and chemical formulae

CFC	Chlorofluorocarbon
CFC-11	CCl_3F
CFC-12	CCl_2F_2
CFC-113	$C_2Cl_3F_3$
CH_3Cl	Methyl chloride
δ	Delta
ε_{App}	Apparent isotope fractionation
GC-MS	Gas chromatography mass spectrometry
GWP	Global warming potential
HCFC	Hydrofluorochlorocarbon
HFC	Hydrofluorocarbon
IR-MS	Isotope ratio mass spectrometry
ITCZ	Intertropical convergence zone
N_2O	Nitrous oxide
PFC	Perfluorocarbon
SCOT	Support coated open tubular
SMOC	Standard mean ocean chloride
SMOW	Standard mean ocean water
UMCIS	UEA methyl chloride isotopologue standard
VPDB	Vienna Pee Dee Belemnite
VSMOW	Vienna standard mean ocean water
WCOT	Wall coated open tubular
ZPE	Zero point energy

References

ALLIN, S. J. 2015. Trace Gases in the Antarctic and Firn Ice: A Record of Carbonyl Sulphide and the Isotopologues of Chlorofluorocarbons. *PhD Thesis,* University of East Anglia, Norwich, UK.

ALLIN, S. J., LAUBE, J. C., WITRANT, E., KAISER, J., MCKENNA, E., DENNIS, P., MULVANEY, R., CAPRON, E., MARTINERIE, P., RÖCKMANN, T., BLUNIER, T., SCHWANDER, J., FRASER, P. J., LANGENFELDS, R. L. & STURGES, W. T. 2015. Chlorine isotope composition in chlorofluorocarbons CFC-11, CFC-12 and CFC-113 in firn, stratospheric and tropospheric air. *Atmos. Chem. Phys.,* 15**,** 6867-6877.

AREGBE, Y., VALKIERS, S., MAYER, K., BIÈVRE, P. D., WESSEL, R. M. & ALINK, A. 1998. Measuring amount ratios of gas isotopes by two primary methods. *Metrologia,* 35**,** 7.

BARKAN, E. & LUZ, B. 2005. High precision measurements of 17O/16O and 18O/16O ratios in H2O. *Rapid Communications in Mass Spectrometry,* 19**,** 3737-3742.

BERNARD, S., RÖCKMANN, T., KAISER, J., BARNOLA, J. M., FISCHER, H., BLUNIER, T. & CHAPPELLAZ, J. 2006. Constraints on N2O budget changes since pre-industrial time from new firn air and ice core isotope measurements. *Atmos. Chem. Phys.,* 6**,** 493-503.

BILL, M., RHEW, R. C., WEISS, R. F. & GOLDSTEIN, A. H. 2002. Carbon isotope ratios of methyl bromide and methyl chloride emitted from a coastal salt marsh. *Geophysical Research Letters,* 29**,** 4-1-4-4.

BLAKE, G. A., LIANG, M.-C., MORGAN, C. G. & YUNG, Y. L. 2003. A Born-Oppenheimer photolysis model of N2O fractionation. *Geophysical Research Letters,* 30**,** 1656.

BRENNINKMEIJER, C. A. M., JANSSEN, C., KAISER, J., RÖCKMANN, T., RHEE, T. S. & ASSONOV, S. S. 2003. Isotope Effects in the Chemistry of Atmospheric Trace Compounds. *Chemical Reviews,* 103**,** 5125-5162.

BRÜHL, C., LELIEVELD, J., CRUTZEN, P. J. & TOST, H. 2012. The role of carbonyl sulphide as a source of stratospheric sulphate aerosol and its impact on climate. *Atmos. Chem. Phys.,* 12**,** 1239-1253.

BUIZERT, C., MARTINERIE, P., PETRENKO, V. V., SEVERINGHAUS, J. P., TRUDINGER, C. M., WITRANT, E., ROSEN, J. L., ORSI, A. J., RUBINO, M., ETHERIDGE, D. M., STEELE, L. P., HOGAN, C., LAUBE, J. C., STURGES, W. T., LEVCHENKO, V. A., SMITH, A. M., LEVIN, I., CONWAY, T. J., DLUGOKENCKY, E. J., LANG, P. M., KAWAMURA, K., JENK, T. M., WHITE, J. W. C., SOWERS, T., SCHWANDER, J. & BLUNIER, T. 2012. Gas transport in firn: multiple-tracer characterisation and model intercomparison for NEEM, Northern Greenland. *Atmos. Chem. Phys.,* 12**,** 4259-4277.

BUTLER, J. H., BATTLE, M., BENDER, M. L., MONTZKA, S. A., CLARKE, A. D., SALTZMAN, E. S., SUCHER, C. M., SEVERINGHAUS, J. P. & ELKINS, J. W. 1999. A record of atmospheric halocarbons during the twentieth century from polar firn air. *Nature,* 399**,** 749-755.

CARPENTER, L. J., REIMANN, S., BURKHOLDER, J. B., CLERBAUX, C., HALL, B. D., HOSSAINI, R., LAUBE, J. C. & YVON-LEWIS, S. A. 2014. Ozone-Depleting Substances (ODSs) and Other Gases of Interest to the Montreal Protocol,

Chapter 1 in Scientific Assessment of Ozone Depletion: 2014, Global Ozone Research and Monitoring Project –

Report No. 55. *World Meteorological Organization, Geneva, Switzerland,* 55.

CHENG, L. & KINDEL, P. K. 1997. Detection and homogeneity of cell wall pectic polysaccharides of Lemna minor. *Carbohydrate Research,* 301**,** 205-212.

CLIFF, S. S., BRENNINKMEIJER, C. A. M. & THIEMENS, M. H. 1999a. First measurement of the 18O/16O and 17O/16O ratios in stratospheric nitrous oxide: A mass-independent anomaly. *Journal of Geophysical Research: Atmospheres,* 104**,** 16171-16175.

CLIFF, S. S., BRENNINKMEIJER, C. A. M. & THIEMENS, M. H. 1999b. First measurement of the 18O/ 16O and 17O/16O ratios in stratospheric nitrous oxide: A mass independent anomaly. *J. Geophys. Res.,* 104**,** 16171-16175.

CLIFF, S. S. & THIEMENS, M. H. 1997. The 18O/ 16O and 17O/16O ratios in atmospheric nitrous oxide: A mass-independent anomaly. *Science,* 278**,** 1774-1776.

CRONIN, J. F. 1971. Recent Volcanism and the Stratosphere. *Science,* 172**,** 847-849.

DAVIDSON, E. A. 2009. The contribution of manure and fertilizer nitrogen to atmospheric nitrous oxide since 1860. *Nature Geosci,* 2**,** 659-662.

DENTENER, F. J. & CRUTZEN, P. J. 1994. A three-dimensional model of the global ammonia cycle. *Journal of Atmospheric Chemistry,* 19**,** 331-369.

DERENDORP, L., WISHKERMAN, A., KEPPLER, F., MCROBERTS, C., HOLZINGER, R. & RÖCKMANN, T. 2012. Methyl chloride emissions from halophyte leaf litter: Dependence on temperature and chloride content. *Chemosphere,* 87**,** 483-489.

DLUGOKENCKY, E. & TANS, P. 2016. *NOAA/ESRL, Earth System Research Laboratory, Global Monitoring Division*.

ESTUPIÑÁN, E. G., NICOVICH, J. M., LI, J., CUNNOLD, D. M. & WINE, P. H. 2002. Investigation of N2O Production from 266 and 532 nm Laser Flash Photolysis of O3/N2/O2 Mixtures. *The Journal of Physical Chemistry A,* 106**,** 5880-5890.

ESTUPIÑÁN, E. G., STICKEL, R. E. & WINE, P. H. 2000. Is quenching of electronically excited NO2 by N2 an important atmospheric source of N2O? *Chemosphere - Global Change Science,* 2**,** 247-253.

FABIAN, P., BORCHERS, R., LEIFER, R., SUBBARAYA, B. H., LAL, S. & BOY, M. 1996. Global stratospheric distribution of halocarbons. *Atmospheric Environment,* 30**,** 1787-1796.

FAHEY, D. W. & HEGGLIN, M. I. 2010. Twenty questions and answers about the ozone layer: 2010 update in *Scientific Assessment of Ozone Depletion*. *Global Ozone Research Monitoring Project, World Meteorological Organisation,* Report number 52, Geneva.

FRAME, C. H. & CASCIOTTI, K. L. 2010. Biogeochemical controls and isotopic signatures of nitrous oxide production by a marine ammonia-oxidizing bacterium. *Biogeosciences,* 7**,** 2695-2709.

FRIEDMAN, L. & BIGELEISEN, J. 1950. Oxygen and Nitrogen Isotope Effects in the Decomposition of Ammonium Nitrate. *The Journal of Chemical Physics,* 18**,** 1325-1331.

GEBHARDT, H., SARNTHEIN, M., GROOTES, P. M., KIEFER, T., KÜHN, H., SCHMIEDER, F. & RÖHL, U. 2008. Carbon and oxygen stable isotopes on G.bulloides of sediment core MD02-2489. *In supplement to: Gebhardt, Holger; Sarnthein, Michael; Grootes, Pieter Meiert; Kiefer, Thorsten; Kühn, Hartmut; Schmieder, Frank; Röhl, Ursula (2008): Paleonutrient and productivity records from the subarctic North Pacific for Pleistocene glacial terminations I to V. Paleoceanography, 23(4), PA4212, doi:10.1029/2007PA001513.* PANGAEA.

GOLDSTEIN, A. H. & SHAW, S. L. 2003. Isotopes of Volatile Organic Compounds: An Emerging Approach for Studying Atmospheric Budgets and Chemistry. *Chemical Reviews,* 103**,** 5025-5048.

GREULE, M., HUBER, S. G. & KEPPLER, F. 2012. Stable hydrogen-isotope analysis of methyl chloride emitted from heated halophytic plants. *Atmospheric Environment,* 62**,** 584-592.

GROSSMAN, A. S., GRANT, K. E., BLASS, W. E. & WUEBBLES, D. J. 1997. Radiative forcing calculations for CH3Cl and CH3Br. *Journal of Geophysical Research: Atmospheres,* 102**,** 13651-13656.

HAMILTON, J. T. G., MCROBERTS, W. C., KEPPLER, F., KALIN, R. M. & HARPER, D. B. 2003. Chloride Methylation by Plant Pectin: An Efficient Environmentally Significant Process. *Science,* 301**,** 206-209.

HARPER, D. B. 1985. Halomethane from halide ion[mdash]a highly efficient fungal conversion of environmental significance. *Nature,* 315**,** 55-57.

HEIL, J., WOLF, B., BRÜGGEMANN, N., EMMENEGGER, L., TUZSON, B., VEREECKEN, H. & MOHN, J. 2014. Site-specific 15N isotopic signatures of abiotically produced N2O. *Geochimica et Cosmochimica Acta,* 139**,** 72-82.

HOLT, B. D., STURCHIO, N. C., ABRAJANO, T. A. & HERATY, L. J. 1997. Conversion of Chlorinated Volatile Organic Compounds to Carbon Dioxide and Methyl Chloride for Isotopic Analysis of Carbon and Chlorine. *Analytical Chemistry,* 69**,** 2727-2733.

HOLTON, J. R., HAYNES, P. H., MCINTYRE, M. E., DOUGLASS, A. R., ROOD, R. B. & PFISTER, L. 1995. Strstosphere-Troposphere Exchange. *Review of Geophysics,* 33**,** 403-439.

HSU, K. J. & DEMORE, W. B. 1994. Rate constants for the reactions of OH with CH3Cl, CH2Cl2, CHCl3, and CH3Br. *Geophysical Research Letters,* 21**,** 805-808.

HU, L., YVON-LEWIS, S. A., BUTLER, J. H., LOBERT, J. M. & KING, D. B. 2013. An improved oceanic budget for methyl chloride. *Journal of Geophysical Research: Oceans,* 118**,** 715-725.

IPCC 2014. *Climate Change 2014: Impacts, Adaptation, and Vulnerability. Part A: Global and Sectoral Aspects. Contribution of Working Group II to the Fifth Assessment Report of the Intergovernmental Panel on Climate Change [Field, C.B., V.R. Barros, D.J. Dokken, K.J. Mach, M.D. Mastrandrea, T.E. Bilir, M. Chatterjee, K.L. Ebi, Y.O. Estrada, R.C. Genova, B. Girma, E.S. Kissel, A.N. Levy, S. MacCracken, P.R. Mastrandrea, and L.L. White (eds.)],* Cambridge, United Kingdom and New York, NY, USA, Cambridge University Press.

JINUNTUYA-NORTMAN, M., SUTKA, R. L., OSTROM, P. H., GANDHI, H. & OSTROM, N. E. 2008. Isotopologue fractionation during microbial reduction of N2O within soil mesocosms as a function of water-filled pore space. *Soil Biology and Biochemistry,* 40**,** 2273-2280.

JOHNSTON, J. C., CLIFF, S. S. & THIEMENS, M. H. 1995. Measurement of multioxygen isotopic ([delta] 18O and [delta]17O) fractionation factors in the stratospheric sink reactions of nitrous oxide. *J. Geophys. Res.,* 100**,** 16801-116804.

KAISER, J. 2008. Reformulated 17O correction of mass spectrometric stable isotope measurements in carbon dioxide and a critical appraisal of historic 'absolute' carbon and oxygen isotope ratios. *Geochimica et Cosmochimica Acta,* 72**,** 1312-1334.

KAISER, J., ENGEL, A., BORCHERS, R. & RÖCKMANN, T. 2006. Probing stratospheric transport and chemistry with new balloon and aircraft observations of the meridional and vertical N2O isotope distribution. *Atmos. Chem. Phys.,* 6**,** 3535-3556.

KAISER, J. & RÖCKMANN, T. 2005. Absence of isotope exchange in the reaction of N2O + O(1D) and the global Δ17O budget of nitrous oxide. *Geophysical Research Letters,* 32**,** n/a-n/a.

KAISER, J., RÖCKMANN, T. & BRENNINKMEIJER, C. A. M. 2004. Contribution of mass-dependent fractionation to the oxygen isotope anomaly of atmospheric nitrous oxide. *Journal of Geophysical Research: Atmospheres,* 109**,** D03305.

KAISER, J., RÖCKMANN, T., BRENNINKMEIJER, C. A. M. & CRUTZEN, P. J. 2002. Wavelength dependence of isotope fractionation in N2O photolysis. *Atmos. Chem. Phys. Discuss.,* 2**,** 1735-1763.

KEENE, W. C., KHALIL, M. A. K., ERICKSON, D. J., MCCULLOCH, A., GRAEDEL, T. E., LOBERT, J. M., AUCOTT, M. L., GONG, S. L., HARPER, D. B., KLEIMAN, G., MIDGLEY, P., MOORE, R. M., SEUZARET, C., STURGES, W. T., BENKOVITZ, C. M., KOROPALOV, V., BARRIE, L. A. & LI, Y. F. 1999. Composite global emissions of reactive chlorine from anthropogenic and

natural sources: Reactive Chlorine Emissions Inventory. *Journal of Geophysical Research: Atmospheres,* 104**,** 8429-8440.
KEPPLER, F., HARPER, D. B., RÖCKMANN, T., MOORE, R. M. & HAMILTON, J. T. G. 2005. New insight into the atmospheric chloromethane budget gained using stable carbon isotope ratios. *Atmos. Chem. Phys.,* 5**,** 2403-2411.
KEPPLER, F., KALIN, R. M., HARPER, D. B., MCROBERTS, W. C. & HAMILTON, J. T. G. 2004. Carbon isotope anomaly in the major plant C₁ pool and its global biogeochemical implications. *Biogeosciences,* 1**,** 123-131.
KIKUCHI, A., EDASHIGE, Y., ISHII, T. & SATOH, S. 1996. A xylogalacturonan whose level is dependent on the size of cell clusters is present in the pectin from cultured carrot cells. *Planta,* 200**,** 369-372.
KIM, K.-R. & CRAIG, H. 1993. Nitrogen-15 and Oxygen-18 Characteristics of Nitrous Oxide: A Global Perspective. *Science,* 262**,** 1855-1857.
KIM, K. R. & CRAIG, H. 1990. Two-isotope characterization of N 2O in the Pacific Ocean and constraints on its origin in deep water. *Nature,* 347**,** 58-61.
KOMALAVILAS, P. & MORT, A. J. 1989. The acetylation of O-3 of galacturonic acid in the rhamnose-rich portion of pectins. *Carbohydrate Research,* 189**,** 261-272.
KOMATSU, D. D., ISHIMURA, T., NAKAGAWA, F. & TSUNOGAI, U. 2008. Determination of the 15N/14N, 17O/16O, and 18O/16O ratios of nitrous oxide by using continuous-flow isotope-ratio mass spectrometry. *Rapid Communications in Mass Spectrometry,* 22**,** 1587-1596.
KONNO, U. T. A., TAKAI, K. E. N. & KAWAGUCCI, S. 2013. Stable chlorine isotope ratio analysis of subnanomolar level methyl chloride by continuous-flow isotope ratio mass spectrometry. *GEOCHEMICAL JOURNAL,* 47**,** 469-473.
KÖSTER, J. R., WELL, R., TUZSON, B., BOL, R., DITTERT, K., GIESEMANN, A., EMMENEGGER, L., MANNINEN, A., CÁRDENAS, L. & MOHN, J. 2013. Novel laser spectroscopic technique for continuous analysis of N2O isotopomers – application and intercomparison with isotope ratio mass spectrometry. *Rapid Communications in Mass Spectrometry,* 27**,** 216-222.
LAUBE, J. C., KAISER, J., STURGES, W. T., BÖNISCH, H. & ENGEL, A. 2010. Chlorine Isotope Fractionation in the Stratosphere. *Science,* 329**,** 1167-1167.
LAUBE, J. C., KEIL, A., BÖNISCH, H., ENGEL, A., RÖCKMANN, T., VOLK, C. M. & STURGES, W. T. 2013. Observation-based assessment of stratospheric fractional release, lifetimes, and ozone depletion potentials of ten important source gases. *Atmos. Chem. Phys.,* 13**,** 2779-2791.
LEWICKA-SZCZEBAK, D., DYCKMANS, J., KAISER, J., MARCA, A., AUGUSTIN, J. & WELL, R. 2016. Oxygen isotope fractionation during N2O production by soil denitrification. *Biogeosciences,* 13**,** 1129-1144.
LOCKHART, J. 2010. Stable Isotope Fractionation of CFC-12 under UV Photolysis. *MSc Research Project,* University of East Anglia.
LONG, A., EASTOE, C. J., KAUFMANN, R. S., MARTIN, J. G., WIRT, L. & FINLEY, J. B. 1993. High-precision measurement of chlorine stable isotope ratios. *Geochimica et Cosmochimica Acta,* 57**,** 2907-2912.
MARTIN, M. 2011. Temperature Dependence of Chlorine Isotope Fractionation in CF2Cl2 in a Photolysis Reaction. *BSc Undergraduate Research Project,* University of East Anglia.
MARTINERIE, P., NOURTIER-MAZAURIC, E., BARNOLA, J. M., STURGES, W. T., WORTON, D. R., ATLAS, E., GOHAR, L. K., SHINE, K. P. & BRASSEUR, G. P. 2009. Long-lived halocarbon trends and budgets from atmospheric chemistry modelling constrained with measurements in polar firn. *Atmos. Chem. Phys.,* 9**,** 3911-3934.
MAXWELL, S. 2012. Chlorine Isotope Fractionation of Dichlorodifluoromethane in the Presence of Scavenger Ethane. *MSc Research Project,* University of East Anglia, Norwich, UK.

MCILVIN, M. R. & CASCIOTTI, K. L. 2010. Fully automated system for stable isotopic analyses of dissolved nitrous oxide at natural abundance levels. *Limnology and Oceanography: Methods,* 8**,** 54-66.

MCLINDEN, C. A., PRATHER, M. J. & JOHNSON, M. S. 2003. Global modeling of the isotopic analogues of N2O: Stratospheric distributions, budgets, and the 17O–18O mass-independent anomaly. *Journal of Geophysical Research: Atmospheres,* 108**,** 4233.

MEIJER, H. A. J. & LI, W. J. 1998. The Use of Electrolysis for Accurate δ17O and δ18O Isotope Measurements in Water. *Isotopes in Environmental and Health Studies,* 34**,** 349-369.

MICHALSKI, G., SCOTT, Z., KABILING, M. & THIEMENS, M. H. 2003. First measurements and modeling of Δ17O in atmospheric nitrate. *Geophysical Research Letters,* 30**,** n/a-n/a.

MILLER, C. E. & YUNG, Y. L. 2000. Photo-induced isotopic fractionation. *Journal of Geophysical Research: Atmospheres,* 105**,** 29039-29051.

MILLER, L. G., KALIN, R. M., MCCAULEY, S. E., HAMILTON, J. T. G., HARPER, D. B., MILLET, D. B., OREMLAND, R. S. & GOLDSTEIN, A. H. 2001. Large carbon isotope fractionation associated with oxidation of methyl halides by methylotrophic bacteria. *Proceedings of the National Academy of Sciences of the United States of America,* 98**,** 5833-5837.

MOHN, J., WOLF, B., TOYODA, S., LIN, C. T., LIANG, M. C., BRÜGGEMANN, N., WISSEL, H., STEIKER, A. E., DYCKMANS, J., SZWEC, L., OSTROM, N. E., CASCIOTTI, K. L., FORBES, M., GIESEMANN, A., WELL, R., DOUCETT, R. R., YARNES, C. T., RIDLEY, A. R., KAISER, J. & YOSHIDA, N. 2014. Interlaboratory assessment of nitrous oxide isotopomer analysis by isotope ratio mass spectrometry and laser spectroscopy: Current status and perspectives. *Rapid Communications in Mass Spectrometry,* 28**,** 1995-2007.

MOLINA, M. J. & ROWLAND, F. S. 1974. Stratospheric sink for chlorofluoromethanes: chlorine atomc-atalysed destruction of ozone. *Nature,* 249**,** 810-812.

MONTZKA, S. A., DLUGOKENCKY, E. J. & BUTLER, J. H. 2011. Non-CO2 greenhouse gases and climate change. *Nature,* 476**,** 43-50.

MONTZKA, S. A. & REIMANN, S. 2011. Chapter One: ozone Depleting Substances (ODSs) and related chemicals. In WMO (World Meteorological Organization Scientific Assessment of Ozone Depletion 2010 Global Research Monitoring Project - Report No. 52. *World Meteorological Society, Geneva Switzerland,* 52.

MOORE, R. M., GROSZKO, W. & NIVEN, S. J. 1996. Ocean-atmosphere exchange of methyl chloride: Results from NW Atlantic and Pacific Ocean studies. *Journal of Geophysical Research: Oceans,* 101**,** 28529-28538.

MORGAN, C. G., ALLEN, M., LIANG, M. C., SHIA, R. L., BLAKE, G. A. & YUNG, Y. L. 2004. Isotopic fractionation of nitrous oxide in the stratosphere: Comparison between model and observations. *Journal of Geophysical Research: Atmospheres,* 109**,** n/a-n/a.

MYHRE, G., SHINDELL, D., BRÉON, F.-M., COLLINS, W., FUGLESTVEDT, J., HUANG, J., KOCH, D., LAMARQUE, J.-F., LEE, D., MENDOZA, B., NAKAJIMA, T., ROBOCK, A., STEPHENS, G., TAKEMURA, T. & ZHANG, H. 2013. Anthropogenic and Natural Radiative Forcing. *In:* STOCKER, T. F., QIN, D., PLATTNER, G.-K., TIGNOR, M., ALLEN, S. K., BOSCHUNG, J., NAUELS, A., XIA, Y., BEX, V. & MIDGLEY, P. M. (eds.) *Climate Change 2013: The Physical Science Basis. Contribution of Working Group I to the Fifth Assessment Report of the Intergovernmental Panel on Climate Change.* Cambridge, United Kingdom and New York, NY, USA: Cambridge University Press.

O'NEILL, M., ALBERSHEIM, P. & DARVILL, A. 1990. The Pectin Polysaccharides of Primary Cell Walls. *In Dey, D. M. (Ed.) Methods in Plant Biochemistry,* 2**,** 415-441.

PATRA, P. K. & LAL, S. 1997. Variability of eddy diffusivity in the stratosphere deduced from vertical distributions of N2O and CFC-12. *Journal of Atmospheric and Solar-Terrestrial Physics,* 59**,** 1149-1157.

PLUMB, R. A., WAUGH, D. W. & CHIPPERFIELD, M. P. 2000. The effects of mixing on tracer relationships in the polar vortices. *Journal of Geophysical Research: Atmospheres,* 105**,** 10047-10062.

PORTMANN, R. W., DANIEL, J. S. & RAVISHANKARA, A. R. 2012. *Stratospheric ozone depletion due to nitrous oxide: influences of other gases*.

PRASAD, S. S. & ZIPF, E. C. 2000. Atmospheric production of nitrous oxide from excited ozone and its significance. *Chemosphere - Global Change Science,* 2**,** 235-245.

PRATHER, M. J., HOLMES, C. D. & HSU, J. 2012. Reactive greenhouse gas scenarios: Systematic exploration of uncertainties and the role of atmospheric chemistry. *Geophysical Research Letters,* 39**,** L09803.

PRATHER, M. J., HSU, J., DELUCA, N. M., JACKMAN, C. H., OMAN, L. D., DOUGLASS, A. R., FLEMING, E. L., STRAHAN, S. E., STEENROD, S. D., SØVDE, O. A., ISAKSEN, I. S. A., FROIDEVAUX, L. & FUNKE, B. 2015. Measuring and modeling the lifetime of nitrous oxide including its variability. *Journal of Geophysical Research: Atmospheres,* 120**,** 5693-5705.

PRINN, R. G., WEISS, R. F., FRASER, P. J., SIMMONDS, P. G., ALYEA, F. N. & CUNNOLD, D. M. 2014. The ALE/GAGE/AGAGE satabase, Dataset DB-1001.

PROKOPIOU, M., MARTINERIE, P., SAPART, C. J., WITRANT, E., MONTEIL, G. A., ISHIJIMA, K., BERNARD, S., KAISER, J., LEVIN, I., SOWERS, T., BLUNIER, T., ETHERIDGE, D., DLUGOKENCKY, E., VAN DE WAL, R. S. W. & RÖCKMANN, T. 2016. Constraining N2O emissions since 1940 using firn air isotope measurements in both hemispheres. *Atmos. Chem. Phys. Discuss.,* 2016**,** 1-50.

RAHN, T. & WAHLEN, M. 1997. Stable Isotope Enrichment in Stratospheric Nitrous Oxide. *Science,* 278**,** 1776-1778.

RAHN, T. & WAHLEN, M. 2000. A reassessment of the global isotopic budget of atmospheric nitrous oxide. *Global Biogeochemical Cycles,* 14**,** 537-543.

RAVISHANKARA, A. R., DANIEL, J. S. & PORTMANN, R. W. 2009. Nitrous Oxide (N2O): The Dominant Ozone-Depleting Substance Emitted in the 21st Century. *Science,* 326**,** 123-125.

REDEKER, K. R., DAVIS, S. & KALIN, R. M. 2007. Isotope values of atmospheric halocarbons and hydrocarbons from Irish urban, rural, and marine locations. *Journal of Geophysical Research: Atmospheres,* 112**,** n/a-n/a.

RHEW, R. C., MILLER, B. R., VOLLMER, M. K. & WEISS, R. F. 2001. Shrubland fluxes of methyl bromide and methyl chloride. *Journal of Geophysical Research: Atmospheres,* 106**,** 20875-20882.

RHEW, R. C., MILLER, B. R. & WEISS, R. F. 2000. Natural methyl bromide and methyl chloride emissions from coastal salt marshes. *Nature,* 403**,** 292-295.

RIDLEY, B. L., O'NEILL, M. A. & MOHNEN, D. 2001. Pectins: structure, biosynthesis, and oligogalacturonide-related signaling. *Phytochemistry,* 57**,** 929-967.

RÖCKMANN, T., KAISER, J., BRENNINKMEIJER, C. A. M., CROWLEY, J. N., BORCHERS, R., BRAND, W. A. & CRUTZEN, P. J. 2001a. Isotopic enrichment of nitrous oxide (15N14NO, 14N15NO, 14N14N18O) in the stratosphere and in the laboratory. *Journal of Geophysical Research: Atmospheres,* 106**,** 10403-10410.

RÖCKMANN, T., KAISER, J., CROWLEY, J. N., BRENNINKMEIJER, C. A. M. & CRUTZEN, P. J. 2001b. The origin of the anomalous or “mass-independent” oxygen isotope fractionation in tropospheric N2O. *Geophysical Research Letters,* 28**,** 503-506.

RUDOLPH, J., LOWE, D. C., MARTIN, R. J. & CLARKSON, T. S. 1997. A novel method for compound specific determination of δ13C in volatile organic compounds at ppt levels in ambient air. *Geophysical Research Letters,* 24**,** 659-662.

SAITO, T., YOKOUCHI, Y., KOSUGI, Y., TANI, M., PHILIP, E. & OKUDA, T. 2008. Methyl chloride and isoprene emissions from tropical rain forest in Southeast Asia. *Geophysical Research Letters,* 35**,** n/a-n/a.

SCHAUFFLER, S. M., HEIDT, L. E., POLLOCK, W. H., GILPIN, T. M., VEDDER, J. F., SOLOMON, S., LUEB, R. A. & ATLAS, E. L. 1993. Measurements of halogenated organic compounds near the tropical tropopause. *Geophysical Research Letters,* 20**,** 2567-2570.

SCHMIDT, J. A. & JOHNSON, M. S. 2015. Clumped isotope perturbation in tropospheric nitrous oxide from stratospheric photolysis. *Geophysical Research Letters,* 42**,** 3546-3552.

SCHMIDT, J. A., JOHNSON, M. S. & SCHINKE, R. 2011. Isotope effects in N2O photolysis from first principles. *Atmos. Chem. Phys.,* 11**,** 8965-8975.

SINGH, H. B., SALAS, L. J. & STILES, R. E. 1983. Methyl halides in and over the eastern Pacific (40°N–32°S). *Journal of Geophysical Research: Oceans,* 88**,** 3684-3690.

STEVENS, C. M. & ENGELKEMEIR, A. 1988. Stable carbon isotopic composition of methane from some natural and anthropogenic sources. *Journal of Geophysical Research: Atmospheres,* 93**,** 725-733.

SYAKILA, A. & KROEZE, C. 2011. The global nitrous oxide budget revisited. *Greenhouse Gas Measurement and Management,* 1**,** 17-26.

TAYLOR, J. W. & GRIMSRUD, E. P. 1969. Chlorine isotopic ratios by negative ion mass spectrometry. *Analytical Chemistry,* 41**,** 805-810.

THOMPSON, A. E., ANDERSON, R. S., RUDOLPH, J. & HUANG, L. 2002. Stable carbon isotope signatures of background tropospheric chloromethane and CFC113. *Biogeochemistry,* 60**,** 191-211.

TOYODA, S., KUROKI, N., YOSHIDA, N., ISHIJIMA, K., TOHJIMA, Y. & MACHIDA, T. 2013. Decadal time series of tropospheric abundance of N2O isotopomers and isotopologues in the Northern Hemisphere obtained by the long-term observation at Hateruma Island, Japan. *Journal of Geophysical Research: Atmospheres,* 118**,** 3369-3381.

TOYODA, S. & YOSHIDA, N. 1999. Determination of nitrogen isotopomers of nitrous oxide on a modified isotope-ratio mass spectrometer. *Anal. Chem.,* 71**,** 4711-4718.

TOYODA, S., YOSHIDA, N. & KOBA, K. 2017. Isotopocule analysis of biologically produced nitrous oxide in various environments. *Mass Spectrometry Reviews,* 36**,** 135-160.

TRENBERTH, K. E., FASULLO, J. T. & KIEHL, J. 2009. Earth's Global Energy Budget. *Bulletin of the American Meteorological Society,* 90**,** 311-323.

VISSER, J. & VORAGEN, A. 1996. Pectin and Pectinases, Progress in Biotechnology. *Vol. 14,* Elsevier, Amsterdam.

WAHLEN, M. & YOSHINARI, T. 1985. Oxygen isotope ratios in N 2O from different environments. *Nature,* 313**,** 780-782.

WOFSY, S. C., MCELROY, M. B. & YUNG, Y. L. 1975. The chemistry of atmospheric bromine. *Geophysical Research Letters,* 2**,** 215-218.

YOKOUCHI, Y., IKEDA, M., INUZUKA, Y. & YUKAWA, T. 2002. Strong emission of methyl chloride from tropical plants. *Nature,* 416**,** 163-165.

YOSHIDA, N. 1988. 15N-depleted N2O as a product of nitrification. *Nature,* 335**,** 528-529.

YOSHIDA, N. & TOYODA, S. 2000. Constraining the atmospheric N2O budget from intramolecular site preference in N2O isotopomers. *Nature,* 405**,** 330-334.

YOUNG, E. D., GALY, A. & NAGAHARA, H. 2002. Kinetic and equilibrium mass-dependent isotope fractionation laws in nature and their geochemical and cosmochemical significance. *Geochimica et Cosmochimica Acta,* 66**,** 1095-1104.

YUNG, Y. L. & MILLER, C. E. 1997. Isotopic fractionation of stratospheric nitrous oxide. *Science,* 278**,** 1778-1780.

ZELLNER, R., HARTMANN, D. & ROSNER, I. 1992. N2O Formation in the Reactive Collisional Quenching of NO3* and NO2* by N2. *Berichte der Bunsengesellschaft für physikalische Chemie,* 96**,** 385-390.

ZIPF, E. C. & PRASAD, S. S. 1998. Experimental evidence that excited ozone is a source of nitrous oxide. *Geophys. Res. Lett.,* 25**,** 4333-4336.

ZUIDERWEG, A., HOLZINGER, R., MARTINERIE, P., SCHNEIDER, R., KAISER, J., WITRANT, E., ETHERIDGE, D., PETRENKO, V., BLUNIER, T. & RÖCKMANN, T. 2013. Extreme 13C depletion of CCl2F2 in firn air samples from NEEM, Greenland. *Atmos. Chem. Phys.,* 13**,** 599-609.

ZUIDERWEG, A., KAISER, J., LAUBE, J. C., RÖCKMANN, T. & HOLZINGER, R. 2012. Stable carbon isotope fractionation in the UV photolysis of CFC-11 and CFC-12. *Atmos. Chem. Phys.,* 12**,** 4379-4385.

Appendix 1

Work contributing to this thesis has been published in the following publication